Methods in Molecular Biology 1464

Springer Protocols

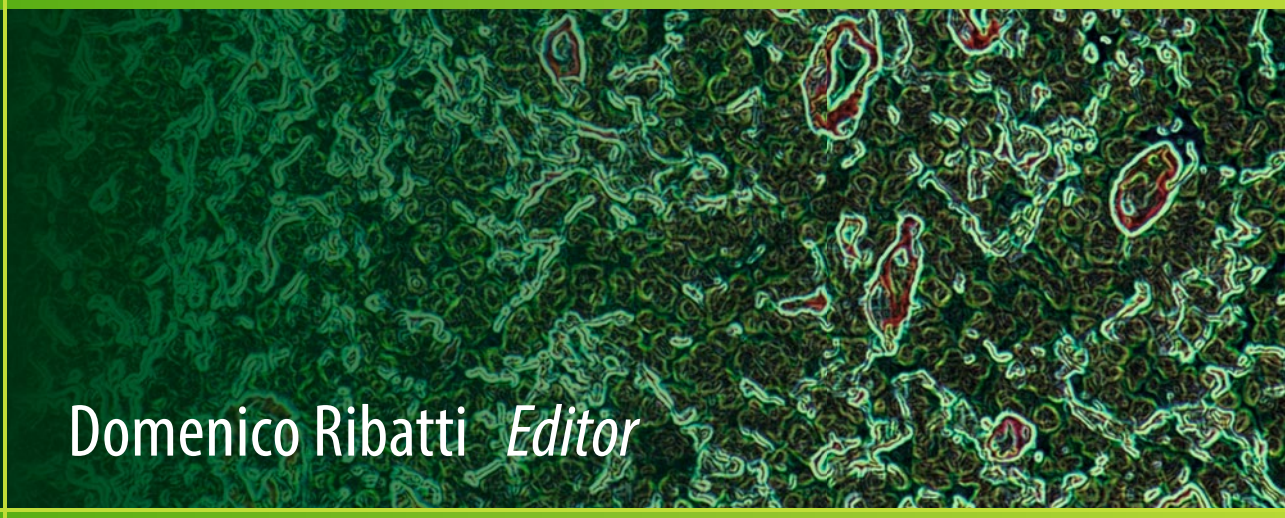

Domenico Ribatti *Editor*

Tumor Angiogenesis Assays

Methods and Protocols

Humana Press

METHODS IN MOLECULAR BIOLOGY

Series Editor
John M. Walker
School of Life and Medical Sciences
University of Hertfordshire
Hatfield, Hertfordshire, AL10 9AB, UK

For further volumes:
http://www.springer.com/series/7651

Tumor Angiogenesis Assays

Methods and Protocols

Edited by

Domenico Ribatti

Department of Basic Medical Sciences, Neurosciences and Sensory Organs, University of Bari Medical School, Bari, Italy; National Cancer Institute "Giovanni Paolo II", Bari, Italy

Humana Press

Editor
Domenico Ribatti
Department of Basic Medical Sciences
Neurosciences and Sensory Organs
University of Bari Medical School
Bari, Italy

National Cancer Institute "Giovanni Paolo II"
Bari, Italy

ISSN 1064-3745 ISSN 1940-6029 (electronic)
Methods in Molecular Biology
ISBN 978-1-4939-3997-8 ISBN 978-1-4939-3999-2 (eBook)
DOI 10.1007/978-1-4939-3999-2

Library of Congress Control Number: 2016942545

Printed on acid-free paper

This Humana Press imprint is published by Springer Nature
The registered company is Springer Science+Business Media LLC
The registered company address is: 233 Spring Street, New York, NY 10013, U.S.A

Preface

There now exists much evidence that growth of solid and hematologic tumors is angiogenesis-dependent. Tumor angiogenesis is generally viewed as the consequence of an angiogenic switch, i.e., a genetic event that endows the tumor with the ability to recruit blood vessels from the neighboring tissue. Tumor tissue is characterized by rapid proliferation, increased permeability, and disorganized architecture, properties which are a cause or a consequence of inadequate perfusion and oxygenation.

The main technical challenge in any study of tumor angiogenesis is the selection of the most appropriate assay. Despite the increasing numbers of both in vitro and in vivo assays, a "gold-standard" angiogenesis assay has yet to be developed; therefore, a combination of assays are required to identify the molecular and/or cellular events in tumor angiogenesis. Despite the discovery and development of numerous antiangiogenic agents for the treatment of cancer, which have showed promising inhibitory effects in preclinical testing, and in some instances tumor regression, these agents have proved very disappointing in clinical trials. This inconsistency of data highlights the need for rigorous preclinical testing using relevant models and the limitations of each assay being taken into consideration, thus avoiding overinterpretation of results.

The aim of this book is to provide a range of methods and protocols for studying tumor angiogenesis in vitro and in vivo to reflect advances in the field. I would like to thank the colleagues who kindly agreed to contribute to this work.

Bari, Italy ***Domenico Ribatti***

Contents

Preface . . . . . *v*
Contributors . . . . . *ix*

1 The Discovery of Tumor Angiogenesis Factors: A Historical Overview 1
Domenico Ribatti

2 Morphological Aspects of Tumor Angiogenesis 13
Ruslan Hlushchuk, Sébastien Barré, and Valentin Djonov

3 Exosomes in Tumor Angiogenesis 25
Karma Z. Salem, Michele Moschetta, Antonio Sacco, Luisa Imberti, Giuseppe Rossi, Irene M. Ghobrial, Salomon Manier, and Aldo M. Roccaro

4 Coculture Assays for Endothelial Cells-Mural Cells Interactions 35
Diana M. Sánchez-Palencia, Alex Bigger-Allen, Magali Saint-Geniez, Joseph F. Arboleda-Velásquez, and Patricia A. D'Amore

5 Characterization of Cancer Stem Cells 49
Stefania Orecchioni and Francesco Bertolini

6 The Aortic Ring Assay and Its Use for the Study of Tumor Angiogenesis 63
Alfred C. Aplin and Roberto F. Nicosia

7 Surface Plasmon Resonance Analysis of Heparin-Binding Angiogenic Growth Factors 73
Marco Rusnati and Antonella Bugatti

8 An Ex Vivo Tissue Culture Model for Anti-Angiogenic Drug Testing 85
Mohammad S. Azimi, Michelle Lacey, Debasis Mondal, and Walter L. Murfee

9 The Chorioallantoic Membrane of the Chick Embryo to Assess Tumor Formation and Metastasis 97
Anne Herrmann, Diana Moss, and Violaine Sée

10 Transgenic Zebrafish 107
Xiaowen Chen, Dafne Gays, and Massimo M. Santoro

11 High-Resolution Intravital Microscopy of Tumor Angiogenesis 115
Ann L.B. Seynhaeve and Timo L.M. ten Hagen

12 Subcutaneous Murine Xenograft Models: A Critical Tool for Studying Human Tumor Growth and Angiogenesis In Vivo 129
Katharina M. Schmidt, Edward K. Geissler, and Sven A. Lang

13 Orthotopic Model of Ovarian Cancer 139
Alessandra Decio and Raffaella Giavazzi

14 The Rip1Tag2 Transgenic Mouse Model 151
Ruben Bill and Gerhard Christofori

15 Tumor Blood Vessel Visualization 163
Clarissa Gillmann and Tobias Bäuerle

16 Uncovering Metabolic Effects of Anti-Angiogenic Therapy in Tumors by Induced Metabolic Bioluminescence Imaging 175
Stefano Indraccolo, Stefan Walenta, and Wolfgang Mueller-Klieser

17 Quantitation of Tumor Angiogenesis In Vitro: An All-In-One Angiogenesis Assay 185
Mahtab Bahramsoltani and Ward De Spiegelaere

Index *193*

Contributors

Alfred C. Aplin • *Department of Pathology, University of Washington, Seattle, WA, USA*
Joseph F. Arboleda-Velásquez • *Schepens Eye Research Institute, Massachusetts Eye and Ear, Department of Ophthalmology, Harvard Medical School, Boston, MA, USA*
Mohammad S. Azimi • *Department of Biomedical Engineering, Tulane University, New Orleans, LA, USA*
Tobias Bäuerle • *Institute of Radiology, University Medical Center Erlangen, Friedrich-Alexander University Erlangen-Nuremberg, Erlangen, Germany*
Mahtab Bahramsoltani • *Faculty of Veterinary Medicine, Institute of Veterinary Anatomy, University of Leipzig, Leipzig, Germany*
Sébastien Barré • *Institute of Anatomy, University of Bern, Bern, Switzerland*
Francesco Bertolini • *Laboratory of Hematology–Oncology, European Institute of Oncology, Milan, Italy*
Alex Bigger-Allen • *Schepens Eye Research Institute, Massachusetts Eye and Ear, Department of Ophthalmology, Harvard Medical School, Boston, MA, USA*
Ruben Bill • *Department of Biomedicine, University of Basel, Basel, Switzerland*
Antonella Bugatti • *Macromolecular Interaction Analysis Unit, Section of Experimental Oncology and Immunology, Department of Molecular and Translational Medicine, University of Brescia, Brescia, Italy*
Xiaowen Chen • *Vesalius Research Center, VIB-KUL, Leuven, Belgium*
Gerhard Christofori • *Department of Biomedicine, University of Basel, Basel, Switzerland*
Patricia D'Amore • *Schepens Eye Research Institute, Massachusetts Eye and Ear, Department of Ophthalmology, Harvard Medical School, Boston, MA, USA*
Ward De Spiegelaere • *Department of Internal Medicine, HIV Translational Research Unit, Ghent University Hospital, Ghent, Belgium*
Alessandra Decio • *Department of Oncology, Laboratory of Biology and Treatment of Metastasis, IRCCS—Istituto di Ricerche Farmacologiche Mario Negri, Milan, Italy*
Valentin Djonov • *Institute of Anatomy, University of Bern, Bern, Switzerland*
Dafne Gays • *Vesalius Research Center, VIB-KUL, Leuven, Belgium*
Edward K. Geissler • *Department of Surgery, University Hospital Regensburg, University of Regensburg, Regensburg, Germany*
Raffaella Giavazzi • *Department of Oncology, Laboratory of Biology and Treatment of Metastasis, IRCCS—Istituto di Ricerche Farmacologiche Mario Negri, Milan, Italy*
Clarissa Gillmann • *Institute of Radiology, University Medical Center Erlangen, Friedrich-Alexander University Erlangen-Nuremberg, Erlangen, Germany*
Irene M. Ghobrial • *Department of Medical Oncology, Dana-Farber Cancer Institute, Harvard Medical School, Boston, MA, USA*
Anne Herrmann • *Department of Biochemistry, University of Liverpool, Liverpool, UK; Department of Cellular and Molecular Physiology, University of Liverpool, Liverpool, UK*
Ruslan Hlushchuk • *Institute of Anatomy, University of Bern, Bern, Switzerland*

Luisa Imberti • *ASST Spedali Civili, Department of Medical Oncology, CREA Laboratory, Brescia, BS, Italy*
Stefano Indraccolo • *Istituto Oncologico Veneto - IRCCS, Padova, Italy*
Michelle Lacey • *Department of Mathematics, Tulane University, New Orleans, LA, USA*
Sven A. Lang • *Department of Surgery, University Hospital Regensburg, University of Regensburg, Regensburg, Germany*
Salomon Manier • *Department of Medical Oncology, Dana-Farber Cancer Institute, Harvard Medical School, Boston, MA, USA*
Debasis Mondal • *Department of Pharmacology, Tulane University, New Orleans, LA, USA*
Michele Moschetta • *Department of Medical Oncology, Dana-Farber Cancer Institute, Harvard Medical School, Boston, MA, USA*
Diane Moss • *Department of Cellular and Molecular Physiology, University of Liverpool, Liverpool, UK*
Wolfgang Mueller-Klieser • *Institute of Pathophysiology, University Medical Center of the Johannes Gutenberg University, Mainz, Germany*
Walter L. Murfee • *Department of Biomedical Engineering, Tulane University, New Orleans, LA, USA*
Roberto F. Nicosia • *Department of Pathology, University of Washington, Seattle, WA, USA; Division of Pathology and Laboratory Medicine, Veterans Administration Puget Sound Health Care System, Seattle, WA, USA*
Stefania Orecchioni • *Laboratory of Hematology–Oncology, European Institute of Oncology, Milan, Italy*
Domenico Ribatti • *Department of Basic Medical Sciences, Neurosciences and Sensory Organs, University of Bari Medical School, Bari, Italy; National Cancer Institute "Giovanni Paolo II", Bari, Italy*
Aldo M. Roccaro • *Department of Medical Oncology, Dana-Farber Cancer Institute, Harvard Medical School, Boston, MA, USA; ASST Spedali Civili, Department of Medical Oncology, CREA Laboratory, Brescia, BS, Italy*
Giuseppe Rossi • *ASST Spedali Civili, Department of Medical Oncology, CREA Laboratory, Brescia, BS, Italy*
Marco Rusnati • *Macromolecular Interaction Analysis Unit, Section of Experimental Oncology and Immunology, Department of Molecular and Translational Medicine, University of Brescia, Brescia, Italy*
Magali Saint-Geniez • *Schepens Eye Research Institute, Massachusetts Eye and Ear, Department of Ophthalmology, Harvard Medical School, Boston, MA, USA*
Karma Z. Salem • *Department of Medical Oncology, Dana-Farber Cancer Institute, Harvard Medical School, Boston, MA, USA*
Antonio Sacco • *Department of Medical Oncology, Dana-Farber Cancer Institute, Harvard Medical School, Boston, MA, USA*
Diana M. Sánchez-Palencia • *Schepens Eye and Research Institute, Massachusetts Eye and Ear, Department of Ophthalmology, Harvard Medical School, Boston, MA, USA*
Massimo M. Santoro • *Vesalius Research Center, VIB-KUL, Leuven, Belgium; Department of Molecular Biotechnology and Health Sciences, Molecular Biotechnology Center, University of Torino, Torino, Italy*
Katharina M. Schmidt • *Department of Surgery, University Hospital Regensburg, University of Regensburg, Regensburg, Germany*
Violaine Sée • *Department of Biochemistry, University of Liverpool, Liverpool, UK*

Ann L.B. Seynhaeve • *Laboratory Experimental Surgical Oncology, Section Surgical Oncology, Department of Surgery, Erasmus MC, Rotterdam, The Netherlands*
Timo L.M. ten Hagen • *Laboratory Experimental Surgical Oncology, Section Surgical Oncology, Department of Surgery, Erasmus MC, Rotterdam, The Netherlands*
Stefan Walenta • *Institute of Pathophysiology, University Medical Center of the Johannes Gutenberg University, Mainz, Germany*

Chapter 1

The Discovery of Tumor Angiogenesis Factors: A Historical Overview

Domenico Ribatti

Abstract

Starting with the hypothesis formulated by Judah Folkman that tumor growth is angiogenesis-dependent, this area of research has a solid scientific foundation, and inhibition of angiogenesis is a major area of therapeutic development for the treatment of cancer. This chapter offers an account of the most relevant discoveries in this field of biomedical research.

Key words Angiogenesis, Anti-angiogenesis, History of medicine, Tumor growth

1 Early Evidence of Tumor Cells Releasing Specific Growth Factor for Blood Vessels

Tumor vascularization was first studied systematically by Goldman, who described the vasoproliferative response of the organ in which a tumor develops as follows: "The normal blood vessels of the organs in which the tumor is developing are disturbed by chaotic growth, there is a dilatation and spiralling of the affected vessels, marked capillary budding, and new vessel formation, particularly at the advancing border" [1].

In 1939, Ide et al. suggested that tumors release specific factors capable of stimulating the growth of blood vessels [2]. In 1945, Algire and Chalkley demonstrated that growing malignancies could continuously elicit new capillary growth from the host [3]. They used a transparent chamber implanted in a cat's skin and showed that the vasoproliferative response induced by tumors was more substantial and earlier than that induced by normal tissues or following a wound and concluded that the growth of a tumor is closely connected to the development of an intrinsic vascular network. In 1956, Merwin and Algire found that the vasoproliferative response of normal or neoplastic tissues transplanted into muscle was not significantly different with respect to the time of onset of new blood vessels, though it was stronger when the implantation

Domenico Ribatti (ed.), *Tumor Angiogenesis Assays: Methods and Protocols*, Methods in Molecular Biology, vol. 1464,
DOI 10.1007/978-1-4939-3999-2_1,

was performed in a resection area [4]. In addition, while normal tissues induced a vasoproliferative response confined to the host, tumor tissues induced the formation of neovessels that pierced the implant. Lastly, the intensity of the response seemed to be influenced by the distance between the implant and the host's vessels: normal tissue was unable to induce a response if placed more than 50 μm away, whereas tumor tissue had a longer activity range [4].

In 1968, Greenblatt and Shubik implanted Millipore chambers into a hamster's cheek pouch and placed some tumor fragments, and in a few days, the growing tumor mass engulfed the whole chamber, whose pores were permeable to the tumor interstitial fluid, but not to the tumor cells [5]. New blood vessels were formed in any case very likely through the release of a diffusible factor that could pass through the pores. In 1968, Ehrman and Knoth confirmed these data with tumor fragments laid on Millipore filters planted on the chick embryo chorioallantoic membrane (CAM) [6].

In the 1970s, Pietro M. Gullino and colleagues observed that the resting adult rodent mammary gland has limited, if any, angiogenic capacity, whereas this is consistently acquired by mammary carcinomas. Lesions with a high frequency of neoplastic transformation induce angiogenesis at a much higher rate than those with a low frequency. This elevated angiogenic capacity was observed long before any morphological sign of neoplastic transformation. Hyperplastic human mammary gland lesions behave in the same way and angiogenesis may thus be an early marker of neoplastic transformation [7–10].

2 Absence of Angiogenesis in Tumors in Isolated Perfused Organs and First Evidence of the Existence of the Avascular and Vascular Phases in Solid Tumor Growth

Judah Folkman (Fig. 1) and colleagues observed that when tumor cells were inoculated into isolated perfused organs, tumors were limited in size to 1–2 $mm^{3,}$ and found that neovascularization did not occur in isolated perfused organs and that tumors transplanted from these organs to syngeneic mice became vascularized and grew rapidly to 1–2 mm^3, more than 1000 times their original volume in the perfused organ [11]. This was the first evidence that the absence of neovascularization correlated with severe restriction of tumor growth.

In another series of experiments, 1 mm fragments from Brown-Pearce and V2 carcinomas were implanted into the avascular rabbit cornea 1–6 mm away from the limbic vessels, and observed the tumor growth daily with a stereomicroscope. After 1 week, new blood vessels had invaded the cornea starting from the edge closer to the site of implantation and developed in that direction at 0.2 mm and then about 1 mm/day, and once the vessels reached the tumor, it grew very rapidly to permeate the entire globe within 4 weeks [12, 13].

Fig. 1 A portrait of Judah Folkman

3 First Formulation of the Hypothesis That Tumor Growth Is Angiogenesis-Dependent and Isolation of the First Tumor Angiogenic Factor

In 1971, Folkman published in the "New England Journal of Medicine" a hypothesis that tumor growth is angiogenesis-dependent and that inhibition of angiogenesis could be therapeutic [14]. This paper also introduced the term anti-angiogenesis to mean the prevention of new vessel sprout from being recruited by a tumor. The hypothesis predicted that tumors would be able to grow beyond a microscopic size of 1–2 mm^3 without continuous recruitment of new capillary blood vessels [14].

Until the early 1970s it was widely assumed that tumors did not produce specific angiogenic proteins. The conventional wisdom was that tumor vasculature was an inflammatory reaction to dying or necrotic tumor cells. In 1971, Folkman, isolated an angiogenic factor subsequently called "tumor angiogenesis factor" (TAF) [15]. TAF has since been extracted from different tumor cell lines, and several low molecular weight angiogenic factors have been isolated, again from the Walker 256 carcinoma. These factors induced a vasoproliferative response in vivo when tested on rabbit cornea or chick CAM, and in vitro on cultured endothelial cells [16–18].

In 1984, Shing and Klagsbrun, working in the Folkman laboratory, purified to homogeneity the first pro-angiogenic molecule from tumors, able to bring with high affinity to heparin, and identified as basic fibroblast growth factor (bFGF).

4 The Development of the "Angiogenic Switch" Concept

The angiogenic switch whereby the normally quiescent vasculature grows new capillaries separates the avascular phase characterized by a dormant tumor and the vascular phase in which exponential tumor growth ensues. In the prevascular phase, tumor cells proliferate, but the rate of tumor cell death counterbalances this proliferation and maintains the tumor mass in a steady state. Dormant tumors (carcinoma in situ) have been discovered during autopsies of 98% of individuals aged 50–70 years who died of causes other causes, but was diagnosed in only 0.1% during life.

Activation of the switch itself has been attributed to the synthesis or release of angiogenic factors. The balance hypothesis assumes that the level of angiogenesis inducers and inhibitors governs cell differentiation states of quiescence or angiogenesis. This balance is altered by increasing activator gene expression, changing the bioavailability or activity of the inducer proteins, or reducing the concentrations of endogenous angiogenesis inhibitors [19].

The mechanism of the switch was first described in 1985 by Dug Hanahan (Fig. 2) who developed transgenic mice in which the large T oncogene is hybridized to the insulin promoter [20]. In this islet cell tumorigenesis (RIP1-TAG2 model), these mice express the large T antigen (TAG) in all their islet cells at birth, and express the SV40 TAG under the control of the insulin gene promoter, which elicits the sequential development of tumors in the islets over a period of 12–14 weeks. Tumor development proceeds by stages during which about half the 400 islets become hyperproliferate, while a subset (about 25%) subsequently acquire the ability to switch to angiogenesis. Some 15–20% of these angiogenic islets develop into benign tumors, encapsulated lesions, and invasive carcinomas [20].

Fig. 2 A portrait of Dug Hanahan

5 Prognostic Significance of Tumor Vascularity

In 1972, Brem in the Folkman laboratory reported the first quantitative method for histologic grading of tumor angiogenesis. He correlated neovascularization in human brain tumors with tumor grade [21]. In the early 1990s, Weidner and co-workers showed that measurement of microvascular density within isolated regions of high vessel concentration was a prognostic indicator for human breast and prostate carcinomas [22]. Microvascular density counting protocols have become the morphological gold standard to assess the neovasculature in human tumors. This method requires the use of specific markers to vascular endothelium and of immunohistochemical procedures to visualize microvessels, and microvascular density in primary tumors is significantly associated with metastasis and prognosis in several solid and hematological tumors [23].

6 The Importance of Tumor Stroma

In his treatise "Il Cancro", published by Ambrosiana in 1946, Pietro Rondoni, Professor of General Pathology at the University of Milan, and Director of the Milan Cancer Institute, stated with regard to the stroma of tumors that: "a tumor acts both angioplastically and angiotactically, in other words it promotes the formation of new vessels and attracts vascular outgrowths (capillaries and pluripotent perivasal cells) so as to build up and shape a stroma of its own, a newly formed stroma. It must thus be unreservedly admitted that tumors are partly vascularized by the already existing network of vessels around them. As in other pathological processes, therefore, vascular neoformation takes place from budding of the existing capillaries" [24]. The importance of this passage lies in the fact that Rondoni refers to the ability of a tumor to induce the formation of new blood vessels from those that already surround it. He also asserts that this angiogenic activity occurs in its stroma.

In 1986, Harold Dvorak (Fig. 3) first highlighted the role played by the stromal component in tumor progression and proposed a similarity between tumors and wounds by defining cancer as a *wound that does not heal* [25]. Subsequent research has demonstrated that the tumor microenvironment plays an active role through adhesion molecules, angiogenesis, and stromal host cells. These latter not only passively support neoplastic cells by providing a scaffold for their growth, but also promote neoplastic development and regulate progression to malignancy. It has been estimated that 15% of malignancy worldwide can be attributed to chronic inflammatory diseases.

The peritumoral inflammatory infiltrate surrounding newly formed blood vessels consists of fibroblasts, macrophages, mast

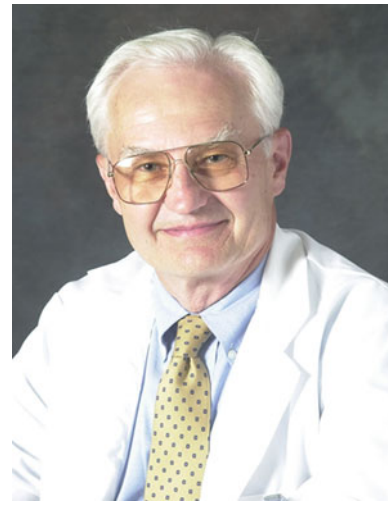

Fig. 3 A portrait of Harold Dvorak

cells, and other leukocytes that may contribute to the induction of an angiogenic response by secreting angiogenic cytokines and proteolytic enzymes which, in turn, mobilize angiogenic factors in the extracellular matrix [26].

7 Anti-angiogenesis

The existence of specific angiogenesis inhibitors was first postulated by Folkman in 1971 in an editorial [14]. No angiogenesis inhibitors existed before 1980, and few scientists thought at that time that such molecules would ever be found. The accumulating literature on angiogenesis inhibitors reported during the 1980s and early 1990s led to the development by pharmaceutical and biotechnology companies of angiogenesis inhibitors for clinical use.

In 1973, Eisenstein et al. found the first angiogenesis inhibitor in cartilage, an avascular tissue that resists invasion by many tumors [27]. In 1975, Brem and Folkman demonstrated that tumor-induced vessels were inhibited by a diffusible factor from neonatal rabbit cartilage. The partially purified inhibitor suppressed tumor growth when it was infused into the vascular bed of murine and rabbit tumors [28].

In 1982, Denekamp, who noticed that tumor blood vessels had different characteristics than normal blood vessels, hypothesized that the local disruption of the tumor vasculature would result in the death of tumor cells and that only a few endothelial cells within the vessels need to be killed to completely occlude the vessels [29]. This strategy relies on the ability of vascular disrupting agents (VDAs, also referred to as vascular targeting agents) to distinguish the endothelial cells of tumor capillaries from normal

ones. Compared to anti-angiogenesis agents, VDAs are much more toxic, and like conventional chemotherapeutics, they are most effective at their maximum tolerated doses.

8 The Discovery of Angiostatin and Endostatin

Angiostatin and endostatin were discovered by M. O'Reilly in Folkman laboratory based on Folkman's hypothesis of a mechanism to explain the phenomenon that surgical removal of certain tumors leads to rapid growth of remote metastases. This hypothesis said that if tumors produce both stimulators and inhibitors of angiogenesis, an excess of inhibitors could accumulate within an angiogenic tumor. In the circulation, however, the ratio would be reversed. Angiogenesis inhibitors would increase relative to stimulators, because of rapid clearance of stimulators from the blood.

Folkman formulated this hypothesis after reading Bouck's first report that the emergence of tumor angiogenesis was the result of a shift in balance between positive and negative regulators of angiogenesis in a tumor. Bouck reported that the switch to angiogenesis during tumorigenesis of transformed hamster cells was associated with downregulation of an inhibitor of angiogenesis, thrombospondin (TSP), and suggested that the switch to the angiogenic phenotype could be the result of a shift in the net balance of positive and negative regulators of angiogenesis [30].

In 1994, O'Reilly began to screen a variety of transplantable murine tumors for their ability to suppress metastases. A Lewis lung carcinoma was the most efficient. When the metastasis-suppressing primary tumor was present in the dorsal subcutaneous position, micrcoscopic lung metastases remained dormant at a diameter of less than 200 μm surrounding a pre-existing microvessel, but revealed no new vessels. Within 5 days after surgical removal of the primary tumor, lung metastases became highly angiogenic and grew rapidly, killing their host by 15 days. This striking evidence that primary tumor could suppress angiogenesis in its secondary metastases by a circulating inhibitor was further supported by the demonstration that a primary tumor could also suppress corneal angiogenesis by an implanted pellet of bFGF. O'Reilly then succeeded in purifying this inhibitor from the serum and urine of tumor-bearing animals. It was a 38-kD internal fragment identical in amino acid sequence to the first four kringle structures of plasminogen and it was named angiostatin. Angiostatin inhibited growth of primary tumors by up to 98% and was able to induce regression of large tumors and maintain them at a microscopic dormant size [31].

In 1997, O'Reilly isolated and purified another angiogenesis inhibitor from a murine hemangioendothelioma. This inhibitor, called endostatin is a 20-kD protein with an N-terminal amino acid

sequence identical to the carboxyterminus of collagen XVIII. It was purified directly from tumor cell-conditioned medium. Endostatin is slightly more potent than angiostatin, and also causes regression of large tumors to a microscopic size. However, the use of endostatin in clinical trials for the treatment of neuroendocrine tumors did not demonstrate therapeutic benefits. A modified version of recombinant endostatin has been developed and used in combination with chemotherapy for the treatment of cancer patients in China [32].

9 Metronomic Chemotherapy

Browder in the Folkman laboratory was the first to demonstrate the concept that by optimizing the dosing schedule of conventional cytotoxic chemotherapy to achieve more sustained apoptosis of endothelial cells in the vascular bed of a tumor, it is possible to achieve more effective control of tumor growth in mice, even if the tumor cells are drug-resistant [33].

Conventional chemotherapy is administered at maximum tolerated doses followed by off-therapy intervals of 2–3 weeks to allow the bone marrow and gastrointestinal tract to recover. In contrast, anti-angiogenic chemotherapy is administered more frequently at lower doses, without long interruptions in therapy and with little or no toxicity. In an editorial published in 2000, Hanahan et al. coined the term "metronomic chemotherapy" to indicate the new schedules of cytotoxic agents given regularly at sub-cytotoxic doses and having the activated endothelium as principal target [34].

During anti-angiogenic chemotherapy, endothelial cell apoptosis and capillary dropout precede the death of tumor cells that surround each capillary and continuous administration of cyclophosphamide in the drinking water inhibited tumor growth in mice by 95 % and significantly increased circulating levels of TSP-1 [35]. The low-dose "metronomic chemotherapy" was ineffective in TSP-1 null mice, indication that the low-dose oral chemotherapy was in part dependent on its capacity to induce an increase in circulating TSP-1.

10 Inhibitors of vascular endothelial growth factor (VEGF)

In 1993, Napoleone Ferrara (Fig. 4) laboratory reported that anti-VEGF monoclonal antibodies exerted a potent inhibitory effect on the growth of three tumor cell lines injected subcutaneously in nude mice, the G55 glioblastoma multiforme, the SK-LMS-1 leiomyosarcoma and the A673 rhabdomyosarcoma, whereas the antibody had no effects on the tumor cell in vitro, consistent with the hypothesis that the inhibition of angiogenesis is the mechanism of tumor suppression in vivo [36]. The growth inhibition ranged

Fig. 4 A portrait of Napoleone Ferrara

between 70% and more than 95%. These findings provided the first direct demonstration that inhibition of the action of an endogenous endothelial cell mitogen may result in suppression of tumor growth in vivo.

Avastin (Bevacizumab) is a humanized anti-VEGF monoclonal antibody. Avastin was the first angiogenesis inhibitor approved by the FDA for the treatment of colorectal cancer in February 2004, administered in combination with irinotecan, 5-fluorouracil, and leucovirin [37], and was subsequently approved for use, in combination with cytotoxic chemotherapy, in breast, lung, and renal cancers, demonstrating a significant improvement in overall survival or delayed tumor progression compared to chemotherapy alone. However, treatment with Avastin can be accompanied by a variety of adverse effects, including hypertension, proteinuria, gastrointestinal perforation, bleeding, and thromboembolism.

A variety of small molecules receptor tyrosine kinase (RTK) inhibitors targeting the VEGF receptors (VEGFRs) have been developed [38]. Other anti-VEGF agents including VEGF-Trap, a soluble receptor targeting VEGF-A, VEGF-B, and placental growth factor (PlGF), an antisense oligonucleotide VEGF-AS targeting VEGF-A, VEGF-C, and VEGF-D are at various stages of clinical development. Inhibitors of VEGF signalling not only stop angiogenesis but also cause regression of some tumor vessels, transform some tumor capillaries into a more normal phenotype, and have direct cytotoxic effects on tumor cells that aberrantly express VEGFRs.

Removal of VEGF inhibition causes tumor re-growth due to the fact that pericytes provide a scaffold for the rapidly re-growing of tumor vessels [39]. Pericytes have been indicated as putative targets in the pharmacological therapy of tumors by using the

synergistic effect of anti-endothelial and anti-pericytic molecules. Removal of pericyte coverage leads to exposed tumor vessels, which may explain the enhanced effect of combining inhibitors that target both tumor vessels and pericytes. Bergers et al. [40] showed that combined treatment or pretreatment with anti-platelet derived growth factor-B (PDGF-B)/PDGF recptor beta (PDGFR-β) reducing pericyte coverage increases the success of anti-VEGF treatment in the mouse RIP1-TAG2 model.

11 Concluding Remarks

The number of patients receiving anti-angiogenic therapies for cancer treatment will increase rapidly in the coming years and the development of anti-angiogenic and anti-vascular drugs has prompted a search for suitable biomarkers. In fact, a clinical challenge in anti-angiogenesis is the finding of biological markers that help to identify subsets of patients more likely to respond to a given anti-angiogenic therapy, to detect early clinical benefit or emerging resistances and to decide whether to change therapy in second-line treatments.

The results from clinical trials have not shown the dramatic antitumor effects that were expected following preclinical studies, which revealed a much higher efficacy of these type of agents in animal models. Patients with different types of tumors respond differently to anti-angiogenic therapy, and future research will focus on determining the tumor types and stages that will benefit most from anti-angiogenic therapy.

Preclinical and clinical data have shown the possibility that tumors may acquire resistance to anti-angiogenic drugs or may escape anti-angiogenic therapy via compensatory mechanisms. Most of the FDA-approved drugs, as well as those in phase III clinical trials, target a single pro-angiogenic protein. However, multiple angiogenic molecules may be produced by tumors, and tumors at different stages of development may depend on different angiogenic factors for their blood supply. Therefore, blocking a single angiogenic molecule might have little or no impact on tumor growth. Cancer genomics and proteomics are likely to identify novel, tumor-specific endothelial targets and accelerate drug discovery. Finally, a particular area of research concerns the assessment of cumulative toxicities that arise from combination therapies.

Acknowledgements

The research leading to these results has received funding from the European Union Seventh Framework Programme (FP7/2007-2013) under grant agreement n°278570 to DR.

References

1. Goldman E (1907) The growth of malignant disease in man and the lower animals with special reference to the vascular system. Lancet ii:1236–1240
2. Ide AG, Baker NH, Warren SL (1939) Vascularization of the Brown-Pearce rabbit epithelioma transplant as seen in the transparent ear chambers. Am J Roentgenol 32:891–899
3. Algire GH, Chalkley HW (1945) Vascular reactions of normal and malignant tissue in vivo. J Natl Cancer Inst 6:73–85
4. Merwin RM, Algire GH (1956) The role of graft and host vessels in vascularization of grafts of normal and neoplastic tissues. J Natl Cancer Inst 17:23–33
5. Greenblatt M, Shubik P (1968) Tumor angiogenesis: transfilter diffusion studied in the hamster by the transparent chamber technique. J Natl Cancer Inst 41:111–124
6. Ehrmann RL, Knoth M (1968) Choriocarcinoma: transfilter stimulation of vasoproliferation in the hamster cheek pouch studied by light and electron microscopy. J Natl Cancer Inst 41:1239–1241
7. Gimbrone MA Jr, Gullino PM (1976) Neovascularization induced by intraocular xenografts of normal, preneoplastic, and neoplastic mouse mammary tissues. J Natl Cancer Inst 56:306–318
8. Gimbrone MA Jr, Gullino PM (1976) Angiogenic capacity of preneoplastic lesions of the murine mammary gland as a marker of neoplastic transformation. Cancer Res 36:2611–2620
9. Brem SS, Gullino PM, Medina P (1977) Angiogenesis: a marker for neoplastic transformation of mammary papillary hyperplasia. Science 195:880–882
10. Brem SS, Jensen HM, Gullino PM (1978) Angiogenesis as a marker of preneoplastic lesions of human breast. Cancer 41:239–244
11. Folkman MJ, Long DM, Becker FF (1963) Growth and metastasis of tumor in organ culture. Cancer 16:453–467
12. Gimbrone MA, Leapman SB, Cotran RS, Folkman J (1972) Tumor dormancy in vivo by prevention of neovascularization. J Exp Med 136:261–276
13. Gimbrone MA, Leapman S, Cotran RS, Folkman J (1973) Tumor angiogenesis: iris neovascularization at a distance from experimental intraocular tumors. J Natl Cancer Inst 50:219–228
14. Folkman J (1971) Tumor angiogenesis: therapeutic implications. New Engl J Med 285: 1182–1186
15. Folkman J, Merler E, Abernathy C, Williams G (1971) Isolation of a tumor fraction responsible for angiogenesis. J Exp Med 133: 275–288
16. Mc Auslan BR, Hoffman H (1979) Endothelium stimulating factor from Walker carcinoma cells. Relation to tumor angiogenic factor. Exp Cell Res 119:181–190
17. Tuan D, Smith S, Folkman J, Merler E (1973) Isolation of the non histone proteins of rat Walker 256 carcinoma. Their association with tumor angiogenesis. Biochemistry 12: 3159–3165
18. Weiss JB, Brown RA, Kumar S, Phillips P (1979) An angiogenic factor isolated from tumours: a potent low-molecular weight compound. Br J Cancer 40:493–496
19. Hanahan D, Folkman J (1996) Patterns and emerging mechanisms of the angiogenic switch during tumorigenesis. Cell 86:353–364
20. Hanahan D (1985) Heretable formation of pancreatic b-cell tumors in transgenic mice expressing recombinant insulin/simian virus 40 oncogene. Nature 315:115–122
21. Brem S, Cotran R, Folkman J (1972) Tumor angiogenesis: a quantitative method for histologic grading. J Natl Cancer Inst 48:347–356
22. Weidner N, Sample JP, Welch WR, Folkman J (1991) Tumor angiogenesis and metastasis. Correlation in invasive breast carcinoma. N Engl J Med 324:1–8
23. Nico B, Benagiano V, Mangieri D, Maruotti N, Vacca A, Ribatti D (2008) Evaluation of microvascular density in tumors: pro and contra. Histol Histopathol 23:601–607
24. Rondoni P (1946) Il cancro. Casa Editrice Ambrosiana, Milano, Italy
25. Dvorak HF (1986) Tumors: wounds that do not heal. Similarities between tumor stroma generation and wound healing. N Engl J Med 315:1650–1659
26. Ribatti D, Crivellato E (2009) Immune cells and angiogenesis. J Cell Mol Med 13: 2822–2833
27. Eisenstein R, Sorgente R, Soble LW, Miller A, Kuettner KE (1973) The resistance of certain tissues to invasion: penetrability of explanted tissues by vascularized mesenchyme. Am J Pathol 73:765–774
28. Brem H, Folkman J (1975) Inhibition of tumor angiogenesis mediated by cartilage. J Exp Med 141:427–439
29. Denekamp J (1982) Endothelial cell proliferation as a novel approach to targeting tumour therapy. Br J Cancer 45:136–139

30. Rastinejad F, Polverini PJ, Bouck NP (1989) Regulation of the activity of a new inhibitor of angiogenesis by a cancer suppressor gene. Cell 56:345–355
31. O'Reilly MS, Holmgren L, Shing Y, Chen C, Rosenthal RA, Moses M et al (1994) Angiostatin: a novel angiogenesis inhibitor that mediates the suppression of metastases by a Lewis lung carcinoma. Cell 79:315–328
32. O'Reilly MS, Boehm T, Shing Y, Fukai N, Vasios G, Lane WS et al (1997) Endostatin: an endogenous inhibitor of angiogenesis and tumor growth. Cell 88:277–285
33. Browder T, Butterfield CE, Kraling BM, Shi B, Marshall B, O'Reilly MS et al (2000) Antiangiogenic scheduling of chemotherapy improves efficacy against experimental drug-resistant cancer. Cancer Res 60:1878–1886
34. Hanahan D, Bergers G, Bergsland E (2000) Less is more, regularly: metronomic dosing of cytotoxic drugs can target tumor angiogenesis in mice. J Clin Invest 105:1045–1047
35. Bocci G, Francia G, Man S, Lawler J, Kerbel RS (2003) Thrombospondin-1, a mediator of the antiangiogenic effects of low-dose metronomic chemotherapy. Proc Natl Acad Sci U S A 100:12917–12922
36. Kim KJ, Li B, Winer J, Armanini M, Gillett N, Phillips HS, Ferrara N (1993) Inhibition of vascular endothelial growth factor-induced angiogenesis suppresses tumor growth in vivo. Nature 362:841–844
37. Hurwitz H, Fehrenbacker K, Novotny W, Cartwright T, Hainsworth J, Heim W et al (2004) Bevacizumab plus irinotecan, fluoro-uracil, and leucovorin for metastatic colorectal cancer. N Engl J Med 350:2335–2342
38. Ribatti D (2010) Tyrosine kinase inhibitors as antiangiogenic drugs in multiple myeloma. Pharmaceuticals 3:1225–1231
39. Mancuso MR, Davis R, Norberg SM, O'Brien S, Sennino B, Nakahara T et al (2006) Rapid vascular regrowth in tumors after reversal of VEGF inhibition. J Clin Invest 116: 2610–2621
40. Bergers G, Song S, Mayer-Morse N, Bergsland E, Hanahan D (2003) Benefits of targeting both pericytes and endothelial cells in the tumor vasculature with kinase inhibitors. J Clin Invest 111:1287–1295

Chapter 2

Morphological Aspects of Tumor Angiogenesis

Ruslan Hlushchuk, Sébastien Barré, and Valentin Djonov

Abstract

The tumor vasculature is a chaotic mixture of abnormal, hierarchically disorganized vessels that differ from those of normal tissues with respect to organization, structure and function. Firstly, tumor vessel wall structure is abnormal and heterogeneous within the tumor. Besides contractile wall components, the perivascular compartment is often lacking pericytes, what makes the tumor vessels fragile and leaky. Secondly, another group of abnormalities involves distortions in angioarchitecture and vasculature as network. Common features of tumor vessels, irrespective of their origin, size and growth pattern, are absence of hierarchical organization, formation of vessels with irregular contours and their heterogeneous distribution within the tumor.

Key words Angiogenesis, Tumorangiogenesis, Tumor growth, Anti-angiogenesis, Quantification of tumorangiogenesis

1 Angiogenic Research

Angiogenesis, the formation of new blood vessels from existing ones, is an extensively investigated process with an enormous medical, scientific, and economic impact. It plays a major role in cardiovascular disorders and cancer progression, which together account for about 2/3 of the worldwide mortality [1]. Accordingly, the interest in the field is enormous and the number of registered clinical trials dealing with angiogenesis is impressive. Preclinical research is critical: out of 5000 compounds that enter pre-clinical testing, only five (0.1%(!)), on average, are tested in human trials [2]. Moreover, the frequently disappointing results from late-stage clinical trials indicate an urgent need for improved assessment of the effects of applied angiomodulating compounds in preclinical models [3].

2 Tumorangiogenesis

With increasing tumor mass, new vascular segments are needed for its supply with oxygen and nutrients and clearance of metabolites.

Domenico Ribatti (ed.), *Tumor Angiogenesis Assays: Methods and Protocols*, Methods in Molecular Biology, vol. 1464,
DOI 10.1007/978-1-4939-3999-2_2,

Lack of adequate vasculature constrains further tumor growth that should result from continuous cell proliferation, the hallmark of cancer pathogenesis [4]. Therefore, the "angiogenic switch," when the tumor cells gain the capability to produce angiogenic factors and induce angiogenesis, is a crucial step for the tumor growth. There are many angiomodulating factors that are produced and secreted by tumor cells, and the progression of tumor angiogenesis depends on the balance between these pro- and antiangiogenic factors [5, 6].

3 Abnormality of Tumor Blood Vessels

The normal vasculature is arranged in a regular hierarchy of evenly distributed, well-differentiated arteries, arterioles, capillaries, venules, and veins. In contrast, the tumor vasculature is a chaotic mixture of abnormal, hierarchically disorganized vessels that differ from those of normal tissues with respect to organization, structure, and function [7, 8].

The vessel wall structure is abnormal and also heterogeneous, even within the same tumor. For example, in MMTV/c-neu carcinoma xenograft tumor model it was observed that the smooth muscle cell presence depends on the location of the vasculature within the tumor: in the periphery the vessels possess a much more pronounced coverage with smooth muscle cells than the ones located more centrally (*see* Fig. 1) [9]. Besides contractile wall components, the perivascular compartment is often lacking pericytes, what makes the tumor vessels fragile and leaky. Their leakiness or hyperpermeability leads to local edema and extravascular clotting of plasma. As a result, a cross-linked fibrin gel is deposited; it serves as a provisional matrix for cell migration, stimulates angiogenesis and subsequent stroma formation [10].

Further abnormalities in the tumor vessels may be observed in the basement membrane (interruptions or even its absence) or endothelial cell layer. One of the frequent findings is the activation of endothelial cells followed by their vacuolization and proliferation. Of special importance is the incomplete or lacking endothelial lining due to detachment of the endothelium or aberrant angiogenesis (*see* Fig. 2). In the case of missing endothelial lining the role of endothelial cells can be overtaken by tumor cells, the process called vasculogenic mimicry that was first described in uveal melanomas in 1999 [11]. It is actually a separate mode of vascular channel formation that does not involve endothelial cells.

The second group of abnormalities is dealing with the angioarchitecture and vasculature as network. As already mentioned above the tumor vasculature is chaotic and disorganized in almost every possible sense. The vascular segments often have irregular contours and the vascular tree lacks the hierarchy and the vessel distribution within a tumor is heterogeneous (*see* Fig. 3). There are multiple arteriovenous shunts or the vascular segments where the

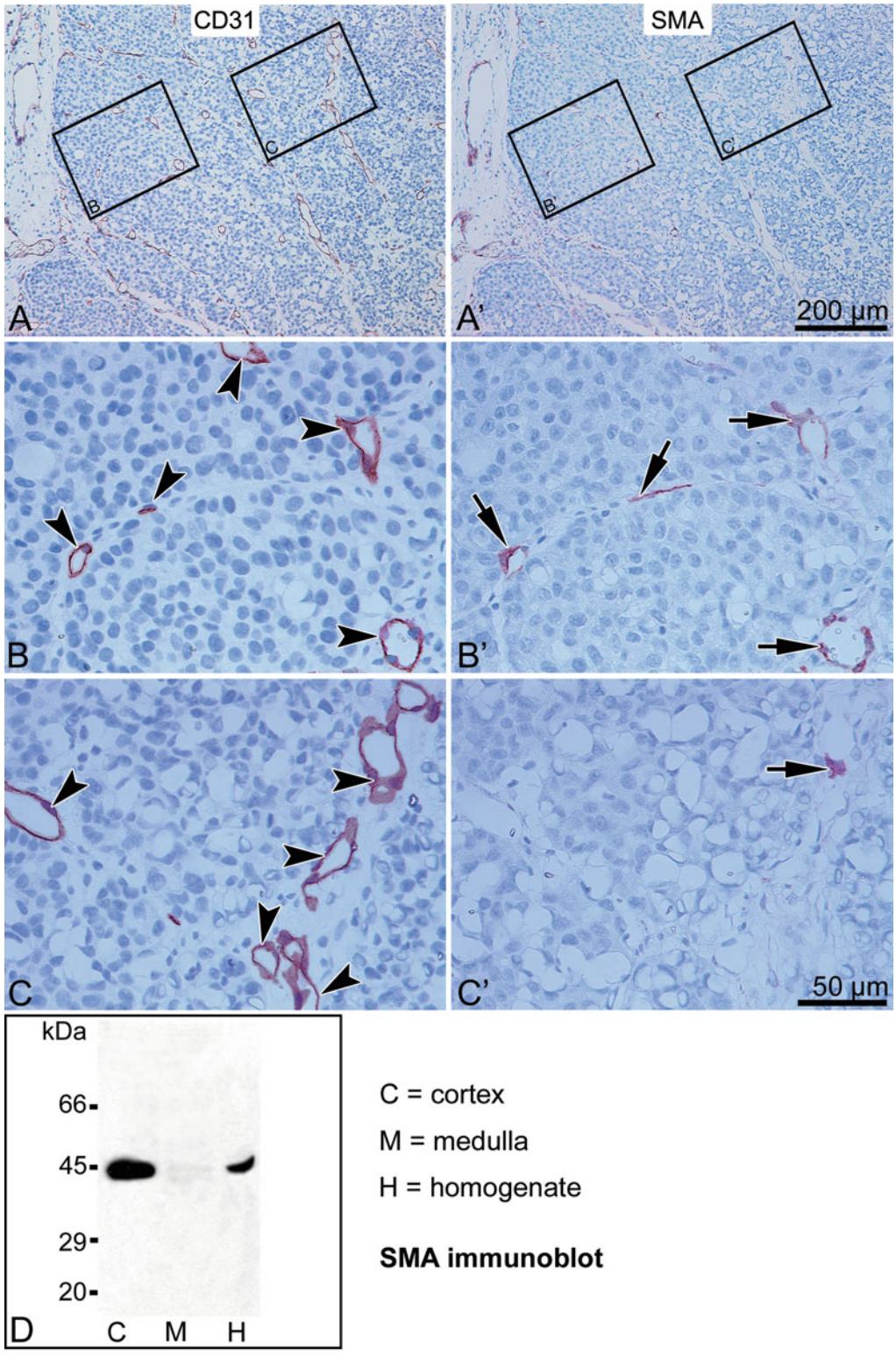

Fig. 1 Consecutive sections through MMTV/c-neu mammary carcinoma xenografts showing immunostaining for CD31 (**a**, **b**, **c**) and SMA (**a'**, **b'**, **c'**). Multiple vessels within the cortex (*arrowheads* in **b**) bear a covering of SMA-positive cells (*arrowheads* in **b'**), whereas those within the medulla (*arrowheads* in **c**) are mainly SMA-negative (positive is marked with *arrow* in **c'**). The spatial distribution of SMA accords with the distribution revealed by immunoblotting (**d**). Adapted with permission from Hlushchuk et al. 2008

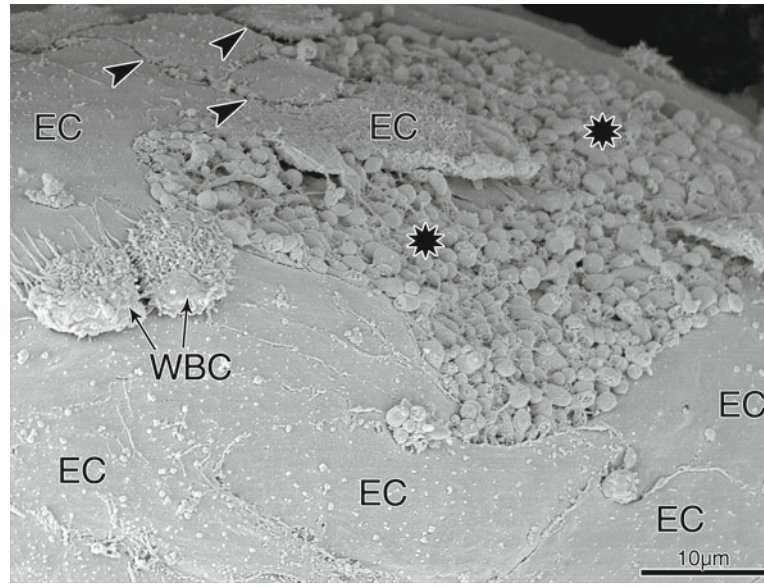

Fig. 2 Endothelial lining of a bigger vessel in the murine liver tumor. *Asterisks* indicate the areas lacking endothelial cells (EC): these areas are covered by platelets. *Black arrowheads* point to the borders between the detaching endothelial cells (EC). White blood cells (WBC) attached to the endothelium are marked with *arrows*. Special thanks to Dr. David Semela for providing the sample

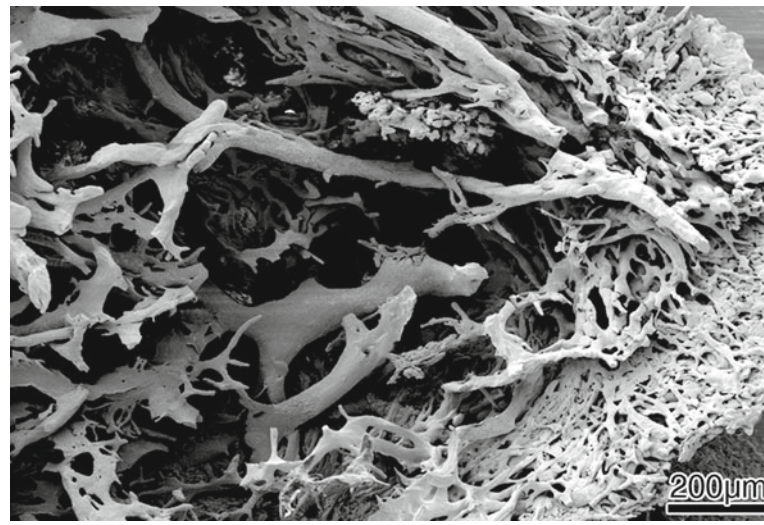

Fig. 3 Scanning electron micrograph of the vascular corrosion cast of the vasculature of treated MMTV/c-neu mammary carcinoma xenograft. The image displays the heterogeneity of the vasculature and its density within the tumor. Most vessels have irregular contours and irregular branching pattern. Adapted with permission from Hlushchuk et al. 2008

flow changes direction. The architectural abnormalities collectively increase the resistance against blood flow. The elevated geometric resistance and heterogeneous vessel density cause unstable blood flow, and heterogeneous blood supply [5].

The tumor vessels are often tortuous, with irregular branching pattern, and, on average, are larger than their normal counterparts. As a result, and also because of arteriovenous shunts, nutrients are not taken up efficiently by tumors, as is demonstrated by the higher than normal oxygen content of the venous blood draining tumors [8]. High glycolytic activity of tumor cells combined with insufficient clearance of metabolites, including carbon dioxide, results in an acidic tumor microenvironment (pH ~7.2 versus pH ~7.4 in normal tissues) [12, 13]. Such combination leads to formation of the zones of metabolic insufficiency and ischemia, sometimes necrosis. As a consequence of ischemia, the transcription factor HIF-1 is stabilized, an event with important consequences for new blood vessel formation: it further shifts the balance between the anti- and pro-angiogenic factors towards promotion of tumorangiogenesis [14].

4 Classification of the Tumor Vessels

Since decades it is recognized that tumor blood vessels are heterogeneous and not of a single type, but only few attempts have been made to define their individual properties. One of the earliest attempts was done by Warren BA [7]. Writing in the late 1970s, he classified tumor blood vessels into eight distinct types, not all of which were found in any one tumor [8]. Warren concluded that the main difference between normal and tumor blood vessels was that, in the latter, capillaries and veins became tortuous and "dilated." The term "dilation" was actually a misnomer in this case, as it was used for description of the enlargement of the vessels, but not through relaxation of smooth muscle cells [8]. One of the most recent attempts was done by the group of Dvorak. In their manuscript, they have identified six structurally and functionally distinct blood vessel types in human cancers, and surrogates of each of these can be induced in mice with an adenoviral vector engineered to express VEGF-A^{164} (Ad-VEGF-A^{164}) (*see* Table 1, reprinted with permission from ref. 8).

The presented classification includes the involved type of vessel formation and its dependency on VEGF-A, suggesting that only some types of tumor vessels can be responsive to the anti-VEGF therapy. In other words, the morphology of tumor vessels (tumor vessel wall) may be critical for the efficacy of the antiangiogenic treatment, giving one more explanation to a rather modest success of antiangiogenic drugs in human cancer patients. Another important parameter in the presented table is the vessel formation process, mainly angiogenesis. Noteworthy, angiogenesis has a few modes.

Table 1
Classification of tumor blood vessels

Vessel type	Vessel properties		
Angiogenesis		Hyperpermeable	VEGF-A dependent
MV	Large, thin-walled, hyperpermeable, lightly fenestrated pericyte-poor Sinusoids that are engorged with red blood cells	+	+
Capillaries	Formed from MV by a process that involves internal division	–	–/?
Glomeruloid Microvascular Proliferations	Poorly organized vascular structures that macroscopically resemble Renal glomeruli. They are composed of endothelial cells and pericytes with minimal vascular lumens and reduplicated basement membrane	+	+
Vascular malformations	MV that have acquired an often asymmetrical coat of smooth muscle Cells and/or fibrous connective tissue. Resemble arteriovenous Malformations found in other settings	–	–
Arterio-venogenesis			
Feeder arteries Draining veins	Enlarged, often tortuous structures that are derived from preexisting Arteries and veins. They extend radially from the tumor mass supplying and draining the angiogenic vessels within	–	–
Other			
Vascular mimicry	Blood-filled spaces lined by tumor cells that have acquired some Endothelial cell properties and may contribute to tumor circulation	?	?

VEGF vascular endothelial growth factor, *MV* mother vessel

5 Modes of Tumorangiogenesis

Two major modes of angiogenesis have been described, namely sprouting and intussusception (often also called "nonsprouting" or splitting) [15]. Sprouting angiogenesis was described more than 150 years ago and has been in the focus of research groups for many decades. This mode of angiogenesis occurs by outgrowth of ablumi-

nal sprouts which subsequently merge with existing capillaries. Degradation of endothelial basement membranes (obviously associated with increased vessel permeability), as well as proliferation of endothelial cells, is essential for this process [16, 17]. Sprouting angiogenesis is often, but not quite correctly, understood or used as a synonym for "angiogenesis." It is surely the more widely studied mode of angiogenesis and many of the molecular and cellular mechanisms involved have already been elucidated (*see* reviews [16, 18]).

In contrast, intussusceptive angiogenesis (IA) is achieved by intraluminal growth. A transluminal pillar, the hallmark of intussusceptive angiogenesis, is formed when endothelial cells of the opposing sides of the vascular lumen finally make contact [15] (*see also* Fig. 4). In contrast to sprouting, the intussusception does not necessarily require endothelial cell proliferation or basement membrane degradation. These features make it more "resistant" to the influences that cause inhibition of endothelial cells proliferation, e.g., anti-VEGF therapy or radiation therapy [9]. The mentioned therapies lead to increase in perivascular cell coverage what again should be supportive to later stages of intussusceptive angiogenesis and remodeling.

Other less-well-characterized forms of angiogenesis are wrapping and hollowing, glomeruloid angiogenesis, co-option of preexisting vessels, or vasculogenic mimicry [19].

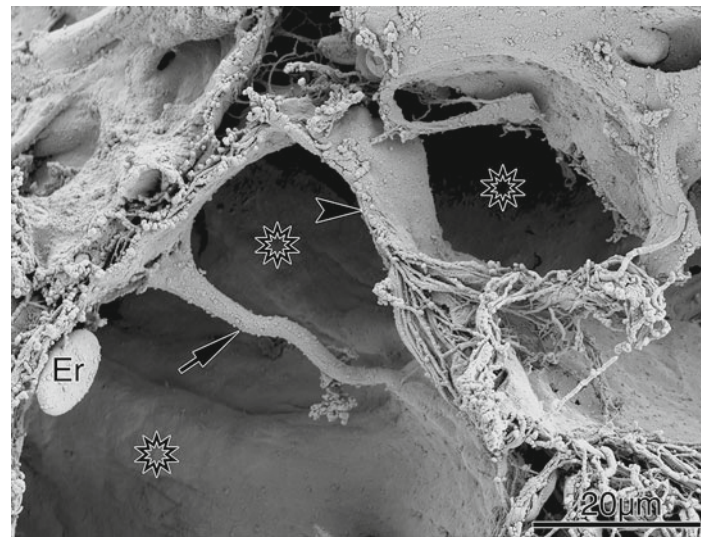

Fig. 4 Scanning electron microscopy image of transluminar pillars at various stages. Early stage of pillar formation (*arrow*) is characterized by connection of opposing endothelial cells by their protrusions. At later stages the pillar (*arrowhead*) is increasing in girth and its core is invaded by perivascular cells, fibroblasts, and fibers. Lumen of the vessel is marked with *asterisks. Er* erythrocyte. Critical point-dried tissue of the ostrich lung. Special thanks to Dr. Andrew M. Makanya for providing the sample

6 Normalization of the Tumor Vasculature

In 1971 Folkman has postulated his idea of inhibiting the neovascularization in order to treat cancer disease. His classical paper can be considered an official "start" of the era of antiangiogenic research [20]. In the last decade the initial idea of letting the tumor starve by "killing" the tumor vessels has undergone metamorphosis. Nowadays, the aim of the antiangiogenic therapy is the normalization of the tumor vasculature and not its regression [21]. Caused by bringing of pro- and anti-angiogenic factors into the balance the tumor vasculature should undergo transient "normalization" that leads to improved perfusion of the tumor. In that way, the delivery of other (e.g., cytostatic) drugs to the tumor mass is substantially improved. The normalization of the vasculature has direct influence on the morphology of the vasculature on both aforementioned levels: at the level of the vessel wall components (increase of pericyte and smooth muscle cell coverage; decreased leakiness) and at the level of angioarchitecture and the vasculature as network (pruning of superfluous segments, more regular contours and branching pattern, improved hierarchy etc.). All mentioned changes could also be explained by the switch from sprouting to intussusceptive mode of angiogenesis as angioadaptive response to antiangiogenic treatment (for details see review [17]). Better understanding of the mechanisms underlying the intussusception and the mentioned switch could potentially improve our control over the tumor vasculature and tumor growth itself.

7 Remarks to Quantification of the Tumor Angiogenesis in Animal Models

Profound quantification is missing in most of the preclinical animal studies concerning compound effects on the tumor vasculature. Such effects are often evaluated using the intratumoral microvessel density (IMD or MVD) in the so-called "vascular hot spots The hypothesis behind the "vascular hot spots" is to evaluate the most aggressive sites within the tumor, but there is no guarantee that there are any on a particularly chosen histological section. There are further issues that can be easily criticized, e.g., the most observer-dependent step is the selection of these densely vascularised areas in a tumor tissue section. This has even led to the negative judgement of the College of American Pathologists concerning microvessel density as a prognostic factor in breast cancer [22] : Quantification of tumor angiogenesis by counting microvessels in immunostained tissue sections was ranked in category III, encompassing "all factors which are not sufficiently

studied to demonstrate their prognostic value." The issues of methodological variation mentioned include: antibody selection, type of fixative used, methods of counting vessels, calculation of microvessel density, **inter-observer variability** (especially of the selection of the field in which to count) and cut-off value for "increased" vascularity [23]. The MVD results are biased, hardly reproducible, and often controversial [24]. Another critical issue: Are the evaluated hot spots "representative" for the whole tumor? [25]. Besides having high methodological variability, this approach can hardly provide any physiologically relevant information or meaningful parameters of the tumor vasculature. Another major disadvantage is that the vascular tree as such is completely omitted. One of the suggested ways to reduce the methodological variability is to use the Chalkley point overlap morphometric technique [26]: it abolishes the observer-dependent step, namely the frequent decision on whether two immunostained and adjacent structures are the projection of one single or two separate blood vessels. Unfortunately, the rest of the weaknesses of IMD approach remain. The Chalkley count is the number of grid points that hit stained microvessels. It is a relative vessel area estimate rather than a true vessel count. But in some instances it provides more physiologically relevant values that better correlate with blood perfusion/hypoxia reduction than IMD (*see* Fig. 5, reprinted with permission from ref. 9). Further possible evaluation parameter could be the vascular surface (exchange) area density. Nonetheless, the inherent inter-observer variability remains the critical disadvantage of the aforementioned and other histological surrogate markers of tumor angiogenesis [23]. The application of that or other value does not provide fundamental solution of the problem. The evaluation is still done in the so called "hot spots," which should be the sites of most aggressive angiogenesis in the tumor. But histology does not provide visualization of the whole tumor (in 3D) in order to localize such "vascular hot spots."

At the moment, probably the most promising visualization method for 3D analysis of the tumor vasculature is the μangio-CT with the usage of the novel polymer-based contrast agent μAngiofil (Fumedica AG, Switzerland) (*see* Fig. 6).

Combined with modern desktop microCT equipment this agent provides superior images and enables three-dimensional resolution of the vascular structures down to the capillary level. Obtained datasets can then be used for localization and analysis of the vascular hot spots within the whole tumor. The contrast agent allows consequent histological investigation of the volumes of interest, making its application even more attractive. Furthermore, such an approach also enables analysis of architectural abnormalities of the tumor vasculature (in 3D and through the whole

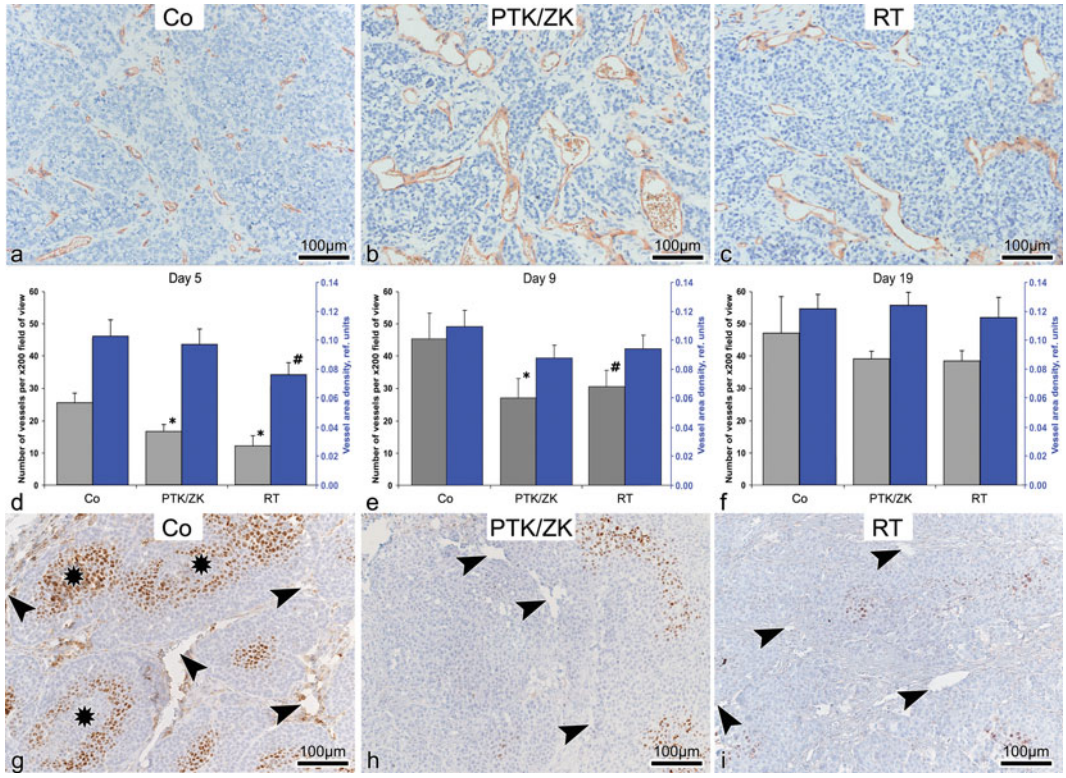

Fig. 5 (**a**, **b**, **c**): Immunohistochemical staining of MMTV/c-neu mammary carcinoma xenografts for CD31 revealing a multitude of tiny vessels in control tumors and fewer, but larger sinusoidal ones in the treated groups (*PTK/ZK* anti-VEGF treatment, *RT* radiotherapy). Changes in the intratumoral microvascular density (IMD) and vessel area density on days 5, 9, and 19 reflect a switch in the mode of angiogenesis: intussusception on day 9 and a second wave of sprouting on day 19. The values significantly different from control values are marked with * ($p \leq 0.02$) or # ($p \leq 0.05$). The HIF-1α staining (**g–i**) reveals the differences in oxygenation level of the tumor cells on day 14: in nontreated tumors (**g**) there is apparent hypoxia demonstrated by plentiful HIF-1α-positive cells on the distance of more than 100–130 µm from the vessels (arrowheads in **g–i**). There are necrotic areas on the similar distance from the vessels (*asterisks* in **g**). On day 14 in both treated groups the level of oxygenation is apparently better with only some HIF-1α-positive cells (**h** and **i**). The vessels are marked with *arrowheads* (**g–i**). Adapted with permission from Hlushchuk et al. 2008

sample). Already now in numerous preclinical studies the blood vessels are visualized and quantified by means of (µ)CT approach [27–32].

With time and easier access to µCT-equipment such an approach will surely gain on even more popularity and will most probably become the modern golden standard for the evaluation of tumor vasculature.

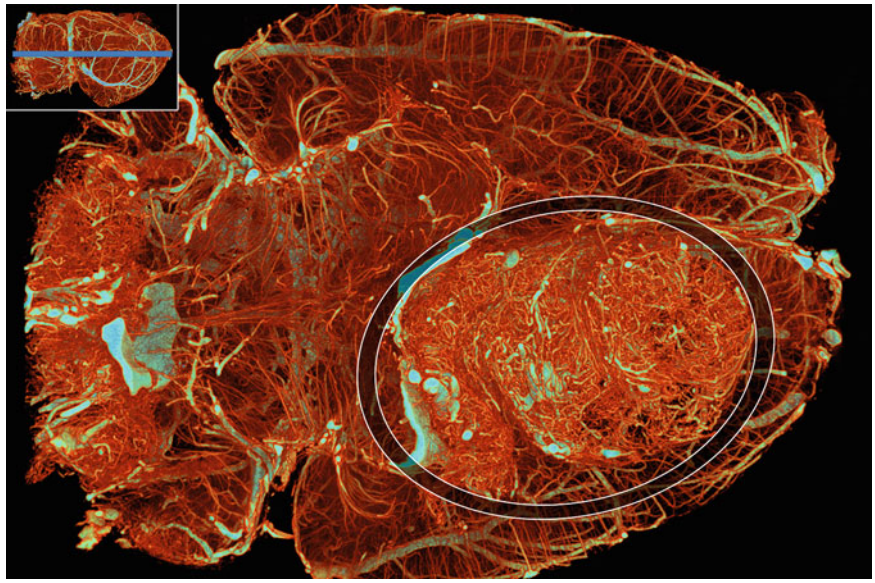

Fig. 6 Superior visualization of the vasculature of the rat brain with gliosarcoma (*encircled*) using μangioCT with the novel polymer-based contrast agent μAngiofil. The *inset* in the *left upper corner* displays the lateral view of the scanned brain; the *blue line* indicates the level of the virtual section shown in the main image. Please note that before μCT scan the sample is fixated and can, therefore, be further processed for histological observation after the site of interest are determined based on the analysis of the obtained 3D-datasets

Below you will find a number of tumor angiogenesis assays, please be aware that in some of them the proper quantification might be a major challenge.

Reference

1. Carmeliet P, Jain RK (2011) Molecular mechanisms and clinical applications of angiogenesis. Nature 473(7347):298–307. doi:10.1038/nature10144
2. Kraljevic S, Stambrook PJ, Pavelic K (2004) Accelerating drug discovery. EMBO Rep 5(9):837–842. doi:10.1038/sj.embor.7400236
3. Singh M, Ferrara N (2012) Modeling and predicting clinical efficacy for drugs targeting the tumor milieu. Nat Biotechnol 30(7):648–657. doi:10.1038/nbt.2286
4. Hanahan D, Folkman J (1996) Patterns and emerging mechanisms of the angiogenic switch during tumorigenesis. Cell 86(3):353–364
5. Gaustad JV, Simonsen TG, Leinaas MN, Rofstad EK (2012) Sunitinib treatment does not improve blood supply but induces hypoxia in human melanoma xenografts. BMC Cancer 12:388. doi:10.1186/1471-2407-12-388
6. Carmeliet P, Jain RK (2000) Angiogenesis in cancer and other diseases. Nature 407(6801):249–257. doi:10.1038/35025220
7. Warren BA (1979) The vascular morphology of tumors. In: Peterson H-I (ed) Tumor blood circulation: angiogenesis, vascular morphology and blood flow of experimental and human tumors. CRC Press Inc., Boca Raton, FL, pp 1–47
8. Nagy JA, Chang SH, Shih SC, Dvorak AM, Dvorak HF (2010) Heterogeneity of the tumor vasculature. Semin Thromb Hemost 36(3):321–331. doi:10.1055/s-0030-1253454
9. Hlushchuk R, Riesterer O, Baum O, Wood J, Gruber G, Pruschy M, Djonov V (2008) Tumor recovery by angiogenic switch from sprouting to intussusceptive angiogenesis after treatment with PTK787/ZK222584 or ionizing radiation. Am J Pathol 173(4):1173–1185. doi:10.2353/ajpath.2008.071131

10. Dvorak HF (2003) Rous-Whipple Award Lecture. How tumors make bad blood vessels and stroma. Am J Pathol 162(6):1747–1757
11. Maniotis AJ, Folberg R, Hess A, Seftor EA, Gardner LM, Pe'er J, Trent JM, Meltzer PS, Hendrix MJ (1999) Vascular channel formation by human melanoma cells in vivo and in vitro: vasculogenic mimicry. Am J Pathol 155(3):739–752. doi:10.1016/S0002-9440(10)65173-5
12. Stubbs M, McSheehy PM, Griffiths JR, Bashford CL (2000) Causes and consequences of tumour acidity and implications for treatment. Mol Med Today 6(1):15–19
13. Kimbrough CW, Khanal A, Zeiderman M, Khanal BR, Burton NC, McMasters KM, Vickers SM, Grizzle WE, McNally LR (2015) Targeting acidity in pancreatic adenocarcinoma: multispectral optoacoustic tomography detects pH-low insertion peptide probes in vivo. Clin Cancer Res 21(20):4576–4585. doi:10.1158/1078-0432.CCR-15-0314
14. Semenza GL (2001) Hypoxia-inducible factor 1: oxygen homeostasis and disease pathophysiology. Trends Mol Med 7(8):345–350
15. Burri PH, Hlushchuk R, Djonov V (2004) Intussusceptive angiogenesis: its emergence, its characteristics, and its significance. Dev Dyn 231(3):474–488. doi:10.1002/dvdy.20184
16. van Hinsbergh VW, Koolwijk P (2008) Endothelial sprouting and angiogenesis: matrix metalloproteinases in the lead. Cardiovasc Res 78(2):203–212. doi:10.1093/cvr/cvm102
17. Hlushchuk R, Makanya AN, Djonov V (2011) Escape mechanisms after antiangiogenic treatment, or why are the tumors growing again? Int J Dev Biol 55(4–5):563–567. doi:10.1387/ijdb.103231rh
18. Carmeliet P, De Smet F, Loges S, Mazzone M (2009) Branching morphogenesis and antiangiogenesis candidates: tip cells lead the way. Nat Rev Clin Oncol 6(6):315–326. doi:10.1038/nrclinonc.2009.64
19. Dome B, Hendrix MJ, Paku S, Tovari J, Timar J (2007) Alternative vascularization mechanisms in cancer: Pathology and therapeutic implications. Am J Pathol 170(1):1–15. doi:10.2353/ajpath.2007.060302
20. Folkman J (1971) Tumor angiogenesis: therapeutic implications. N Engl J Med 285(21):1182–1186. doi:10.1056/NEJM197111182852108
21. Jain RK (2005) Normalization of tumor vasculature: an emerging concept in antiangiogenic therapy. Science 307(5706):58–62. doi:10.1126/science.1104819
22. Fitzgibbons PL, Page DL, Weaver D, Thor AD, Allred DC, Clark GM, Ruby SG, O'Malley F, Simpson JF, Connolly JL, Hayes DF, Edge SB, Lichter A, Schnitt SJ (2000) Prognostic factors in breast cancer. College of American Pathologists Consensus Statement 1999. Arch Pathol Lab Med 124(7):966–978. doi:10.1043/0003-9985(2000)124<0966:PFIBC>2.0.CO;2
23. Vermeulen PB, Gasparini G, Fox SB, Colpaert C, Marson LP, Gion M, Belien JA, de Waal RM, Van Marck E, Magnani E, Weidner N, Harris AL, Dirix LY (2002) Second international consensus on the methodology and criteria of evaluation of angiogenesis quantification in solid human tumours. Eur J Cancer 38(12):1564–1579
24. Elagoz S, Egilmez R, Koyuncu A, Muslehiddinoglu A, Arici S (2006) The intratumoral microvessel density and expression of bFGF and nm23-H1 in colorectal cancer. Pathol Oncol Res 12(1):21–27, doi:PAOR.2006.12.1.0021
25. Marson LP, Kurian KM, Miller WR, Dixon JM (1999) Reproducibility of microvessel counts in breast cancer specimens. Br J Cancer 81(6):1088–1093. doi:10.1038/sj.bjc.6690811
26. Fox SB, Leek RD, Weekes MP, Whitehouse RM, Gatter KC, Harris AL (1995) Quantitation and prognostic value of breast cancer angiogenesis: comparison of microvessel density, Chalkley count, and computer image analysis. J Pathol 177(3):275–283. doi:10.1002/path.1711770310
27. Ehling J, Bartneck M, Wei X, Gremse F, Fech V, Möckel D, Baeck C, Hittatiya K, Eulberg D, Luedde T (2014) CCL2-dependent infiltrating macrophages promote angiogenesis in progressive liver fibrosis. Gut 63(12):1960–1971
28. Kiessling F, Greschus S, Lichy MP, Bock M, Fink C, Vosseler S, Moll J, Mueller MM, Fusenig NE, Traupe H (2004) Volumetric computed tomography (VCT): a new technology for noninvasive, high-resolution monitoring of tumor angiogenesis. Nat Med 10(10):1133–1138
29. Gremse F, Grouls C, Palmowski M, Lammers T, de Vries A, Grüll H, Das M, Mühlenbruch G, Akhtar S, Schober A (2011) Virtual elastic sphere processing enables reproducible quantification of vessel stenosis at CT and MR angiography. Radiology 260(3):709–717
30. Schambach SJ, Bag S, Steil V, Isaza C, Schilling L, Groden C, Brockmann MA (2009) Ultrafast high-resolution in vivo volume-CTA of mice cerebral vessels. Stroke 40(4):1444–1450
31. Figueiredo G, Brockmann C, Boll H, Heilmann M, Schambach SJ, Fiebig T, Kramer M, Groden C, Brockmann MA (2012) Comparison of digital subtraction angiography, micro-computed tomography angiography and magnetic resonance angiography in the assessment of the cerebrovascular system in live mice. Clin Neuroradiol 22(1):21–28
32. Sawall S, Kuntz J, Socher M, Knaup M, Hess A, Bartling S, Kachelrieß M (2012) Imaging of cardiac perfusion of free-breathing small animals using dynamic phase-correlated micro-CT. Med Phys 39(12):7499–7506

Chapter 3

Exosomes in Tumor Angiogenesis

Karma Z. Salem, Michele Moschetta, Antonio Sacco, Luisa Imberti, Giuseppe Rossi, Irene M. Ghobrial, Salomon Manier, and Aldo M. Roccaro

Abstract

Exosomes are small vesicles ranging in size between 30 and 150 nm, derived from the luminal membranes of the endosome and are constitutively released by fusion with the cell membrane. Several studies have revealed that exosomes play crucial roles in mediating local and systemic cell communication through the horizontal transfer of information in the form of nucleic material and proteins. This is particularly relevant in the context of the tumor-microenvironment cross talk. Here we describe the method of isolating exosomes and their role in modifying the tumor environment and more specifically in enabling metastasis and promoting angiogenesis.

Key words Exosome, Angiogenesis, Cancer, Tumor, Microenvironment, Pre-metastatic niche

1 Introduction

Exosomes have recently come to be recognized as critical components of intercellular communication capable of producing local and systemic changes. They are defined as small vesicles ranging in size between 30 and 150 nm and are released by all cells and particularly tumor cells. These vesicles represent a rich source of novel biomarkers in the diagnosis and prognosis of disease. In fact, the functional impact of exosomes is imparted by the molecular components they carry—including protein and nucleic acids such as micro RNAs. At present, exosome-mediated processes have been implicated in the pathobiology of both solid tumors and hematologic malignancies. These microvesicles play an important role in angiogenesis [1] and in promoting tumorigenesis in many cancer types, in particular through the transfer of miRNAs, mRNA, and proteins [2–4]. The function of exosomes in tumor progression can be explained in part by the capacity of tumor-derived exosomes to modulate the host microenvironment—in a distant site—and produce conditions favorable for the proliferation and spread of neoplastic cells [5–8]. These findings have raised the concept of

Domenico Ribatti (ed.), *Tumor Angiogenesis Assays: Methods and Protocols*, Methods in Molecular Biology, vol. 1464,
DOI 10.1007/978-1-4939-3999-2_3,

the pre-metastatic niche, in which exosome-induced neoangiogenesis plays a central role.

In spite of the advances in elucidating the role of exosomes in cancer, there is an experimental challenge in studying these nanovesicles because of their small size and the difficulty in obtaining high yields of these vesicles from biological fluids such as plasma. Cell culture media and physiologic fluids are known to contain several types of shed membrane fragments and vesicles. For this reason, it is imperative to ensure that the purified vesicles are indeed exosomes and not other contaminating material before performing any functional analysis.

Here we will develop the different methods to isolate exosomes and describe their role in inducing tumor progression and metastasis by inducing neoangiogenesis.

2 Methods of Exosome Isolation

One of the challenges involved in exosome research is a lack of standard methodologies evaluating the usability, vesicle purity, and yield from cell-culture-conditioned media and biological fluids. Currently, the gold standard in the purification of exosomes is a process of differential centrifugation, consisting of low speed centrifugation to remove cells and debris followed by high speed centrifugation to pellet the exosomes The main disadvantage of this process is that it can be cumbersome when dealing with large volumes and can also negatively impact the yield and quality of isolated exosomes. Alternatives to ultracentrifugation are process involving ultrafiltration, or exosome isolation reagents.

Characterizing and assessing the purity of the isolated exosomes is also imperative before performing any functional analysis to ensure that they are not contaminated with other vesicles.

For exosomes from cell culture supernatants, FBS used in cell culture should be precleared of exosomes by ultracentrifugation at $100{,}000 \times g$ for 3 h at 4 °C to remove any preexisting bovine-derived exosomes.

The ultracentrifugation process consists of several differential centrifugations. The first few centrifugation steps are designed to remove dead cells and large debris. At each of these centrifugation steps, the pellet is discarded and the supernatant is spun down again. The final supernatant is then ultracentrifuged at $100{,}000 \times g$ to pellet the exosomes. The pellet is then washed in a large volume of PBS to remove any contaminating proteins or other vesicles and centrifuged one last time at the same high speed [9].

An alternative method is the ultrafiltration process in which supernatant fractions of cell-cultured media are filtered on 0.2 μM pore filters to remove contaminating apoptotic bodies, microvesicles, and cell debris. The resulting filtrate is then ultracentrifuged

at 20,000 × *g* for 20 min. Exosomes are then harvested by ultracentrifugation at 100,000 × *g* for 70 min.

Other options include employing exosome isolation reagents such as ExoQuick (System Bioscience), Exosome Isolation Reagent (Life Technologies) or Exo-spin (Cell Guidance System). In this case, the biofluid is collected and centrifuged at 3000 × *g* for 15 min to remove cell debris. The supernatant is then transferred to a new sterile tube and the exosome isolation reagent is added to precipitate exosomes. At this point, the exosomes should appear as a beige/white pellet at the bottom of the tube. The use of exosome isolation reagent is more controversial as the potential for contamination by other vesicles is likely increased.

Once the isolation of exosomes is complete, the next step consists of the identification of isolated vesicles as exosomes and requires morphological analysis. Due to their small size, the most effective means of characterizing and visualizing exosomes is by electron microscopy combined with immunogold labeling of exosome-specific markers such as CD81 and CD63. Other methods to identify exosome-specific markers such as flow cytometry (requiring bead-conjugated antibodies) and western blot can be used. Characterizing the size of the vesicles by NanoSight is also helpful as it indicates the potential contamination by other vesicles.

3 Exosomes Are Involved in the Metastatic Process

Tumorigenicity and metastatic spread is instigated by cancer initiating cells that require a niche at the distant target site referred to as the pre-metastatic niche. Evidence suggests that these cancer-initiating cells prepare their homing bed before arrival, implying the involvement of soluble mediators in this process. Today, a large variety of contributing factors have been identified as being involved in preparing the pre-metastatic niche with tumor-derived exosomes being heralded as the driving force behind this process. Exosomes carry mRNA, miRNA, and proteins that are function-competent. These microvesicles spread throughout the body but bind to and get taken up by only select target cells. The process of binding and uptake can severely affect the target cells. It initiates activation of signal transduction and transferred RNA and proteins then account for gene silencing as well as over-expression of specific mRNA or proteins. Rapid progress in understanding the early role of exosome in metastasis has led to new hopes that we may be able to prevent metastatic spread by interfering with the pre-metastatic niche.

Mounting evidence suggests the central role of tumor-derived exosomes in modulating the distant tumor microenvironment. Melanoma-derived exosomes injected in naïve mice have been shown to induce neoangiogenesis at pre-metastatic niche sites

before the presence of any tumor cells [3]. In this process, melanoma tumor cells with high expression of the RAB family members were more prone to metastasize. The RAB proteins are regulators of membrane trafficking and exosome formation and their expression correlates with the secretion of exosomes. In this study, RAB27A RNA interference decreased exosome production, preventing bone marrow pre-metastatic education and reducing tumor growth and metastasis, suggesting a central role for exosomes in the pre-metastatic process.

In the context of multiple myeloma, it has been recently reported that the protein content of exosomes isolated from myeloma bone marrow stromal cells was enriched for oncogenic proteins, cytokines, and kinases, including IL-6, CCL2, and fibronectin [4]. This supports the notion that bone marrow stromal cells support tumorigenesis not only through paracrine mechanisms like growth factors [10, 11] but also through direct transfer of microRNAs and proteins from exosomes thus creating a favorable niche for the expansion of the malignant clone.

A recent study by Hoshino et al. demonstrated that various different types of tumor-derived exosomes fuse preferentially with resident cells at their predicted destination [12]. This concept of metastatic organotropism argues that exosomes taken up by organ-specific cells prepare and prime the pre-metastatic niche. Proteomic analysis of exosomes revealed distinct integrin expression patterns perhaps indicating the predilection for exosomes to target specific cells types or organs. Integrins α6β4 and α6β1 were associated with lung metastasis while exosomal integrins αvβ5 was linked to liver metastasis. Targeting these integrins in turn decreased exosome uptake as well as lung and liver metastasis.

Studies investigating pancreatic ductal adenocarcinoma (PDAC) have also demonstrated that intercellular communication is critical for metastatic progression in this aggressive cancer [13]. In fact, PDAC-derived exosomes were shown to induce liver pre-metastatic niche formation in mice and consequently increase liver metastatic burden. Uptake of these tumor-derived exosomes by the liver resulted in TGF-β secretion and upregulation of fibronectin production. This resulting fibrotic microenvironment then enhanced the recruitment of bone marrow derived macrophages. It was also noted that macrophage migration inhibitory factor (MIF) was highly expressed in tumor-derived exosomes and its blockade prevented the formation of this liver pre-metastatic niche and thus inhibited metastasis. Additionally, patients with pancreatic tumors that did not progress had markedly lower MIF in their exosomes than patients who later developed liver metastasis. These results suggest that exosomal MIF does indeed prime the liver in preparation for metastasis and may have potential prognostic and therapeutic implications in preventing the progression of this cancer.

In addition to the role of exosomes in promoting tumor metastasis, their function and mechanism of action has been shown to extend to enhancing angiogenesis in the microenvironment. In fact, recent evidence suggests that exosomes' capability to induce angiogenesis in the pre-metastatic niche plays a central role in the metastatic process.

4 Angiogenesis in Cancer

Angiogenesis, the growth of new blood vessels from pre-existing ones, is an important process in the pathogenesis of malignant, infectious, fibro-proliferative, and inflammatory diseases [14]. This process is controlled by multiple growth factors and signaling pathways, and critically depends upon the tight balance of pro-angiogenic and antiangiogenic factors [14].

It is widely accepted that acquiring angiogenic capacities represents a fundamental hallmark leading pre-cancerous cells to become cancerous. After neoplastic transformation the net balance between pro-angiogenic and anti-angiogenic molecules in the tumor tissue is tipped to favor angiogenesis, the so called 'angiogenic switch' [15]. The vascular endothelial growth factor, VEGF, is thought to be the most important as VEGF acts pro-angiogenic by augmenting all steps of angiogenesis: vascular permeability, endothelial cell proliferation, endothelial cell migration or invasion into the surrounding tissue, and finally capillary-like tube formation [16]. Various inhibitors interfering with VEGF/VEGFR have received FDA approval and are currently approved in clinical use [16]. Many other growth factors and pathways have also been implicated in the formation of cancer associated vessels.

The family of fibroblast growth factors (FGF) is involved in neurogenesis, embryonic and post-natal organ development, branching morphogenesis, angiogenesis, and in the pathogenesis of cancer. FGF-2 by binding to its receptor FGFR-1, is thought to be the major family member mediating neongiogenesis [17]. The platelet-derived growth factor (PDGF) is frequently upregulated in tumors and has been shown to cooperate with FGF-2 to promote tumor angiogenesis and metastasis development [15]. Delta-like ligand 4 (Dll4) is a member of the Delta/Jagged family of transmembrane ligands binding to Notch receptor [15, 16]. The delta-Notch pathway regulates the artery–vein differentiation but it seems to be also importantly implicated in the stimulation of blood vessel formation. Its major role is to mediate cell–cell communication and controls of cell determination thus playing a pivotal role in vascular development. The role of Angiopoietin 2 in angiogenesis is generally considered as an antagonist for Ang1, thereby inhibiting Ang1-promoted Tie2 signaling, which is critical for blood vessel maturation and stabilization [18]. However the

role of Ang1/Ang2/Tie2 pathways in tumor-associated angiogenesis remain controversial. While some studies have shown that upregulation of Ang2 correlates with tumor growth and angiogenesis development of various types of cancers, other studies have reported that specific induction of Ang2 in gliomas, mammary carcinomas, and lung carcinomas inhibited tumor growth and metastasis [18].

Apart from these growth factors and signaling pathways many other subcellular systems also contribute to the process of neovessel formation.

Proteolytic degradation of matrix proteins is essential for transmigration of activated endothelial cells through the basal membrane into surrounding matrix [19]. In this context, the plasminogen system, the matrix-metalloproteinase (MMP) system, as well as the heparanase and chymase families are thought to be important [20]. For example, a large body of in vitro and in vivo data has shown an important role of the urokinase (uPA)/plasminogen system in angiogenesis and cancer. Moreover blood vessel formation critically depends on extracellular signaling as well as the connection with the extracellular matrix (ECM) proteins, such as fibronectin, fibrinogen, vitronectin, and laminin as well as collagens [19]. The attachment to the ECM is adjusted by integrin adhesion receptors [21]; integrins operate as bidirectional transducer molecules by matching signals from both, the outside to the inside of the cell, or from the inside to the outside of the cell. Both signaling directions are tightly regulated in focal adhesion to support cell adhesion, spreading, and motility of endothelial cells. Both endothelial cell integrins and ECM proteins have been implicated in cancer associated angiogenesis and may represent important therapeutic targets [21].

Integrins have to interact with several kinases as well as related adaptor proteins since they have no intrinsic kinase activity. Integrins can activate Focal Adhesion Kinase (FAK) signaling thereby communicating signals that can induce cell migration or cell proliferation [22]. FAK activation then leads to activation of src family kinases which control not only the activity of Rho GTPases but also downstream kinases such as AKT, thereby affecting endothelial cell proliferation, migration, and survival [22]. All these downstream kinases may represent important therapeutic targets for the development of new antiangiogenic drugs. Finally, tumor microenvironment, which consists of several cytotypes including fibroblasts, pericytes, mesenchymal-stem cells, and inflammatory-immune cells, also contributes to angiogenesis via secretion of angiogenic molecules and cell-to-cell interactions [15, 23].

Given the molecular and biological complexity of angiogenesis in cancer, the understanding of how cancer and non cancer derived exosomes participate in this process represents an important challenge that can open new paths for the development of novel and effective anticancer drugs able to inhibit the neoangiogenic process during cancer development.

5 Exosomes in Cancer-Associated Angiogenesis

Numerous studies have identified that exosomes can be released from various cell types: dendritic cells, B lymphocytes, stem cells, mesenchymal stem cells, tumor cell lines, platelets, cardiomyocytes, endothelial cells have all been implicated in the release of exosomes which in turn then mediate important biological functions mediating distant cell-to-cell interactions [24].

Endothelial cells can release different types of membrane vesicles, including microvesicles, exosomes, and apoptotic bodies, in response to cellular activation or apoptosis [24]. Defining the specific biological functions mediated by the specific types of vesicles remains an important methodological challenge, as previously discussed. Data reported in literature needs to be carefully interpreted after taking into consideration methodological aspects.

It has been shown that endothelial exosomes might be involved in vascular development through incorporation and transfer of Delta-like ligand 4 (Dll4; Delta 4) protein to neighboring endothelial cells. This leads to an inhibition of Notch signaling and an increased capillary-like structure formation in vitro and in vivo [25]. This suggests that the Delta like ligand/Notch pathway may not require the direct cell–cell contact and that exosome release by endothelial cells may work in the place of cell-to-cell contact thus expanding the range of cell signaling potential for angiogenesis regulation. Other studies have also shown that endothelial-derived exosomes contain proteins, microRNA, and mRNA with pro-angiogenic potential. For example, it has been reported that matrix metalloproteinases harbored by exosomes from endothelial cells are functionally active and can mediate endothelial cell invasion and capillary-like formation [26]. All together it seems that endothelial cell-derived exosomes containing proteins and mRNAs/microRNAs which may function as paracrine or autocrine factors thus having the ability to facilitate cancer associated angiogenesis and metastasis [24, 27]. For example, it has been shown that exosomes from LAMA84 chronic myeloid leukemia (CML) cells affect vascular remodeling in vitro through an IL-8 mediated activation of VCAM-1 [28]. Umezu et al. [29] have found that miRNA-enclosed exosomes have a critical role in mediating leukemia cell-to-endothelial cell communication. Exosomes, collected from miR-92a-overexpressing leukemia cells (K562 cells), did enter into endothelial cells, resulting in increased endothelial cell migration and tube formation.

Glioblastoma cell-derived exosomes have been shown to interact with endothelial cells and thereby stimulate endothelial cell proliferation [30, 31]. In this same disease it has been observed that exosomes derived from tumor cells grown in hypoxia as compared to those derived by cells grown in normoxic conditions significantly stimulated angiogenesis [31].

King et al. [32] reported that hypoxia promoted the release of exosomes from breast cancer cells, and the hypoxically regulated miR-210 was presented at elevated levels in hypoxic exosomes.

Squamous carcinoma and colorectal cancer cells can secrete exosomes enriched in proteins and cell cycle-related mRNAs that can facilitate angiogenesis and metastasis [33, 34].

Cancer cells can indirectly stimulate angiogenesis via platlets-activation and subsequent release of platelet derived endothelial-stimulating exosomes. For example, Janowska-Wieczorek et al. [1] have shown that exosomes released from human platelet α-granules could contribute to tumor metastasis and angiogenesis. Finally, cancer cells can also stimulate the release of pro-angiogenic exosomes from cells of the tumor microenvironment, i.e., fibroblasts, macrophages, other immune cells, and mesenchymal stem cells (ref. 24 for review). In summary this evidence supports the hypothesis that exosomes contribute to cancer angiogenesis via several mechanisms and may represent a target for future anti-angiogenic drugs. However studies in this field are still limited so far.

6 Conclusions

Exosomes are small nanovesicles secreted by all cell types in the body, especially tumor cells, and are involved in cell-to-cell communications. They represent attractive biomarkers in cancer as they are accessible in the peripheral blood and represent a mirror of the tumor cell's content. Functionally, recent evidence has shown the primordial role of exosomes in tumor metastasis. In fact, exosomes are involved in priming the distant niche before the arrival of the first metastatic cell, thus initiating what is referred to as the pre-metastatic niche. Tumor-derived exosomes release a specific content of miRNA, mRNA, and proteins in recipient cells, therefore modifying their properties. This phenomenon leads to angiogenesis that promotes tumor progression and metastasis. The knowledge of these mechanisms could lead to therapeutic advances, especially in regards to the use of exosomes to deliver drugs or small interfering RNA to specific targeted cells.

References

1. Janowska-Wieczorek A, Wysoczynski M, Kijowski J et al (2005) Microvesicles derived from activated platelets induce metastasis and angiogenesis in lung cancer. Int J Cancer 113:752–760
2. Melo SA, Sugimoto H, O'Connell JT et al (2014) Cancer exosomes perform cell-independent microRNA biogenesis and promote tumorigenesis. Cancer Cell 26:707–721
3. Peinado H, Aleckovic M, Lavotshkin S et al (2012) Melanoma exosomes educate bone marrow progenitor cells toward a pro-metastatic phenotype through MET. Nat Med 18:883–891
4. Roccaro AM, Sacco A, Maiso P et al (2013) BM mesenchymal stromal cell-derived exosomes facilitate multiple myeloma progression. J Clin Invest 123:1542–1555

5. Andreola G, Rivoltini L, Castelli C et al (2002) Induction of lymphocyte apoptosis by tumor cell secretion of FasL-bearing microvesicles. J Exp Med 195:1303–1316
6. Kim JW, Wieckowski E, Taylor DD, Reichert TE, Watkins S, Whiteside TL (2005) Fas ligand-positive membranous vesicles isolated from sera of patients with oral cancer induce apoptosis of activated T lymphocytes. Clin Cancer Res 11:1010–1020
7. Liu C, Yu S, Zinn K et al (2006) Murine mammary carcinoma exosomes promote tumor growth by suppression of NK cell function. J Immunol 176:1375–1385
8. Clayton A, Mitchell JP, Court J, Linnane S, Mason MD, Tabi Z (2008) Human tumor-derived exosomes down-modulate NKG2D expression. J Immunol 180:7249–7258
9. Théry C, Amigorena S, Raposo G, Clayton A (2006) Isolation and characterization of exosomes from cell culture supernatants and biological fluids. Curr Protocol Cell Biol 30(3.22):3.22.1–3.22.29
10. Gupta D, Treon SP, Shima Y et al (2001) Adherence of multiple myeloma cells to bone marrow stromal cells upregulates vascular endothelial growth factor secretion: therapeutic applications. Leukemia 15:1950–1961
11. Kumar S, Witzig TE, Timm M et al (2004) Bone marrow angiogenic ability and expression of angiogenic cytokines in myeloma: evidence favoring loss of marrow angiogenesis inhibitory activity with disease progression. Blood 104:1159–1165
12. Hoshino A, Costa-Silva B, Shen TL et al (2015) Tumour exosome integrins determine organotropic metastasis. Nature 527:329–335
13. Costa-Silva B, Aiello NM, Ocean AJ et al (2015) Pancreatic cancer exosomes initiate pre-metastatic niche formation in the liver. Nat Cell Biol 17:816–826
14. Welti J, Loges S, Dimmeler S, Carmeliet P (2013) Recent molecular discoveries in angiogenesis and antiangiogenic therapies in cancer. J Clin Invest 123:3190–3200
15. Prager GW, Poettler M, Unseld M, Zielinski CC (2012) Angiogenesis in cancer: Anti-VEGF escape mechanisms. Transl Lung Cancer Res 1:14–25
16. Chung AS, Ferrara N (2011) Developmental and pathological angiogenesis. Annu Rev Cell Dev Biol 27:563–584
17. Lieu C, Heymach J, Overman M, Tran H, Kopetz S (2011) Beyond VEGF: inhibition of the fibroblast growth factor pathway and anti-angiogenesis. Clin Cancer Res 17:6130–6139
18. Shim WS, Ho IA, Wong PE (2007) Angiopoietin: a TIE(d) balance in tumor angiogenesis. Mol Cancer Res 5:655–665
19. Campbell NE, Kellenberger L, Greenaway J, Moorehead RA, Linnerth-Petrik NM, Petrik J (2010) Extracellular matrix proteins and tumor angiogenesis. J Oncol 2010:586905
20. Rundhaug JE (2005) Matrix metalloproteinases and angiogenesis. J Cell Mol Med 9:267–285
21. Desgrosellier JS, Cheresh DA (2010) Integrins in cancer: biological implications and therapeutic opportunities. Nat Rev Cancer 10:9–22
22. Bolos V, Gasent JM, Lopez-Tarruella S, Grande E (2010) The dual kinase complex FAK-Src as a promising therapeutic target in cancer. Onco Targets Ther 3:83–97
23. Bergers G, Hanahan D (2008) Modes of resistance to anti-angiogenic therapy. Nat Rev Cancer 8:592–603
24. Ribeiro MF, Zhu H, Millard RW, Fan GC (2013) Exosomes function in pro- and anti-angiogenesis. Curr Angiogenes 2:54–59
25. Sheldon H, Heikamp E, Turley H et al (2010) New mechanism for Notch signaling to endothelium at a distance by delta-like 4 incorporation into exosomes. Blood 116:2385–2394
26. Taraboletti G, D'Ascenzo S, Borsotti P, Giavazzi R, Pavan A, Dolo V (2002) Shedding of the matrix metalloproteinases MMP-2, MMP-9, and MT1-MMP as membrane vesicle-associated components by endothelial cells. Am J Pathol 160:673–680
27. Taverna S, Flugy A, Saieva L et al (2012) Role of exosomes released by chronic myelogenous leukemia cells in angiogenesis. Int J Cancer 130:2033–2043
28. Mineo M, Garfield SH, Taverna S et al (2012) Exosomes released by K562 chronic myeloid leukemia cells promote angiogenesis in a Src-dependent fashion. Angiogenesis 15:33–45
29. Umezu T, Ohyashiki K, Kuroda M, Ohyashiki JH (2013) Leukemia cell to endothelial cell communication via exosomal miRNAs. Oncogene 32:2747–2755
30. Skog J, Wurdinger T, van Rijn S et al (2008) Glioblastoma microvesicles transport RNA and proteins that promote tumour growth and provide diagnostic biomarkers. Nat Cell Biol 10:1470–1476
31. Kucharzewska P, Christianson HC, Welch JE et al (2013) Exosomes reflect the hypoxic status of glioma cells and mediate hypoxia-dependent activation of vascular cells during tumor development. Proc Natl Acad Sci U S A 110:7312–7317

32. King HW, Michael MZ, Gleadle JM (2012) Hypoxic enhancement of exosome release by breast cancer cells. BMC Cancer 12:421
33. Park JE, Tan HS, Datta A et al (2010) Hypoxic tumor cell modulates its microenvironment to enhance angiogenic and metastatic potential by secretion of proteins and exosomes. Mol Cell Proteomics 9:1085–1099
34. Hong BS, Cho JH, Kim H et al (2009) Colorectal cancer cell-derived microvesicles are enriched in cell cycle-related mRNAs that promote proliferation of endothelial cells. BMC Genomics 10:556

Chapter 4

Coculture Assays for Endothelial Cells-Mural Cells Interactions

Diana M. Sánchez-Palencia, Alex Bigger-Allen, Magali Saint-Geniez, Joseph F. Arboleda-Velásquez, and Patricia A. D'Amore

Abstract

Coculture assays allow the investigation of the role of endothelial cell and mural cell interactions in small vessel development and function. Different setups for coculture can be used to assay questions of interest. We include here methods for direct coculture, indirect coculture, and coculture in a three-dimensional extracellular matrix scaffold for studies of either a simple and direct association between the two cell types, the exchange of soluble molecules, or the interaction within a biomimetic tissue microenvironment.

Key words Angiogenesis, Endothelial cells, Pericytes, Coculture, Matrigel, Small intestinal submucosa, Intercellular interactions, Paracrine, Juxtacrine, Microvessels

1 Introduction

Cocultures have been used successfully over the years to study the interactions between endothelial cells and cells collectively known as mural cells (smooth muscle cells and pericytes). Two-dimensional (2D) direct and indirect coculture methods in cell culture plates are useful to examine interactions that require direct contact (juxtacrine) or those that are made through diffusion of soluble factors (paracrine). Three-dimensional (3D) techniques involve the use of agarose, matrigel, or a fibrous decellularized extracellular matrix (ECM) scaffold to investigate interactions within a 3D-biomimetic environment. We have investigated through the use of cocultures the effect of heterotypic cell interactions on cell proliferation [1–3], migration [4, 5], apoptosis [6], activation of growth factors [2], cord formation [6, 7], and Notch signaling [8]. Coculture set-ups have allowed us to examine signaling pathways that dictate the behavior of endothelial cells [2, 4–7] during vessel formation, and the maturation and stabilization of neovessels through communication with pericytes [1–3, 6, 8].

Domenico Ribatti (ed.), *Tumor Angiogenesis Assays: Methods and Protocols*, Methods in Molecular Biology, vol. 1464,
DOI 10.1007/978-1-4939-3999-2_4,

We describe here three different methods of coculture including direct coculture, indirect coculture using transwells, and coculture in a 3D matrix using an ECM scaffold [9]. The methodologies include detailed culture conditions for primary human endothelial cells and an updated protocol for isolating and culturing bovine retinal pericytes [2, 10].

2 Materials

All materials should be sterilized by autoclaving, filtering, or ethylene oxide sterilization.

2.1 Materials for the Culture of Human Retinal Microvascular Endothelial Cells (HRECs)

1. Primary human retinal microvascular endothelial cells (catalog number ACBRI 181) (Cell Systems).
2. 0.2% gelatin in PBS (must be tissue culture grade) autoclaved.
3. HREC culture medium: EBM-2 supplemented with 2% fetal bovine serum (FBS) (catalog number S11150) (Atlanta Biologicals), EBM-2, 100 U/mL penicillin and 100 mg/mL streptomycin (1% P/S), 2 mM L-glutamine (1% L-glutamine), Single Quot (catalog number CC-4176) (Lonza). FBS must be refiltered and complete media must be filtered after preparation.
4. 1× phosphate buffer saline (PBS) without calcium and magnesium, must be autoclaved.
5. Trypsin-versene (catalog number 17-161E) (Lonza).
6. HREC freezing media: 90% FBS and 10% DMSO solution.
7. Six-well or 24-well transwell supports.

2.2 Materials for Isolation and Culture of Bovine Retinal Pericytes (BRPs)

1. Calf eyes shipped on ice (*see* **Note 1**).
2. 4 L of sterile PBS.
3. Two No. 15 surgical blades.
4. Poly-lined sterile field drapes, 18″ × 26″, one per eye.
5. Surgical spears, one per eye (catalog number Q604230) (Fabco).
6. Cell strainers, 100 μm pore size mesh (catalog number 352360) (Corning).
7. Cell strainers, 70 μm pore size mesh (catalog number 352350) (Corning).
8. Two sets of sterile scissors and forceps.
9. Two 150 × 25 mm culture dishes per eye.
10. Two 50 mL conical tubes per eye.
11. Two sterile 1 L beakers.

12. One 2 L beaker.
13. One L of 0.4% betadine solution in PBS (*see* **Note 2**).
14. 15 mL of collagenase (digest enzyme) solution per eye (prepare the day prior to isolation): 51,051 units collagenase and 0.25% of FBS in PBS; filter sterilize.
15. PBS-EDTA solution: 2.5 mL of 0.5 M (pH 8.0) in 500 mL of PBS; filter sterilize.
16. Trypsin-EDTA (0.25%) (catalog number 25200-056) (Life Technologies).
17. BRP washing medium (prepare the day prior to isolation): Dulbecco's modified Eagle's medium (DMEM) (catalog number DMEM 12-708F) (Lonza) supplemented with 10% calf serum (catalog number SH30072.03) (HyClone), 1% P/S, 1% L-glutamine, 0.025 mg/mL nystatin (catalog number N3503-5MU) (Sigma); filter sterilize.
18. BRP culture medium (prepare the day prior to isolation): DMEM (catalog number DMEM 12-708F) (Lonza) supplemented with 10% calf serum (catalog number SH30072.03) (HyClone), 1% P/S and 1% L-glutamine; filter sterilize.
19. BRP growth medium: DMEM (catalog number DMEM 12-708F) (Lonza), 20% bovine calf serum (catalog number 12133C) (Sigma), 1% P/S and 1% L-glutamine; filter sterilize (*see* **Note 3**).
20. BRP freezing medium: 85% FBS, 10% DMSO and 5% DMEM (catalog number DMEM 12-708F) (Lonza).

2.3 Materials for the Preparation of an ECM Scaffold from Porcine Small Intestine and for 3D ECM Coculture

1. Hydrogen peroxide solution (catalog number 216763) (Sigma).
2. Sodium hypochlorite solution (catalog number 425044) (Sigma).
3. 1 L autoclaved deionized water (DI).
4. 500 mL autoclaved PBS.
5. Four-well chamber slide system (catalog number 177399) (Thermo Scientific).
6. Sterile forceps and scissors.
7. ECM coculture medium: DMEM (catalog number DMEM 12-708F) (Lonza), 10% FBS (catalog number S11150) (Atlanta Biologicals), 1% P/S and 1% L-glutamine; filter sterilize.

3 Methods

Work in a biosafety cabinet. Use a surgical mask to protect yourself from exposure to enzymes.

3.1 Culture of HRECs

3.1.1 Thawing of HRECs

1. Coat T75 flasks with 5 mL of 0.2 % gelatin in PBS, by adding gelatin evenly to the culture surface of the flask, incubating at 37 °C (inside incubator) for at least 30 min, aspirating gelatin from flasks and washing twice with 10 mL of PBS.
2. Warm to 37 °C the HREC culture medium.
3. Transfer cells from a vial with 1×10^6 cells to a 15 mL tube.
4. Add 5 mL of HREC culture medium to resuspend the cells and mix by pipetting.
5. Spin at $423 \times g$ for 4 min.
6. Aspirate media without disturbing the pellet.
7. Resuspend in 10–12 mL of media and mix by pipetting.
8. Plate in one T75 flask.

3.1.2 Passaging of HRECs

1. Passage at a 1:3 to 1:5 ratio (*see* **Note 4**).
2. Warm to 37 °C the HREC culture medium, trypsin-versene and PBS without calcium and magnesium.
3. Accordingly with the desired passage ratio, coat T75 flasks as indicated in Subheading 3.1.1.
4. Wash cells to be passaged with 5 mL PBS.
5. Add 3 mL of trypsin-versene and incubate at 37 °C for 3–5 min, until cells detach; gently tap the sides of the flask to assist detachment.
6. Add 6 mL of complete media to quench the trypsin and mix by pipetting.
7. Transfer cells to a 15 mL conical tube and spin at $423 \times g$ for 4 min.
8. Aspirate media without disturbing the pellet.
9. Resuspend and plate in the chosen passage ratio in 10–12 mL of complete media.
10. Change media every other day.

3.1.3 Freezing of HRECs

1. Wash cells to be frozen with 5 mL PBS.
2. Add 3 mL of trypsin-versene and place in 37 °C incubator for 3–5 min, until cells detach; gently tap the sides of the flask to assist detachment.
3. Add 6 mL of complete media to quench the trypsin and mix by pipetting.
4. Transfer cells to a 15 mL conical tube and spin at $423 \times g$ for 4 min.
5. Aspirate media without disturbing the pellet.
6. Count cells using an automated cell counter or a hemocytometer and resuspend in freezing media as 1×10^6 cells/mL; freeze in 1 mL volumes.

3.2 Isolation of Bovine Retinal Pericytes (BRPs)

3.2.1 Isolation of BRPs

1. Upon arrival place eyes on ice.
2. Set up the following materials inside the biosafety cabinet: 1 L sterile beakers, sterile drape, culture dishes, surgical spears, surgical tools, surgical blades, 500 mL PBS, sterile filtered wash medium, 50 mL conical tubes and the collagenase solution.
3. Outside the biosafety cabinet, immerse the eyes in betadine (enough to cover the eyes) inside a 2 L beaker for 15 min.
4. Fill two sterile 1 L beakers with sterile PBS; remove the eyes from the betadine one at a time and submerge in one of the 1 L beakers with sterile PBS.
5. Prepare 130 mL per eye of the stock BRP wash medium diluted 1/25 with sterile PBS. Arrange one separate conical tube per eye, each containing 25 mL of solution.
6. Place the lid of one of the culture dishes upside down under the sterile drape and manipulate the eye on the drape (*see* **Note 5**). Place the bottom part of the dish diagonally behind the dissection area while on the sterile drape, and use for collecting waste tissue.
7. Remove the orbital fat and muscle surrounding the eyeball using sterile scissors and forceps. This can be done for all eyes on the same sterile drape prior to beginning dissection. After trimming, place the eyes in the other 1 L beaker filled with PBS. Change the sterile drape.
8. Place one eye on the clean sterile drape placed over the culture dish lid. While holding the eye with forceps by the optic nerve, make an incision with the surgical blade roughly 5 mm posterior from the iris. Using scissors, cut around the entire eyeball to remove the anterior segment and place in the waste dish (Fig. 1a). The vitreous body (which is also waste) should come out with the anterior segment. Pull the vitreous out using forceps if it did not come out with the anterior segment.
9. Applying very light pressure, use a scalpel blade to cut out a thin circular section in the center of the posterior segment (about 0.1 mm deep and 40 mm in diameter) (Fig. 1b). Use a moist surgical spear to gather up the sectioned tissue towards the center (*see* **Note 6**). Cut the optic nerve and place the circular section in the waste dish (*see* **Note 7**).
10. Use a moist surgical spear to gather towards the center of the posterior segment the remainder of the retina (which will have a circular hole in the center after the removal of the circular section in the previous step) (*see* **Note 8**). Carefully lift the gathered retina with a pair of forceps. Cut the remaining attachments of the retina to the optic nerve and then remove the retina with the second pair of sterile forceps. Place in the conical tube containing the 25 mL diluted BRP wash medium solution.

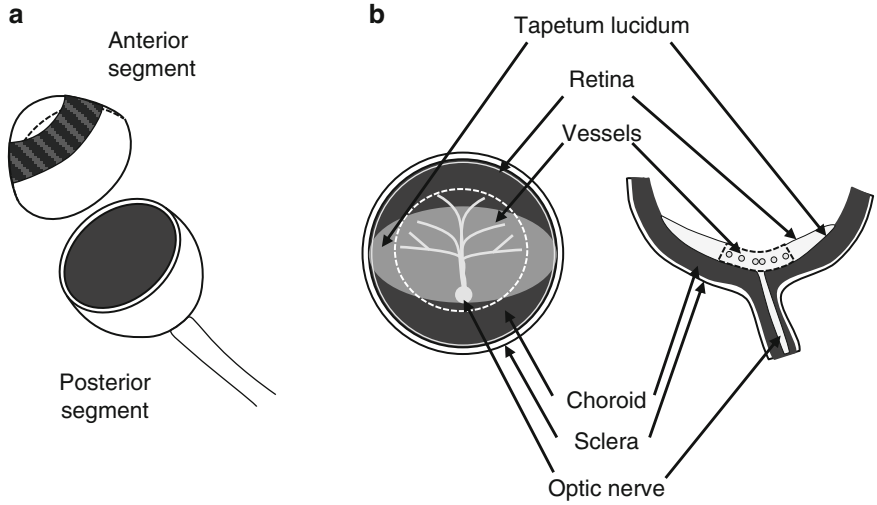

Fig. 1 Dissection of a bovine retina. (**a**) Dissection of the anterior and posterior segments of the eye. (**b**) Removal of a circular section (*dashed line*) of the retina in the center of the posterior segment containing the larger retinal vasculature

11. Repeat the dissection on the remaining eyes. Keep the retinas in the previously arranged separate conical tubes containing diluted BRP wash medium solution (*see* **Note 9**). Keep at room temperature for less than 1 h.
12. Wash each retina by gently inverting the tube three to four times. Carefully pour out the wash solution into a waste container without pouring out the retina. Wash twice more with BRP wash medium solution for a total of three washes. Remove as much of wash solution as possible and then transfer the retina to a clean sterile culture dish by pouring (*see* **Note 10**).
13. Aspirate 1 mL of collagenase solution into a p1000 pipette and force the tissue through the pipette four to seven times until it flows easily. After the first or second pipetting movements, check if there are any visible large vessels (such as those present in the circular section removed in **step 9**) and pipette them out in a separate area of the culture dish.
14. Continue to inspect and pipette the retina in collagenase solution four to seven more times until fully digested. Remove any visible large vessels to the waste dish. Add 13 mL of collagenase solution to the dish and pipette up and down with a p1000 pipette four to seven times.
15. Incubate at 37 °C and 5% CO_2 for 1 h.
16. Pipette up and down the digested tissue 10–15 times with a 10 mL pipette, and check under the microscope for detached single cells.

17. When a single cell suspension is obtained, pass the solution through a 100 μm mesh into a clean sterile 50 mL conical tube containing 25 mL of BRP wash medium solution.
18. Spin at 751 × *g* for 4 min.
19. Aspirate the supernatant and repeat washing twice with 10–15 mL of BRP wash medium solution.
20. Resuspend cells in 25 mL of BRP culture medium and plate by passing through a 70 μm mesh into a T175 flask. Culture at 37 °C and 5 % CO_2.
21. The following day, aspirate the medium, wash twice with 10 mL of PBS and replenish with 25 mL of BRP culture medium. Repeat on the sixth day of culture. *See* Fig. 2a–c for images of cells on the second and fourth day of culture.
22. On the eighth day of culture (Fig. 2d), replace the media with PBS and observe each flask under a microscope to determine the presence of non-pericyte cells such as endothelial cells, astrocytes, and fibroblasts, considered here as "contaminants" (Fig. 2b, e). Mark the location of contaminant colonies on the bottom of the flask. Colonies are easily detached using a rapid EDTA treatment as follows: wash the cells with PBS and then add 10 mL of PBS-EDTA solution. After 2 min, contaminants will be fully lifted of the plate while pericytes will only start to round up. Tap firmly the sides of the flask to assist detachment of contaminants, aspirate and wash twice with PBS.

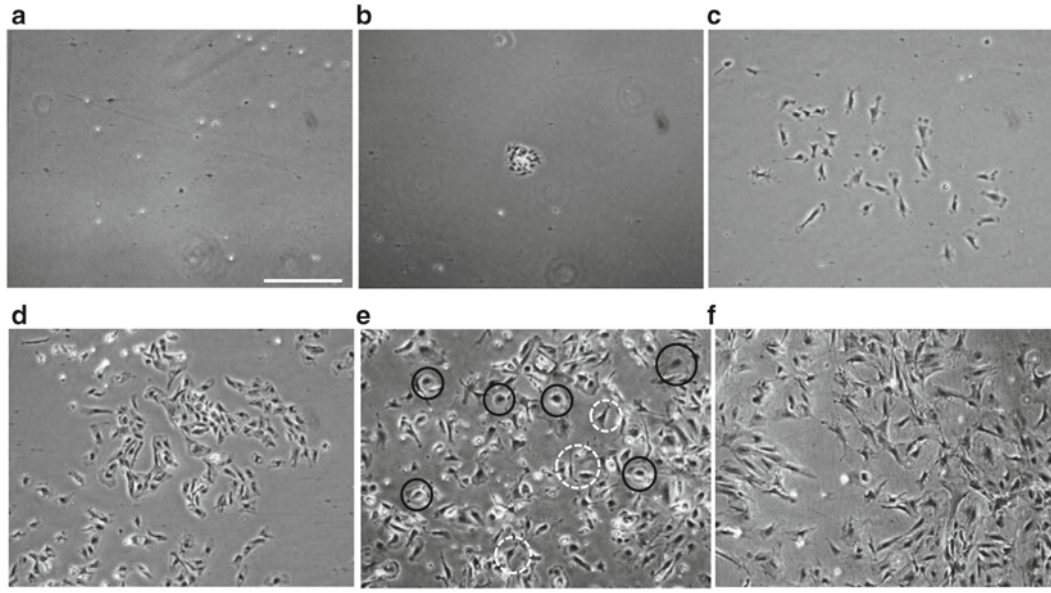

Fig. 2 Isolation of bovine retinal pericytes. 2 (P0) (**a**, **b**), 4 (P0) (**c**), 8 (P0) (**d**), 10 (P0) (**e**), and 18 (P1) (**f**) days of culture. Pericytes begin spreading on the plate after 4 days and take around 10–12 days to achieve confluency. Contaminants in culture after 2 (**b**) and 10 days of culture (**e**, *black solid line*). Pericytes are shown in *white dashed line circles* in (**e**). Bar: 500 μm

Add 25 mL of BRP growth medium. Confirm that all contaminants are removed under the microscope using the marked location as guide. Make sure there are no more "contaminants" before passaging (*see* **Notes 11** and **12**).

23. Passage cells at a 1:1.5 ratio when they reach 90% confluency (between day 8 and 14) by using the standard passaging procedure described in Subheading 3.2.2. P1 cells can be maintained in culture for 1–2 weeks without changes in morphology (Fig. 2f).
24. If "contaminant" cells are visible in the next 1–2 weeks, use trypsin-versene (5 mL for a T175 flask) to remove them. Generally, endothelial and smooth muscle cells will detach before pericytes. Wash cells with 13 mL PBS, aspirate, add trypsin-versene, swirl it around in the flask and use the microscope to observe detachment of "contaminants". Add twice the volume of culture medium to quench the trypsin, aspirate and wash twice with 13 mL PBS. Then passage pericytes using trypsin-EDTA by the standard passaging procedure in Subheading 3.2.2. P2 and P3 cells can be frozen 2–3 days later, using the procedure described in Subheading 3.2.2.
25. Use BRPS up to P6 and always passage before 90% confluency (avoid 100% confluence, since they start to pile up).

3.2.2 Passaging and Freezing of BRPs

1. Wash cells with 13 mL PBS and aspirate.
2. Add 5 mL of trypsin-EDTA and incubate at 37 °C for 3–5 min, until cells detach; gently tap the sides of the flask to assist detachment.
3. Add 10 mL of BRP growth medium to quench the trypsin and mix by pipetting.
4. Transfer cells to a 50 mL conical tube and spin at 423 × *g* for 4 min.
5. Aspirate media without disturbing the pellet.
6. To passage: resuspend in 6–9 mL of BRP growth medium and passage at a 1:3 ratio. Add media to complete a volume of 12 mL of BRP growth medium in T75 flasks or 25 mL BRP growth medium in T175 flasks.
7. To freeze: count cells using an automated cell counter or a hemocytometer, resuspend in freezing medium as 1×10^6 cells/mL and freeze in 1.0 mL volumes.

3.3 Direct Coculture of Endothelial Cells and Pericytes

1. Expand BRPs and HRECs in their respective culture media splitting at 1:3 ratios (Fig. 3a, b).
2. For assays of pericyte recruitment, pericyte differentiation or endothelial cell proliferation (determined through the final total number of endothelial cells plus pericytes in the plate),

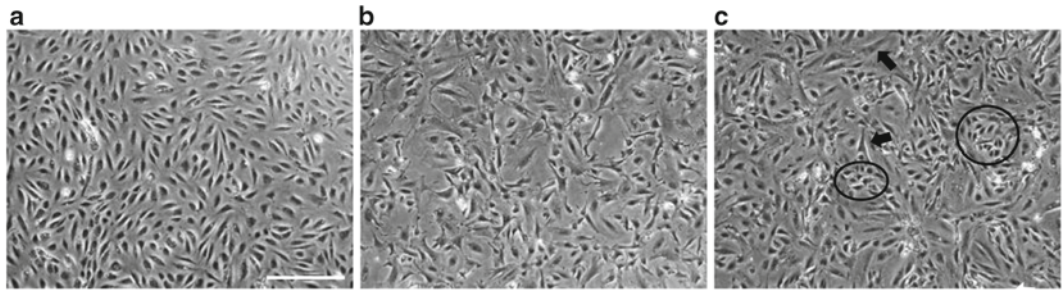

Fig. 3 Direct endothelial cell-pericyte coculture. (**a**) Human retinal endothelial cells in monoculture. (**b**) Bovine retinal pericytes in monoculture. (**c**) Example of direct coculture of endothelial cells (*circles*) and pericytes (*arrows*) plated at a 1:1 ratio and allowed to grow for 2 days. Bar: 500 μm

proliferation of pericytes can be arrested at 80 % confluence by incubating in mitomycin C (10 μg/mL) for 2 h.

3. Wash BRPs with PBS and detach from flask with trypsin-EDTA.
4. Plate in 24-well plates at a density of 2.0×10^4 cells per well in BRP culture media and allow to attach overnight.
5. Next day, detach HRECs as described in Subheading 3.1.2 and add an equal number of HRECs in BRP culture medium.
6. Incubate and assay as desired (Fig. 3c).
7. Simultaneously and using identical conditions, establish individual cultures of HRECs and proliferation-arrested BRPs as controls.

3.4 Indirect Coculture of Endothelial Cells and Pericytes in Transwells

1. Expand BRPs and HRECs in their respective culture media splitting at 1:3 ratios (*see* **Note 13**).
2. Wash BRPs with PBS and detach from flask with trypsin-EDTA.
3. Plate BRPs in 24-well plates at a density of 2.0×10^4 cells per well or in 6-well plates at a density of 1.5×10^5 cells per well in BRP culture media and allow to attach overnight.
4. Next day, detach HRECs as described in Subheading 3.1.2 and plate an equal number of HRECs into the upper chamber of transwells and allow to attach for 90 min.
5. Place transwells into the wells containing the BRPs (Fig. 4a).
6. Add 1 mL of BRP culture media.
7. Incubate and assay as desired.
8. Simultaneously and using identical conditions, establish individual cultures of HRECs and BRPs as controls, as well as a direct contact coculture control. For the latter, plate BRPs on the underside of the transwells and allow to attach overnight; flip over the transwells, insert into wells, and plate HRECs into the upper chamber of the transwells (Fig. 4b).

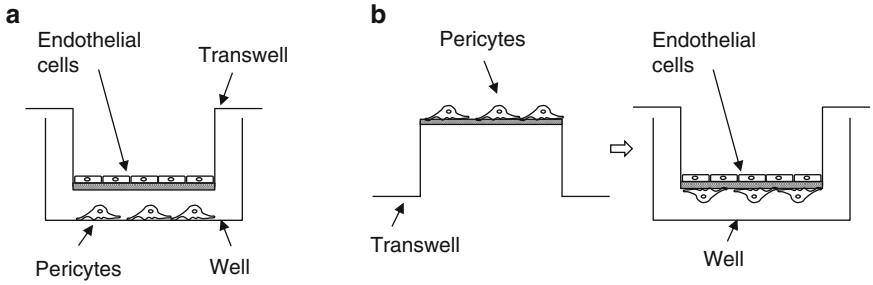

Fig. 4 (**a**) Indirect coculture of endothelial cells and pericytes in transwells. Pericytes are plated on 6- or 24-well plates overnight. Endothelial cells are plated at 1:1 ratio the next day on the upper chamber of correspondent 6- or 24-well transwells. (**b**) Control with direct contact through the transwell membranes. Pericytes are incubated overnight on the underside of the transwells, which are then flipped over and inserted in wells. Endothelial cells are plated on the upper chambers of the transwells

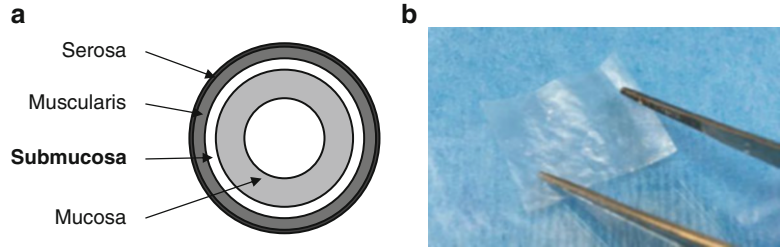

Fig. 5 Preparation of an extracellular matrix scaffold. (**a**) Cross-section of the porcine small intestine. (**b**) Rectangular scaffold after preparation

3.5 Coculture in a Three-Dimensional ECM Scaffold

3.5.1 Preparation of an ECM Scaffold from Porcine Small Intestine

1. Obtain the jejunum portion of the small intestine of a market-weight porcine donor, section into 30 cm long segments and open each segment longitudinally to form a rectangle.
2. Rinse well with tap water and scrape off the exterior (serosa and muscularis) and interior (mucosa) layers of the intestine with the edge of a scalpel handle. The remaining tissue is the submucosa layer (Fig. 5a).
3. Wash for 1 h in DI with rapid agitation on an orbital shaker.
4. Decellularize and disinfect to obtain acellular ECM scaffolds, by washing for 15 min in a solution of oxidizing agents such as 2.0% sodium hypochlorite and 2.0% hydrogen peroxide in DI with fast agitation.
5. Wash for 15 min once in sterile PBS and twice in sterile DI.
6. Let dry for 1–2 h inside a biosafety cabinet on top of clean saran wrap cleaned with 70% ethanol.
7. Sterilize each ECM scaffold separately with ethylene oxide and use within 6 months.

3.5.2 Coculture

1. Expand BRPs and HRECs in their respective culture media splitting at 1:3 ratios.
2. Use sterile scissors and forceps to cut 27 × 21 mm rectangles from a sterile ECM scaffold (Fig. 5b).
3. Use forceps to place a scaffold on the bottom of each well in a chamber slide (Fig. 6a).
4. Detach HRECs as described in Subheading 3.1.2, culture 5.0×10^4 HRECs per well on top of the ECM scaffold and incubate for 2 h in 1 mL of HREC culture media.
5. Carefully aspirate the HREC media (without touching the ECM scaffold), add an equal number of BRPs in 500 μL of coculture media to each well and allow to attach for 2 h.
6. Culture as desired; assay gene expression or image by immunofluorescent staining as desired (Fig. 6b) (*see* **Notes 14–16**).
7. Simultaneously and using identical conditions, establish cocultures of HRECs and BRPs as controls on chamber slides without a scaffold.

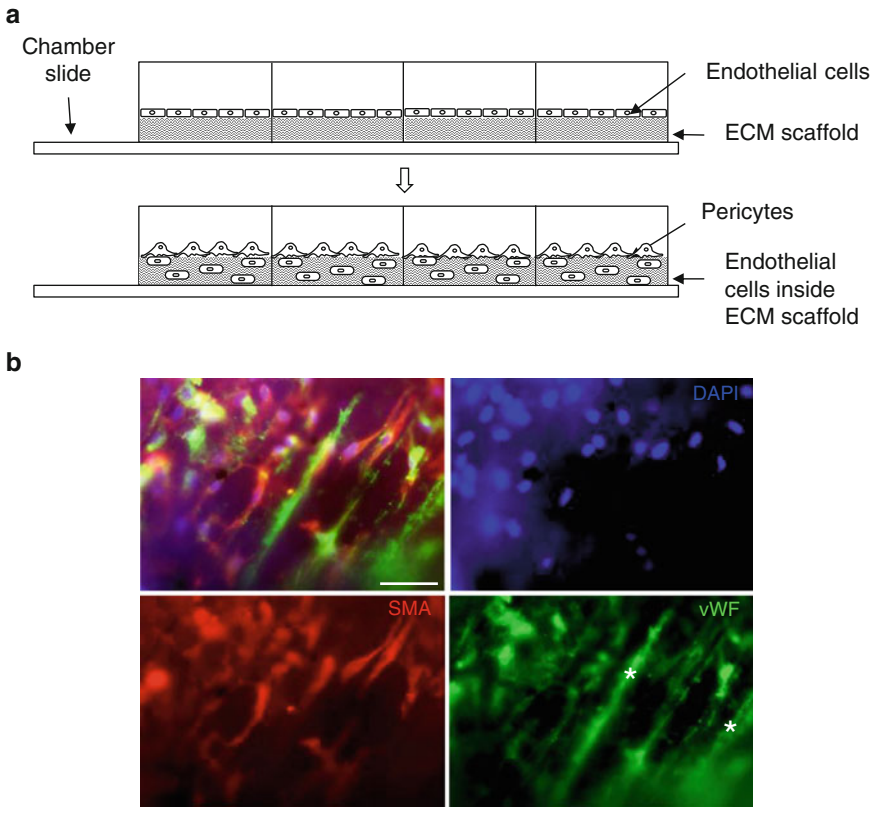

Fig. 6 Coculture of endothelial cells and pericytes in an ECM scaffold (decellularized small intestinal submucosa). (**a**) Endothelial cells are incubated in an ECM scaffold placed on the bottom of a chamber slide. Pericytes are added after 2 h. (**b**) Endothelial cells (stained with von Willebrand factor, vWF) and pericytes (stained with smooth muscle actin, SMA) locate inside the scaffold after 2 h of coculture. Scaffold fibers fluoresce in the green channel (*stars*). The out of focus location of multiple cells shows the 3D character of this coculture method. Bar: 50 μm

4 Notes

1. Calf eyes yield a higher number of pericytes with a higher proliferative potential than cells isolated from adult eyes.
2. Use glass flasks, not plastic, to make dilution.
3. Bovine calf serum 12133C from Sigma induces increased proliferation of pericytes.
4. Passage at 90% confluence. Confluence at these passage ratios is achieved in 3–6 days.
5. The dish prevents the eye from rolling and maintains sterility.
6. Keep the spear moist with PBS to avoid the retina from sticking to the spear.
7. The larger vessels in the retina, where mural cells are mainly smooth muscle cells, will be removed with this section. These vessels are visible with the naked eye. The remaining retina in the posterior segment will contain the pericyte-covered microvasculature (which is not visible with the naked eye).
8. Be careful not to remove any underlying pigmented tissue (i.e., the tapetum lucidum) or the retinal pigment epithelium.
9. If any loose pigmented tissue is observed, carefully remove it by aspiration (do with care as it can result in the aspiration of the entire retina).
10. Wash medium can be aspirated (instead of poured), but once again should be done with care to avoid the aspiration of the retina.
11. If "contaminants" are still visible after the EDTA treatment, keep the cells in BRP culture medium for a few more days and then repeat this step.
12. The most common "contaminants" are endothelial cells and fibroblasts. If left unattended, endothelial cells can become the 70% of the total cell population. Fibroblasts hardly reach populations higher than the 10% of the total cell population.
13. Arrest of cell growth is only necessary for direct culture, where endothelial cell growth is determined by final cell number including both endothelial cell and pericyte total count. This is not needed in coculture since cells are physically separated.
14. Interactions between HRECs and BRPs are observed after 2–4 days.
15. Image scaffold without sectioning as cells tend to detach from thinner sections during the washes of staining procedures.
16. Imaging of scaffolds works very well with upright fluorescence microscopy. Note in Fig. 4 the out of focus (i.e. out of plane) location of several cells, due to the 3D character of this coculture method. vWF antibody (catalog number A0082) (Dako)

at a 1:100–200 dilution clearly stains endothelial cells (Fig. 6b). We have not obtained good results working with lectin for staining of endothelial cells on SIS membranes. For pericytes, SMA antibody (catalog number C6198) (Sigma) works very well at a 1:400 dilution (Fig. 6b). Alternatively, live cells can be prelabeled before seeding on the chamber slide using a PKH26 cell membrane linker kit (catalog number PKH26GL) (Sigma) to label endothelial cells red and a PKH67 cell linker kit (catalog number PKH67GL) (Sigma) to label pericytes green. To label 1×10^6 live cells, detach cells from flask and wash twice with serum-free media. Add 0.5 μL of PKH dye to 50 μL of diluent-C and vortex. After second wash, resuspend cells in 50 μL diluent-C and mix with dye solution. Incubate for 3–5 min at room temperature. Add complete media (with serum) to quench reaction and wash two to three more times in complete media. Resuspend and culture as desired.

Acknowledgements

This work was supported by NIH grants R00EY021624 (JA) and R01EY005318 (PDA).

References

1. Orlidge J, D'Amore P (1987) Inhibition of capillary endothelial cell growth by pericytes and smooth muscle cells. J Cell Biol 105(3): 1455–1462
2. Antonelli-Orlidge A, Saunders K, Smith S, D'Amore P (1989) An activated form of transforming growth factor beta is produced by cocultures of endothelial cells and pericytes. Proc Natl Acad Sci 86(12):4544–4548
3. Dodge A, Lu X, D'Amore P (1993) Density-dependent endothelial cell production of an inhibitor of smooth muscle cell growth. J Cell Biochem 53:21–31
4. Hirschi K, Rohovsky S, D'Amore P (1998) PDGF, TGFbeta and heterotypic cell-cell interactions mediate endothelial cell-induced recruitment of 10T1/2 cells and their differentiation to a smooth muscle fate. J Cell Biol 141(3):805–814
5. Hirschi K, Rohovsky S, Beck L, Smith S, D'Amore P (1999) Endothelial cells modulate the proliferation of mural cell precursors via platelet-derived growth factor-BB and heterotypic cell contact. Circ Res 84(3): 298–305
6. Darland D, Massingham L, Smith S, Piek E, Saint-Geniez M, D'Amore P (2003) Pericyte production of cell-associated VEGF is differentiation-dependent and is associated with endothelial survival. Dev Biol 264(1):275–288
7. Darland D, D'Amore P (2001) TGFb is required for the formation of capillary-like structures in three-dimensional cocultures of 10T1/2 and endothelial cells. Angiogenesis 4:11–20
8. Arboleda-Velasquez JF, Primo V, Graham M, James A, Manent J, D'Amore P (2014) Notch signaling functions in retinal pericyte survival. Invest Ophthalmol Vis Sci 55(8):5191–5199
9. Sánchez-Palencia D, Rathan S, Ankeny C, Fogg R, Briceno J, Yoganathan A (2015) Mechanotransduction in small intestinal submucosa scaffolds: fabrication parameters potentially modulate the shear-induced expression of PECAM-1 and eNOS. J Tissue Eng Reg Med. doi:10.1002/term.2040
10. Bryan B, D'Amore P (2008) Pericyte isolation and use in endothelial/pericyte coculture models. In: Cheresh D (ed) Methods of enzymology, 1st edn. Elsevier, San Diego, CA

Chapter 5

Characterization of Cancer Stem Cells

Stefania Orecchioni and Francesco Bertolini

Abstract

There is biological and clinical evidence that mammalian tumors are highly heterogeneous at single-cell level, and that only a minority of the cancer cells have limitless replicative potential in vitro and in vivo. Here we review the different strategies currently used for the functional isolation of cancer cells with in vivo cancer initiation potential and self-renewal. These tools are currently used to better define their molecular, phenotypic, and drug-resistance characteristics in preclinical and clinical studies.

Key words Cancer stem cells, Cancer-initiating cells, Methods, FACS, Side population, Aldehyde dehydrogenase, Tumorspheres, Tumorigenicity

1 Introduction

The majority of human cancers display a significant degree of intratumor heterogeneity in various phenotypic and functional features, such as differentiation grade, cellular morphology, gene expression, proliferative rate, and angiogenic and metastatic potential [1]. Growing evidence suggests that tumor cell heterogeneity might be attributed to a clonal evolutionary process, driven by genetic instability, and to differentiation of stem-like cells, the so-called cancer stem cells or cancer-initiating cells (CSCs/CICs) [2]. CSCs are described as a small population of undifferentiated cells characterized by indefinite self-renewal ability (through asymmetrical cell division), high tumorigenicity, and differentiation into non-CSC progeny that leads to the production of all cell types in the tumor, thus contributing to intratumor heterogeneity. According to the CSC hypothesis, tumorigenic stem-like cells within heterogeneous tumors are responsible for the tumor initiation and for the generation of distant metastasis [3, 4]. Moreover, since CSCs are highly resistant to chemotherapeutics, they are involved in local or metastatic tumor recurrence after therapy [5, 6].

Malignant stem cells were first identified in 1994 by John Dick and colleagues in acute myeloid leukemia (AML) [7]. The Dick

Domenico Ribatti (ed.), *Tumor Angiogenesis Assays: Methods and Protocols*, Methods in Molecular Biology, vol. 1464,
DOI 10.1007/978-1-4939-3999-2_5,

laboratory isolated a phenotypically distinct subset of leukemic cells (CD34+CD38−) from the peripheral blood of AML patients, characterized by a rate of self-renewal higher than normal hematopoietic stem cells. Only these cells, with stem-like properties, were able to recapitulate the morphological features of the original malignancy upon transplantation into immunocompromised mice in limiting dilution assays. This pioneering work provided the paradigm for the general CSC model and laid the foundations for all CSC-related studies in solid tumors that followed.

Based on similar techniques previously applied to the hematopoietic model, Al-Hajj and colleagues have been the first to identify and characterize CSCs from breast cancer [8]. Since then, CSCs have been identified in various solid tumors, including melanoma [9], glioblastoma [10], lung carcinoma [11], prostate [12], and ovarian cancer [13], still using the same approach of combined flow cytometry and serial xenotransplantation in mice.

However, since the identification of rare malignant stem cells via flow cytometry is a critical step [14, 15], further methodologies for CSC isolation have been improved by using marker-independent strategies. Thus, the use of CSC-specific surface markers must be associated with other functional assays, namely (a) detection of side-population (SP) phenotypes by Hoechst 33342 dye exclusion [16, 17], (b) assessment of aldehyde dehydrogenase (ALDH) enzymatic activity [18, 19], and (c) evaluation of growth potential as floating spheres in serum-free medium [20, 21].

Since all the methods above mentioned have their limitations in identifying CSCs unequivocally, it might be more advantageous to use combinatorial markers and methodologies, especially when a whole tumor tissue is analyzed [22]. Indeed, prospective identification and isolation of CSCs from solid tumors, and a better understanding of the properties of these cells, will lead to the development of novel therapeutic strategies aimed to eradicate the engine of tumor progression. We describe here methods currently used for CSC identification and characterization, starting from primary solid tumors.

2 Materials

2.1 Laboratory Equipment

1. Laminar flow biosafety cabinet (BSL2).
2. Water bath.
3. Hemocytometer.
4. Inverted microscope.
5. 37 °C Humidified incubator with 5 % CO_2.
6. Falcon 40 μm cell strainers.
7. 0.20 μm Syringe filters.

2.2 Sample Acquisition and Dissociation

1. Dissociation solution: Dulbecco's modified Eagle's medium:Ham's nutrient mixture F-12 (1:1) (DMEM/F12) supplemented with 1× collagenase/hyaluronidase mixture (10× stock, Stem Cell Technologies) and 125 U/mL DNasi I (Life Technologies).
2. RNAlater RNA Stabilization Reagent (QIAGEN).
3. 4% Formaldehyde solution.
4. Optimal cutting temperature (O.C.T.) solution (Bio Optica).
5. Nalgene cryogenic vials.
6. Nalgene Cryo 1 °C cell-freezing container.
7. Dimethyl sulfoxide (DMSO).
8. Liquid nitrogen transfer container.
9. Dry ice.
10. Forceps.
11. Scalpels.

2.3 Cell Culture

1. Complete growth medium: DMEM/F12 supplemented with 10% fetal bovine serum (FBS) heat inactivated, 2 mM L-glutamine, 100 U/mL penicillin, and 100 μg/mL streptomycin.
2. Trypsin-EDTA 1× in PBS without Phenol Red Ca^{2+} and Mg^{2+}.
3. PBS without Ca^{2+} and Mg^{2+}.
4. T-25 and T-75 tissue culture flasks.
5. Various-sized multiwell plates.

2.4 Antigen Expression and Cell Sorting

1. Navios Flow Cytometer (Beckman Coulter).
2. Influx cell sorter (BD Biosciences).
3. Ethylenediamine tetraacetic acid (EDTA).
4. Bovine serum albumin (BSA).
5. Red blood cell lysis buffer: 10 mM Potassium bicarbonate ($KHCO_3$), 155 mM ammonium chloride (NH_4Cl), 0.1 mM EDTA.
6. 7-Aminoactinomycin D (7-AAD) Viability Dye (Beckman Coulter).
7. SYTO 16 Green Fluorescent Nucleic Acid Stain (Life Technologies).
8. CD133/1 (AC133, Prominin1) (Miltenyi Biotec) and respective isotype control.

2.5 Marker-Independent Methods

1. Verapamil (Sigma-Aldrich).
2. Hoechst 33342 (Sigma-Aldrich).

3. ALDEFLUOR™ kit (STEMCELL Technologies).
4. Complete tumorsphere medium: DMEM/F12 supplemented with 5 μ/mL insulin, 20 ng/mL epidermal growth factor (EGF), 20 ng/mL basic fibroblast growth factor (bFGF), and 1× B27 supplement (50× stock, Life Technologies).
5. Ultra-low-attachment plates.

2.6 In Vivo Tumorigenicity

1. NOD/SCID interleukin-2 receptor γ (IL-2Rγ)–null (NSG) immunocompromised mice.
2. BD Matrigel™ Basement Membrane Matrix (BD Biosciences).
3. Round-bottomed 96-well microplates.
4. Insulin syringes or Hamilton syringe (2biological Instruments).
5. Avertin (2,2,2-Tribromoethanol) (Sigma-Aldrich).
6. Hematoxylin and eosin.

3 Methods

3.1 Tumor Specimen Acquisition and Collection

Written informed consent and institutional review board (IRB) approval for research on human samples are basic prerequisites for all specimen acquisition. Fresh tissue sample from cancer resection should be collected in a sterile container as soon as possible after removal from the operating room. For nucleic acid isolation, it is crucial that the specimen must be frozen within 20 min in order to prevent degradation (RNA starts to degrade within minutes). Tumor fragments should be flash frozen and kept at −20 °C or −80 °C, or in liquid nitrogen for long-term storage. This provides excellent tissue integrity and a wide array of options for tissue analysis. Alternatively, immediately stabilize the sample in RNAlater RNA Stabilization Reagent (*see* **Note 1**). For xenotransplantation studies time is less critical, but the tissue should be kept refrigerated and in medium until transplantation. In our experience, patient-derived xenografts have been successfully established by implanting tumor samples after overnight storage at 4 °C. Additionally, save part of the specimen for further histological characterization by embedding a portion of the tumor in optimal cutting temperature (O.C.T.) solution, followed by flash freezing (*see* **Note 2**), or by fixing one part of the tumor in 4% phosphate-buffered formalin and embedding in paraffin.

3.2 Sample Dissociation

Carry out all procedures in aseptic conditions under a laminar flow hood to minimize contaminations. Note that all fresh tissue should be handled in a biosafety cabinet using Biosafety Level 2 (BSL2) techniques.

1. Prepare dissociation solution as described in Subheading 2.2 and place into a 50 mL conical tube.
2. Transfer the tumor to a sterile petri dish using sterile forceps.
3. Mince the sample with two scalpels in a cross-wise manner until tumor is reduce to a paste and the final tissue fragments are small enough to pass through the tip of a 5 mL pipette (*see* **Note 3**).
4. Transfer the cut-up tumor to the tube containing the dissociation solution (prepared in **step 1**) and incubate into a 37 °C water bath (*see* **Note 4**).
5. Mix up and down the tumor fragments every 15 min using a 5 mL pipette, and then a 1000 µL micropipette to further disintegrate cell clumps, until the tumor is well dissociated (*see* **Note 5**).
6. Filter the cell suspension through a 40 µm nylon mesh cell strainer into a new 50 mL sterile tube and use the rubber end of the syringe plunger to break up clumps by gently squeezing cells against the cell strainer.
7. Thoroughly rinse the strainer with PBS and recover any residual from underneath the cell strainer in order to minimize cell loss.
8. Centrifuge for 5 min at 350×*g*, discard the supernatant, and resuspend the cell pellet in a small volume of cold ammonium chloride lysis buffer (prepared as described in Subheading 2.4) to lyse red blood cells (*see* **Note 6**); incubate on ice for 5–10 min, wash with a 10× volume of PBS, and centrifuge again.
9. Resuspend cells in DMEM/F12 and calculate the viable cell concentration with a hemocytometer and trypan blue.

3.3 In Vitro Expansion of Primary Tumor Cells

1. After evaluation of viability, resuspend cells in complete growth medium described in Subheading 2.3.
2. Plate the primary cell suspension in standard tissue culture flasks; use T25 flasks or multiwell plates depending on how many cells are available.
3. Culture cells in a 37 °C humidified incubator with 5% CO_2; viable tumor cells should attach to the flask within 12–24 h.
4. Inspect the culture regularly by inverted microscope to monitor cell growth and confluency; replace medium weekly, or when required as it looks depleted (orange/yellow color), by changing half volume with fresh complete culture medium (*see* **Note 7**).
5. Split the culture when cells are 70–90% confluent by trypsinization with an appropriate volume of 0.25% trypsin and 0.02% EDTA until all adherent cells detach (about 3–5 min).
6. When all cells are detached, inactivate trypsin by adding an equal volume of complete DMEM/F12 and wash the flask with PBS to collect all detached cells into a 15 mL tube.

7. Centrifuge at 350 × *g* for 5 min, discard supernatant, and resuspend the cell pellet in fresh complete culture medium.
8. Perform a cell count using trypan blue exclusion assay on a hemacytometer (*see* **Note 8**).
9. Replate cells at a concentration between ranges of 1 and 2×10^4 cells/cm^2.
10. Continue cell culture for up to five passages.

3.4 Methods to Characterize CSCs

The two main methods that are used to prospectively purify and characterize CSCs include marker-dependent and marker-independent strategies. Flow cytometry played a crucial role in identifying CSCs either by marker-dependent and by marker-independent methods, such as side-population analysis, aldefluor assay, and sphere formation assays, combined with limiting dilution xenotransplantation in immunodeficient mice. Here, we describe the principal in vitro and in vivo strategies used to identify CSCs. Importantly, the CSC-specific detection methods illustrated hereinafter have their limitations in identifying malignant stem cells unequivocally, especially when tumor tissue is analyzed. Therefore, the use of combinatorial markers and methodologies is imperative in order to isolate and characterize a putative CSC population.

3.4.1 Antigen Expression and Cell Sorting

CSCs are frequently identified and characterized by multiparametric flow cytometric analysis that represents a powerful technique to simultaneously interrogate the phenotype of single cells in suspension with high performance and reliability. Furthermore, it enables the separation of living cells by fluorescence-activated cell sorting (FACS), using antibodies directed at cell-surface markers in order to isolate rare CSCs from a large heterogeneous cell population.

1. Harvest cells within 7 days of primary cultures, wash with PBS, and perform a cell count and viability analysis.
2. Split cells in two aliquots for flow cytometric analysis and for cell sorting, respectively.
3. Adjust cell number to a concentration of $1–5 \times 10^6$ cells/mL in FACS buffer (PBS with 2 mM EDTA and 0.5 % bovine serum albumin).
4. Add the appropriate number of cells to be stained into FACS tubes.
5. Add conjugated antibody (0.1–10 μg/mL, or a previously titrated amount) or respective isotype controls and vortex gently to mix. Incubate cells for at least 15 min at 4 °C in the dark (*see* **Note 9**).
6. Remove any unbound antibody by washing cells in FACS buffer. Centrifuge at 350 × *g* for 5 min and decant the buffer.

7. Resuspend stained cells in 200–400 μL of FACS buffer for flow cytometric analysis (*see* **Note 10**). Keep the cells at 4 °C until your scheduled time for analysis.
8. Acquire cells (at least 1×10^6 total cells per sample) on a standard flow cytometer and perform analysis after selection of DNA+ (Syto16+) and viable (7-AAD−) cells. Set the analysis gates with the aid of "fluorescence minus one" isotype controls.
9. The staining panel, both for analysis and cell sorting, includes various markers depending on the tumor type (an overview of markers used for the characterization of CSCs in different tumors is given in ref. 23). For instance, CD133 (prominin-1) has been recognized as a putative CSCs marker for glioblastoma, breast, colon, prostate, kidney, pancreatic, and lung carcinomas, liver and brain tumors, and melanoma [4] (*see* **Note 11**).
10. For cell sorting, resuspend stained cells from **step 7** in appropriate volume of FACS buffer so that the final cell concentration is $4–5 \times 10^6$ cells/mL.
11. Sort CD133-positive and CD133-negative fractions using a three laser Influx high speed cell sorter (BD Biosciences) equipped with a Class I biosafety cabinet (*see* **Note 12**). The purity of CD133+ and CD133− sorted populations is routinely 90%.
12. Culture sorted cell populations in standard medium for further in vitro and in vivo experiments.

3.4.2 Side-Population Assay

The side-population (SP) discrimination assay is a flow cytometric strategy used to isolate CSCs by efflux of incorporated dyes like Hoechst 33342, via multi-drug resistance (MDR) and ATP-binding cassette (ABC) transporters expressed within the cell membrane. A peculiar characteristic of both normal and malignant stem cells is the overexpression of ABC transporters as efflux pumps protect stem cells from damage by xenobiotic substances [24]. Then, the flow cytometric profile of the cells which actively efflux the dye out has a distinctive feature and they form a distinct small cell population (<0.1% of the total cell number), termed the "side population," that shows little or no fluorescence with Hoechst 33342 [25]. Thus, the use of Hoechst 33342 to detect CSCs as an SP overcomes the lack of a tumor-specific phenotype and replaces it with a more direct and functional marker. Results obtained with this method must be rigorously validated anyway using other CSC-specific detection methods described in the previous and following sections.

1. Count viable nucleated cells, resuspend in pre-warmed standard medium, and divide cells in two aliquots; adjust cell number to a concentration of 1×10^6 cells/mL in medium.
2. Add to both cell suspensions the Hoechst 33342 stock solution to obtain a final concentration of 5 μg/mL.

3. Add only to the aliquot control 50 μM verapamil (ABCB1 and ABCC1 transporter inhibitor, *see* **Note 13**) and leave the other aliquot untreated.
4. Incubate the cell/dye suspensions for 90 min at 37 °C in the dark and gently invert the tubes every 15–20 min to avoid cell settling and clumping (*see* **Note 14**).
5. After 90 min, spin the cells down at 4 °C (in a precooled rotor) and resuspend the cell pellets in an appropriate volume of cold FACS buffer (*see* **Note 15**).
6. If the SP assay is combined with staining for cell surface phenotyping, the cells can now be processed for antibody staining as described in Subheading 3.4.1. Matching the SP assay with the classical cell-surface staining protocols can lead to a further characterization of putative CSC populations.
7. Immediately prior to flow cytometry, add 7-AAD (to a final concentration of 2 μg/mL) and incubate cells for 15 min at 4 °C in the dark. Maintain cell suspensions at 4 °C and protected from light at all times.
8. Acquire at least 500,000 total cells per sample on a suitable flow cytometer.
9. The Hoechst 33342 dye is excited at 350 nm ultraviolet (UV). Therefore, an optimal SP resolution requires a flow cytometer equipped with a UV laser. To measure the resultant fluorescence at two wavelengths use a 450/20 band-pass filter and 675 long-pass filter for detection of Hoechst Blue and Red, respectively, and the 610 short-pass dichroic mirror to split the emission wavelengths.
10. Create the following two-parameter plots (*x*-axis vs. *y*-axis) with all the parameters in linear scale:
    (a) Forward scatter (FSC) versus side scatter (SSC)
    (b) 7-AAD versus SSC
    (c) Hoechst Red versus Hoechst Blue
11. Exclude debris and dead cells in plots a and b, respectively.
12. Identify the SP on the Hoechst Red versus Hoechst Blue plot (on the left side of the plot, showing low fluorescence intensity at both emission wavelengths).
13. Optional: Sort SP-positive and SP-negative fractions and evaluate the purity. Culture sorted cell populations in standard medium for further in vitro and in vivo experiments.

3.4.3 Aldehyde Dehydrogenase (ALDH) Activity

The aldehyde dehydrogenase 1 (ALDH1) isoform catalyzes the conversion of retinol to retinoic acid in normal and malignant stem cells and its activity has been used as a functional stem cell marker to isolate CSCs in different tumor types [26]. Cells with ALDH1 enzymatic activity can be detected using a simple and rapid method

that is now commercially available (STEMCELL Technologies) and it works with cultured cells as well as with cells isolated from solid tumors.

1. Perform a viable cell count and resuspend cells in ALDEFLUOR™ assay buffer containing the ALDH substrate Bodipy™-aminoacetaldehyde (BAAA) and efflux inhibitor (*see* **Notes 16** and **17**).
2. Transfer portion of cells from **step 1** to negative control tube containing the ALDH enzyme inhibitor diethylaminobenzaldehyde (DEAB, 50 mmol/L).
3. Incubate at 37 °C for 30–60 min.
4. Spin the cells down at 4 °C (in a precooled rotor) and resuspend the cell pellets in an appropriate volume of cold FACS buffer (*see* **Note 18**).
5. If the aldefluor assay is combined with staining for cell surface phenotyping, the cells can now be processed for antibody staining as described in Subheading 3.4.1.
6. Measure the cellular fluorescence with the green fluorescence channel (520–540 nm) of a standard flow cytometer and perform analysis setting up proper gate according to instruction in ALDEFLUOR™ kit. Since only cells with an intact cellular membrane can retain BAA^-, only viable $ALDH^{bright}$ cells are identified.
7. Optional: Sort ALDH-positive and ALDH-negative fractions and evaluate the purity. Culture sorted cell populations in standard medium for further in vitro and in vivo experiments.

3.4.4 Sphere Formation Assay

In the sphere formation assay, cells from solid tumors are grown in serum-free, non-adherent conditions forming spherical structures (tumorspheres). This assay can be used to estimate the percentage of CSCs present in a population of tumor cells since only malignant stem cells can survive and proliferate in this environment.

1. Resuspend freshly isolated tumor cells or sorted cells into a single-cell suspension in complete tumorsphere medium described in Subheading 2.5. Importantly, B27 should be freshly added before use.
2. Perform a viable cell count with trypan blue.
3. Plate cell suspension onto ultra-low-attachment plates at appropriate density in triplicate. The optimum density is usually between 200 and 600 cells/cm^2 depending on cell type.
4. Maintain cells in a 5% CO_2-humidified incubator at 37 °C for 1 week without replenishing the medium so as not to disturb the formation of the tumorspheres.

5. After 1-week incubation, analyze sphere formation under an inverted light microscope and count the number of tumorspheres (at 40× magnification) whose size can vary from less than 50 to 250 μm. They are easily distinguishable from aggregated cells as the cells seem to be fused together and single cells cannot be identified.
6. Sphere-forming efficiency (%) is calculated according to the formula (number of spheres per wells/number of cells seeded per well) × 100.

3.4.5 In Vivo Tumorigenicity Evaluation

A crucial characteristic of CSCs is their ability to generate tumors as xenografts in immunodeficient mice. This unique feature must therefore be rigorously verified in animal models to prove the self-renewal and differentiation potential of the cellular subpopulation isolated with FACS and other marker-independent methods described above.

1. Count viable cells, and serially dilute in PBS using a broad range of cell doses (from 10^2 to 10^6) to assess the optimum range of tumorigenicity.
2. Thaw on ice an aliquot of Matrigel and mix equivalent volume of cell and Matrigel in a round-bottomed 96-well plate that is resting on ice (*see* **Note 19**).
3. Prior to injection into mice, gently mix the cells/Matrigel suspensions and aspirate 20–100 μL per injection into cooled insulin syringe or a Hamilton syringe for the smallest volumes (*see* **Note 20**).
4. Anesthetize mice with Avertin (375 mg/kg) intraperitoneally.
5. Inject orthotopically at least five mice with each cell dose.
6. Determine an approximate median of tumorigenic frequency and then use tighter dilutions to identify the minimum tumorigenic dose.
7. Once xenografts are established, tumors should be compared histologically to the primary patient specimen (*see* Subheading 3.1) by hematoxylin and eosin staining.

4 Notes

1. For RNAlater long-term storage at −20 °C, first incubate tumor fragments (placed in separate cryovials) overnight in the RNA stabilization reagent at 4 °C. Then transfer the tissue, in the reagent, to −20 °C for archival storage.
2. Cover the cryomold with a thin layer of O.C.T. and, using sterile forceps, transfer the specimen to the cryomold. Fill it with more O.C.T. by paying attention to avoid air bubble for-

mation, and freeze the mold in liquid nitrogen by holding the cryomold with a forceps over the opening of the liquid nitrogen transfer container (freezer gloves and a face shield should be used during this procedure).

3. Many studies report that the implantation of tumor fragments in mice has a higher transplantation success rate than single-cell suspension injection. Then, in this step, it is important to keep aside small fragments (2–3 mm square) of tumor for both cryopreservation and direct implantation of the primary sample into immunodeficient mice. For cryopreservation: place no more than five fragments in a cryovial and fill it with a 90% FBS + 10% DMSO solution. Freeze the fragments by slowly decreasing the temperature 1 °C/min in a Nalgene Cryo 1 °C cell-freezing container filled with isopropanol. Place the container at −80 °C overnight before transferring the vials to liquid nitrogen cryotanks.
4. Gentle agitation of tissue fragments may improve tumor dissociation. If use a shaker, or a tube rotator in a 37 °C incubator, set motion at low to moderate speed.
5. The digestion progression can be monitored by gross observation and microscopic evaluation of the digestion medium (large undigested material may contain cell debris, fat, and extracellular matrix). Depending on the sample type, tumor dissociation should take from 30 min to 4 h. Since longer incubation times will reduce cell viability, the sample should not be left in the digestion medium for longer than necessary. Stop digestion by adding DMEM/F12 in equal amount of collagenase mix added.
6. Adjust the pH to 7.2 and sterilize the solution using a 0.20 μm filter before use. Keep at 4 °C.
7. At the first medium change, collect also culture supernatant containing unattached cells and plate it into a new flask to provide a backup culture.
8. When possible, freeze earlier passages of the primary culture in 90% FBS + 10% DMSO and store in liquid nitrogen for further experiments.
9. If you use primary unlabeled antibodies, after completing **step 5**, dilute the fluorochrome-labeled secondary antibody in FACS buffer (see individual antibody data sheet for the appropriate dilution) and then resuspend the cells in this solution. Incubate for at least 30 min at 4 °C in the dark. Wash the cells twice by centrifugation at 350 × *g* for 5 min and resuspend the cell pellet in 200–400 μL of FACS buffer for flow cytometric analysis.

10. If you need to preserve cells for several days, after completing **step 6** instead of resuspending cells in FACS buffer, add 100–200 μL 4% paraformaldehyde and incubate for 15 min at room temperature. Centrifuge samples at 350×*g* for 5 min and resuspend the cell pellet in 200–400 μL of FACS buffer. Fixation will stabilize the light scatter and inactivate most biohazardous agents. The fixation for different antigens will require optimization by the user.
11. While CD133 has been efficiently used as a single marker for the isolation of CSCs in colorectal cancer and brain tumors, intratumoral heterogeneity makes it difficult to define universal stemness markers. Thereby, a set of markers are necessary to identify and characterize CSCs from other tumor types (*see* ref. 23).
12. Continuously cool the samples to 4 °C during the procedure. Perform a forward scatter pulse height and side scatter analysis to exclude cell clusters and doublets. Perform a two-way cell sorting procedure with a 140 μm nozzle with a 5.5-PSI pressure, and with an event rate of 1000 events per second, using a sort pure mode (optimal conditions need to be optimized depending on the instrument and/or the cells sorted). Collect samples into sterile polypropylene tubes containing sterile FACS buffer, and use for further in vitro and in vivo studies.
13. A significant number of ABC transporter inhibitors is available; based on both the tumor type and the type and content of ABC transporters, the use of a different inhibitor could be required (e.g., verapamil, cyclosporine A, and probenecid target the ABCB1 protein, while fumitremorgin C blocks the ABCG2 transporter).
14. It is crucial that the temperature throughout the sample is maintained at 37 °C. To ensure a correct temperature control, the Hoechst incubation step is usually performed in a water bath. Otherwise, in order to avoid manual mixing of the tubes, dye incubation step can also be successfully carried out in a 37 °C incubator equipped with a gentle shaker.
15. In order to inhibit further dye efflux, the cells must be kept at 4 °C for the rest of the experiment. Thus, steps following the Hoechst staining (e.g., washing, centrifugation, antibody staining, and data acquisition) should be carried out in the cold and in the dark, for minimizing metabolic activity and preserving the Hoechst profile.
16. Perform the assay using different sample concentrations (range from 1×10^5 to 2×10^6 cells/mL) and select the cell concentration that better discerns between $ALDH^{bright}$ and $ALDH^{low}$ cells minimizing background ratio.
17. BAAA is a visible light excitable fluorochrome that diffuses freely across the plasma membrane of intact viable cells. Only

cells with ALDH activity convert BAAA into the fluorescent product Bodipy™-aminoacetate (BAA–). The reaction product BAA– is retained inside cells since its exclusion through ABC transporters is blocked by efflux inhibitors contained into the assay buffer. To optimize the assay, it may be useful to add other efflux inhibitors (e.g., verapamil, probenecid, or 2-deoxy-D-glucose).

18. In order to inhibit efflux of BAAA and of BAA– and to prevent loss of fluorescence intensity, the cells must be kept at 4 °C for the rest of the experiment.
19. The final 1:1 cells/Matrigel suspension volume depends upon the injection site ranging from 20 μL (e.g., renal capsule and brain) to 100 μL (subcutaneous and mammary fat pad).
20. Traditionally, CSC research has been carried out using severe combined immunodeficient (SCID) or nonobese diabetic SCID (NOD/SCID) mice. However, the use of more highly immunocompromised NOD/SCID interleukin-2 receptor γ (IL-2Rγ)–null (NSG) mice lacking T, B, and NK cells can increase the detection of tumorigenic cells.

Acknowledgments

Supported in part by AIRC (Associazione Italiana per la Ricerca sul Cancro), Fondazione Umberto Veronesi, and Ministero della Salute.

References

1. Marusyk A, Polyak K (2010) Tumor heterogeneity: causes and consequences. Biochim Biophys Acta 1805:105–117
2. Singh AK, Arya RK, Maheshwari S, Singh A, Meena S, Pandey P, Dormond O, Datta D (2015) Tumor heterogeneity and cancer stem cell paradigm: updates in concept, controversies and clinical relevance. Int J Cancer 136:1991–2000
3. Reya T, Morrison SJ, Clarke MF, Weissman IL (2001) Stem cells, cancer, and cancer stem cells. Nature 414:105–111
4. Ribatti D (2012) Cancer stem cells and tumor angiogenesis. Cancer Lett 321:13–17
5. Martin-Padura I, Marighetti P, Agliano A, Colombo F, Larzabal L, Redrado M, Bleau AM, Prior C, Bertolini F, Calvo A (2012) Residual dormant cancer stem-cell foci are responsible for tumor relapse after antiangiogenic metronomic therapy in hepatocellular carcinoma xenografts. Lab Invest 92:952–966
6. Dawood S, Austin L, Cristofanilli M (2014) Cancer stem cells: implications for cancer therapy. Oncology 28:1101–1107
7. Lapidot T, Sirard C, Vormoor J, Murdoch B, Hoang T, Caceres-Cortes J, Minden M, Paterson B, Caligiuri MA, Dick JE (1994) A cell initiating human acute myeloid leukaemia after transplantation into SCID mice. Nature 367:645–648
8. Al-Hajj M, Wicha MS, Benito-Hernandez A, Morrison SJ, Clarke MF (2003) Prospective identification of tumorigenic breast cancer cells. Proc Natl Acad Sci U S A 100:3983–3988
9. Fang D, Nguyen TK, Leishear K, Finko R, Kulp AN, Hotz S, Van Belle PA, Xu X, Elder DE, Herlyn M (2005) A tumorigenic subpopulation with stem cell properties in melanomas. Cancer Res 65:9328–9337
10. Singh SK, Clarke ID, Terasaki M, Bonn VE, Hawkins C, Squire J, Dirks PB (2003) Identification of a cancer stem cell in human brain tumors. Cancer Res 63:5821–5828

11. Eramo A, Lotti F, Sette G, Pilozzi E, Biffoni M, Di Virgilio A, Conticello C, Ruco L, Peschle C, De Maria R (2008) Identification and expansion of the tumorigenic lung cancer stem cell population. Cell Death Differ 15:504–514
12. Collins AT, Berry PA, Hyde C, Stower MJ, Maitland NJ (2005) Prospective identification of tumorigenic prostate cancer stem cells. Cancer Res 65:10946–10951
13. Bapat SA, Mali AM, Koppikar CB, Kurrey NK (2005) Stem and progenitor-like cells contribute to the aggressive behavior of human epithelial ovarian cancer. Cancer Res 65:3025–3029
14. Zimmerlin L, Donnenberg VS, Donnenberg AD (2011) Rare event detection and analysis in flow cytometry: bone marrow mesenchymal stem cells, breast cancer stem/progenitor cells in malignant effusions, and pericytes in disaggregated adipose tissue. Methods Mol Biol 699:251–273
15. Tirino V, Desiderio V, d'Aquino R, De Francesco F, Pirozzi G, Graziano A, Galderisi U, Cavaliere C, De Rosa A, Papaccio G, Giordano A (2008) Detection and characterization of CD133+ cancer stem cells in human solid tumours. PLoS One 3:e3469
16. Hadnagy A, Gaboury L, Beaulieu R, Balicki D (2006) SP analysis may be used to identify cancer stem cell populations. Exp Cell Res 312:3701–3710
17. Song J, Chang I, Chen Z, Kang M, Wang CY (2010) Characterization of side populations in HNSCC: highly invasive, chemoresistant and abnormal Wnt signaling. PLoS One 5:e11456
18. Ma I, Allan AL (2011) The role of human aldehyde dehydrogenase in normal and cancer stem cells. Stem Cell Rev 7:292–306
19. Storms RW, Trujillo AP, Springer JB, Shah L, Colvin OM, Ludeman SM, Smith C (1999) Isolation of primitive human hematopoietic progenitors on the basis of aldehyde dehydrogenase activity. Proc Natl Acad Sci U S A 96:9118–9123
20. Liu JC, Deng T, Lehal RS, Kim J, Zacksenhaus E (2007) Identification of tumorsphere- and tumor-initiating cells in HER2/Neu-induced mammary tumors. Cancer Res 67:8671–8681
21. Zhong Y, Guan K, Guo S, Zhou C, Wang D, Ma W, Zhang Y, Li C, Zhang S (2010) Spheres derived from the human SK-RC-42 renal cell carcinoma cell line are enriched in cancer stem cells. Cancer Lett 299:150–160
22. Tirino V, Desiderio V, Paino F, De Rosa A, Papaccio F, La Noce M, Laino L, De Francesco F, Papaccio G (2013) Cancer stem cells in solid tumors: an overview and new approaches for their isolation and characterization. FASEB J 27:13–24
23. Greve B, Kelsch R, Spaniol K, Eich HT, Götte M (2012) Flow cytometry in cancer stem cell analysis and separation. Cytometry A 81:284–293
24. Dean M, Fojo T, Bates S (2005) Tumour stem cells and drug resistance. Nat Rev Cancer 5:275–284
25. Golebiewska A, Brons NH, Bjerkvig R, Niclou SP (2011) Critical appraisal of the side population assay in stem cell and cancer stem cell research. Cell Stem Cell 8:136–147
26. Sládek NE (2003) Human aldehyde dehydrogenases: potential pathological, pharmacological, and toxicological impact. J Biochem Mol Toxicol 17:7–23

Chapter 6

The Aortic Ring Assay and Its Use for the Study of Tumor Angiogenesis

Alfred C. Aplin and Roberto F. Nicosia

Abstract

This chapter describes protocols developed in our laboratory to prepare and analyze angiogenic cultures of rat aorta. Rings of rat aorta cultured in collagen gels produce neovessel outgrowths which reproduce ex vivo key steps of the angiogenic process including endothelial migration, proliferation, proteolytic digestion of the extracellular matrix, capillary tube formation, pericyte recruitment, and vascular regression. The angiogenic response of aortic explants can be stimulated with growth factors or inhibited with anti-angiogenic molecules. Aortic ring cultures can also be used to study tumor angiogenesis. Protocols outlined in this chapter describe how this assay can be modified to investigate the angiogenic activity of cancer cells.

Key words Collagen, Endothelial cells, Pericytes, Neovascularization, Cancer cells

1 Introduction

Angiogenesis contributes to the progression of many debilitating and life-threatening diseases but it also plays a critical role in embryonal development, the revascularization of ischemic organs, and the regeneration of tissues [1]. Basic research conducted during the last 40 years has greatly enhanced our understanding of how blood vessels form, mature, and remodel and has uncovered key molecular pathways of angiogenic regulation that can be targeted pharmacologically for therapeutic intervention [1]. Successful translational studies and clinical trials have led to the approval for therapeutic applications of many angiogenesis-targeting drugs [2, 3]. Research in this field has created the need for bioassays to test the activity of pro- and anti-angiogenic compounds. Among the many systems that have been developed to study angiogenesis [4], the aortic ring model has emerged as one of the most widely used assays particularly for the evaluation of new drugs. A Medline review shows that nearly 500 studies have been published to date

Domenico Ribatti (ed.), *Tumor Angiogenesis Assays: Methods and Protocols*, Methods in Molecular Biology, vol. 1464,
DOI 10.1007/978-1-4939-3999-2_6,

with the aortic ring assay and that its use has steadily increased in recent years [5].

The aortic ring assay recapitulates ex vivo the main steps of the angiogenic process including endothelial migration, proliferation, proteolytic digestion of the extracellular matrix, capillary tube formation, recruitment of pericytes, and vascular regression [6]. Except for the lack of blood flow, the angiogenic response of the aortic explants resembles angiogenesis in vivo and is regulated by paracrine interactions between endothelial cells, macrophages, fibroblasts, and pericytes involving a variety of angiogenic factors and inflammatory cytokines/chemokines [5].

In this chapter we provide a detailed description of protocols currently used in our laboratory to prepare aortic ring cultures and analyze angiogenesis in this model. We also describe how this assay can be used to study tumor angiogenesis.

2 Materials and Reagents

1. 1–2-month-old rat.
2. Styrofoam dissecting board.
3. 80% Ethanol.
4. Hair clippers with size 40 A5 blade.
5. Size 2.0 silk sutures.
6. One pair of 17 cm curved Mayo scissors.
7. Two Halsted-Mosquito hemostats.
8. Size 22 surgical blades and scalpel blade handle.
9. Small forceps.
10. Small curved scissors.
11. 100 mm four-compartment Felsen dishes.
12. Four-well tissue culture dishes (NUNC—IVF dishes).
13. Endothelial Basal Medium (EBM, Lonza).
14. Rat tail collagen solution (1.3 mg/ml, either commercial or prepared in-house).
15. Fine-curved microdissection forceps (Dumont #7).
16. 14 mm straight blade Noyes iridectomy scissors.
17. Sterile 23.4 mg/mL sodium bicarbonate solution.
18. Sterile 10X minimum essential medium (MEM) solution.
19. Micropipettors and sterile tips.
20. Humidified 5% CO_2 tissue culture incubator.
21. Dissecting microscope.

3 Methods

3.1 Excision of the Aorta

1. Sacrifice rats by CO_2 asphyxiation or intraperitoneal injection of sodium pentobarbital.
2. Shave thoracic and abdominal skin using hair clippers, and disinfect with 80% ethanol.
3. Pin the animal onto a dissection board.
4. Make a Y-shaped incision with a scalpel from the top of each shoulder to the xyphoid process of the sternum and down to the lower abdomen.
5. Dissect the skin from the underlying muscle with a scalpel and open the abdominal cavity using small scissors.
6. Cut the ribs with scissors from each side of the animal toward the manubrium of the sternum. Using a hemostat, gently displace the sternal plate to the right side of the animal exposing the thoracic cavity.
7. Using sterile forceps, displace the intestines, stomach, spleen, and liver to the right side of the animal.
8. Cut the diaphragm with sterile small curved scissors toward the midline and back, avoiding the diaphragmatic vessels: this will expose the thoracic aorta along the vertebral column.
9. Tie a knot with a silk suture at the distal end of the thoracic aorta, just below the diaphragm. While holding the suture with forceps, dissect the aorta from the posterior mediastinum with small curved scissors. Excise the aorta at the aortic arch level.
10. Cut the aorta below the knot and place it in a Felsen dish containing serum-free EBM.

3.1.1 Notes

1. We recommend using the thoracic portion of the aorta which has a uniform diameter and a regular pattern of collateral (intercostal) arteries. The abdominal artery (below the diaphragm) is an additional source of rings, but its tapering lumen may introduce variability in the angiogenic response.
2. Attention should be given not to damage the aorta by stretching or letting it dry. The isolation procedure should be completed within 10–15 min of animal sacrifice.

3.2 Preparation of Aortic Rings

1. Working under a dissecting microscope, clean the aorta of periaortic fibroadipose tissue and blood using curved microdissection forceps and Noyes iridectomy scissors.
2. Remove the intraluminal blood clot using fine microdissection forceps.
3. Cut away the collateral vessels as close to the aorta as possible.

4. As the cleaning proceeds, transfer the aorta into the adjacent compartments of the Felsen dish, always ensuring that the aorta is submerged in fresh medium.
5. Prepare aortic rings by serially cross-sectioning the aortic tube at 1–1.5 mm intervals with a scalpel. Discard the proximal and distal rings.
6. Wash the rings through eight sequential baths of serum-free EBM using two Felsen dishes. Lift and hold rings between washes using the capillary action of medium trapped between the microdissection forceps prongs.
7. After washing, re-examine rings to ensure that they are uniform in size. Trim off any remaining fibroadipose tissue. The aortic rings are now ready to be embedded in collagen gels.

3.2.1 Notes

1. The thoracic aorta of a 2-month-old rat should yield 20–25 rings.
2. When cutting rings from the aorta with a scalpel, it is helpful to remove some of the growth medium from the chamber so that the aorta is kept wet but no longer floats.
3. When transferring rings between washes, take care not to crush or otherwise damage the rings.
4. The total time required to clean a rat aorta, cut individual rings, and perform eight washes should not take longer than 30–45 min.
5. Once aortic rings have been prepared, they may be stored in EBM in a humidified tissue culture incubator at 37 °C for periods of up to 24 h prior to embedding in collagen gels.

3.3 Embedding Aortic Rings in Collagen Gel

1. Prepare the working collagen solution by mixing 1 volume 10× MEM with 1 volume 23.4 mg/ml $NaHCO_3$ in a sterile tube. Next add eight volumes of 1.3 mg/ml collagen solution and mix by pipetting slowly up and down several times taking care not to generate bubbles. Keep all solutions on ice.
2. Transfer aortic rings with fine-curved microdissection forceps into four-well IVF dish. Place one ring on the bottom of each culture well.
3. Pipette a 30 μl drop of working collagen solution onto each ring.
4. Using a sterile pipette tip, reposition the aortic ring so that it is suspended in the collagen solution and oriented with the luminal axis parallel to the bottom of the culture dish.
5. Spread the collagen solution around the explant into a thin disc of approximately 8 mm in diameter by slowly drawing the collagen outward around the ring in a circular motion.

6. Incubate the IVF dish containing four aortic ring cultures into a tissue culture incubator at 37 °C for 10 min to induce collagen gelation.
7. Carefully add 500 μl of serum-free EBM to each culture in a dropwise fashion.
8. Replace growth medium with fresh medium three times a week starting from day 3.

3.3.1 Notes

1. This method is optimized for assaying angiogenic growth from collagen gel cultures of rat aortic rings. The same method can be applied to mouse aortic rings with minor modifications of the culture conditions [6–8].
2. Always prepare four aortic ring cultures per experimental group including an untreated set of cultures.
3. The collagen solution can be prepared from rat tail tendons as described [6, 9] or obtained from commercial sources [7].
4. Alternative matrices such as fibrinogen or Matrigel may be used, as needed [10–12].
5. The procedure should be carried out without interruptions, always keeping the aortic rings submerged in culture medium to avoid drying of the aortic explants.
6. It is important not to stretch or crush the aorta or the aortic rings at any stage of the procedure.
7. Always mix the 10× MEM and $NaHCO_3$ solutions thoroughly before adding the collagen solution.
8. Keep all reagents for the collagen gel on ice.
9. The collagen solution should not be less than 1.3 mg/ml dry weight and all reagents should be of tissue culture grade and LPS (endotoxin)-free. Aortic rings are very sensitive to LPS which can stimulate or inhibit angiogenesis depending on its concentration [13].
10. Before adding collagen to the aortic ring, remove excess medium carried over during transfer to the IVF dish by gently dragging the wet ring across the surface of the dish.
11. Neutral pH should be maintained throughout the culture period.
12. Control and experimental aortic rings should always be dissected from animals of the same age, ideally from the same aorta.
13. Feeding is not required if the cultures are not supplemented over time with exogenous agents. If the cultures are not fed, the angiogenic response of the rings is more pronounced and the aortic neovessels survive longer, likely due to accumulation of endogenous angiogenic factors in the culture medium.

3.4 Preparation of Cancer Cell Aggregates

1. Pipette 4 ml of a 1×10^6 suspension of cancer cells in EBM + 10 % FBS into a sterile 25 ml Erlenmeyer flask.
2. Place flask on an orbital shaker set at ~75 rpm, and culture for 48 h in a humidified incubator at 37 °C.
3. Look for clustering of cells and formation of aggregates in the middle of the flask.
4. Transfer to a 15 ml tube and let aggregates sediment by gravity to the bottom of the tube. If aggregates are too small (this will depend on the cancer cell type), centrifuge at low speed to facilitate sedimentation.
5. Remove supernatant, resuspend aggregates in 0.5 ml collagen solution (see above), and mix with a micropipettor P1000. Keep suspension of cancer cell aggregates in collagen solution on ice.

3.5 Co-culture of Aortic Rings with Cancer Cell Aggregates

1. Pipette 5 μl of collagen/cell aggregates onto bottom of a four-well IVF dish, and incubate at 37 °C for 5 min to induce gel formation. This will generate a collagen gel drop containing cancer cell aggregates.
2. Place an aortic ring next to the cancer cell/collagen gel drop, and pipette an additional 30 μl collagen solution onto the culture dish to cover both aortic ring and adjacent cancer cell/collagen gel drop.
3. Use a pipette tip to ensure that the collagen gel is uniformly spread around the aortic explant and adjacent cancer cells.
4. Incubate for 10 min at 37 °C.
5. Add 500 μl serum-free EBM and incubate at 37 °C. Feed 3× a week.

3.6 Treatment of Aortic Ring Cultures with Tumor-Conditioned Medium

1. Prepare tumor-conditioned medium by incubating subconfluent cultures of cancer cells in serum-free EBM for 3 days. Use fresh or store at –70 °C.
2. Prepare aortic ring cultures as described above.
3. Feed the aortic ring cultures with a 1:1 mixture of fresh serum-free EBM and tumor-conditioned medium. Dose–response experiments can be performed by varying the ratio of fresh EBM and tumor-conditioned EBM.

3.6.1 Notes

1. For the co-culture experiments, place the ring within 1 mm from the cancer cell aggregates to ensure maximum exposure to tumor angiogenic factors.
2. The size of the cancer cell aggregates will vary depending on the cancer cell line.
3. If cancer cells have special media requirements, prepare tumor-conditioned medium with the cancer cell-specific medium, always without serum. Use this medium for the 1:1 mixture with EBM in the untreated control.

4 Measurement of Angiogenesis

Angiogenesis can be measured either by manually counting vessels with an inverted microscope or by image analysis. Image analysis provides an objective measurement of the angiogenic response including vessel number and length but it may be time consuming unless it is automated. For the method with Image J software used in our laboratory, refer to a previously published paper [14]. The manual counting method allows rapid assessment of angiogenic response from living cultures. This method only requires a trained observer and an inverted microscope. The speed and extent of the angiogenic response are analyzed by graphing the number of neovessels produced by individual cultures over time [15, 16]. A brief description of the manual method [6] is outlined below.

4.1 Measurement of Angiogenesis by Counting Neovessels

1. Use an inverted microscope with 4× to 10× magnification equipped with bright-field optics. Adjust the condenser diaphragm to obtain optimal contrast and depth of field.
2. Start by visualizing a landmark of the outgrowth and then count all the visible vessels in either a clockwise or a counterclockwise direction.
3. Identify microvessels by their greater thickness and cohesive pattern of growth compared to isolated cells.
4. Count each branch as a separate vessel; a Y-shaped branching vessel is therefore counted as three vessels; loops are counted as two vessels; for anastomosing vessels forming polygonal patterns, count each side of the polygon as a separate vessel.
5. Count microvessels every 2–3 days and record the results for a period of 10–14 days.
6. Use statistical methods (*t*-test, analysis of variance) to analyze data and determine levels of significance between control and treated cultures.

4.1.1 Notes

1. Beware of adventitial collagen fibers or contaminating extraneous fibers which may mimic vessel sprouts.
2. The three-dimensional nature of the angiogenic growth requires frequent readjustment of the focus to accurately visualize vessels.
3. Vessel counts should be done by the same observer throughout the experiment.
4. The angiogenic outgrowth of a typical unstimulated collagen gel culture of rat aorta contains 60–100 microvessels.
5. As vessel number exceeds 200 per culture (cultures treated with exogenous angiogenic stimuli) the visual count method may become challenging and labor intensive. Since the outgrowths in these cultures are generally symmetrical, counting microves-

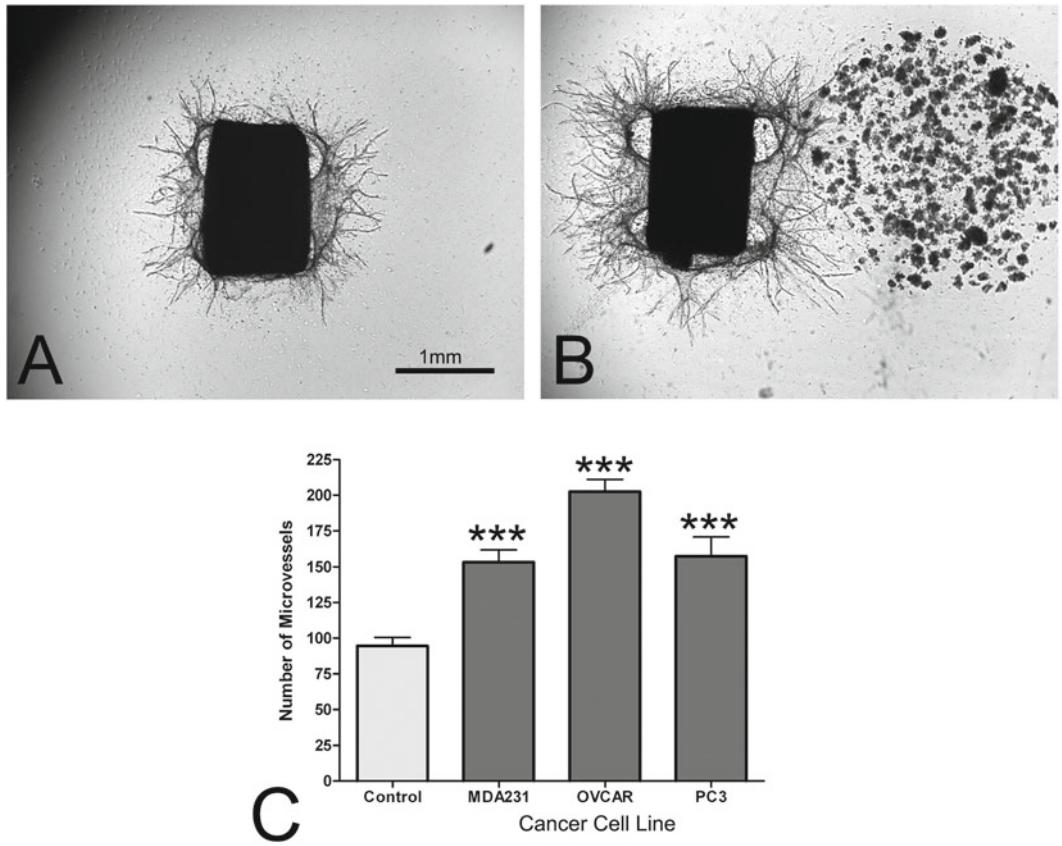

Fig. 1 Co-culture of aortic rings and cancer cell aggregates. (**a**) Angiogenic sprouting from aortic ring in control culture. (**b**) Angiogenesis stimulated by cancer cells in co-culture of aortic ring with aggregates of PC3 cancer cells. (**c**) Measurement of tumor angiogenesis in co-cultures of aortic rings with breast (MDA231), ovarian (OVCAR), and prostate cancer (PC3) cell lines ($N=4$; ***$p<0.001$)

sels in half the culture and then doubling the number will give a close approximation of the angiogenic response. Alternatively these cultures can be measured by image analysis [14].

6. We do not recommend the manual vessel count method if the aortic rings are cultured in Matrigel due to the complexity and highly branched nature of the outgrowths in this matrix. Angiogenesis in Matrigel is best visualized by image analysis after the cultures have been stained with endothelial specific markers.
7. Phase contrast is an acceptable alternative if sufficient contrast cannot be achieved with bright-field optics.

5 Expected Results

Most of the neovessels in aortic cultures originate from the cut edges of the explants. Sprouting endothelial cells form branches, anastomoses, loops, and networks which become coated with pericytes

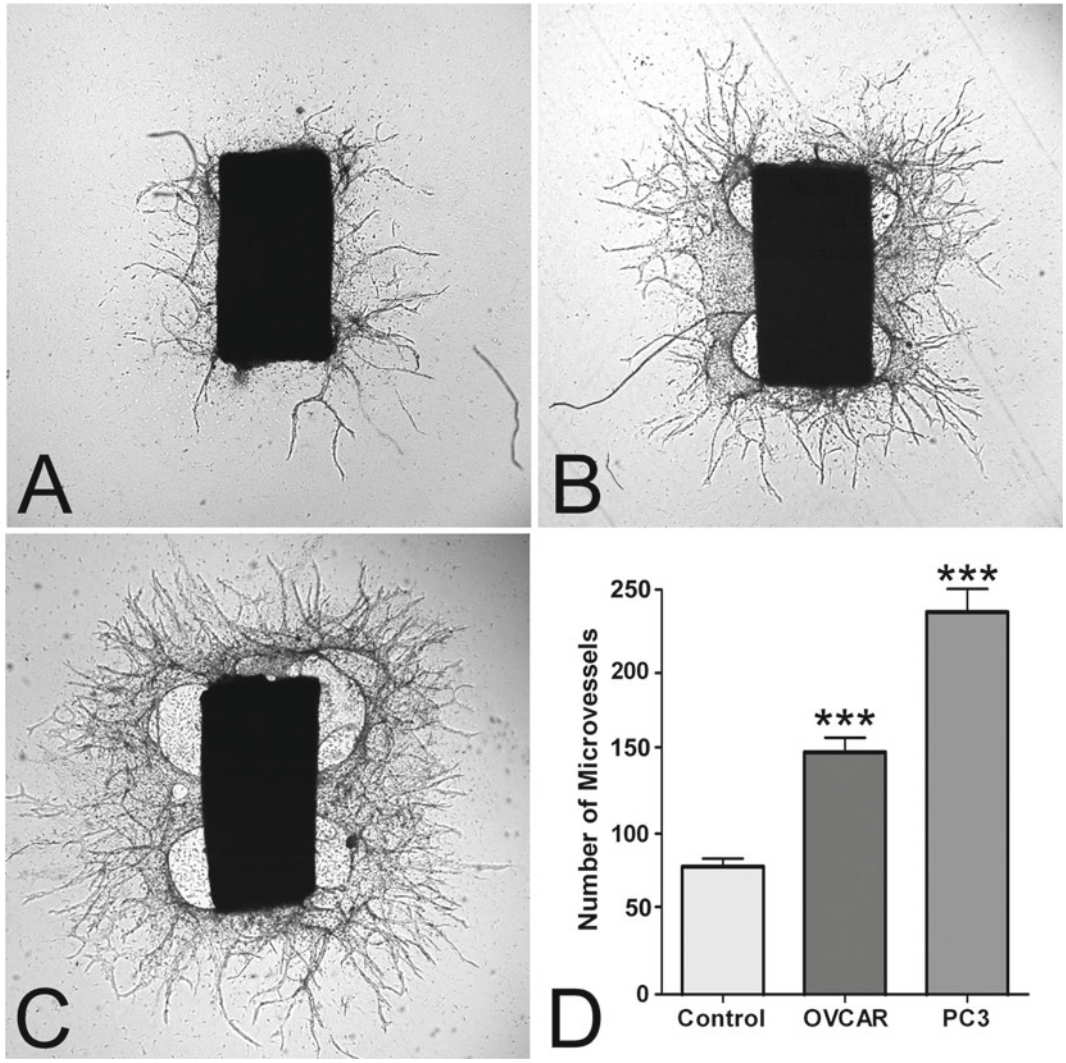

Fig. 2 Cultures of aortic rings stimulated with tumor-conditioned media. Control culture (**a**) and cultures treated with conditioned media from OVCAR (**b**) or PC3 (**c**) cancer cells. (**d**) Measurement of tumor angiogenesis in aortic ring cultures treated with tumor-conditioned media ($N=4$; ***$p<0.001$)

over time [5, 6, 9]. Endothelial sprouts become visible at days 2–3 and increase in number and length over the next 4–5 days. Angiogenic sprouting stops after 6–8 days of culture and is followed by vascular regression. Aortic angiogenesis can be greatly enhanced by exposing the cultures to endothelial growth stimuli including recombinant growth factors/cytokines or angiogenic factor-producing cells or tissue explants [5, 6, 9]. Figures 1 and 2 show the angiogenic effect in aortic cultures of human prostate, breast, and ovarian cancer cells or media conditioned by these cancer cells. This modification of the assay can be used to investigate mechanisms of tumor angiogenesis and test the efficacy of drugs designed to interfere with angiogenesis in different types of malignancy.

Acknowledgements

This work was supported in part by a Merit Review Award from the US Department of Veterans Affairs Biomedical Laboratory Research and Development Service. The contents do not represent the views of the US Department of Veteran Affairs or the US Government. We gratefully acknowledge the support of a grant-in-aid from the American Heart Association and Dr. B. Knudsen, Cedars-Sinai Medical Center, Los Angeles, CA for providing the PC3 cells.

References

1. Carmeliet P, Jain RK (2011) Molecular mechanisms and clinical applications of angiogenesis. Nature 473:298–307
2. Welti J, Loges S, Dimmeler S, Carmeliet P (2013) Recent molecular discoveries in angiogenesis and antiangiogenic therapies in cancer. J Clin Invest 123:3190–3200
3. Shojaei F, Ferrara N (2007) Antiangiogenesis to treat cancer and intraocular neovascular disorders. Lab Invest 87:227–230
4. Simons M, Alitalo K, Annex BH, Augustin HG, Beam C et al (2015) State-of-the-art methods for evaluation of angiogenesis and tissue vascularization: a scientific statement from the American Heart Association. Circ Res 116:e99–e132
5. Nicosia RF (2009) The aortic ring model of angiogenesis: a quarter century of search and discovery. J Cell Mol Med 13:4113–4136
6. Aplin AC, Fogel E, Zorzi P, Nicosia RF (2008) The aortic ring model of angiogenesis. Methods Enzymol 443:119–136
7. Masson V, Devy L, Grignet-Debrus C, Bernt S, Bajou K et al (2002) Mouse aortic ring assay: a new approach of the molecular genetics of angiogenesis. Biol Proced Online 4:24–31
8. Baker M, Robinson SD, Lechertier T, Barber PR, Tavora B et al (2011) Use of the mouse aortic ring assay to study angiogenesis. Nat Protoc 7:89–104
9. Nicosia R, Ligresti G, Aplin AC (2012) Preparation and analysis of aortic ring cultures for the study of angiogenesis ex vivo. In: Zudaire E, Cuttitta F (eds) The textbook of angiogenesis and lymphangiogenesis: methods and applications. Springer, New York, pp 127–148
10. Nicosia RF, Ottinetti A (1990) Growth of microvessels in serum-free matrix culture of rat aorta. A quantitative assay of angiogenesis in vitro. Lab Invest 63:115–122
11. Malinda KM, Nomizu M, Chung M, Delgado M, Kuratomi Y et al (1999) Identification of laminin alpha1 and beta1 chain peptides active for endothelial cell adhesion, tube formation, and aortic sprouting. FASEB J 13:53–62
12. Boscolo E, Folin M, Nico B, Grandi C, Mangieri D et al (2007) Beta amyloid angiogenic activity in vitro and in vivo. Int J Mol Med 19:581–587
13. Aplin AC, Ligresti G, Fogel E, Zorzi P, Smith K et al (2014) Regulation of angiogenesis, mural cell recruitment and adventitial macrophage behavior by Toll-like receptors. Angiogenesis 17:147–161
14. Aplin AC, Nicosia RF (2015) The rat aortic ring model of angiogenesis. In: Ribatti D (ed) Vascular morphogenesis: methods and protocols. Springer, New York, pp 255–264
15. Zhu WH, Guo X, Villaschi S, Francesco NR (2000) Regulation of vascular growth and regression by matrix metalloproteinases in the rat aorta model of angiogenesis. Lab Invest 80:545–555
16. Aplin AC, Zhu WH, Fogel E, Nicosia RF (2009) Vascular regression and survival are differentially regulated by MT1-MMP and TIMPs in the aortic ring model of angiogenesis. Am J Physiol Cell Physiol 297:C471–C480

Chapter 7

Surface Plasmon Resonance Analysis of Heparin-Binding Angiogenic Growth Factors

Marco Rusnati and Antonella Bugatti

Abstract

Surface plasmon resonance (SPR) is an optical technique to evaluate biomolecular interactions. Briefly, SPR measures the capacity of two molecules to bind each other by detecting reflected light from a prism-gold film interface. One of the two putative interactants (called ligand) is chemically immobilized onto the gold film. When the sensor is exposed to a sample containing the second interactant (called analyte), its binding to the immobilized ligand causes a change of the refractive index of the material above the gold surface that is monitored as a real-time graph of the response units against time, producing a real-time graph called sensorgram. SPR has become a golden standard technology for label-free, real-time interaction analysis in basic research and drug discovery in a wide array of biomedical areas, including oncology and virology [1, 2]. Here we describe the exploitation of SPR for the study of the capacity of the pro-oncogenic, pro-angiogenic HIV-1 p17 matrix protein [3, 4] to bind to heparin, a structural analog of heparan sulfate proteoglycans (HSPGs) receptors, and for the identification of novel HSPGs-antagonists to be used as anti-p17 drugs.

Key words Surface plasmon resonance, Biosensor, Heparin, Protein binding, Affinity calculation

1 Introduction

Surface plasmon resonance (SPR) is an optical technique to evaluate biomolecular interactions by detecting reflected light from a prism-gold film interface. A typical setup of a solid-phase bioassay based on SPR spectroscopy is schematized in Fig. 1. Briefly, it is composed by:

1. A light source that emits a monochromatic laser beam.
2. An optical detector system that monitors the changes in SPR signal brought about by binding events in real time.
3. An exchangeable gold slide (called sensorchip), upon which one of the two putative interactants is immobilized.
4. A microfluidic system that allows the injection of the sample containing the second interactant over the sensor surface.

Domenico Ribatti (ed.), *Tumor Angiogenesis Assays: Methods and Protocols*, Methods in Molecular Biology, vol. 1464,
DOI 10.1007/978-1-4939-3999-2_7,

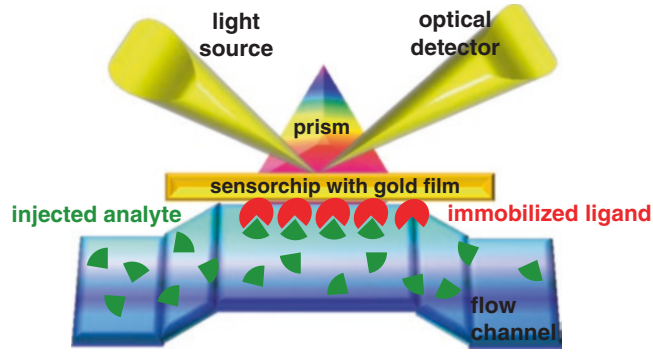

Fig. 1 Schematic representation of a surface plasmon resonance apparatus. The molecule immobilized onto the gold sensorchip is named ligand whereas the putative partner injected into the flow channel is called analyte. In the presence of the ligand/analyte interaction, the refractive index at the gold surface changes, resulting in the shift of the resonance angle that provides label-free transduction of the binding event

5. These four integrated systems communicate with a computer equipped with control and data evaluation software.

The biophysical bases of the SPR operating principles are extensively described elsewhere [5]. Briefly, the polarized beam of monochromatic visible light is passed through a prism fitted with the sensorchip. The light is reflected off the gold surface and its intensity is detected at the specular angle. An electric field intensity, known as evanescent wave, is generated when the light strikes the surface. It interacts with and is absorbed by free electron clouds in the gold layer, generating electron charge density waves called plasmons, causing a reduction in the intensity of the reflected light. The angle corresponding to the sharp intensity minimum that occurs at the SPR condition is called resonance angle. It depends on the refractive index of the material near (below 300 nm) the gold surface, as it is sampled by the evanescent light intensity. The resonance angle can be monitored by following the specularly reflected light intensity *versus* angle at fixed wavelengths or *versus* wavelength at fixed angle. In an SPR assay, one of the two molecules for which a binding analysis is required is chemically immobilized onto the gold film (and is defined ligand). Then, the sensor is exposed to a sample containing the second molecule to be analyzed (defined analyte) that is injected through the microfluidic system. If the binding of the analyte to the ligand occurs, this causes a change of the refractive index at the metal surface, resulting in the shift of the resonance angle that provides label-free transduction of the binding event. The raw data are then processed and presented as a real-time graph of the response units (RU) against time, a graph referred to as sensorgram (*see* Fig. 3).

In respect to conventional techniques such as fluorescent-, enzyme-, or radio-labeled assays, SPR analysis adds to label-free molecular recognition several advantages: the ability to manipulate very low concentrations of molecules semi-automatically in real time, the possibility to detect analytes over a wide range of molecular weights and binding affinities (including weakly interacting small chemical compounds), and the access to information spanning from straight ON-OFF sensing to binding kinetics and thermodynamics. In details:

1. Kinetics analysis that allows the determination of the association and dissociation rates (k_{on} and k_{off}, respectively) that give a measure of how fast a molecule binds to and detaches from another (*see* **Note 1**). The k_{off}/k_{on} ratio allows the determination of the dissociation constant (K_d) value, inversely proportional to the affinity of the interaction.
2. Equilibrium analysis that allows the calculation of the equilibrium K_d in a kinetic-independent way (*see* **Note 2**).
3. Calculation of the stoichiometry of the interaction, particularly important for the binding of a multivalent interactant such as heparin/heparan sulfate proteoglycans (HSPGs) that set up complex interactions with multiple copies of its partners [6] (*see* **Note 3**).
4. Competition experiments, aimed at the identification of compounds able to prevent/displace the binding of a ligand to its receptor. This ability is predictive of the in vivo antagonist capacity of the identified compounds, with implications in drug discovery programs [7–9] (*see* **Note 4**).

In our laboratory, SPR has been successfully exploited to screen a large number of proteins for their capacity to bind to heparin, a structural analog of HSPGs receptors expressed onto all the eukaryotic cells and involved in various physiological and pathological processes including virus infection, inflammation, angiogenesis, and oncogenesis [1, 2].

2 Materials

Prepare all solutions and samples using ultrapure water (deionized water with a sensitivity of 18 MΩ cm at 25 °C) and analytical grade reagents. Filter all reagents and samples by 0.22 μm PVDF Stericup (Merk Millipore, Darmstadt, Germany) before using it in the SPR apparatus (*see* **Note 5**). Follow all waste disposal regulations when disposing waste materials. When working with the Biacore X-100 apparatus (see below) prepare all the samples in Biacore 1.5 ml polypropylene vials with rubber caps compatible with the automated injection rack system.

2.1 SPR Apparatus and Sensorchips

Two different SPR apparatus (a Biacore X and a Biacore X-100, GE Healthcare, Milwaukee, WI) are routinely used in our laboratory. Although similar results can be obtained with the two apparatus when performing simpler analysis (i.e., direct interaction of a protein with heparin), the newer and powerful Biacore X-100 allows more complex analysis (i.e., competition experiments with small chemical compounds) otherwise not manageable with the Biacore X (*see* **Notes 4** and **6**).

Depending on the requirements of appropriate experimental conditions, different sensorchips can be used:

1. SA sensorchip, composed of a carboxymethylated dextran matrix covalently attached to a gold surface. Streptavidin is already covalently bound via carboxyl moieties of the dextran for the quick immobilization of biotinylated partners. In respect to CM3 sensorchip (described below), SA sensorchip is characterized by longer carboxymethylated dextran chains, allowing high-efficiency immobilization, particularly searched in competition experiments (*see* **Note 4**).
2. CM3 sensorchip has a shorter carboxymethylated dextran matrix in respect to sensorchip SA. The shorter matrix may give reduced nonspecific binding (*see* **Note 7**). On the other hand, due to the shorter matrix, the immobilization yield is approximately 30% of that obtained on sensorchip SA under the same experimental conditions (*see* **Note 8**).

Biacore apparatus are always kept with a maintenance sensorchip inside. All the procedures described are performed at a fixed temperature equal to 25 °C.

2.2 Heparin, Proteins, and Heparin-Like Antagonists for Immobilization and SPR Analysis

1. Streptavidin (Sigma-Aldrich).
2. Heparin is a structural analog of the glycosaminoglycan chains of HSPGs. A high-molecular-weight heparin (13.6 kDa) (*see* **Note 9**) is routinely used in our laboratory that is obtained from a commercial batch preparation of unfractionated sodium heparin from beef mucosa (Laboratori Derivati Organici S.p.A., Milan, Italy) purified from contaminants (up to 95%) according to described methodologies. Its ^{13}C NMR spectrum showed 78% *N*-sulfate glucosamine, 80% 6-*O*-sulfate glucosamine, and 59% 2-*O*-sulfate iduronic acid. Heparin is biotinylated as already described [10].
3. HIV-1 p17 is a novel, non-conventional angiogenic growth factor that contributes to tumor angiogenesis in HIV-1-positive patients [3]. The coding sequence of HIV-1 p17 clade B isolate BH10 (aa 1-132) is amplified by polymerase chain reaction with specific primers that allows the cloning of the p17 sequence into the BamH1 site of the prokaryotic expression vector pGEX-2T (GE, Healthcare, Milwaukee,

WI). HIV-1 p17 is then expressed and purified as already described [11].

4. The capsular *E. coli* K5 polysaccharide has the same structure as the heparin precursor *N*-acetyl heparosan [7, 12]. K5-sulfated derivatives are obtained by *N*-deacetylation/*N*-sulfation and/or *O*-sulfation of a single batch of K5 polysaccharide as described [13]. Selected K5-sulfated derivatives have been already demonstrated to act as heparin/HSPGs antagonists in different pathological settings [14].

2.3 Buffers for Surface Preparation (Streptavidin Immobilization and Heparin Capture) and for Binding and Competition Analysis

1. 0.01 M HEPES pH 7.4 containing 0.15 M NaCl, 3 mM EDTA, 0.05% Tween 20 (HBS-EP+).
2. 10 mM Sodium acetate, pH 4.8.
3. 100 mM *N*-hydroxysuccinimide (NHS).
4. 400 mM *N*-ethyl-*N*-(3-dimethylaminopropyl)-carbodiimide hydrochloride (EDC).
5. 1 M Ethanolamine.
6. Wash solution: 50 mM NaOH containing 1 M NaCl.
7. Extrawash solution: 50% Isopropanol in 50 mM NaOH containing 1 M NaCl.
8. Regeneration solution: 2 M NaCl in deionized water.

3 Methods

3.1 Streptavidin Immobilization

Apart from the use of SA sensorchip, on which streptavidin is precoated, when CM3 sensorchip is preferred (*see* **Notes 6** and **7**) the immobilization of streptavidin is required that is obtained as follows:

1. The sensorchip is usually kept in the fridge, so that it must be equilibrated at 25 °C for at least 30 min before starting any procedure.
2. Undock and remove the maintenance sensorchip, insert and dock the new sensorchip.
3. Activate the CM3 surface by injecting a mixture of EDC/NHS (1:1) at a flow rate of 10 µl/min for 7 min.
4. Inject streptavidin (30 µg/ml in 10 mM sodium acetate, pH 4.8) over the activated CM3 sensorchip at a flow rate of 10 µl/min for 7 min.
5. Deactivate the excess of reactive groups of the sensorchip by injecting 1 M ethanolamine at a flow rate of 10 µl/min for 7 min.

3.2 Heparin Capture

Biotinylated heparin is captured onto streptavidin-coated sensorchip as follows:

1. Surface conditioning with three consecutive injections of 1 M NaCl in 50 mM NaOH. Flow rate equal to 5 µl/ml and contact time equal to 1 min are recommended.
2. Inject biotinylated heparin (10 µg/ml in HBS-EP+) onto the streptavidin sensorchip at a flow rate of 5 µl/min for 8 min.
3. Wash with an injection of 40 µl of extrawash solution at a flow rate equal to 5 µl/min. This is intended to wash only the fluidic channels (*see* **Note 5**) without entering into contact with the flow cell where heparin has been immobilized.

In Fig. 2 is reported a typical sensorgram obtained for the immobilization of heparin onto a streptavidin-precoated SA sensorchip.

3.3 Kinetics and Affinity Measurements with HIV-1 p17

1. Make serial dilutions (ideally from five to eight, see legend to Fig. 3) of HIV-1 p17 in HBS-EP+. The concentrations chosen should cover a wide range centered on the value for the K_d for the interaction under analysis (*see* **Note 10**).
2. Inject the first of the HIV-1 p17 dilutions (usually from the less to the more concentrated ones) at a flow rate equal to 5 µl/min for 120 s ("contact time"), followed by a 600s "dissociation time" in which HBS-EP+ alone is passed onto the surface at the same flow rate.
3. Regenerate the sensorchip by one injection of regeneration solution at a flow rate equal to 5 µl/min for 30 s ("contact time") followed by a 60 s "stabilization period" in which HBS-EP+ alone is passed onto the surface at the same flow rate.

In Fig. 3 is shown a representative analysis resulting from the study of the interaction occurring between HIV-1 p17 and sensorchip-immobilized heparin. In Table 1 are reported the binding parameters calculated for the same interaction [15].

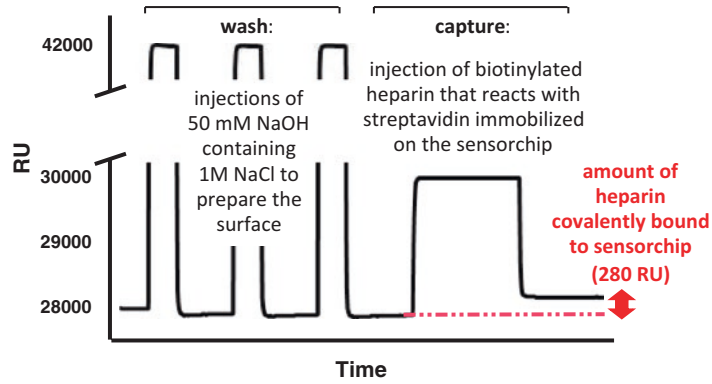

Fig. 2 Sensorgram resulting from a representative procedure of immobilization of heparin onto streptavidin-coated sensorchip. The final amount of immobilized heparin (280 RU) corresponds to about 20 femtomoles/mm^2

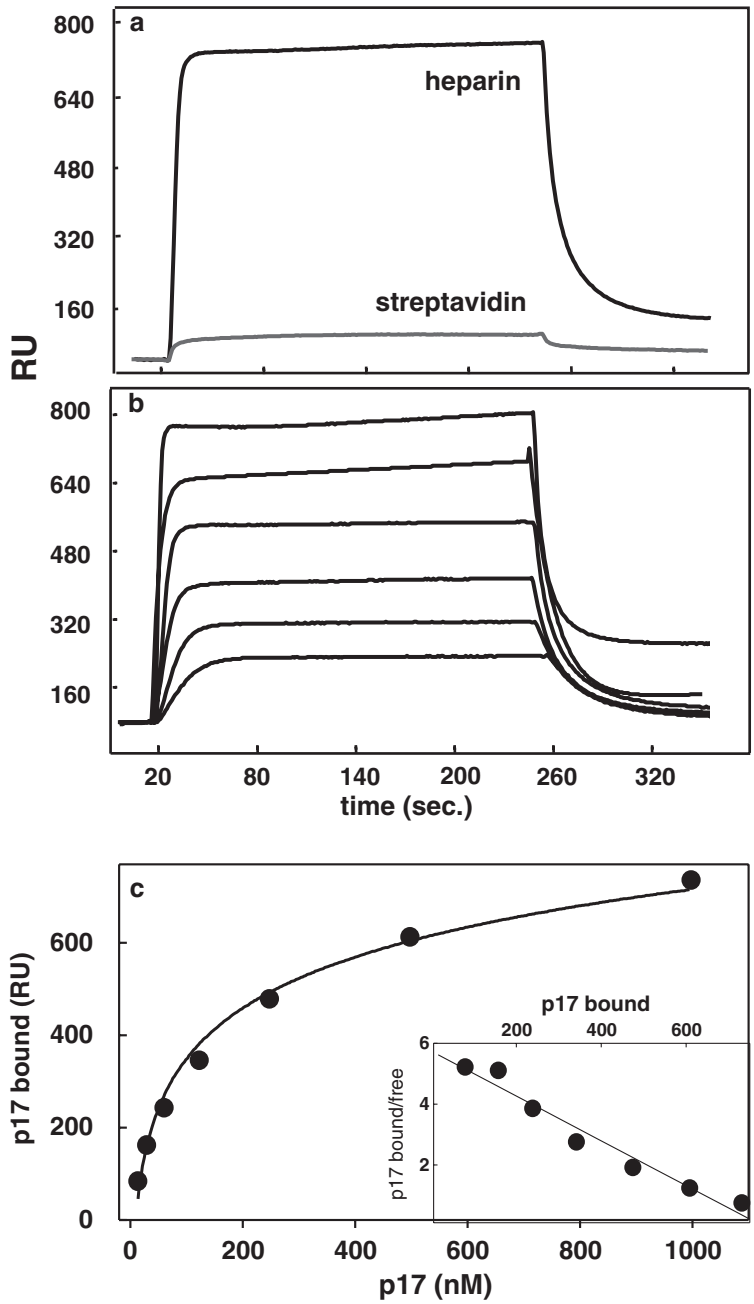

Fig. 3 SPR analysis of HIV-1 p17/heparin interaction. (**a**) Sensorgrams showing the binding of HIV-1 p17 (500 nM) to the heparin- or streptavidin-coated sensorchips. (**b**) Blank-subtracted sensorgrams overlay showing the binding of increasing concentrations of HIV-1 p17 (1000, 500, 250, 125, 62.5, 31.25 nM) to the heparin-coated sensorchip. In **a** and **b**, the response (in RU) is recorded as a function of time. (**c**) Saturation curve obtained by the values of RU bound at equilibrium derived from the injection of the increasing concentrations of HIV-1 p17 onto the heparin-coated sensorchip. *Inset* in panel **c**: Scatchard plot analysis of the equilibrium binding data shown in **c**. The correlation coefficient of the linear regression is equal to –0.96. Reproduced from ref. 15 with permission from ASBMB

Table 1
Binding parameters of the interaction of HIV-1 p17 to heparin

	k_{on} (1/Ms)	k_{off} (1/s)	K_d (M) k_{off}/k_{on}	K_d (M) at equilibrium
HIV-1 p17/heparin				
Native p17	3.39×10^5	0.0643	1.9×10^{-7}	1.36×10^{-7}
Heat-denatured p17	4.32×10^5	0.217	5.03×10^{-7}	4.23×10^{-7}

k_{on} and k_{off} are reported. K_d value was derived either from the k_{off}/k_{on} ratio or by Scatchard plot analysis of the equilibrium binding data. The results shown are representative of other two that gave similar results. *n.d.* not determinable. Reproduced from ref. 15 with permission from ASBMB

3.4 Competition Experiments with K5-Sulfated Derivatives

Once the best SPR conditions to characterize the HIV-1 p17/heparin interaction are set, this knowledge can be translated in the optimization of a reliable SPR model for a first-line screening aimed at the identification of putative inhibitors of HIV-1 p17. To this aim:

1. Make serial dilutions (ideally from three to eight, *see* legend to Fig. 4) of each K5-sulfated derivative in the presence of a fixed concentration (100 nM) of HIV-1 p17 in HBS-EP+. For the choice of the fixed concentration of HIV-1 p17 and of the range of concentrations of K5-sulfated derivatives *see* **Notes 11** and **12**, respectively.
2. Inject the first of the samples containing the mixture of HIV-1 p17 and the putative inhibitor (usually from the more to the less concentrated ones) at a flow rate equal to 10 μl/min for 120 s ("contact time") followed by a 600 s of "dissociation time" in which HBS-EP+ alone is passed onto the surface at the same flow rate.
3. Regenerate the sensorchip by one injection of regeneration solution at a flow rate equal to 10 μl/min for 30 s ("contact time") followed by a 60 s "stabilization period" in which HBS-EP+ alone is passed onto the surface at the same flow rate.

In Fig. 4 is shown a representative competition experiment in which a series of sulfated K5 derivatives have been assayed in dose–response for their capacity to inhibit the interaction of HIV-1 p17 to sensorchip-immobilized heparin.

The preparation of the samples and the performing of the steps described above are different when using the Biacore X or Biacore X-100 apparatus since the latter is endowed with a certain degree of automatization that quickens the procedure (*see* **Note 13** for further details).

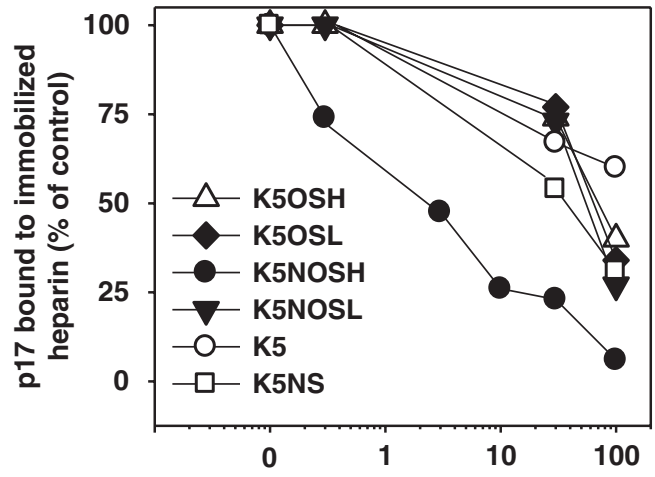

Fig. 4 Effect of K5-sulfated derivatives on the interaction of HIV-1 p17 to heparin. K5 derivatives (at concentrations spanning from 300 to 0.3 nM) were evaluated for their capacity to inhibit the interaction of HIV-1 p17 (100 nM) with heparin immobilized to the sensorchip. The responses are plotted as percentage of the binding of HIV-1 p17 measured in the absence of any polysaccharide. Each point is the mean ± S.E.M. of three separate determinations. Reproduced from ref. 15 with permission from ASBMB

4 Notes

1. To perform accurate kinetics analysis, the phenomenon of mass transport [16, 17] should be avoided or minimized. To this aim, optimal assay conditions consist in a combination of high flow rates and low surface binding capacity. Regarding the former, flow rates >30 μl/min are recommended when possible. Regarding the latter, it translates in the immobilization of limited amount of ligand (usually lower than 500 RU) (*see also* **Notes** 7 and **8** for related issues).
2. In an ideal SPR analysis, the K_d values calculated either by kinetic or equilibrium analysis must coincide (*see* Table 1), thus ensuring the quality and reliability of the measurements. In particular analysis however this is hardly achievable (i.e., binding involving large aggregates [virions, extracellular vesicles] or small chemical compounds resuspended in dimethyl sulfoxide [DMSO] [*see also* **Note 6** for related issues]). In these cases, the more trustworthy K_d value is that provided by equilibrium analysis that, being independent from kinetic parameters, is not influenced by artifacts such as those derived by the presence of DMSO.
3. The binding stoichiometry can be calculated by the following equation:

$$S = \frac{M_W L}{M_W A} \times \frac{A}{L}$$

where S is stoichiometry; M_wL and M_wA are the molecular weight (mass) of the ligand and of the analyte, respectively; A is the analyte binding level at saturation; and L is the level of ligand immobilization (the last two parameters expressed in RU).

4. In competition experiments, a high ligand density translates in a high binding capacity functional to an easier evaluation of the inhibitory potency of a putative antagonist. This can be obtained by immobilizing heparin to a SA instead of a CM3 sensorchip.
5. Due to its capillary-like geometry, the fluidic system of the Biacore apparatus is particularly prone to clotting caused by debris present in the buffers and/or samples to be injected. Particular attention to avoid this events must be then adopted.
6. Putative drugs are often low-molecular-weight (LMW) organic compounds that require organic solvents like DMSO (usually from 1 to 3%) in order to become soluble in aqueous buffers. In turn, SPR analysis in the presence of DMSO requires special care. Biacore X-100 Plus Package provides the necessary software to correctly process raw data from this type of analysis. The response obtained from the analysis of the direct binding of LMW analytes to their target ligands can be very low (a few RU) because of the equally very low molecular size (down till 200 Da). In addition, binding affinities are often weak (K_d values in the range of μM) which further reduces the response. For this reason, sensor surfaces for LMW screening must be prepared with high levels of ligand (from 8000 to 10,000 RU for average-sized ligands). Accordingly, high concentrations of analytes (expected to be weak binders) are required to saturate the surface (typically 0.1–2 mM). Phosphate buffers are generally recommended for work with small molecules. Using organic buffers such as HEPES can bind to the small organic ligand, thus interfering with the analysis. Physiological ionic strength (150 mM monovalent cations) should be used to reduce nonspecific binding and inclusion of detergent (0.05% Surfactant P20) generally improves data quality by reducing drift and signal disturbances. The composition of running buffer and sample buffer must be matched as closely as possible, particularly with respect to organic solvent concentration. Variations in DMSO content between samples resulting from both evaporation and absorption of water are however unavoidable. An alternative approach to study the direct binding of LMW analytes to their target ligands is represented by competition experiments (*see also* **Notes 4** and **11** for related issues).
7. Heparin-binding proteins are cationic peptides containing stretches of basic amino acids that have thus the tendency to bind aspecifically to negatively charged surfaces such as the carboxymethylated dextran matrix. The shorter dextran chains

(and the consequent lower negative charge) of CM3 sensorchip may reduce this nonspecific binding.

8. The lower yield of immobilization that can be obtained with CM3 sensorchip is useful in kinetic applications, where low ligand densities are required to obtain solid kinetic data (*see also* **Note 1** for related issues).
9. The immobilization of longer heparin chains (13.6 kDa) in respect to shorter ones (usually up to 9 kDa) ensures the presence of a higher number of binding sites also in the presence of low-density immobilization, allowing the better discrimination of the specific *versus* aspecific binding of cationic proteins (*see also* **Note 7**).
10. In practice, the K_d value is often not known, and the range of concentrations that can be used may be limited by availability or solubility of the analyte. Whenever possible, the range of concentration of the analyte can be tentatively decided by comparison to previous, similar analysis. As for HIV-1 p17, a good indication has been provided by the K_d values already calculated for the interaction of heparin with other cationic peptides.
11. Usually, a sub-saturating concentration of analyte is chosen on the basis of the already performed kinetics and affinity measurements. In sub-saturating concentrations, the analyte is more easily challenged by the inhibitor, facilitating the performing of good dose–response curves, overall in those cases in which the inhibitor is available in small amount or its solubility is limited. Note that the use of sub-saturating amount of analyte (that generates low RU responses) is in contrast with the requirement for high RU responses mentioned in **Notes 4**, **6**, and **9**. A good balance between these two contrasting requirements must be searched for in an optimal ligand/analyte ratio.
12. The range of concentrations of the inhibitor is centered on the K_d value calculated for the interaction to be challenged and that has been calculated in the kinetics and affinity measurements. Usually a few doses spanning from 100 times lower to 100 times higher the K_d are firstly assayed and, on the basis of these first results, the range of concentrations can be refined.
13. The preparation of the samples and the performing of the steps described in paragraphs in Subheadings 3.1–3.4 are different when using the Biacore X or Biacore X-100 apparatus, with the latter endowed with a certain degree of automatization that quickens the procedure. When using the Biacore X apparatus each injection must be performed manually and each singly generated sensorgram must be merged with the others (overlay) and analyzed with the dedicated software. At variance, the automatization available in the Biacore X-100 allows the creation of "Wizard" procedure (here not described) that automatically performs all the

injections required for the procedure. To this aim, a rack is available in which a dialog shows you where the buffers and the reagents should be placed and how much of each sample is needed. Make sure that you do not make bubbles while putting the reagents into the vials (*see also* **Note 5**). Close all the vials with the orange rubber caps and place them in the right order.

Acknowledgement

This work was supported by grants from MIUR to Marco Rusnati.

References

1. Rusnati M, Presta M (2015) Angiogenic growth factors interactome and drug discovery: the contribution of surface plasmon resonance. Cytokine Growth Factor Rev 26:293–310
2. Rusnati M, Chiodelli P, Bugatti A et al (2015) Bridging the past and the future of virology: surface plasmon resonance as a powerful tool to investigate virus/host interactions. Crit Rev Microbiol 41:238–260
3. Caccuri F, Giagulli C, Bugatti A et al (2012) HIV-1 matrix protein p17 promotes angiogenesis via chemokine receptors CXCR1 and CXCR2. Proc Natl Acad Sci U S A 109:14580–14585
4. Martorelli D, Muraro E, Mastorci K et al (2015) A natural HIV p17 protein variant up-regulates the LMP-1 EBV oncoprotein and promotes the growth of EBV-infected B-lymphocytes: implications for EBV-driven lymphomagenesis in the HIV setting. Int J Cancer 137:1374–1385
5. Piliarik M, Vaisocherova H, Homola J (2009) Surface plasmon resonance biosensing. Methods Mol Biol 503:65–88
6. Rusnati M, Tulipano G, Spillmann D et al (1999) Multiple interactions of HIV-I Tat protein with size-defined heparin oligosaccharides. J Biol Chem 274:28198–28205
7. Rusnati M, Oreste P, Zoppetti G et al (2005) Biotechnological engineering of heparin/heparan sulphate: a novel area of multi-target drug discovery. Curr Pharm Des 11:2489–2499
8. Urbinati C, Chiodelli P, Rusnati M (2008) Polyanionic drugs and viral oncogenesis: a novel approach to control infection, tumor-associated inflammation and angiogenesis. Molecules 13:2758–2785
9. Rusnati M, Bugatti A, Mitola S et al (2009) Exploiting surface plasmon resonance (SPR) technology for the identification of fibroblast growth factor-2 (FGF2) antagonists endowed with antiangiogenic activity. Sensors (Basel) 9:6471–6503
10. Rusnati M, Urbinati C, Caputo A et al (2001) Pentosan polysulfate as an inhibitor of extracellular HIV-1 Tat. J Biol Chem 276:22420–22425
11. Giagulli C, Marsico S, Magiera AK et al (2011) Opposite effects of HIV-1 p17 variants on PTEN activation and cell growth in B cells. PLoS One 6:e17831
12. Casu B, Grazioli G, Razi N et al (1994) Heparin-like compounds prepared by chemical modification of capsular polysaccharide from *E. coli* K5. Carbohydr Res 263:271–284
13. Leali D, Belleri M, Urbinati C et al (2001) Fibroblast growth factor-2 antagonist activity and angiostatic capacity of sulfated *Escherichia coli* K5 polysaccharide derivatives. J Biol Chem 276:37900–37908
14. Rusnati M, Vicenzi E, Donalisio M et al (2009) Sulfated K5 *Escherichia coli* polysaccharide derivatives: a novel class of candidate antiviral microbicides. Pharmacol Ther 123:310–322
15. Bugatti A, Giagulli C, Urbinati C et al (2013) Molecular interaction studies of HIV-1 matrix protein p17 and heparin: identification of the heparin-binding motif of p17 as a target for the development of multitarget antagonists. J Biol Chem 288:1150–1161
16. Myszka DG, Jonsen MD, Graves BJ (1998) Equilibrium analysis of high affinity interactions using BIACORE. Anal Biochem 265:326–330
17. Karlsson R (1999) Affinity analysis of non-steady-state data obtained under mass transport limited conditions using BIAcore technology. J Mol Recognit 12:285–292

Chapter 8

An Ex Vivo Tissue Culture Model for Anti-angiogenic Drug Testing

Mohammad S. Azimi, Michelle Lacey, Debasis Mondal, and Walter L. Murfee

Abstract

Angiogenesis, defined as the growth of new blood vessels from existing ones, plays a key role in development, growth, and tissue repair. Its necessary role in tumor growth and metastasis has led to the creation of a new category of anti-angiogenic cancer therapies. Preclinical development and evaluation of potential drug candidates require models that mimic real microvascular networks. Here, we describe the rat mesentery culture model as a simple ex vivo assay that offers time-lapse imaging of intact microvascular network remodeling and demonstrate its application for anti-angiogenic drug testing.

Key words Angiogenesis, Microvascular network, Endothelial cell, Mesentery, Drug screening, Pericytes, Tissue culture

1 Introduction

Models that mimic angiogenesis are extremely valuable for the preclinical evaluation of anti-angiogenic tumor therapies. Consequently, an emerging need is the development of more biomimetic models that recapitulate the complexity of a real tissue. For example, consider single-cell two-dimensional in vitro assays. While such approaches have proven extremely useful in identifying mechanistic signaling information, they are limited in their complexity and capability to mimic physiologically relevant scenarios [1]. In face of these limitations, three-dimensional culture systems [1], ex vivo tissue explant models [2], microfluidic platforms [3, 4], and integrated computational approaches [5] have been developed in an attempt to incorporate the multicellular complexity of a real microvascular network, and yet these assays are also inherently limited by their "bottom-up" approach and do not fully recapitulate the in vivo scenario. The utility of any model depends on the scientific question being investigated or the application. Recently, we have introduced the rat mesentery tissue culture model as a

Domenico Ribatti (ed.), *Tumor Angiogenesis Assays: Methods and Protocols*, Methods in Molecular Biology, vol. 1464,
DOI 10.1007/978-1-4939-3999-2_8,

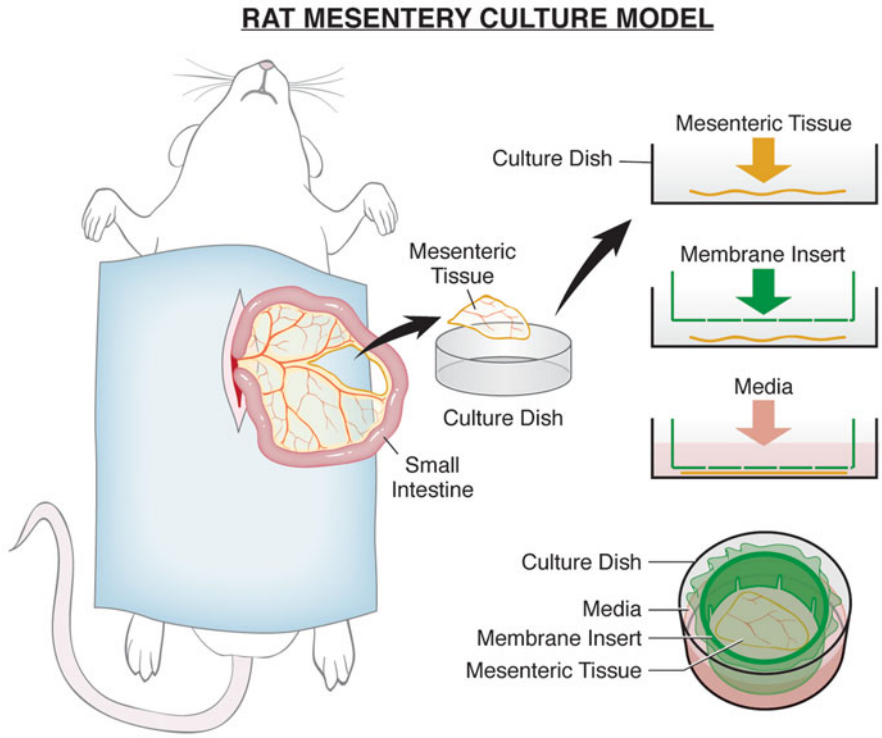

Fig. 1 Illustration of rat mesentery culture model. The mesenteric tissue, harvested from the small intestine of an adult Wistar rat, is transferred into a culture dish, quickly spread out on the bottom of a well, secured in place with a membrane insert, and covered with media. Tissues are cultured in standard conditions (37 °C, 5 % CO_2)

novel, alternative ex vivo model that offers time-lapse imaging of intact microvascular networks. Culturing of the rat mesentery was first described as a useful model for recapitulating mast cell dynamics during wound healing [6]. Our laboratory has further established the ex vivo tissue model as a tool for investigating cell dynamics involved in microvascular remodeling [7, 8] (Fig. 1). Despite the lack of flow incorporation, features of this model made possible by the "top-down" preservation of a real tissue characteristics include (1) viable blood and lymphatic vessels (Fig. 2a) and cell proliferation (Fig. 2d) in an intact microvascular network scenario, (2) stimulation of angiogenesis and lymphangiogenesis (Fig. 2c), (3) the ability to probe pericyte-endothelial cell interactions (Fig. 2b), and (4) time-lapse imaging [7, 8]. The key advantages of the rat mesentery culture model are its simplicity and self-containment, which eliminate the need for matrix embedding.

The objective of this chapter is to detail the rat mesentery culture model methodology for anti-angiogenic drug testing. The thickness of the mesentery tissue (20–40 μm) [9] combined with our technically simple protocol enables tissue-specific comparisons before and after treatment to investigate its effects on entire microvascular networks. Validation of this method for anti-angiogenic drug testing has been demonstrated using sunitinib, a tyrosine kinase

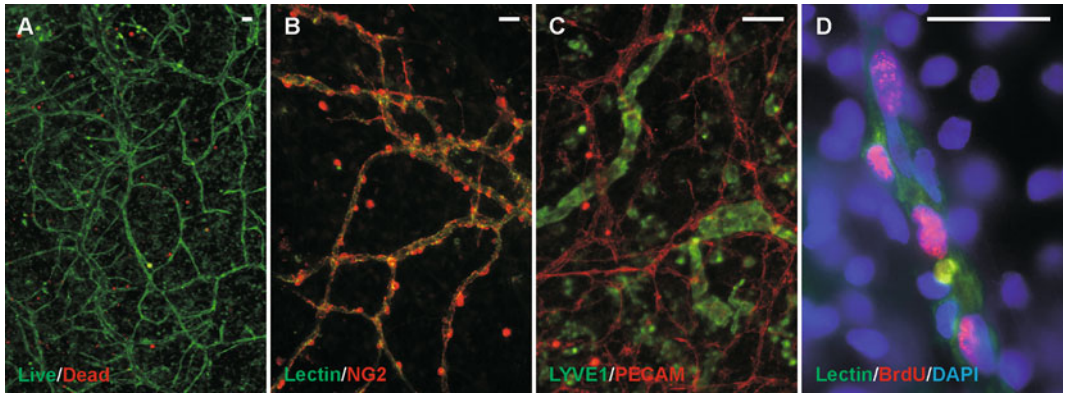

Fig. 2 Presence of viable cells, pericytes, lymphatic/blood vessels, and proliferative cells within microvascular network. Live/dead assay after 3 days of culture exhibits a high ratio of live to dead cells, especially along the microvasculature (**a**); BSI-lectin/NG2 labeling confirms the presence of pericytes along microvessels (**b**); LYVE1/PECAM labeling confirms the presence of lymphatic and blood vessels (**c**); and vascular cell proliferation is supported by BrdU-DAPI-positive cells along a capillary segment labeled with BSI-lectin (**d**). Scale bars = 100 μm

inhibitor targeting VEGFR-2, and bevacizumab, a known VEGF-A inhibitor [8]. The rat mesentery culture model potentially serves to offer a valuable preclinical drug screening platform.

2 Materials and Surgical Tools

2.1 Solutions and Reagents

1. Media: Minimum essential media (MEM), supplemented with 1% penicillin-streptomycin (PenStrep), and 10% fetal bovine serum (FBS).
2. Phosphate-buffered saline with calcium and magnesium.
3. 0.9% Sodium chloride (saline).
4. BSI-lectin labeling solution: MEM supplemented with 2.5% FITC-conjugated BSI-lectin (25 μg/ml).
5. Zetamine.
6. Beuthanasia-D.
7. AnaSed.
8. 70% Ethanol.
9. 70% Isopropyl alcohol.
10. Povidone-iodine.

2.2 Tools

1. Microdissecting scissors.
2. Microdissecting forceps.
3. Scalpel handle.
4. Sterile surgical blade.
5. Culture dish.
6. Six-well plate.

2.3 Other

1. Surgical stage: The surgical stage is created by drilling an elliptical hole approximately 2 in. by 1 in. in the center of a 100 mm culture dish. Next, the sharp edges of the hole are polished using sandpaper, and a layer of silicon glue is added to the edges to create a raised, smooth surface for the tissues.
2. Electric heating pad.
3. Pre-cut surgical drape with an elliptical hole (2 by 1 in.) at the center.
4. Absorbent bench underpad with waterproof barrier.
5. Gauze sponge.
6. Cotton tip applicators.
7. 5 ml Syringe.
8. Membrane insert: Inserts are assembled using hydrophilic polycarbonate filter membrane with 5 μm pores and commercially available membrane inserts.

3 Methods

3.1 Preparation

1. Anesthetize the rat with intramuscular injection of Zetamine (80 mg/kg body weight), and AnaSed (8 mg/kg body weight) (*see* **Note 1–3**).
2. Wait for approximately 5 min and confirm that the rat is under anesthesia by pinching between the animal's toes. The pinching should not cause any reflexes.
3. Shave the abdominal area, and ensure complete removal of hair.
4. Wipe the shaved area with alternating 70% isopropyl alcohol and povidone-iodine solution twice.

3.2 Mesenteric Tissue Exteriorization

Before harvesting the tissue, prepare the surgical bench by wiping the station with 70% ethanol. Pre-warm PBS and media to approximately 37 °C in separate culture dishes using the heating pad (*see* **Notes 4–9**).

1. Spread the absorbent underpad on the bench.
2. Place the anesthetized rat on its back on the underpad.
3. Starting 1 in. below the sternum, use a scalpel blade to make an approximately 2-in. longitudinal incision through the skin and then the linea alba.
4. Place the pre-cut drape over the abdominal section so that the opening aligns with the incision.
5. Place the sterilized surgical stage on the abdominal section so that the opening aligns with the incision.
6. Gently pull out the small intestine through the opening of the surgical stage using sterile cotton-tip applicators without any

contacts with mesenteric windows, and locate the ileum. Lay out the exposed tissue on the surgical stage.

7. Euthanize the rat via intracardiac injection of Beuthanasia-D (0.2 ml).
8. Make sure that the rat is euthanized by palpating the heart. Make sure that there is no pulse before initiating the harvesting process.

3.3 Harvesting Mesenteric Tissues

1. Identify vascularized mesenteric windows starting in the ileum (*see* **Notes 10** and **11**).
2. Locate a desired mesenteric window by cotton-tip applicators, fully spread it out, and place it on the surgical stage.
3. Pull up an arbitrary part of the selected tissue's fat border with the forceps, and cut around the entire mesenteric window using the microscissors (*see* **Note 12** and **13**). Make sure to include a fat border approximately 0.2 mm thick around the mesenteric windows. The fat border provides a cushion between the membrane insert and the dish (*see* Subheading 3.4, part 3) in culture.
4. Rinse the harvested mesenteric window by immersion in PBS solution.
5. Place the tissue in a culture dish containing media.
6. Repeat steps 2–4 until all desired mesenteric tissues have been harvested.

3.4 Mounting the Tissues for Culture

1. Take one tissue out of the media and place it inside the well of a 6-well plate.
2. Using forceps, spread out the tissue on the bottom of the well by grabbing different parts of the peripheral fat pad and pulling them apart, until the tissue is fully exposed and flattened.
3. Place the membrane insert inside the well and on top of the tissue, to keep the tissue in place, and add media supplemented with 10% FBS to fully cover the membrane (*see* **Note 14** and **15**). In order to keep the tissue secured and flat, ensure that the membrane touches the fat pad around the tissue and rests gently against it. Avoid pressing the membrane insert against the tissue as it could cause cell death.
4. Repeat steps 1–3 for all tissues.
5. Transfer the plate to an incubator under standard conditions (5% CO_2).

3.5 Imaging Microvascular Networks for Time-Lapse Comparisons

1. On the day of imaging (*see* **Note 16**), replace the culture media with BSI-lectin labeling solution (*see* **Note 17**).
2. Incubate the tissues for 30 min under standard culture conditions.

3. After the incubation, aspirate the lectin-supplemented media, and wash the tissues with lectin-free media twice.
4. Replace the wash media with the desired culture media.
5. Using a fluorescent microscopy unit equipped with a motorized stage, take images of the networks (*see* **Note 18**). Make sure to record the coordinates of the images so they will be accessible for multiple imaging over the period of the culture. However, if a motorized stage is not available, finding the same region is possible by following the patterning landmarks within the microvascular network (*see* **Note 19–21**).

3.6 Example Application Study

The use of the rat mesentery culture model for drug testing was demonstrated with a validation study evaluating the anti-angiogenic effects of sunitinib, an established tyrosine kinase inhibitor targeting VEGFR-2, and bevacizumab, a well-known VEGF-A inhibitor [8]. Here we showcase a potential application of the model for evaluating unknown effects of potential repositioning based on FDA-approved drug combinations. The combination of nelfinavir and curcumin was recently shown by our laboratories to produce synergistic anticancer effects [10]. While nelfinavir has been reported to cause endothelial dysfunction [11, 12] and curcumin, an antioxidant and NF-kβ inhibitory dietary supplement, is known to have anti-angiogenic effects [13], a question remains whether or not the dose-specific anti-tumor effect of the combination was associated with anti-angiogenesis. Use of the rat mesentery tissue culture model, to evaluate the anti-angiogenic effects of a nelfinavir/curcumin drug combination, highlights its dose and tissue-specific sensitivity. In this study, tissues were exposed to curcumin (4.5 μM) in the presence of a low dose (1.5 μM) or high dose (4.5 μM) of nelfinavir for 3 days. The results suggest that the high-dose drug treatment has inhibitory effects on capillary sprouting and vascular density (Fig. 3). While future studies are undoubtedly needed to

Fig. 3 (continued) sprouting observed in the control group is inhibited with drug treatment. Scale bars = 100 μm. The effect of 3-day exposure to these drugs on 10% serum growth was evaluated for two angiogenic metrics: vessel density (**e**), and number of capillary sprouts per vascular area (**f**). Control tissues were stimulated with 10% serum only. Each pair of bars represents a tissue from a rat. The number following the letter R (from 1 to 4) identifies the rat and the second number (from 1 to 6) identifies the tissue. Changes in segments and sprouts per vascular area were analyzed using mixed effects linear models. Models account for differences in tissue samples from rats. Differences among drug treatment groups were compared using the Tukey method for multiple comparisons. Increases in both vessel density and number of capillary sprouts per tissue were significantly diminished in the high-dose group compared to those in the control group ($p < 0.001$ for both; represented by *). The response was also attenuated in the high-dose group relative to the low-dose group for both capillary sprouts and vessel density ($p = 0.002$ and $p < 0.001$, respectively; represented by +). Differences between the control and the low-dose groups were not statistically significant. The mean increase in vascular density in control group was 59.4 vessel segments compared to 43.5 for the low-dose and 7.6 for high-dose groups. The mean increases in number of capillary sprouts were 11.4, 11.2, and 3.2 for control, low-dose, and high-dose groups, respectively

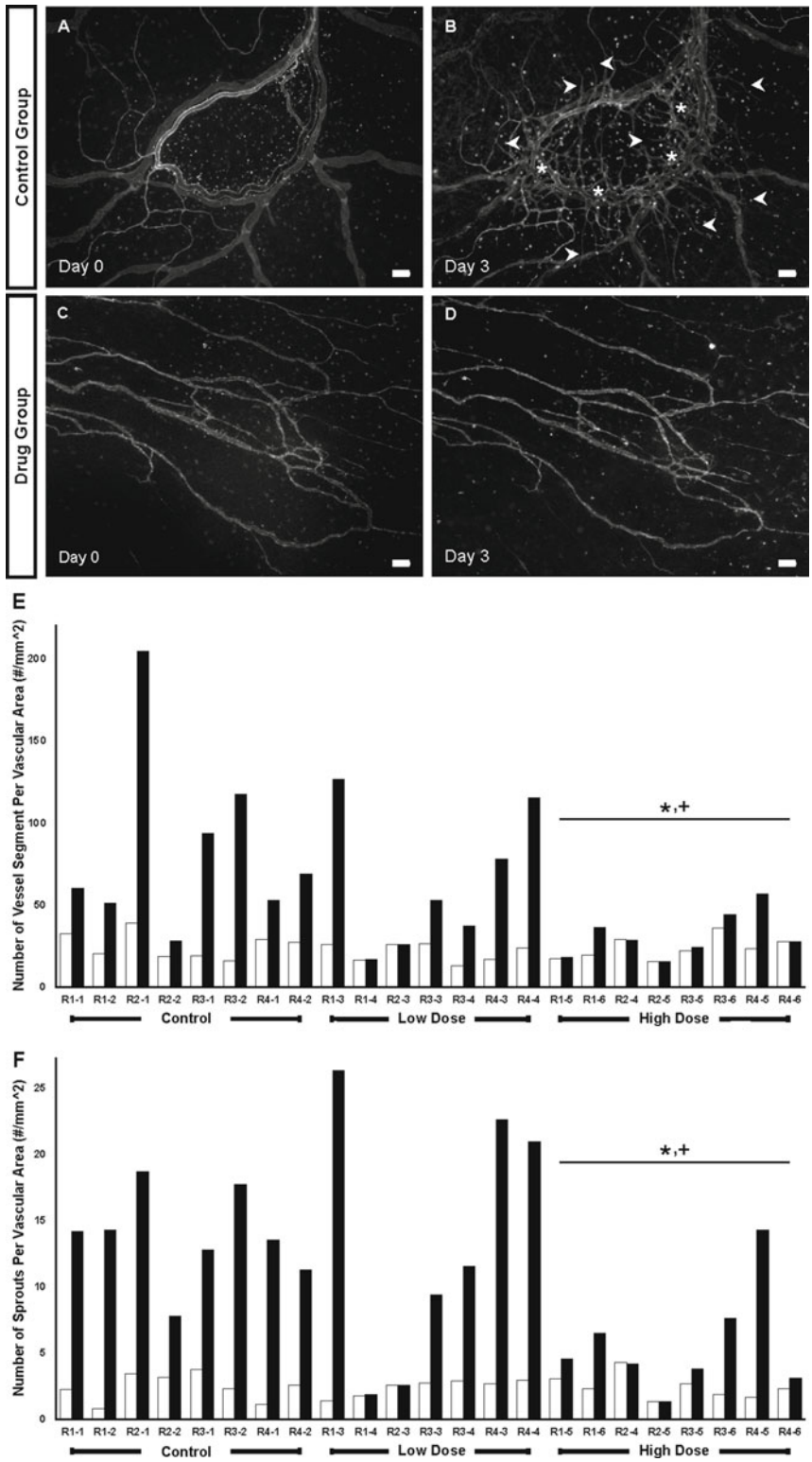

Fig. 3 The inhibition of angiogenesis in rat mesenteric microvascular networks by nelfinavir/curcumin treatment. Day 0 (**a**) and day 3 (**b**) images for tissues stimulated with 10% serum (control). *Arrowheads* indicate the newly formed sprouts caused by the stimulation. *Asterisks* show the regions with high vascular density; day 0 (**c**) and day 3 (**d**) images for tissues stimulated with 10% serum + high-dose drug treatment. The capillary

elucidate the individual dose effects of curcumin and nelfinavir and to evaluate the comparative advantage of drug combination repositioning, the results demonstrate the ability to identify concentration-dependent effects in an intact network scenario—a utility that could be valuable for therapeutic dose determination, which would be influenced by the presence of tissue constituents more than just blood vessels or blood endothelial cells. As a final note, the relevance of the rat mesentery for chemotherapy and anti-angiogenic drug testing is supported by numerous chronic in vivo animal studies [14, 15]. The results from this application study serve to expand the usefulness of this tissue by demonstrating the ability to evaluate drugs, for which the anti-angiogenic effects are unknown, in a "high-content" ex vivo scenario.

4 Notes

1. All animal experiments should be approved by an institutional animal and care use committee (IACUC) or its equivalent.
2. Although this method is based on male adult Wistar rats (325–350 g), other rat strains and ages can be used as tissue sources.
3. This method has been demonstrated with rat mesenteric tissues. The presence of microvascular networks in mouse mesenteric tissues remains in question, and based on our experience, mouse mesenteric tissue windows are largely avascular and lack branching microvascular networks.
4. Bring all the materials and reagents to 37 °C before use.
5. Make sure to use sterile materials and avoid exposing them to open air or mixing them with non-sterile materials. All materials should be handled under the biological hood before surgery to prevent contamination.
6. All surgical tools and instruments should be sterilized before the surgery to prevent culture contamination.
7. All the non-liquid tools and applicators should either be sterile or autoclaved if possible.
8. Plastic parts that are not suitable for high-temperature autoclave should be soaked in 70 % ethanol and thoroughly washed with sterile saline prior to harvesting.
9. Aseptic techniques should be applied throughout the surgery and the culture period. This includes wearing sterile gloves, surgical mask, eye protector, and lab coat.
10. When harvesting tissues, consider the level of vascularization in each tissue, as it is often possible to identify vascular networks just by examining the tissue closely with the naked eye. Although there are approximately 15–20 mesenteric windows

to harvest from adult rats, some of those tissues might not be vascularized.

11. Make sure to start harvesting tissues from the ileum and move towards the jejunum. Based on our experience, tissues from the ileum are likely to be vascularized.
12. During surgery, try to avoid cutting peripheral vessels present in the fat border, as it will lead to bleeding and blood clot formation inside the surgical stage. Occasional bleeding, however, can be stopped by applying pressure on the vessel using a sterile gauze sponge and rinsing the tissues with saline. Make sure to soak up all the blood in the surgical stage with a sterile gauze sponge before harvesting proceeds.
13. During the harvesting period, use the sterile 5.0 ml syringe to intermittently drip saline on the exteriorized tissues to ensure that tissues do not dry out.
14. While spreading the tissue at the bottom of the well, try not to trap air bubbles underneath the tissue. The presence of air bubbles underneath the tissue, occurring during mounting tissues, will cause blackout regions for the imaging.
15. FBS was used in this method since it is relatively inexpensive and causes a robust angiogenic response within 3 days at 10% level [8, 16]. Other concentrations of FBS could be used to cause angiogenesis. Alternatively, FBS can be substituted with different angiogenic and lymphangiogenic growth factors, such as VEGF-A [7], bFGF [7], and VEGF-C [17].
16. Time and repetition of imaging must be determined based on specific aims. The first imaging session is usually done on the day culture starts (day 0), and after that, it could be repeated multiple times throughout the culture.
17. BSI-lectin is used in this chapter to visualize microvascular networks. The decision to choose FITC-conjugated BSI-lectin was based on its robust labeling of blood vessels across the hierarchy of the intact microvascular networks in a relatively short period of time. Alternatively, antibody labeling could represent a potential method to visualize specific cell types.
18. Imaging should be done as fast as possible to reduce possible negative effects associated with live tissue imaging such as potential fluorophore photo-toxicity and temperature fluctuations.
19. Tissues should be re-labeled with BSI-lectin for each imaging session.
20. The 3-day period was selected for this study mainly because 10% FBS causes a robust angiogenic response in mesenteric windows after 3 days (*see* **Note 15**). However, previous viability tests have confirmed that cells remain alive for at least 7 days even in the absence of serum [7]. Furthermore, multiple

studies have shown the presence of cell proliferation, smooth muscle cells, pericytes, and angiogenesis [7, 8]. Nevertheless, future studies are needed to determine how long cells stay viable in this culture past 7 days.

21. For the reported method, an environmental chamber was not used.

Acknowledgment

This work was supported by National Institutes of Health Grant 5-P20GM103629-04 to WLM and the Tulane Center for Aging and the Tulane Hypertension and Renal Center of Excellence.

References

1. Kaunas R, Kang H, Bayless KJ (2011) Synergistic regulation of angiogenic sprouting by biochemical factors and wall shear stress. Cell Mol Bioeng 4(4):547–559. doi:10.1007/s12195-011-0208-5
2. Nicosia RF, Ottinetti A (1990) Growth of microvessels in serum-free matrix culture of rat aorta. A quantitative assay of angiogenesis in vitro. Lab Invest 63(1):115–122
3. Chan JM, Zervantonakis IK, Rimchala T, Polacheck WJ, Whisler J, Kamm RD (2012) Engineering of in vitro 3D capillary beds by self-directed angiogenic sprouting. PLoS One 7(12):e50582. doi:10.1371/journal.pone.0050582
4. Song JW, Munn LL (2011) Fluid forces control endothelial sprouting. Proc Natl Acad Sci U S A 108(37):15342–15347. doi:10.1073/pnas.1105316108
5. Peirce SM, Mac Gabhann F, Bautch VL (2012) Integration of experimental and computational approaches to sprouting angiogenesis. Curr Opin Hematol 19(3):184–191. doi:10.1097/MOH.0b013e3283523ea6
6. Norrby K, Franzen L (1980) A tissue model for the study of cell proliferation in vitro. In Vitro 16(1):31–37
7. Stapor PC, Azimi MS, Ahsan T, Murfee WL (2013) An angiogenesis model for investigating multicellular interactions across intact microvascular networks. Am J Physiol Heart Circ Physiol 304(2):H235–245. doi:10.1152/ajpheart.00552.2012
8. Azimi MS, Myers L, Lacey M, Stewart SA, Shi Q, Katakam PV, Mondal D, Murfee WL (2015) An ex vivo model for anti-angiogenic drug testing on intact microvascular networks. PLoS One 10(3):e0119227. doi:10.1371/journal.pone.0119227
9. Norrby K (2006) In vivo models of angiogenesis. J Cell Mol Med 10(3):588–612
10. Mathur A, Abd Elmageed ZY, Liu X, Kostochka ML, Zhang H, Abdel-Mageed AB, Mondal D (2014) Subverting ER-stress towards apoptosis by nelfinavir and curcumin coexposure augments docetaxel efficacy in castration resistant prostate cancer cells. PLoS One 9(8):e103109. doi:10.1371/journal.pone.0103109
11. Mondal D, Pradhan L, Ali M, Agrawal KC (2004) HAART drugs induce oxidative stress in human endothelial cells and increase endothelial recruitment of mononuclear cells: exacerbation by inflammatory cytokines and amelioration by antioxidants. Cardiovasc Toxicol 4(3):287–302
12. Mondal D, Liu K, Hamblin M, Lasky JA, Agrawal KC (2013) Nelfinavir suppresses insulin signaling and nitric oxide production by human aortic endothelial cells: protective effects of thiazolidinediones. Ochsner J 13(1):76–90
13. Bhandarkar SS, Arbiser JL (2007) Curcumin as an inhibitor of angiogenesis. Adv Exp Med Biol 595:185–195. doi:10.1007/978-0-387-46401-5_7
14. Lennernas B, Albertsson P, Damber JE, Norrby K (2004) Antiangiogenic effect of metronomic paclitaxel treatment in prostate cancer and non-tumor tissue in the same animals: a quantitative study. APMIS 112(3):201–209. doi:10.1111/j.1600-0463.2004.apm1120306.x

15. Albertsson P, Lennernas B, Norrby K (2012) Low-dosage metronomic chemotherapy and angiogenesis: topoisomerase inhibitors irinotecan and mitoxantrone stimulate VEGF-A-mediated angiogenesis. APMIS 120(2):147–156. doi:10.1111/j.1600-0463.2011.02830.x
16. Phamduy TB, Sweat RS, Azimi MS, Burow ME, Murfee WL, Chrisey DB (2015) Printing cancer cells into intact microvascular networks: a model for investigating cancer cell dynamics during angiogenesis. Integr Biol (Camb) 7(9):1068–1078. doi:10.1039/c5ib00151j
17. Sweat RS, Sloas DC, Murfee WL (2014) VEGF-C induces lymphangiogenesis and angiogenesis in the rat mesentery culture model. Microcirculation 21(6):532–540. doi:10.1111/micc.12132

Chapter 9

The Chorioallantoic Membrane of the Chick Embryo to Assess Tumor Formation and Metastasis

Anne Herrmann, Diana Moss, and Violaine Sée

Abstract

The chorioallantoic membrane (CAM) of the chick embryo is a suitable and convenient platform for the assessment of tumor formation and metastatic dissemination. Here, we describe tumor cell engraftment on the extraembryonic CAM and further monitoring of tumor growth and metastasis.

Key words Chick embryo, CAM, Tumor model, Metastasis, Tumorigenesis

1 Introduction

The ability to quantify tumor growth and metastasis in vivo is critical not only to advance our understanding of the multistep cancer progression but also for preclinical pharmacological drug testing. While various model organisms exist, the chick embryo can present advantages over more routinely used rodent models and has been used for more than a century. In 1911 Rous and Murphy reported that avian sarcoma cells form tumors when implanted on the chorioallantoic membrane (CAM) [1] and tumorigenesis has since been shown for cancer cells of murine, human, or other origin (reviewed in ref. 2). This is not surprising, as the CAM offers the ideal microenvironment for the engraftment of cancer cells. It benefits from a rich capillary network and supply of nutrients, and is easily accessible and suitable for all cell types without the need of a special, immunodeficient host as the chick embryo naturally has no immune system during most of its development [3]. In addition, its in ovo development allows noninvasive monitoring including the ability for live in vivo imaging of tumorigenesis and metastasis [4]. Some of the metastatic processes can be monitored by direct injection of tumor cells intravenously, in the yolk sac or in a target organ. Their behavior in blood vessels and their ability to form tumors can be imaged upon injection or several days later [4, 5]. However, to obtain a complete picture of all metastatic cascade events from

Domenico Ribatti (ed.), *Tumor Angiogenesis Assays: Methods and Protocols*, Methods in Molecular Biology, vol. 1464,
DOI 10.1007/978-1-4939-3999-2_9,

primary tumor formation, invasion, intravasation to extravasation proliferation in the metastatic site and formation of secondary tumors, the implantation onto the CAM is the most suitable model. Here, we explain the different experimental steps required for spontaneous metastasis assessment using the CAM model including the storage of fertilized chicken eggs, their incubation and windowing, tumor cell engraftment on the CAM, and the assessment of tumor formation and metastasis.

2 Materials

2.1 Tissue Culture

1. CO_2 incubator.
2. Sterile phosphate-buffered saline (PBS).
3. Trypsin-EDTA.
4. Fetal calf serum containing media for cell culture.
5. 15 ml conical tubes.
6. Centrifuge.
7. Ice.

2.2 Egg Incubation and Windowing

1. Refrigerator for fertilized egg storage at 12–14 °C.
2. Blue tack (Bostik) and petri dish for "egg holder" (*see* **Note 1**).
3. Power Craft PKW-160W Combitool Mini-drill, used with a Combi disk as rotary tool (*see* **Note 2**).
4. Egg incubator (OvaEasy 190 advance Series II, Brinsea) including removable trays and humidity pump (Humidity Management Module H22, Brinsea).
5. Egg incubator (Multihatch Mark II, Brinsea) (*see* **Note 3**).
6. Egg piercer (Fox Run Boiled Egg Piercer).
7. Sterile 10 ml syringe (BD, Catalogue no.: 302188) and needle (Terumo Neolus, 20 G × 1″, 0.9 × 25 mm).
8. Waste container.
9. Rough tissue wipes.
10. Adhesive tape to attach egg window (3 M, Scotch Magic tape, Catalogue no.: 5210460).
11. Adhesive tape to cover albumin hole (Nev's Ink, Inc. Brand Labelling Tape).
12. Sterile scalpel (Swann Morton, Catalogue no.: 0501).

2.3 CAM Implantation

1. Sterile flow cabinet.
2. Pipette and pipette tips.
3. Lens cleaning tissue (Fisher Scientific Catalogue no.: FB13066), cut in 0.5 × 3 cm stripes, autoclaved.

4. Dumont Tweezers 4 (T5389, straight).
5. Marker pen or pencil.

2.4 Collection of Tumor Samples and Dissection

1. 4% Formaldehyde prepared in PBS (Sigma Aldrich).
2. Ice.
3. Dissection scissors and tweezers (springbow dissection scissors (T5372), Dumont tweezers 7 (T5392, curved), Dumont tweezers 4 (T5389, straight), delicate operating scissors (straight; sharp-sharp; 30 mm blade length; 4 3/4″ overall length)).
4. PBS (Life Technologies, with $MgCl_2$ and $CaCl_2$).
5. Petri dishes (100 mm).
6. Leica M165FC fluorescent stereomicroscope with 16.5:1 zoom optics, Leica DFC425 C camera.

3 Methods

All procedures are carried out at room temperature unless otherwise stated. Cell preparation and CAM implantation have to be performed under a sterile laminar flow hood to avoid contamination. Cell preparation is described for the use of a T-75 cm flask (surface area of 7500 mm^2).

3.1 Incubation of Chicken Eggs

1. Fertilized white leghorn chicken eggs should be stored in a cool damp place. We suggest adding a water tray to a refrigerator set at 12–14 °C. Fertilized eggs can be stored under these conditions for up to 14 days without significant delay of embryonic development when transferred to 37.8 °C.
2. Incubation should commence 7 days prior to CAM implantation. The desired number of fertilized eggs should be removed from the refrigerator and labeled for further identification.
3. Eggs are incubated, labeled side uppermost, in a humidified incubator (40%) at 37.8 °C. The first day of incubation is classed as embryonic day 0 (E0).

3.2 Fenestration of Chicken Eggs

1. On E3 (72 h after start of incubation) eggs are removed from the incubator and gently cleaned with rough tissue wipes sprayed with a little 70% ethanol. As the egg shell is permeable ethanol should be used with caution and not be sprayed directly on the egg as it can impair the survival of the embryos.
2. Rotate the eggs from side to side several times to ensure that the embryo and its membrane are not sticking to the inner side of the egg shell.
3. Place the egg on a cushioned holder (*see* **Note 1**), labeled side facing up.

4. Puncture the wide base of the egg (air cell) with egg piercer and insert a 10 ml syringe with 19 G needle to remove about 3 ml of albumen. This will result in a dropping of the embryo and ensure a free space between the shell and embryonic structures and avoid its disruption during fenestration. The needle should be inserted delicately to avoid damaging of the egg yolk. Needle blockage can occur due to the chalazae, which hold the yolk in place. In that case, the needle should be carefully removed and reinserted.
5. The aspirated albumen can be discarded. The amount removed (~3 ml) might need to be adjusted depending on the size of the egg.
6. Seal pierced hole with Nev's Ink tape. Use as little tape as possible; usually a 0.5×0.5 cm piece is sufficient to seal the hole to minimize the loss of gas exchanges between the embryo and the egg shell.
7. A rectangular window (1×2 cm) is carefully cut in the egg shell using a rotary tool with cutting disk attachment. The fine opaque inner shell membrane beneath the eggshell must not be damaged; otherwise egg shell dust will fall on the embryo and its extra-embryonic membrane, with a risk of the window falling onto the embryo (*see* **Note 2**).
8. Separate the connection of the inner shell membrane on three sides with a sterile scalpel. Avoid cutting all sides as this will cause the window to fall on top of the embryo.
9. Attach about 2.5 cm of Scotch Magic adhesive tape on the fenestrated area and carefully remove the window completely. The embryo should be located directly beneath the fenestrated opening.
10. Reclose the window and incubate the egg in a humidified incubator (40% humidity is recommended) at 37.8 °C (*see* **Note 3**). It is important that the tape is sealed neatly around the cuts, but a corner of the tape should be left unattached for ease of handling later on (Fig. 1).

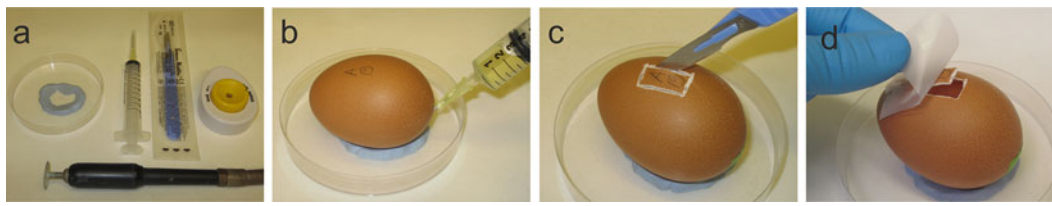

Fig. 1 Representative images of egg fenestration. (**a**) Tools needed for egg fenestration showing cushioned egg holder, syringe with needle, sterile scalpel, egg piercer (*left* to *right*), and rotary-tool (*bottom*). (**b**) Removal of albumen, **step 3.2.4**. (**c**) Careful incision of membrane, **step 3.2.8**. (**d**) Use of adhesive tape to glue the window in place, **step 3.2.9**

3.3 Cell Preparation at E7

1. In order to easily and reliably identify tumor cells, their labeling with a fluorescent protein (stable cell line) is highly recommended.
2. For adherent cells remove supernatant and wash once with 5 ml of PBS.
3. Remove PBS and add 1 ml of trypsin-EDTA and incubate for as required at 37 °C.
4. Add 10 ml of media containing 10% FCS, count cells with a hemocytometer or similar, and collect cell suspension in conical tube.
5. Centrifuge for 5 min at 101 × *g*.
6. Remove supernatant completely and use pipette to carefully transfer the pellet to a microtube. The pellet should have a thick liquid consistency (*see* **Note 4**) and be stored on ice until CAM implantation (*see* **Note 5**).

3.4 Cell Implantation onto the CAM at E7

1. At E7 remove the eggs from the incubator and discard unfertilized eggs or dead embryos. This can be assessed by opening the window and observing the developmental stage and/or presence of a heartbeat.
2. Place the egg on an egg holder, carefully remove the window, and, using a stereomicroscope with bright field, locate the CAM (it should be right beneath the fenestrated area above the embryo, *see* **Note 6**).
3. Use tweezers to pick up and fold a strip of sterile lens tissue paper and lower it into the window until it touches the CAM. Remove tissue paper carefully; the part of the CAM that was in contact with the lens tissue should be dry and ideally have a small fold.
4. Pipet 2×10^6 cells directly into the fold (*see* **Note 7**), reseal the fenestrated area, and label the side of the egg with a number or other form of identification. This should be done as quickly as possible after the target area has been dried with tissue paper.
5. Without disturbing the cell pellet on the CAM, place the egg back into the incubator and incubate for a further 7 days until E14.

3.5 Collection of Tumor Samples at E14

1. At E14, the end of the experimental period, tumor formation and metastasis are investigated using a fluorescence stereomicroscope.
2. Place the egg on an egg holder and remove window.
3. Using a forceps, carefully remove the shell surrounding the fenestrated area to increase the field of view. Remove as much shell as possible without disturbing the extra-embryonic membranes or embryo.

4. Use bright-field and fluorescence imaging to locate the primary tumor and/or any dried cell patches.
5. Acquire images of the tumor using fluorescence and bright-field.
6. Use dissection scissors and tweezers to carefully remove the tumor from the CAM and place it in a petri dish containing sterile PBS for further image acquisition.
7. Tumors are imaged from three perspectives: anterior, posterior, and lateral view (*see* **Note 8**).
8. For immunohistochemistry (IHC) (*see* **Note 9**), place the tumor in 4% formaldehyde solution and incubate for 4 h to overnight. As a general rule, incubate tumor samples for 1 h per 1 mm of tissue thickness.
9. Tumors should not be stored in formaldehyde solution for a long term and the fixation protocol might need to be adapted depending on the tissue and labeling technique.

3.6 Dissection and Detection of Metastasis

1. To monitor metastatic potential, embryos have to be removed from their shell and dissected, after primary tumor excision.
2. The embryo is picked up by the neck using curved tweezers and detached from the allantois and extra-embryonic membranes with scissors.
3. Place the embryo in a petri dish and kill it in accordance with ethical standards, *e.g.*, quick decapitation. Both head and body should be immersed in some PBS to prevent tissues from drying out.
4. Remove organs carefully and assess each tissue and organ for fluorescence to identify potential metastatic deposits.
5. Depending on the metastatic potential of the cell used (*see* **Note 10**), metastasis can be non-existent or limited to a few cells only; hence a careful and thorough examination is recommended (*see* **Note 11**) (Fig. 2).

4 Notes

1. Use blue-tack to form a cushioned mold for the egg, *e.g.*, in a 100 mm petri dish.
2. A sharp pair of scissors can also be used for fenestration. After performing **steps 3.2.1–3.2.6** an egg piercer should be used to punch two holes in the area of the window. The sharp tip of the scissors is then used to increase the size of the punched holes. A piece of adhesive tape should be attached to the top of the area to prevent egg shell pieces from falling on top of the embryo during the window incision. Scissor blades are inserted in the holes and used to cut out the window. Protocol is continued from **step 3.2.9**.

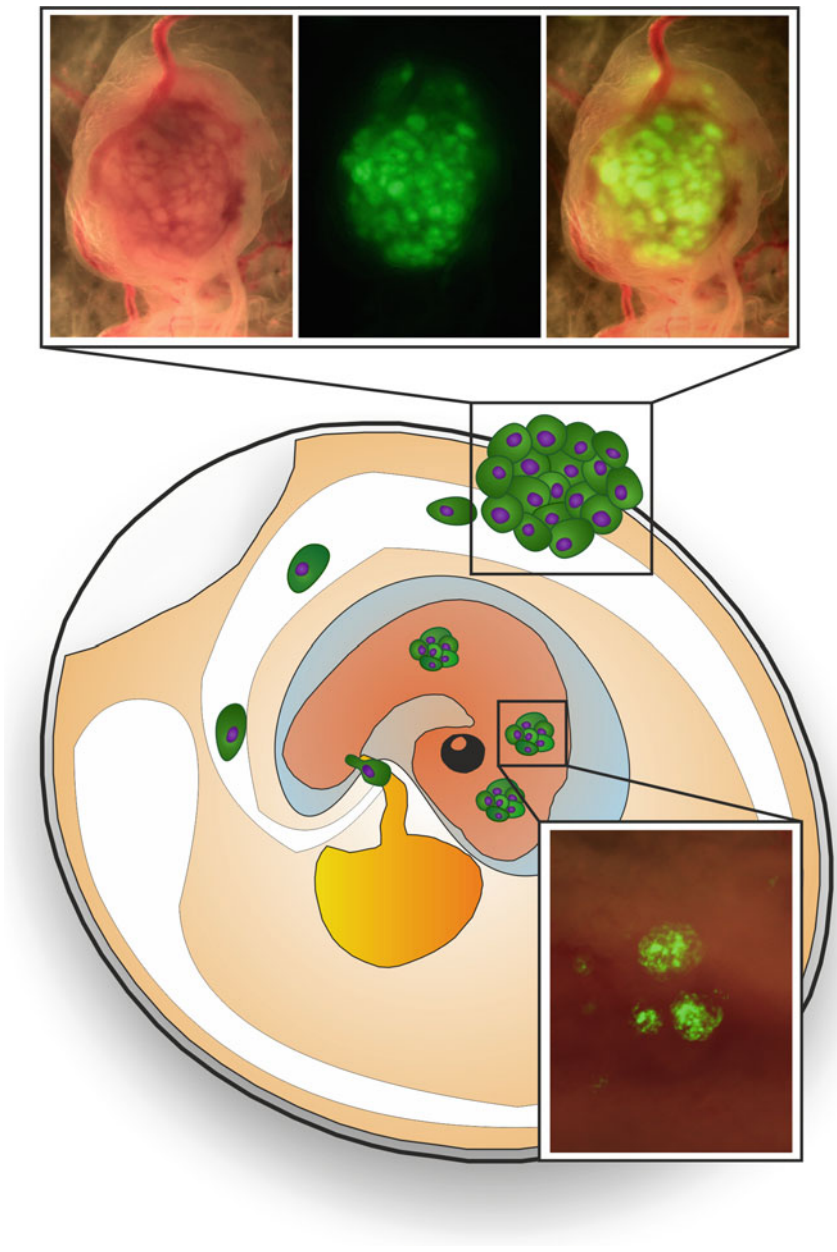

Fig. 2 Scheme of chick embryo and its embryonic CAM with representative images of primary tumors grown on the CAM (*top panel*, taken at E14) and secondary tumors formed in the embryo itself (*bottom image*). Cells have been transduced with GFP for ease of identification

3. Ideally different incubators for different egg incubation steps should be used, in order to avoid contamination and to keep changes of temperature and humidity to a minimum. As a suggestion, one incubator should be used to incubate eggs before windowing, one for windowed eggs and another one post-CAM implantation.

4. Cell pellets should be resuspended in a minimum volume of liquid. The consistency of the cell solution should be so viscous that a droplet of cells can be implanted on the CAM without spreading over the CAM's surface. For human cancer cells we recommend about 2×10^6 cells in 2 μl per egg.
5. Cells should be implanted on the CAM immediately after preparation. A delay of more than 15 min is not recommended.
6. If embryonic development is delayed, the CAM could be absent in an early E7 embryo. It is recommended to check the presence of the CAM before cell preparation. A further incubation for a few more hours is usually sufficient for completion of CAM formation.
7. The cell number for tumor formation might have to be adjusted depending on cell and tumor type. For neuroblastoma, glioblastoma, and breast cancer cell lines (SK-N-AS, SK-N-BE(2)C, SH-SY-5Y, U87, D566, MDA-MB-31, ZR-75) 2×10^6 cells results in consistent and reliable tumor formation. If the efficiency with which the cell line of interest forms tumors is low or zero, pretreatment of the CAM with trypsin-EDTA can improve this. Following treatment of the CAM with lens tissue, 5 μl of trypsin-EDTA is added to the surface of the CAM and then the cell pellet is added. However, this step could also facilitate metastasis, which has to be considered when studying spontaneous metastatic dissemination.
8. Pictures of anterior, posterior, and lateral views are taken in order to allow a rough estimate of tumor volume.
9. For other applications, *e.g.*, quantitative real-time PCR, tumors can be placed in RNA later and stored on ice until they can be processed.
10. Metastatic occurrence can be triggered or enhanced by precondition of cells in 1 % O_2 for 3 days or DMOG (Enzo Life Sciences, 0.5 mM, 24 h) as observed for neuroblastoma cells [4].
11. In order to guarantee a reliable and quick identification of even a small amount of metastasized cells it is recommended to transduce cells with a fluorescent viral vector. Viral transduction should be optimized for each cell line to guarantee bright fluorescent intensity. It is also recommended to work with a pure cell population where at least 95 % of the cells express the fluorescent protein. Fluorescence-activated cell sorting (FACS) can be used to enrich the population.

References

1. Rous P, Murphy JB (1911) Tumor implantations in the developing embryo. Experiments with a transmissible sarcoma of the fowl. J Am Med Assoc 56:741–742
2. Ribatti D (2008) The chick embryo chorioallantoic membrane in the study of tumor angiogenesis. Rom J Morphol Embryol 49:131–135
3. Meirowsky E, Freeman LW, Woodard JS (1954) The response of embryonic chick membrane to Bowen's intraepithelial cancer. J Invest Dermatol 22:417–429
4. Herrmann A, Rice M, Levy R et al (2015) Cellular memory of hypoxia elicits neuroblastoma metastasis and enables invasion by non-aggressive neighbouring cells. Oncogenesis 4:e138
5. Carter R, Mullassery D, See V et al (2012) Exploitation of chick embryo environments to reprogram MYCN-amplified neuroblastoma cells to a benign phenotype, lacking detectable MYCN expression. Oncogenesis 1:e24

Chapter 10

Transgenic Zebrafish

Xiaowen Chen, Dafne Gays, and Massimo M. Santoro

Abstract

The generation and use of transgenic animals carrying exogenous pieces of DNA stably integrated in their genome is a quite common practice in modern laboratories. Zebrafish have been increasingly used for transgenesis studies mainly due to easy egg accessibility and manipulation together with relatively short generation time. The zebrafish transgenic technology becomes very useful when coupled to continuous in vivo observation of the vertebrate embryonic vasculature. Here we describe the most common technique to generate zebrafish transgenic fish using the Tol2-based methodology and their applications to visualize vascular tissues or endothelial cells in vivo and for functional tumor angiogenesis studies.

Key words Zebrafish embryos, Gateway cloning system, Tol2 system, Transgenesis

1 Introduction

The zebrafish (*D. rerio*) is a small tropical fish, which has become very popular in laboratories worldwide mainly for its advantages compared to rodent models to study vertebrate development and disease [1, 2]. Among the several advantages of the zebrafish model system is the large amount embryos that are generated at each adult mating. This large amount of eggs (e.g., embryos) generated an extraordinary resource for further experimental needs. Moreover, the optical clarity of embryos easily allows live imaging of cells and dynamics tracking in the context of a whole organism. A good example is the use of transgenic zebrafish animals marking endothelial cells with a genetically encoded marker [3]. To this purpose in last decade, a considerable number of zebrafish transgenic lines have been generated to better characterize different components of vascular system such us arteries, veins, and lymphatic tissues. These lines express a fluorescent protein under control of a selected promoter, offering the chance to in vivo identify single cells as well as the anatomical structure they take part [4]. Thus, transgenic (Tg) tissue-specific zebrafish lines are commonly applied in in vivo studies to characterize molecular and genetics

*Author contributed equally with all other contributors.

Domenico Ribatti (ed.), *Tumor Angiogenesis Assays: Methods and Protocols*, Methods in Molecular Biology, vol. 1464,
DOI 10.1007/978-1-4939-3999-2_10,

pathways responsible for vascular system development and morphogenesis [5–7]. Most importantly, such Tg zebrafish lines have been generated to study vascular-associated pathological conditions such as tumor angiogenesis [8, 9].

Here we describe a method to generate Tg fish lines based on the Tol2-mediated transgenesis protocol. Briefly, a Tol2-based construct can be assembled by using the Tol2 Kit and three-fragment gateway recombination cloning strategy [10, 11]. The plasmid containing the Tol2 region is then mixed with mRNA for Tol2 transposase and microinjected into one-cell-stage wild-type embryos. Injected embryos were raised to adulthood and founders were screened for fluorescence in the entire vascular system. Recent improvement of the Tol2-based Tg system in zebrafish has also allowed the control of enzyme expression in time and space by coupling the insertion of the gene with regulatory elements such as GAL4/UAS or Cre/LoxP [12, 13]. For all these reasons, the zebrafish transgenesis is one of the most used technologies established within the scientific community.

2 Materials

2.1 Reagents

1. Wild-type (WT) AB zebrafish strain or others (http://zfin.org/action/feature/wildtype-list).
2. Egg water: Instant Ocean Sea Salts dissolved in distilled water to 60 μg/ml [14].
3. Agarose (A9539, Sigma Aldrich).
4. Plasmid DNA containing the transgene of interest.
5. High Pure Plasmid Isolation Kit (11754777001, Roche).
6. pCS-TP plasmid carrying Tol2 transposase [15].
7. Restriction enzyme NotI (10 U/μl, ER0591, ThermoFisher Scientific).
8. E.Z.N.A.® Gel Extraction Kit (D2500, Omega Bio-tek).
9. mMESSAGE mMACHINE® SP6 Transcription Kit (AM1340, ThermoFisher Scientific).
10. Phenol red stock: Dissolve 2 g of phenol red in 10 ml of H_2O, P5530, Sigma-Aldrich, final concentration is 0.2% (w/v).
11. Tricaine (3-aminobenzoic acid ethyl ester, A-5040, Sigma-Aldrich): Stock solution is 0.16% in H_2O. Store at 4 °C.
12. Mineral oil (M5904, Sigma-Aldrich).
13. RNaseZap® RNase Decontamination Solution (AM9780, ThermoFisher Scientific).

2.2 Equipments

1. Air incubator set at 28 °C (Thermostatic cabinet, Lovibond®).
2. Stereo microscope (M80, Leica).
3. Epifluorescence stereomicroscope (SMZ18, Nikon).

4. NanoDrop2000 spectrophotometer (ThermoFisher Scientific).
5. Plastic mold (4.0 × 6.5 cm, TU-1, Adaptive Science Tools).
6. Horizontal puller (P-97 Flaming/Brown).
7. Borosilicate glass capillaries (3.5 nl, 4878, World Precision Instruments).
8. Microinjection apparatus (Picospritzer III, Parker Hannifin Corporation).
9. Micromanipulator (World Precision Instruments).
10. Micrometric slide (PYSER-SGI).
11. Microloader tips (0.5–10 ml, Eppendorf).
12. Glass or plastic pipettes for embryo transfer.
13. Parafilm® (P7793, Sigma).

3 Methods

3.1 The Following Step Can Be Performed Any Time Before the Injection

1. Preparation of microinjection needles: A good needle is key to this technique. Needles with a long shank tend to break more easily and can bend on, rather than penetrate, the chorion. They can also easily get plugged. Needles with a short shank do not break easily, but they can damage the embryos as they tend to thicken quite quickly. Good needles could be obtained from borosilicate glass capillaries pulled using P-97 Flaming/Brown puller using the following parameters: heat = 788; pull = 100; Vel = 250; time = 150; and pressure = 500.
2. Preparation of agarose microinjection plates: Different methods could be used as previously described [16, 17] (*see* **Note 1**). Agarose plates can be reused. After use, remove all fluid and seal the dish with Parafilm® and keep at +4 °C. Warm up plates before injection by adding room-temperature fish water to the plate, or putting them in the incubator at 28 °C.
3. Preparation of the plasmid DNA containing the transgene of interest: Plasmid should be designed and prepared following the Tol2 system guidelines [10, 11]. Plasmid should be purified using high-purity plasmid preparation kit. Measure DNA concentration by NanoDrop2000. Samples can be stored at −20 °C until required.
4. Preparation of *transposase* capped-mRNA: pCS2-TP plasmid should be purified using high-purity plasmid preparation kit and eluted in nuclease-free water. The plasmid is linearized by NotI and purified using a commercial gel extraction kit. For mRNA synthesis we use the Ambion mMACHINE® SP6 Transcription Kit following the manufacturer's instructions. mRNA concentration is determined by NanoDrop2000. mRNA quality could be evaluated by agarose gel electrophoresis if necessary. Aliquot the RNA in small quantities (3–5 µl) and store at −80 °C.

3.2 The Day Before Injection, Day 0

Set up 10–15 pairs of WT fish in the late afternoon, keeping the male and female separated from one another (*see* **Note 2** for more tips).

3.3 The Day of Injection, Day 1

1. Prepare the injection solution. Mix plasmid DNA containing the transgene of interest (15 ng/μl), *transposase* mRNA (25 ng/μl), and phenol red (1×) (*see* **Note 3**). Usually a volume of 5 μl is sufficient to inject more than 500 eggs. Heat the solution at 65 °C for 10 min to denature the mRNA and chill on ice. Centrifuge and keep on ice until use. The injection solution should be freshly made and not reused.
2. Prepare the needle and assemble the injection apparatus. Needles can be cut open either in the air or in the egg water. Using the highest magnification on your stereomicroscope, cut a very small amount of the tip of the needle using clean forceps. The inner diameter should be around 10 μm. Backfill the needle, loading 2–3 μl using Eppendorf microloader tips. Instead of loading bigger volumes, it is better to reload repeatedly the needle with few μl of fresh solution. Insert the needle in the holder of the micromanipulator. To calibrate the needle adjust the microinjector pressure and time setting. The time setting differs between needles and usually ranges from 25 to 300 ms. Under the stereomicroscope inject a small amount of solution into a drop of mineral oil on a micrometric slide. Measure the size of the injected droplet to determine its volume. Set the microinjector time in the way that the droplet volume is around 2–4 μl. The volume must not exceed 1/10 of the cell's volume (*see* **Note 4**). More details can also be found in a video protocol [18].
3. Collect the eggs. Remove the separator from the breeding tanks and wait until fish lay eggs. About 20 min later eggs can be collected using an egg strainer. Do not wait for more time; injection should be done in the one-cell eggs.
4. Inject embryos. Align eggs in the agarose microinjection plate with the help of a plastic pipette. Inject in the cytoplasm of the first cell and avoid injection in the yolk. This will ensure the integration of the transgene in the genome of the first cell and then the inheritance of the same modification in all the other cells. Inject a large amount of eggs. Typically 20–40% of the injected embryos express the transgene and the mortality rate is about 60%. To have 20–30 positive embryos, around 200 should be injected. Leave 15–30 eggs uninjected to check their viability (*see* **Note 5**). After injecting the eggs, use a gentle stream of egg water to move the injected eggs into a clean Petri dish.
5. (Optional) Few hours after the injection, select the eggs according to the presence or not of phenol red in the cells. Remove eggs that do not have red cells or that are not fertilized.

This step can be avoided if the transgenic construct contains a fluorescent marker that can be used later on to select the eggs. Conversely, if genotyping is made by PCR, red phenol selection will decrease the number of negative embryos.

3.4 Day 1/2/3 After Injection

Check the survival of the injected embryos (*see* **Note 6**) and remove the unfertilized or abnormal eggs. Check the expression of the transgene of interest. Very often, the transgenic construct contains a fluorescent marker which can be used for embryos selection (Fig. 1). Otherwise, you can co-inject the transgene of interest with a fluorescent reporter construct [19] or you can put all these elements into one construct (to exclude the possibility that fusion protein may affect function of the transgene) or use 2A peptide [20]. In the case using an epifluorescence stereomicroscope to check the expression of fluorescent marker in the tissue and developmental stage where it is expected to be expressed. In this step, embryos will show a mosaic expression of the transgene [21]. If embryos move, tricaine could be added to the medium. If the transgenic construct does not contain a fluorescent marker, PCR could be done to verify the presence of the transgene. To do so, sacrifice 5–10 injected embryos, and extract genomic DNA (*see* **Notes 7** and **8**).

3.5 Day 5–12 Weeks

Raise the positive embryos to sexual maturity. This step will take at least 9–12 weeks. These fish are potential F0 founder fish. Each of them contains the transgene, integrated in a different position and copy number in the genome. Some of them will have the transgene integrated in the germline and will be able to transmit it to the next generation.

3.6 Obtain Stable Transgenic Lines

Outcross F0 fish to wild-type and screen the resulting F1 embryos for the expression of the transgene. The percentage of F1 embryos expressing the transgene may vary from 1 to 50%. Raise the positive F1 embryos to sexual maturity. Establish the transgenic line from at least three different F0 embryos (*see* **Note 9**).

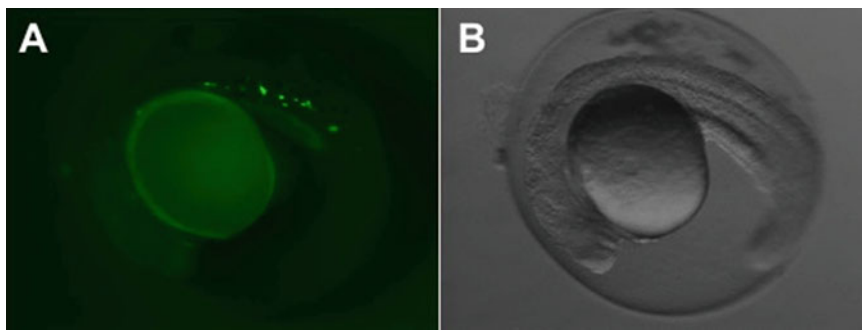

Fig. 1 Representative image of a mosaic transgenic embryo. (**a**) GFP expression in some blood vessels driven by the *kdrl* promoter using the Tol2-based method described in the manuscript. (**b**) Bright-field image of the same embryo

4 Notes

1. In our lab we use plastic mold to make injection plate. We pour 1.5 % hot agarose into petri dish (about 25 ml) and place the mold carefully onto the agarose using forceps so that no bubbles are trapped and remove the mold after the agarose solidifies. You can put the plate in the fridge to speed up the solidification.
2. To increase the release of eggs many tricks can be applied during the setup of the cross.
   (a) Provide plastic "grass" as a hiding place for the fish.
   (b) Set up fish with a male:female ratio of 1:2.
   (c) Before removing the separator, transfer the fish into a tank with freshwater.
   (d) If the fish do not lay eggs, combine more pairs in the same one tank.
   (e) Keep adult males and females separated for few days (around 1 week) before mating.
3. Be careful to handle with RNA and always clean surfaces and pipettes with RNase Zap and use RNase-free tips. In respect to the concentration of the plasmid for injection, we indicate here the dose we always try at first; otherwise, you need to determine the dose by yourselves.
4. Here we use the air injection system. Besides, there is frequently used another system that is driven by mineral oil. In detail, you can inject the mineral oil directly into the needle, and assemble the needle into microinjection base. The advantage of the latter system is that you can easily set up the injection dose manually and suck the injection solution by "PULL" button in the system. But if mineral oil interferes with what you inject, it is better to use the air-driven system.
5. In some cases, the needle gets plugged. Here are some troubleshootings.
   (a) Try to remove visible debris at the tip by scratching carefully the needle over Parafilm®.
   (b) Re-break the tip and recalibrate the needle.
   (c) Phenol red is one of the causes why needles get plugged. Check the quality of phenol red and filter in the case you see debris. It is also possible to use it at lower concentration. However, in this case egg selection will be more difficult. For proficient persons, phenol red could be removed from the injection solution.
6. Sometimes, high mortality of injected eggs could be observed; there are many different reasons.

(a) The needle is too big. Optimize the puller with different time and pressure settings.

(b) Bad eggs: If fish are laying bad eggs, the mortality rate will be high also in uninjected controls. If the problem persists, use a different batch of fish.

(c) Poor injection technique: Avoid multiple injection in the same egg. Avoid injecting air bubbles or stretching the yolk.

(d) Toxicity of the transgene: The transgene itself is toxic to embryos or overdose injection.

7. Here we provide an easy and efficient way to extract PCR-grade crude genomic DNA. Put the embryos in a 1.5 ml Eppendorf tube, remove the fish water, and add 20–50 μl of 50 mM NaOH. Boil at 95 °C for 10–20 min. Cool down the samples at 12 °C and add 1/10 volume of 1 M Tris–HCl (pH = 8.0). Use 1–5 μl of the supernatant for PCR.

8. Based on our experiences, several factors can cause low numbers of positive injected embryos.

(a) Injection in the yolk decreases the integration rate in the genome [19]. Inject in the cytoplasm of the first cell and avoid injection in the yolk.

(b) Transgene size: An optimal integration rate is obtained when the transgene size is <2–3 kb. The efficiency of transgene integration and transmission decreases with size.

If the size could not be reduced, inject more eggs to increase the probability of get positive embryos.

(c) Transgene toxicity.

(d) Low quality of *transposase* mRNA: mRNA is easily degraded; thus immediately after synthesis check the quality of mRNA on an agarose gel and prepare small aliquots (2–3 μl) to be stored at −80 °C until use. Frequent freeze/thaw can result in mRNA degradation and loss of activity.

(e) Change the transgene:transposase molar ratio.

9. In some cases, it happens that there is no positive F1 embryo after screening. You need to check the following possibilities.

(a) Screen a higher number of F0 adult fish.

(b) Before considering as negative an F0 fish, be sure to have analyzed at least 80–150 F1 embryos. Since the transgene transmission rate could vary between 1 and 50%, sometimes you will have 1 positive embryo every 100!

(c) Transgene toxicity: Due to the toxicity of the transgene, the positive embryos may die during development and cannot survive until adulthood.

References

1. Shin JT, Fishman MC (2002) From Zebrafish to human: modular medical models. Annu Rev Genomics Hum Genet 3:311–340
2. Lieschke GJ, Currie PD (2007) Animal models of human disease: zebrafish swim into view. Nat Rev Genet 8(5):353–367
3. Lawson ND, Weinstein BM (2002) In vivo imaging of embryonic vascular development using transgenic zebrafish. Dev Biol 248(2): 307–318
4. Asakawa K, Kawakami K (2010) A transgenic zebrafish for monitoring in vivo microtubule structures. Dev Dyn 239(10):2695–2699
5. Torres-Vazquez J, Kamei M, Weinstein BM (2003) Molecular distinction between arteries and veins. Cell Tissue Res 314(1):43–59
6. Lawson ND, Weinstein BM (2002) Arteries and veins: making a difference with zebrafish. Nat Rev Genet 3(9):674–682
7. Stainier DY (2001) Zebrafish genetics and vertebrate heart formation. Nat Rev Genet 2(1):39–48
8. Nicoli S, Ribatti D, Cotelli F, Presta M (2007) Mammalian tumor xenografts induce neovascularization in zebrafish embryos. Cancer Res 67(7):2927–2931
9. Tobia C, De Sena G, Presta M (2011) Zebrafish embryo, a tool to study tumor angiogenesis. Int J Dev Biol 55(4–5): 505–509
10. Villefranc JA, Amigo J, Lawson ND (2007) Gateway compatible vectors for analysis of gene function in the zebrafish. Dev Dyn 236(11):3077–3087
11. Kwan KM, Fujimoto E, Grabher C, Mangum BD, Hardy ME, Campbell DS, Parant JM, Yost HJ, Kanki JP, Chien CB (2007) The Tol2kit: a multisite gateway-based construction kit for Tol2 transposon transgenesis constructs. Dev Dyn 236(11):3088–3099
12. Halpern ME, Rhee J, Goll MG, Akitake CM, Parsons M, Leach SD (2008) Gal4/UAS transgenic tools and their application to zebrafish. Zebrafish 5(2):97–110
13. Langenau DM, Feng H, Berghmans S, Kanki JP, Kutok JL, Look AT (2005) Cre/lox-regulated transgenic zebrafish model with conditional myc-induced T cell acute lymphoblastic leukemia. Proc Natl Acad Sci U S A 102(17):6068–6073
14. Westerfield M (1993) The zebrafish book: a guide for the laboratory use of zebrafish (*Brachydanio rerio*). M. Westerfield, Eugene, OR
15. Kawakami A, Fukazawa T, Takeda H (2004) Early fin primordia of zebrafish larvae regenerate by a similar growth control mechanism with adult regeneration. Dev Dyn 231(4):693–699
16. Detrich HW, Westerfield M, Zon LI (2011) The zebrafish : genetics, genomics and informatics, 3rd edn. Elsevier/Academic, Amsterdam, Netherlands; Boston, MA
17. Nüsslein-Volhard C, Dahm R (2002) Zebrafish: a practical approach, 1st edn. Oxford University Press, Oxford
18. Rosen JN, Sweeney MF, Mably JD (2009) Microinjection of zebrafish embryos to analyze gene function. J Vis Exp 25:1115
19. Rembold M, Lahiri K, Foulkes NS, Wittbrodt J (2006) Transgenesis in fish: efficient selection of transgenic fish by co-injection with a fluorescent reporter construct. Nat Protoc 1(3):1133–1139
20. Provost E, Rhee J, Leach SD (2007) Viral 2A peptides allow expression of multiple proteins from a single ORF in transgenic zebrafish embryos. Genesis 45(10):625–629
21. Koster RW, Fraser SE (2001) Tracing transgene expression in living zebrafish embryos. Dev Biol 233(2):329–346

Chapter 11

High-Resolution Intravital Microscopy of Tumor Angiogenesis

Ann L.B. Seynhaeve and Timo L.M. ten Hagen

Abstract

Real-time evaluation of vascular effects in an animal skinfold window model by intravital microscopy (IVM) provides a powerful tool to improve insight into vascular development and vascular therapy. The potential of IVM to examine processes in tissues (e.g., tumors, inflammatory sites), in a noninvasive way, enables determination of the kinetics of processes under study at any given time point. The introduction of sensitive digital cameras, confocal and multiphoton microscopy, and powerful imaging software greatly improved the quality of the images acquired. Together with the introduction of better fluorescent probes, with a shift towards red and near-infrared fluorescence, confocal and multiphoton microscopy enables deeper imaging with less (photo)toxicity. IVM is particularly useful for examination of processes in time, which span seconds up to days or even weeks, such as tumor vascular development. Here we describe an advanced dorsal skinfold window chamber for high-resolution intravital microscopy of tumor angiogenesis.

Key words Intravital microscopy, Angiogenesis, Cancer, Fluorescence, Confocal, Multiphoton

1 Introduction

Angiogenesis is the development of blood vessels necessary to sustain growth and development. Cells need nutrients and oxygen to survive and grow, while waste needs to be removed. As the diffusion distance of oxygen and nutrients is limited a dense and well-organized vasculature is present. During development, at adult stage for instance during placental establishment, but also in a number of diseases such as retinopathy, inflammation, and cancer, angiogenesis occurs. In cancer angiogenesis is an integral and crucial step during progression of the disease from dormant to malignant; it provides the possibility to grow beyond the diffusion limits and enables hematologic spread [1]. Therefore it is not surprising that in the treatment of cancer not only the tumor cells but also the vasculature are recognized as a potential target.

Since the establishment of the tumor vasculature, and therefore also angiogenesis, as a target for therapy this area became a rapidly

Domenico Ribatti (ed.), *Tumor Angiogenesis Assays: Methods and Protocols*, Methods in Molecular Biology, vol. 1464,
DOI 10.1007/978-1-4939-3999-2_11,

progressing field of research which focused on manipulation, inhibition, and destruction of the tumor-associated vasculature (TAV) [2, 3]. Especially in combination treatment settings, in which an antivascular strategy is combined with for instance chemotherapy, promising results are obtained. For obvious reasons a growing preference developed for in vivo models to study these aspects in high detail. Special interest exists for those models that enable real-time and longitudinal observation of tumor vascular effects. An elegant approach is the skinfold window model, which allows noninvasive and serial examinations [4, 5]. In this model a flap of skin on the back of rodents is sandwiched between two frames, which hold glass windows. Through the windows processes like tumor growth, angiogenesis, vascular function (flow, permeability), and drug delivery or tumor response can be followed in real time by IVM. Using the skinfold window model in combination with multiphoton laser scanning microscopy (MPLSM) the group of Dr. R.K. Jain demonstrated in vivo gene expression, angiogenesis, cell adhesion and migration, and drug delivery [6].

Another major technological development in the spatiotemporal analysis of processes in living material is the introduction of fluorescent protein tags like green fluorescent protein (GFP) [7, 8]. 4D image analysis with GFP fusion proteins (either alone or combined with spectral variants of GFP) is an intensely pursued research avenue, since it can provide novel insight into the behavior of proteins and other molecules and in the organization of biochemical processes. Labeling of tumor cells with GFP enabled in vivo visualization at single-cell level in a mouse skinfold window and intravital imaging using two-photon microscopy [9, 10]. Moreover, the strong fluorescence of GFP-labeled cells in combination with sensitive digital imaging enabled noninvasive visualization of tumors present in liver, bone, or lung [11]. In this noninvasive whole-body imaging-setting vessels can be identified by the absence of fluorescence. These models are particularly useful to examine the development of metastases. Combination of the skinfold window model with fluorescently labeled tumor cells has been used for the examination of the early processes of tumor formation [9]. The success of GFP has generated a plethora of fluorescent proteins enabling dual- or multicolor imaging. Importantly, fluorescent proteins and compounds which are compatible with the life setting have been developed with fluorescence at the red or near-infrared range. As red light penetrates deeper and with higher efficiency in tissues deeper and more detailed examination of processes is possible.

Detailed examination of angiogenesis and vascular effects, especially early processes involving microcapillaries, by noninvasive whole-body imaging of GFP-labeled tumors, is difficult due to the relatively low resolution of these techniques. Moreover, using bright-field microscopy or whole-body imaging positive identification of blood

vessels is difficult. In the skinfold window model blood vessels can be identified as columns of red blood cells in bright-field view, or can be highlighted by injection of a fluorescent blood marker, whereas in the models in which GFP-expressing tumors are used, the vessels are recognized by the absence of fluorescence. Therefore, early, yet non-conducting sprouts, or very small capillaries, nonfunctional or disintegrated vessels, or vessels in very dark tumors (i.e., melanoma) are difficult to identify. Here we describe the use of an eNOS-GFP-expressing transgenic mouse with bright fluorescent endothelial cells. In combination with fluorescent blood markers discrimination between functional or nonfunctional vessels, single endothelial cells, thin sprouts, and endothelial tip cells can be easily detected and in detail imaged. Combination of IVM with proper transgenic mice and fluorescent markers provides an unprecedented tool for detailed and high-resolution imaging of for instance angiogenesis as is described here.

2 Materials

Intravital microcopy (IVM) is performed on a number of animals such as mice, rats, rabbits, hamsters, or guinea pigs. Here we focus on IVM using a dorsal skinfold window chamber on mice. The principal is however not different from for instance rats. Sterility and working clean are important factors determining success, as well as experience and proper tools and instruments. It is therefore mandatory to sterilize or thoroughly clean with alcohol all instruments, materials, and surfaces, also of the mouse as described below. It is advised to perform placement of the window chambers in an operation room, with preferably a dual-head operation microscope.

2.1 Mice

Mice of 12 weeks or older are used which are from a clean facility. Mice should be of reasonable weight preferably above 20 g as younger and lighter mice tend to have lesser skin on the back. If rats are used young rats are preferred, as the skin tends to be thinner and therefore more easy to handle. After installment of the window animals are housed in a climate chamber (32 °C and a humidity of at least 50%), ensure that there is enough clearance to move freely in the cage. Although the animals are able to move freely and without any impairment with the window chamber developed by us and described here, it is important to check if animals can reach their food and water (*see* **Note 1**).

Forced expression of fluorescent cell markers, such as green fluorescent protein (GFP), enables detection and visualization of cells in vitro and in vivo. An increasing selection of mice are available with specific fluorescent markers (*see* **Note 2**). With IVM we show that GFP-expressing cells can be monitored at high magnification at subcellular level; that is, we are able to image inside cells of living mice. Here we use a transgenic mouse model expressing

GFP under the control of an eNOS promotor and localization sequence. As a result endothelial cells express substantial amount of GFP while eNOS levels are not affected. The localization sequence locates expressed GFP to cell membrane and Golgi allowing to distinguish not only individual cells but also membrane extension such as filopodia.

2.2 Anesthesia Procedure

Anesthesia: Air/isoflurane inhalation anesthetics in which flow and isoflurane concentration should be set such that mouse breathing is light and even.

2.3 Equipment and Solutions

1. Heating mattress set at 37 °C.
2. Electric shaver, typically high-end commercial with a small (1 cm width) head.
3. Hair removal gel with no extra additives such as perfumes.
4. Chlorhexidine (2%) in alcohol (70%).
5. Saline (0.9% sterile NaCl solution).
6. Dual-head operation microscope: Although excellent results can be obtained without the use of an operation microscope if one is present use is preferred.
7. Tumor material (*see* Subheading 3) from donor mice or suspension of tumor cells (*see* **Note 3**).
8. Skinfold window chamber parts as depicted in Fig. 1. Per assembly two window frames (made from PEEK), two pairs of bolds and nuts (aluminum), two thin retaining rings, two circular cover glasses (number 1, 0.016 mm thick and 12 or 18 mm in diameter), and a 10 mm diameter filler glass. All materials are autoclaved at 105 °C for 90 min.
9. Surgical instruments including silk suture 4/0, syringe (1 ml), two 23G needles, a 25G needle, scalpel holder + scalpel blade size 15, surgical forceps, surgical microscissors, small needle holder, clamping needle holder (or hemostatic forceps), micro screwdriver, and ear punch (used for marking mice) (Fig. 2). All materials are purchased sterile or sterilized by autoclaving for 90 min at 121 °C.

3 Methods

Perform all procedures under aseptic or sterile conditions.

3.1 Preparation of Mice

1. Mice are sedated by inhalation anesthetics (air/isoflurane) while on a 37 °C heating mattress and thoroughly cleaned with chlorhexidine in alcohol and the skin removed from hair. At all stages put eye ointment on the animal's eye and keep the animal

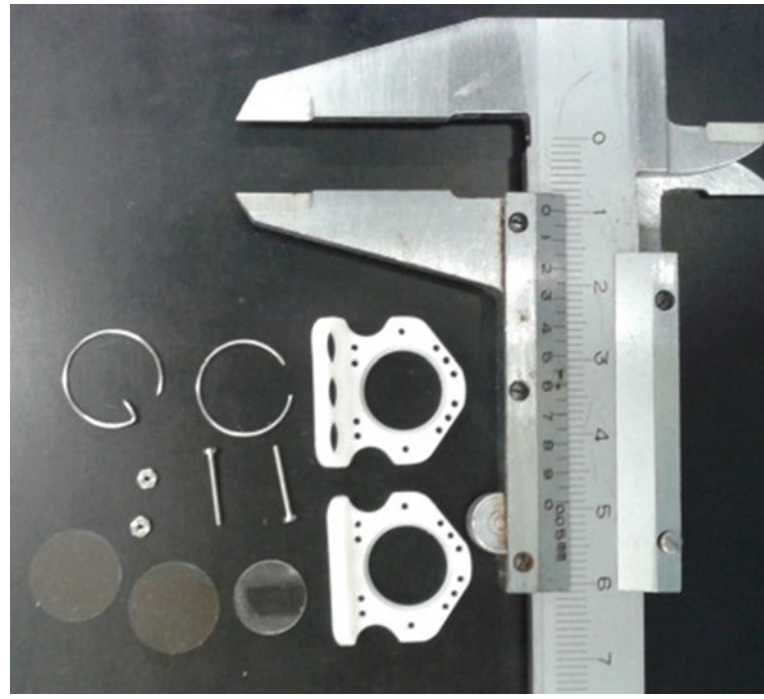

Fig. 1 Doral skinfold window chamber parts. Visible are the two frames (*white*), cover glasses, and filler glass. The retaining rings are thin and do not obscure the view area

Fig. 2 Instrumentation used for establishment of the dorsal skinfold window chamber. Parts are mentioned in the text

properly heated. For this we use a small-sized electric razor followed by application of an ointment to remove the hair, followed by another cleaning step. Mark the center line alone the spine to ensure symmetrical positioning of the window chamber.

2. The skin on the back is examined and pulled into a flap. On one side of the flap the chamber is positioned in middle between front and hind legs, and the window part circled using a marker. Also mark the position on the skin for the bolts. With a light behind the skin flap an area can be selected such that the tumor can be implanted between major vascular branches. Following procedures are preferably done under an operation microscope, but also a stereomicroscope and special operation glasses or if well trained by naked eye. With a scalpel the skin is cut along the circular marker line and the upper skin is removed. Be careful not to damage the underlying layers and vasculature as in the fascia later a tumor will be implanted. Also be sure that the skinfold extends about 2–3 mm above the window frame.
   We use lightweight synthetic window frames (PEEK) which are compatible with MRI and hyperthermia [12, 13]. The frames have spacers included and are fixed together using lightweight bolts and nuts, which can be replaced by sutures when for instance used in an MRI.
3. Pull the skinfold up and punch two holes (1 mm in diameters) for the bolts. Position the window frames, place the bolts and nuts, and tighten lightly. Pull the skin 2–3 mm above the top of the window frames and manipulate the skinfold such that the circular exposed area matches the window and secure the skin with 23G needles through the little holes at the top. Secure the nuts and replace the 23G needles with sutures. At this moment a cover glass can be positioned at the back and secure with a retaining ring (*see* **Note 4**). The window chamber is now ready for tumor implantation.

3.2 Tumor Induction

Important! Steps below should be performed before operation on the mouse is started.

1. Tumor cell suspension (*see* **Note 6**): Use freshly isolated cells, mild trypsin incubation, suspended in PBS at a concentration of approximately 1×10E4 per 20 µl (*see* **Note 5**). If desired the cells can be embedded in collagen gel or Matrigel. Store on ice only for a short period (time to prepare the window). When using a tumor cell suspension spread of cells through the chamber easily occurs. To prevent cells spreading can be suspended in a gel (collagen) or if tumor growth needs to be promoted in Matrigel. It is advised to gently create a pocket using forceps in the fascia without causing a bleeding before injection of cells.

2. Tumor fragment (*see* **Note 6**): In this setting a donor tumor-bearing mouse is used. The tumor should be big enough to provide sufficient material but not too large to prevent presence of necrosis. Remove the tumor from the donor mouse, locate viable tissue, and cut fragments of approximately 1 mm^3.

Secondly, tumor donor material can be used for implantation. Create a small pocket large enough to hold the 1 cm^3 tumor fragment. This pocket can be prefilled and stretched with a 1 mml syringe fitted with a 25G needle. The tip of the needle is slightly bent to allow easy approach of the pocket. The tumor fragment can be either implanted using a needle holder or forceps. Alternatively, the tumor fragment can be placed in the tip of a bent 19G needle and injected carefully, without adding air, in the pocket.

Mice are placed in a climate-controlled space set to 32 °C and above 50% humidity and pain relief are administered (*see* **Note 7**). Perform daily inspection of the mice. Using bright-field microscopy early tumor onset is monitored until the mice are ready for IVM, which depends on tumor type. Generally syngeneic tumors grow faster (or experience is within 14 days) compared to xenografts which may take up to several weeks.

3.3 Intravital Microscopy

Essentially a number of microscopes or imaging methods may be used. As shown below impression of global tumor growth and concomitant vascular changes are possibly observed with a standard digital camera (Fig. 3) or (fluorescence) microscope. Here we show results of IVM with confocal and multiphoton microscopy.

Mouse stage: When ready mice are placed on a preheated temperature-controlled platform which is mounted on the microscope stage. As breathing of the mouse introduces movement artifacts we use a frame to immobilize the window chamber. The frame is bolted to the window chamber, which in turn is bolted to the platform. While the mouse can still move slightly this is not translated to the window chamber.

This chapter does not describe the use of microscopes as this is beyond the scope. However, we shortly list a number of advantages of different imaging technologies. With bright-field microscopy blood flow, perfusion, vascular organization, and cells or regions rich in contrast can be imaged quite good. When equipped with a 3CCD digital camera movies can be made. At low magnification (e.g., 2× or 5× objective lens) this option is sufficient to check the quality of the window. As the window is a relatively thick tissue, compared to a section commonly used for histology, use of a confocal or multiphoton microscope is preferred. We experience good penetration up to 100 μm with confocal and beyond that with multiphoton. Much improved imaging is achieved when using objective lenses with higher magnification and numeric aperture (NA). If possible, water immersion lenses should be used at higher

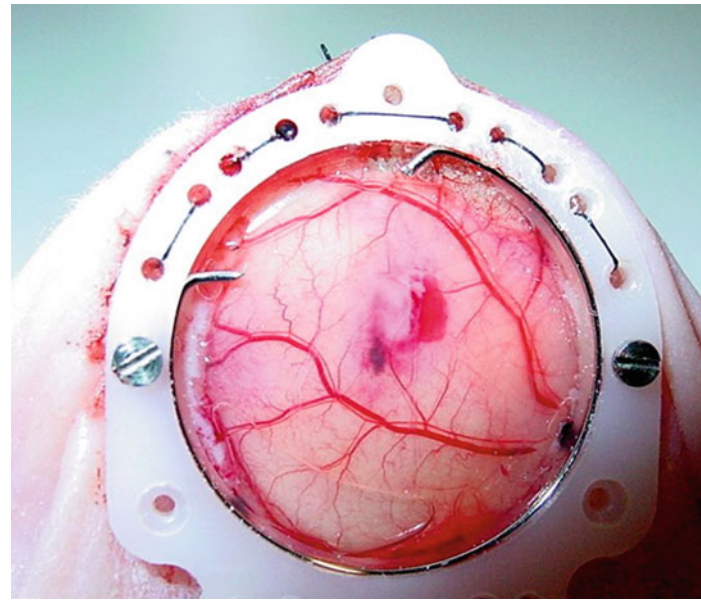

Fig. 3 Image of an 18 mm intravital dorsal skinfold window chamber on a nude mouse. Visible is a human melanoma xenograft producing melanin, with above it an a-vascular region. The tumor is surrounded by a bleeding caused by hyper-permeabilization of the vessels. Image was made with a digital camera

magnification as these lenses have a better NA (higher resolution or resolving power) and better working distance than oil immersion lenses (*see* **Note 8**). Readers are advised to test which method works best and what study needs to be performed. We refer the reader to the following publications for further information.

3.4 Intravital Imaging of Tumor Angiogenesis

IVM based on lightweight synthetic window chambers results in a compatible system. Mice exhibit normal behavior and weight gain. Mice can be maintained for a time frame of at least 1 month depending on tumor growth.

Irrespective of the imaging method, bright-field or confocal microscopy, proper control over the condition of the mouse allows up to 8 h of imaging in one stretch and daily imaging for weeks. Heating of the mouse during imaging to maintain body temperature is crucial; low temperature not only affects perfusion in cooled areas but also negatively influences inhalation anesthetics. Under anesthesia body temperature drops rapidly to room temperature and in our experience mice are more difficult to sedate and may die when body temperature is not maintained at 37 °C.

Several skinfold window systems are used in the literature. Here we use a synthetic window frame with a field of view of 12 of 18 mm in diameter. The ratio between window frame size and field of view is favorable as many other window frames are larger with a field of view of 10 mm. Smaller titanium frames are available with

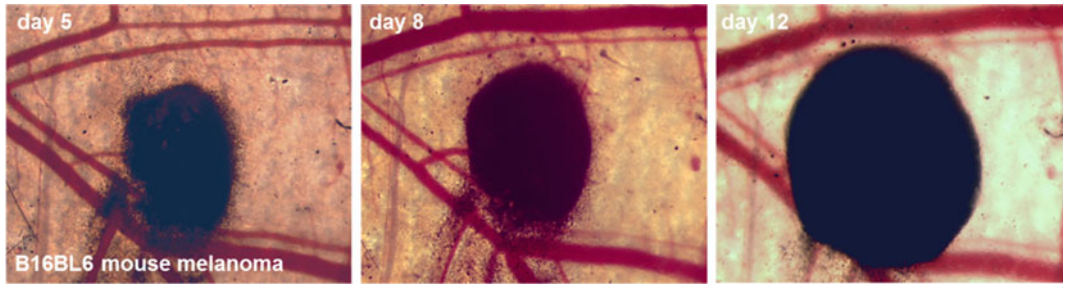

Fig. 4 Longitudinal imaging of a B16Bl6 melanoma in a dorsal skinfold window chamber on a C57Bl6 mouse. The color bright-field images are possible as the melanoma cells are visible because of the abundant production of melanin. While the tumor doubles over a time frame of days vascular growth is not that apparent. Images were made with a fluorescence microscope

12 mm windows. The advantage of the synthetic frame is further reduced weight and compatibility with MRI. Previously we showed dual-modality imaging using confocal IVM and MRI.

Bright-field imaging is especially useful in contrast-rich areas. As vessels generally conduct red blood cells, which are rich in contrast, these are easily detected. Already with a standard digital camera tumor growth, changes in vascular structure, and in this case with a malignant xenograft melanoma, hyperpermeability resulting in hemorrhage is observed. Using bright-field microscopy more detailed imaging of early vascular makeup, changes in vessel density or vessel diameter, and progression of vascular networks during tumor development are demonstrated. Here we show sequential images of a growing melanoma, which stands out clearly because of a high melanin content rendering tumor cells dark (Fig. 4). While the tumor doubles in size growth of this particular syngeneic melanoma growing in the skin seems to attract hardly any vessels. Vascularization inside the tumor is obscured because of accumulated melanin. This phenomenon allowed us however to identify groups of melanoma cells around preexisting vessels; in that setting tumor growth is not depended on angiogenesis but uses the already present vasculature for delivery of oxygen and nutrients, designated cooption. In contrast, growth of Lewis lung carcinoma (LLC) in the skinfold induced massive angiogenesis and recruitment of new vessels towards the tumor (Fig. 5). The bright-field images give the impression that the growing tumor mass is vascularized only at the rim (Fig. 5, left panel). Fluorescence microscopy is invaluable to provide detailed information on tumor vascularization and perfusion of vessels as discussed below.

3.5 Fluorescence Intravital Imaging of Tumor Angiogenesis

Clearly, tumors grow in different patterns depending on their capacity to attract new vessels, abuse existing vascular networks, and ability to survive anoxia or progress irrespective of tumor

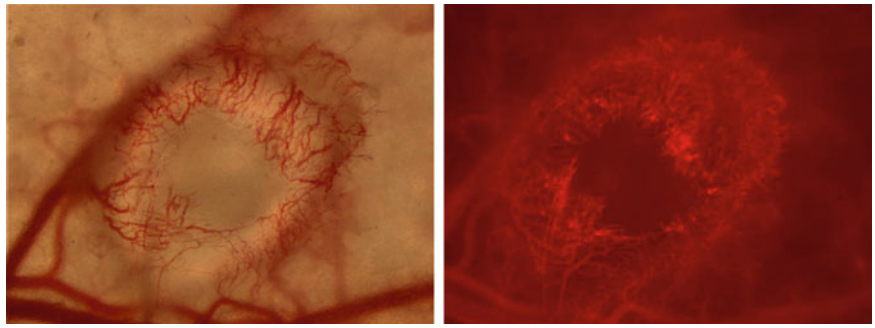

Fig. 5 Lewis lung carcinoma (LLC) in a dorsal skinfold window chamber. *Left*, bright-field image showing ingrowth of new vessels into the tumor leaving a a-vascular center. *Right*, fluorescence image showing perfused vessels after the injection of 100 nm red fluorescent particles confirming the existence of an a-vascular center. Images were made with a fluorescence microscope

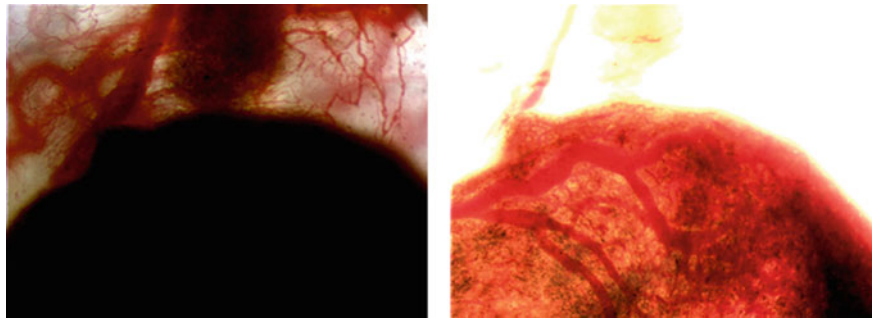

Fig. 6 Dorsal skinfold window chamber imaging of a melanoma rich in melanin. *Left*, any structure obscured by the dark is light-absorbing melanin. It seems that some vascular development does take place at the rim just outside of the tumor. *Right*, increased light power visualizes major vessels inside of the melanoma. These vessels are new and generated by the tumor (angiogenesis). Small vessels however are difficult to detect. Images were made with a fluorescence microscope

necrosis because of poor perfused areas. Bright-field imaging shows that melanoma grows differently from LLC. Figure 5 shows LLC-induced angiogenesis in bright-field and functional vessels in fluorescence mode. After injection of a red fluorescent blood marker vessels growing and extending in the rim of the tumor are visible (Fig. 5, right panel). However, the center of the tumor is not vascularized, which is a typical phenomenon of fast-growing tumors resulting in central necrosis and collapse.

Bright-field imaging of melanoma growth shows marginal vascular changes outside of the tumor (Fig. 6, left panel). At high lamp power, which should not be applied but is done here to show structures obscured by melanin, intratumoral vessels become visible (Fig. 6, right panel). To visualize endothelial cells an eNOS-GFP transgenic mouse was used as described above. Using fluorescence microscopy in combination with bright field on a

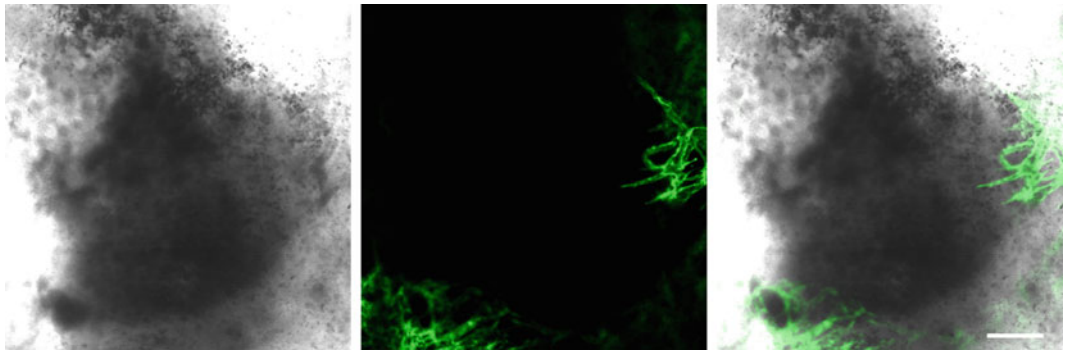

Fig. 7 Scanning confocal microscopy image of a melanoma growing in a dorsal skinfold window chamber. *Left*, bright-field image of the tumor showing melanin-rich cells. *Middle*, image of tumor-induced vessel growth. Vessel penetrates into the tumor mass. These vessels are visible as the endothelial cells produce green fluorescent protein. *Right*, overlay. Bar 200 μm

confocal we observed initial a-vascular growth followed by initiation of vascular budding (Fig. 7). Existing vessels produce sprouts which penetrate into the formed tumor mass (Fig. 8). Over time further ingrowth of vessels into the existing tumor mass occurs. Different from LLC here vascular growth is not restricted to the tumor rim.

At high magnification, using a 20× or 40× water immersion objective lens individual endothelial cells can be identified with clear demarcation of the cell membrane and accumulation of GFP in Golgi (Fig. 9). Endothelial cells are more chaotically organized in tumor vessels compared to healthy blood vessels.

4 Notes

1. House animals with a dorsal skinfold window chamber separately to prevent problems to the chamber.
2. Mice expressing fluorescent proteins expressed in specific cells are available. Combination of markers provides unique insight into localization of cells with respect to each other. It is advised when breeding and crossing these mice to check that fluorescent proteins expressed are compatible with each other and with the compounds used.
3. It is advised to use tumors which grow well in skin of the used animal and will provide a descend tumor within 2–4 weeks. If tumors take too long to grow skin regrowth may interfere with the experiment.
4. If the skin is relatively thick a filler glass (10 mm diameter) can be positioned at the back between cover glass and skin. Be careful not to overdo this as blood flow may be compromised.

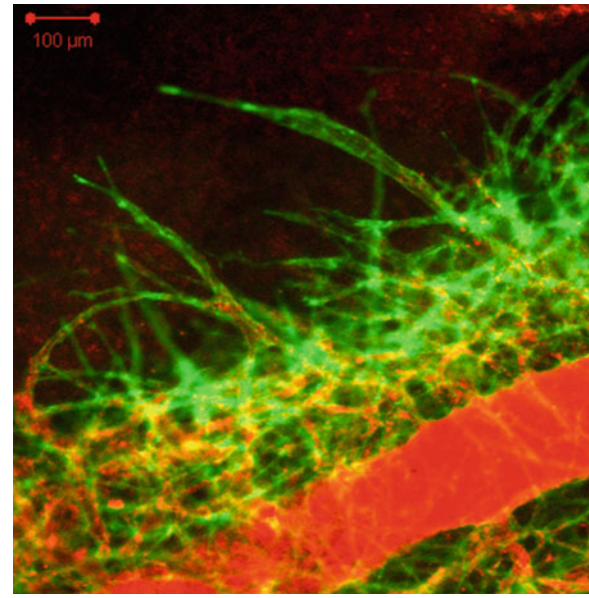

Fig. 8 Laser scanning confocal microscopy image of angiogenesis at the rim of a tumor in a dorsal skinfold window chamber. Vessels are visible because of endothelial cell-specific green fluorescence protein expression. Perfusion is visualized with a red fluorescent blood marker

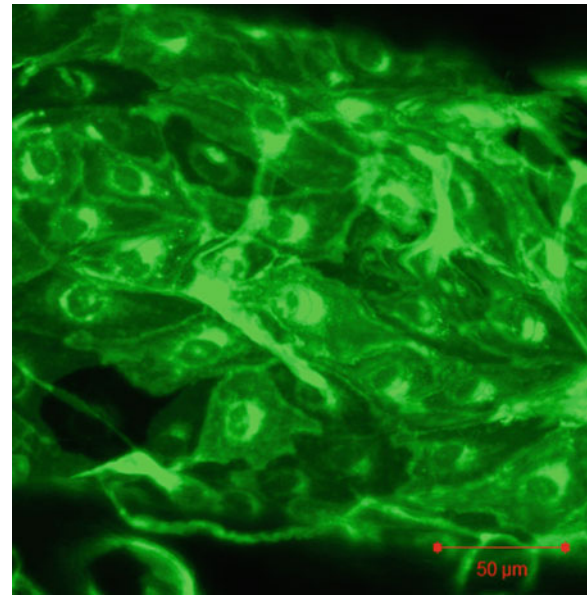

Fig. 9 Laser scanning confocal microscopy image of an angiogenic tumor vessel in a tumor in a dorsal skinfold window chamber. Endothelial cells are visible because of specific green fluorescence protein expression. Expression is mainly in Golgi (next to the nucleus) and cell membrane. In contrast to healthy vessels a relative chaotic pattern of endothelial cells populate the wall of angiogenic tumor vessels

5. Number of injected tumor cells depends on experimental setup, tumor cell growth characteristics, and scientific question.
6. The tumor cell deposit or tumor fragment should be placed in the center of the window chamber.
7. For pain relief 0.01 mg/kg Temgesic or alike is administered before the animals recover from anesthetics.
8. Use of objective lenses with a long working distance is preferred. Generally oil immersion lenses at a magnification of for instance 40× have short working distances around or below 0.2 mm which limit the focus range. Low-magnification lenses on the other hand have a better working distance but 40× long-working-distance (around 2 mm) objective lenses are available, but with poor NA. Water immersion lenses combine high magnification and reasonable NA with compatible working distance, e.g., a 40× with a NA of 0.7–1.0 and a working distance of about 2 mm. Heating of the objective lens to body temperature is advised when immersion lenses are used.

References

1. Kerbel RS (2008) Tumor angiogenesis. N Engl J Med 358(19):2039–2049
2. Folkman J (1971) Tumor angiogenesis: therapeutic implications. N Engl J Med 285(21): 1182–1186
3. Tozer GM, Kanthou C, Baguley BC (2005) Disrupting tumour blood vessels. Nat Rev Cancer 5(6):423–435
4. Palmer GM, Fontanella AN, Shan S, Hanna G, Zhang G, Fraser CL, Dewhirst MW (2011) In vivo optical molecular imaging and analysis in mice using dorsal window chamber models applied to hypoxia, vasculature and fluorescent reporters. Nat Protoc 6(9):1355–1366
5. Jain RK, Munn LL, Fukumura D (2002) Dissecting tumour pathophysiology using intravital microscopy. Nat Rev Cancer 2(4):266–276
6. Brown EB, Campbell RB, Tsuzuki Y, Xu L, Carmeliet P, Fukumura D, Jain RK (2001) In vivo measurement of gene expression, angiogenesis and physiological function in tumors using multiphoton laser scanning microscopy. Nat Med 7(7):864–868, Erratum in: Nat Med 2001;7(9):1069
7. Prasher DC (1995) Using GFP, to see the light. Trends Genet 11(8):320–323
8. Chalfie M, Tu Y, Euskirchen G, Ward WW, Prasher DC (1994) Green fluorescent protein as a marker for gene expression. Science 263(5148):802–805
9. Li CY, Shan S, Huang Q, Braun RD, Lanzen J, Hu K, Lin P, Dewhirst MW (2000) Initial stages of tumor cell-induced angiogenesis: evaluation via skin window chambers in rodent models. J Natl Cancer Inst 92(2): 143–147
10. Potter SM, Wang CM, Garrity PA, Fraser SE (1996) Intravital imaging of green fluorescent protein using two-photon laser-scanning microscopy. Gene 173(1 Spec No):25–31
11. Hoffman RM (2001) Visualization of GFP-expressing tumors and metastasis in vivo. Biotechniques 30(5):1016–1022, 1024–1026
12. Lu T, Lokerse WJ, Seynhaeve AL, Koning GA, Ten Hagen TL (2015) Formulation and optimization of idarubicin thermosensitive liposomes provides ultrafast triggered release at mild hyperthermia and improves tumor response. J Control Release 220(Pt A):425–437
13. Li L, ten Hagen TL, Hossann M, Süss R, van Rhoon GC, Eggermont AM, Haemmerich D, Koning GA (2013) Mild hyperthermia triggered doxorubicin release from optimized stealth thermosensitive liposomes improves intratumoral drug delivery and efficacy. J Control Release 168(2):142–150

Chapter 12

Subcutaneous Murine Xenograft Models: A Critical Tool for Studying Human Tumor Growth and Angiogenesis In Vivo

Katharina M. Schmidt, Edward K. Geissler, and Sven A. Lang

Abstract

Subcutaneous tumor models are widely used in angiogenesis research. Due to the relative simplicity, these mouse models are ideal for the evaluation of molecular hypotheses. In addition, these models are frequently used to assess anti-angiogenic efficacy during drug development. Finally, subcutaneous models can be performed with either xenogeneic or syngeneic tumors, both harboring advantages and drawbacks. Herein, we describe the use of subcutaneous xenograft models in anticancer research.

Key words Tumor models, Xenografts, Mice, Cancer research, Preclinical anticancer therapy, Tumor angiogenesis

1 Introduction

Animal models are a crucial tool for studying molecular mechanisms of cancer and for the development of new anticancer agents [1]. The laboratory mouse (*M. musculus*) is one of the most appropriate model systems owing to the ease of keeping, to the specific breeding possibilities, and to the widespread physiological and molecular analogies to humans [2]. Since the beginnings in the 1950s, murine cancer models have advanced. Particularly, the development of immunocompromised mice enabled the establishment of diverse xenograft models, and so enabled the in vivo assessment of human cells or human tissue in murine organisms [3]. Although xenograft models lack a fully functional immune system, these models are widely used to assess tumor growth independent of immune system influence.

Besides xenografts, models with functional immune system are available. For example, syngeneic injection models with murine cancer cells derived from certain mouse strains being injected into immunocompetent mice (e.g., B16 melanoma cell used in C57BL/6 mice)

Domenico Ribatti (ed.), *Tumor Angiogenesis Assays: Methods and Protocols*, Methods in Molecular Biology, vol. 1464,
DOI 10.1007/978-1-4939-3999-2_12,

are available. Handling of these models is similar to xenografts, although tumors tend to be more aggressive. Furthermore, genetic engineered mice (GEM) with a high incidence of spontaneous cancer development have gained popularity in cancer research during the last years [3, 4]. Although GEM allow the study of specific gene mutations in an immunocompetent organism, they fail to represent the complex heterogeneity of human tumor cells [4].

The subcutaneous tumor model is the most common xenograft model in anticancer drug research [1, 5]. It stands out due to a convenient and less invasive process, causing minimal burden to animals during longitudinal monitoring. The main drawbacks with subcutaneous versus orthotopic xenograft models are the lack of organ-specific microenvironment and the negligible capacity to metastasize (in most models). Nonetheless, subcutaneous xenografts are a proper instrument for testing molecular hypotheses before starting an intricate orthotopic experiment.

Tumors in the subcutaneous model can be established by the use of either cultured tumor cells or tumor tissue fragments. For the xenograft model, immunocompromised mice, e.g., athymic nude mice (nu/nu) [6] or severe combined immune-deficient mice (scid/scid) [7], are typically used. Tumor growth and the efficacy of various treatments (anticancer agents, gene modifications of tumor cells, etc.) are obvious during the whole period of the experiment. With regard to angiogenesis, tumors can be assessed for the development of necrosis or be analyzed for vessel growth immunohistochemically (e.g., staining of CD31-positive vessel area). Factors affecting angiogenesis can be easily determined also by immunohistochemistry, Western blotting or PCR (e.g., HIF-1α, VEGF-A).

The following protocol describes the basic steps of producing subcutaneous xenografts by injection of cultured tumor cells (+/− basement membrane-like matrix/Matrigel) or transplantation of tumor tissue fragments.

2 Materials

2.1 For Injection of Cultured Tumor Cells and Transplantation of Tumor Tissue

1. Immunocompromised mice (e.g., athymic nude mice (nu/nu), severe combined immune-deficient mice (scid/scid)) at an age of 6–8 weeks, maintained under barrier conditions.
2. Depilatory cream (if not using nude mice).
3. Skin disinfection.
4. Syringes (1 ml).
5. Injection needles (27 gauge, 1.5–2.0 cm).
6. Sterile instruments (scalpel, scissors, forceps, needle holder).
7. Vernier caliper.
8. Precision scale.

2.2 Only for Injection of Cultured Tumor Cells

1. Cultured human cancer cells (10^5–10^7 cells per animal; determination of needed cell number *see* **Note 1**).
2. Phosphate-buffered saline (PBS).
3. Trypsin (1×/10×; depending on cells used).
4. Cell culture medium with at least 10% FCS.
5. Centrifuge.
6. Trypan blue.
7. Hemocytometer.
8. Hanks' Balanced Salt Solution (HBSS).
9. Basement membrane-like matrix/Matrigel (optional).
10. Isoflurane.
11. Animal induction chamber.
12. Crushed ice.
13. Vortexer.

2.3 Only for Transplantation of Tumor Tissue

1. Fresh human tumor tissue (from a patient in the operating room or from a donor animal (*see* Subheading 3.4)).
2. Cell culture medium (e.g., Minimum Essential Medium Eagle, Medium 199).
3. Penicillin/streptomycin.
4. Gauze squares.
5. Sodium chloride (NaCl) 0.9%, sterile.
6. Ketamine 10%.
7. Xylazine 2%.
8. Eye ointment.
9. Suture material (monofilament, non-absorbable, USP 4-0).

3 Methods

3.1 Preparation of Tumor Cells or Tissue

3.1.1 Preparation of Cultured Tumor Cells

1. Sterile cell preparation should be conducted under laminar flow hood.
2. Remove cell culture medium.
3. Wash cultured cells with PBS.
4. Add trypsin (2–4 ml/100 cm^2) and incubate at 37 °C until all cells are detached.
5. Quench trypsin by adding two volumes of cell culture medium (with at least 10% FCS).
6. Suspend cells thoroughly by pipetting up and down.
7. Separate 20 µl of cell suspension, add 20 µl of trypan blue, and quantify the cell number using a hemocytometer.

8. Centrifuge cells at 100–150 × *g* and at room temperature for 5 min.
9. Discard supernatant.
10. Resuspend the cell pellet in HBSS at a concentration of 0.2–20×10^8 cells/ml (equivalent to 10^5–10^7 cells per animal finally; determination of needed cell number *see* **Note 1**).
11. Optional: Mix cell suspension and Matrigel in equal parts with a pipette after thawing Matrigel following the manufacturer's instructions.

    Basement membrane-like matrix/Matrigel is a mouse sarcoma-derived basement membrane-like extract containing basement membrane proteins (laminin, entactin, collagen, heparan sulfate proteoglycans) and growth factors (e.g., FGF, EGF, TGF beta) [8]. In vivo Matrigel increases the tumor growth rate [9]; so its use is recommended for tumor cells that grow poorly in vivo.
12. Keep cell suspension on ice.

3.1.2 Preparation of Tissue from Patients' Tumors or from Xenograft Tumors

1. Keep tumor tissue in cold cell culture medium with penicillin/streptomycin (1 % v/v). Process tissue in less than 30 min.
2. Transfer the tumor tissue into a sterile Petri dish containing cell culture medium with penicillin/streptomycin (1 % v/v) and divide the tissue into equally sized cubes of approximately 2 × 2 × 2 mm. Avoid necrosis in these transplants (*see* **Note 2**).
3. For maintaining cell viability tumor tissue should be covered by medium at all times.

3.2 Injection/ Transplantation

Remove hair from the mouse flanks (if not using nude mice) using depilatory cream.

3.2.1 Injection of Cultured Tumor Cells

1. Gently vortex the cell suspension, and aspirate 50 µl of cells (100 µl of cell/Matrigel mixture) per animal into a syringe (1 ml) with a 27-gauge needle. If you treat more animals consecutively, agitate the syringe and change the needle before each injection.
2. For inhalation anesthesia, put the mouse into an animal induction chamber according to the manufacturer's recommendations, taking care for investigator's safety (*see* **Note 3**). Alternatives to inhalation anesthesia are shown in **Notes 4** and **5**.
3. As soon as anesthesia is deep enough (approximately after 1–2 min, *see* **Note 6**), place the mouse onto your operation table in a prone position.
4. Disinfect the dorsal skin.
5. Lift the dorsal skin with your left (right for sinistrals) index finger and thumb, so that the skin is separated from the underlying muscles (*see* Fig. 1a).

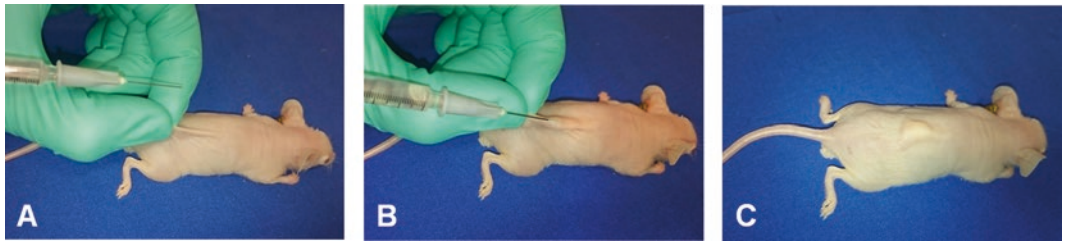

Fig. 1 Tumor cell injection. (**a**) Keep the mouse in prone position and lift a dorsal skin fold. (**b**) Injection of cell suspension into the subcutaneous space. (**c**) At the injection site, a bump remains for a few days

6. Inject 50 µl of the well-vortexed cell suspension (100 µl of the cell/Matrigel mixture) into the lifted skin fold (*see* Fig. 1b, and **Notes** 7 and **8**). If there is a resistance during injection, reset the needle because that means you might be in a false compartment.

3.2.2 Transplantation of Tumor Tissue Fragments

1. Aspirate 100 µl of xylazine, 400 µl of ketamine, and 500 µl of NaCl into a syringe (1 ml). Mix very well.
2. Inject 50–75 µl of the mixture intraperitoneally (equivalent to 4–6 mg xylazine/kg body weight and 80–120 mg ketamine/kg body weight) and put the animal back into the cage. Apply eye ointment to prevent conjunctivitis, keratitis, and blindness.
3. As soon as anesthesia is deep enough (approximately 5–10 min after injection, *see* **Note 6**), place the animal onto your operation table in a prone position.
4. Disinfect the dorsal skin.
5. Transfer the prepared tumor particles onto a wet gauze square.
6. Make a small transverse incision (5 mm) at the right or left lumbar area (*see* Fig. 2a).
7. Stretch the subcutaneous tissue and form a small subcutaneous pocket by carefully and repeatedly opening the scissors (*see* Fig. 2b).
8. Insert a certain number of tumor particles (determination of the optimal number *see* **Note 1**) into the opened pocket (*see* Fig. 2c).
9. Close the subcutaneous pocket with 2–3 single-button sutures (*see* Fig. 2d).
10. Place the treated mouse in a clean cage and observe it until complete recovery from anesthesia. Especially after intraperitoneal injection anesthesia, it is important to keep the sleeping animals warm.

3.3 Monitoring/ Treatment

1. During the first days after tumor cell injection or tumor tissue transplantation there is a small bump at the site of operation (*see* Fig. 1c), which usually diminishes before the tumor starts to grow.

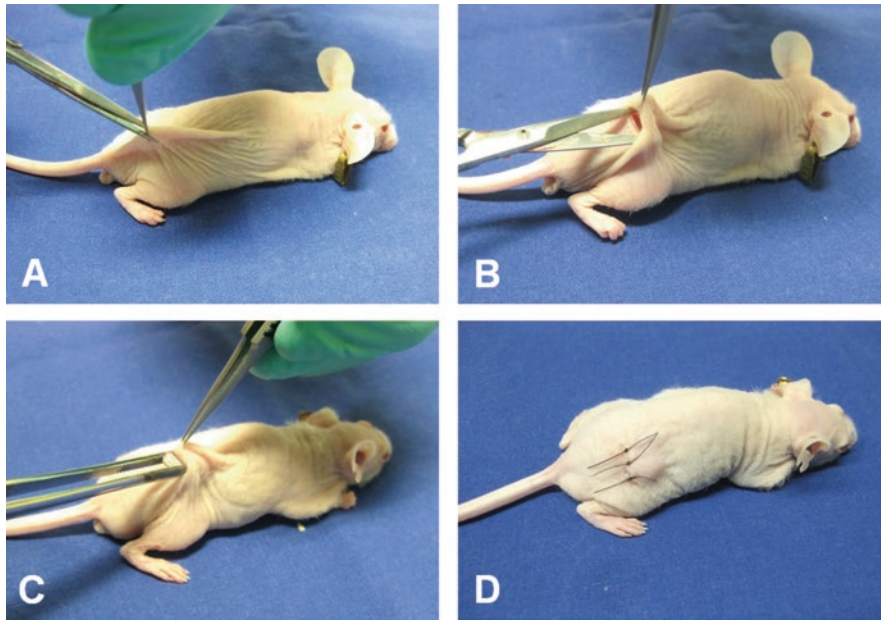

Fig. 2 Tumor tissue transplantation. (**a**) Small incision at the right/left lumbar area. (**b**) Stretching the subcutaneous tissue to form a small pocket. (**c**) Insertion of tumor fragments. (**d**) Wound closure with single-button sutures

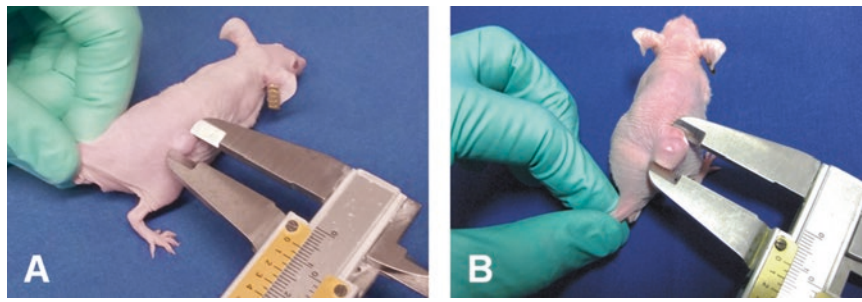

Fig. 3 Tumor measurement by external caliper. (**a**) Early status. (**b**) Advanced status

2. For the next weeks, tumor growth is monitored by regular measurement of the greatest longitudinal diameter (length) and the greatest transverse diameter (width) using a Vernier caliper (*see* Fig. 3a, b).
3. Tumor volume is calculated by the most commonly used modified ellipsoid formula: $0.5 \times \text{length} \times \text{width}^2$ [10, 11]. There are many other formulas that have various pros and cons, as discussed by Tomayko and Reynolds [11].
   Of course, measurement by external caliper is sometimes affected by errors including variable tumor shapes, skin thickness, or interpersonal differences in measuring. New methods

using microCT or microPET imaging reduce these uncertainties, but they are expensive and not available everywhere [12]. **Note 9** addresses how to reduce measurement errors.

4. Treatment, e.g., systemic application of chemotherapy or of targeted agents, should be started when tumors reach a size of approximately 100 mm^3.
5. If the regrown fur disturbs tumor measurement, remove hair from the mouse flanks again.
6. Considering animal welfare it is often recommended that the mean diameter of a single subcutaneous tumor should not exceed 12–15 mm [13]. Termination of the experiment is also indicated when there are skin ulcerations or when the general state of health of the mouse is significantly impaired (*see* **Note 10**).

3.4 Tumor Excision

1. Prepare containers and media for preserving or processing explanted tumor tissue.
2. Sacrifice the animal by cervical dislocation, or other method recommended by the ethics commission.
3. If the regrown fur disturbs tumor excision, remove hair from the mouse flanks again.
4. Make a semicircular skin incision at the tumor edge using scissors (*see* Fig. 4a) and expose the tumor-containing skin (*see* Fig. 4b). If the tumor cells and fragments were properly implanted into the subcutaneous space, there should not be any infiltration of the dorsal musculature (with noninvasive tumors).
5. Enucleate the xenograft by carefully cutting the peritumoral connecting tissue fibers (*see* Fig. 4c and **Note 11**) and making sure that the overlying skin is dissected away.
6. Weigh and measure the enucleated tumor (*see* Fig. 5 and **Note 9**).
7. Preserve or process the tumor tissue according to your further experiments or go on with Subheading 3.1.2.

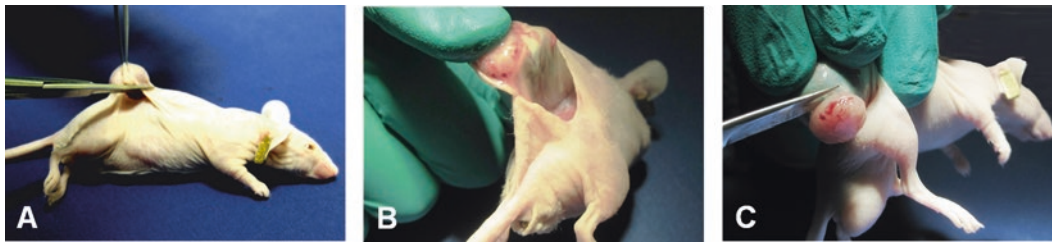

Fig. 4 Tumor excision. (**a**) Semicircular skin incision at the tumor edge. (**b**) Exposition of the tumor-containing skin flap. (**c**) Tumor enucleation

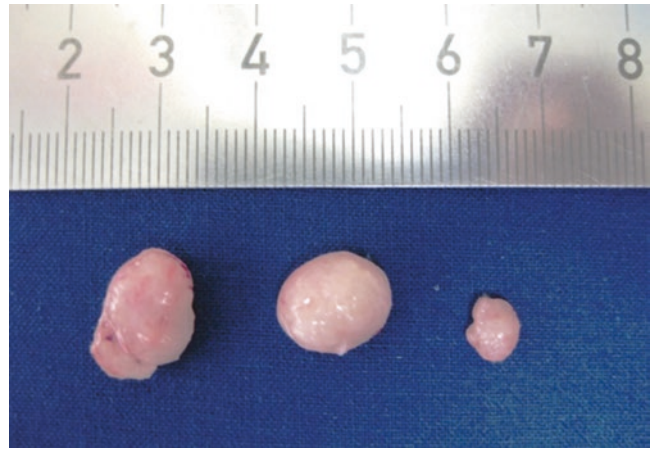

Fig. 5 Differing shapes of excised tumors

4 Notes

1. Before starting the main experiment, determine the optimal number of injected tumor cells or transplanted tumor tissue fragments. Optimal number means that a subcutaneous tumor is visible after an acceptable time interval (2–4 weeks), but that tumor does not reach the criteria of termination (*see* Subheading 3.3, **step 6**) too early. If injected tumor cells (even at high concentrations) do not form a subcutaneous tumor, consider using basement membrane-like matrix/Matrigel (*see* Subheading 3.1.1, **step 10**).
2. The appearance of necrotic tissue can differ in diverse tumor types. In general, necrosis is characterized by dark brownish color and liquid consistency, mostly localized at the center of a large tumor.
3. Avoid inhalation of isoflurane. Conduct anesthesia in an animal induction chamber placed under an appropriate fume hood.
4. For subcutaneous tumor cell injection, anesthesia is not necessary, if the animals are compliant and if an assistant holds the mouse in a prone position.
5. For subcutaneous tumor cell injection, you can also use intraperitoneal injection anesthesia (*see* Subheading 3.2.2, **steps 1–3**).
6. Anesthesia is deep enough, as soon as breathing is calm and pinching of toes or ears does not evoke a withdrawal reflex [14] (http://vetmed.duhs.duke.edu/GuidelinesforAnesthesia.html).
7. It is important not to inject the tumor cells against resistance because that is a sign of injecting into the wrong compartment (probably into the intracutaneous space). If there is a resistance, reset the needle and try to inject again.

8. Some investigators prefer to bend the needle before subcutaneous injection, so that the direction of the needle is parallel to the body surface.
9. Measurement variations can be diminished by ensuring that the same person is involved for the duration of the study. Furthermore, weighing the excised tumors represents an objective endpoint which mostly overcomes errors due to variations in measurement or in tumor shapes [13].
10. To guarantee animal welfare and to identify serious impairments you should assess the body weight, inspect the habitus, and observe the behavior at certain time intervals (e.g., twice a week).
11. Excising the subcutaneous tumor is much more convenient if the skin patch covering the tumor is left attached to the mouse (*see* Fig. 4b). Then you can span the skin patch over your left (right for sinistrals) thumb to stretch the connective tissue fibers to be cut (*see* Fig. 4c).

References

1. Cespedes MV, Casanova I, Parreno M et al (2006) Mouse models in oncogenesis and cancer therapy. Clin Transl Oncol 8:318–329
2. Frese KK, Tuveson DA (2007) Maximizing mouse cancer models. Nat Rev Cancer 7:645–658
3. Talmadge JE, Singh RK, Fidler IJ et al (2007) Murine models to evaluate novel and conventional therapeutic strategies for cancer. Am J Pathol 170:793–804
4. Richmond A, Su Y (2008) Mouse xenograft models vs GEM models for human cancer therapeutics. Dis Model Mech 1:78–82
5. Kelland LR (2004) Of mice and men: values and liabilities of the athymic nude mouse model in anticancer drug development. Eur J Cancer 40:827–836
6. Flanagan SP (1966) 'Nude', a new hairless gene with pleiotropic effects in the mouse. Genet Res 8:295–309
7. Bosma MJ, Carroll AM (1991) The SCID mouse mutant: definition, characterization, and potential uses. Annu Rev Immunol 9:323–350
8. Hughes CS, Postovit LM, Lajoie GA (2010) Matrigel: a complex protein mixture required for optimal growth of cell culture. Proteomics 10:1886–1890
9. Benton G, Kleinman HK, George J et al (2011) Multiple uses of basement membrane-like matrix (BME/Matrigel) in vitro and in vivo with cancer cells. Int J Cancer 128:1751–1757
10. Euhus DM, Hudd C, Laregina MC et al (1986) Tumor measurement in the nude mouse. J Surg Oncol 31:229–234
11. Tomayko MM, Reynolds CP (1989) Determination of subcutaneous tumor size in athymic (nude) mice. Cancer Chemother Pharmacol 24:148–154
12. Jensen MM, Jorgensen JT, Binderup T et al (2008) Tumor volume in subcutaneous mouse xenografts measured by microCT is more accurate and reproducible than determined by 18F-FDG-microPET or external caliper. BMC Med Imaging 8:16
13. Workman P, Aboagye EO, Balkwill F et al (2010) Guidelines for the welfare and use of animals in cancer research. Br J Cancer 102:1555–1577
14. Gargiulo S, Greco A, Gramanzini M et al (2012) Mice anesthesia, analgesia, and care, Part I: anesthetic considerations in preclinical research. ILAR J 53:E55–E69

Chapter 13

Orthotopic Model of Ovarian Cancer

Alessandra Decio and Raffaella Giavazzi

Abstract

Epithelial ovarian cancer (EOC) is the fifth commonest cancer-related cause of female death in the developed world. In spite of current surgical and chemotherapeutic options the vast majority of patients have widely metastatic disease and the survival rate has not much changed over the last years. The anti-angiogenic drugs are driving the field of agents targeting the tumor microenvironment in ovarian cancer. Preclinical models that accurately reproduce the molecular and biological features of ovarian cancer patients are a valuable means of producing reliable data on personalized medicine and predicting the therapeutic response in clinical trials.

In this methodological chapter we describe the orthotopic model of ovarian cancer implanted under the ovarian bursa of mice. In spite of anatomical differences between the rodent and human bursa-fallopian tube, the appropriate primary tumor microenvironment at the site of the implant allows investigation of tumor–stroma interactions (e.g., angiogenesis), and is well suited for studying the tumor dissemination and metastasis typical of this disease.

This model—although fairly labor intensive—may be useful for assessing novel, more selective therapeutic interventions and for biomarker discovery, reflecting the behavior of this disease.

Key words Ovarian cancer, Orthotopic transplant, Intrabursal transplant, Angiogenesis, Metastasis, Patient-derived xenografts, Ovarian cancer cell lines, Optical imaging

1 Introduction

Epithelial ovarian cancer (EOC) is the fifth commonest cancer-related cause of female death in the developed world [1]. The recommended treatment for advanced disease is debulking surgery followed by cytotoxic chemotherapy with carboplatin/paclitaxel (PTX) [2]. While platinum-based chemotherapy gives a high response rate, subsequent maintenance or consolidation therapies have not yet improved overall survival, though our knowledge of the clinical and molecular characteristics of ovarian cancer has improved over the last few decades [3]. Agents targeting the VEGF/VEGFR signaling axis with ligand-binding drugs (i.e., with the antibody bevacizumab) or with low-molecular-weight VEGF

Domenico Ribatti (ed.), *Tumor Angiogenesis Assays: Methods and Protocols,* Methods in Molecular Biology, vol. 1464,
DOI 10.1007/978-1-4939-3999-2_13,

receptor tyrosine kinase inhibitors (i.e., cediranib) have shown efficacy in ovarian cancer clinical trials [4].

Preclinical models that accurately reproduce the molecular, biological, and pharmacological features of ovarian cancer patients are valuable to produce reliable preclinical data for personalized medicine and to predict the therapeutic response of new treatment interventions.

The most widely used preclinical models for the investigation of ovarian cancer include syngeneic murine cancer raised in immunocompetent mice, xenografts from patient tumor specimens (patient-derived xenografts, PDX), or well-established human tumor cell lines cultured in vitro, transplanted in immunodeficient mice, and genetically engineered models (GEMs) [5–7].

Each has advantages and disadvantages. In brief, PDX are nowadays the most used models, because they maintain the original tumor architecture and histological characteristics, the molecular and genetic heterogeneity of the patient tumor of origin [8–11]. A fundamental drawback of PDX models, however, is that the human stroma is replaced by murine stroma with sequential passage [12]. Syngeneic murine models allow examination of how the immune system is involved in cancer development and progression, but a drawback is that they grow so fast that their applications are limited [13]; more important, they do not translate the molecular complexity and heterogeneity of human cancer.

GEMs reproduce well the interactions between tumor and stroma, as well as the impact of the immune system. However, these are only one model of the tumor-specific target, not depicting the genetic complexity of the human disease [14].

Human tumor cell lines are widely used to explore new aspects of cancer biology, from the role of individual molecules to cellular processes involved in invasion and metastasis. However, the different environment to which human tumor cell lines are exposed causes genetic changes that are distinct from the genetic stress imposed on tumors in patients [15].

An extensive analysis of the different models is beyond the scope of this methodology chapter, but several recent reviews describing ovarian cancer experimental models are recommended for further reading [5–7, 16, 17].

Most human solid tumors growing subcutaneously in mice show limited invasiveness, and very often have a fibrous capsule around them. In contrast, orthotopic transplant at the site of the original patient tumor reproduces the appropriate tumor microenvironment, and the tumor–stroma interaction typical of the target organ. Thus orthotopically growing tumors allow the emergence of biological features of cancer progression and metastasis, therapeutic response, or resistance to therapies similar to those in patients. This is the case of the implant of ovarian cancer under the bursa of the mouse ovary, described in detail in this chapter. The transplant of

tumor cell suspensions or fragments directly in the mouse peritoneal cavity (i.p. injection) is also considered an "orthotopic" model of ovarian cancer [8, 18]. Here, however, the artificial dispersion of cancer cells in the peritoneal cavity gives no information on early metastatic events from the ovary, but it is useful for studying ovarian cancer that disseminates in the organs of the peritoneal cavity and the production of ascites. Current studies indicate that ovarian tumors originate in other pelvic organs and involve the ovary only secondarily. Thus, it has been suggested that serous carcinoma arises from the implantation of epithelium from the fallopian tube [19]. This observation warrants for considering the origin of the primary tumors from the ovary.

A downside of orthotopic rather than subcutaneous or i.p. transplant is that the injection technique requires surgery, hence manual skills and practice. Furthermore, monitoring tumor growth in the ovary is not easy, e.g., with PDX, though tumor imaging is possible.

Several approaches are utilized for the orthotopic implantation of ovarian cancer, such as injection of cancer cells under the ovarian bursa [20] or implantation of tumor fragments under the capsule of the ovary [21]. Orthotopic models have been described derived from ovarian cancer PDX [8], or from human ovarian cancer cell lines [22–24] transplanted in immunodeficient mice, or from mouse ovarian cancer cell lines transplanted in syngeneic mice [25].

Here we describe implantation of an ovarian cancer cell suspension under the ovarian bursa (i.b.). The use of this model to test the antitumor activity and mechanism of action of antiangiogenic drugs (i.e., bevacizumab and cediranib) has been recently described [24, 26, 27].

2 Materials

2.1 Mice

1. Pathogen-free C57BL/6 or NCr-nu/nu 6–8-week-old female mice for murine syngeneic or human xenogenic tumors, respectively (*see* **Note 1**).

Other immunodeficient strains, including SCID or NOD/scid/gamma mice, could be used to increase the engraftment [28] and reduce the host-mediated background for immunohistochemical (IHC) analysis.

Approx. ten mice per group are recommended to permit statistical analysis and take account of the inherent variability of the assays.

2.2 Tumor Lines (*See* Note 2)

1. Murine model: ID8 cell line obtained from MOSEC (mouse ovarian surface epithelial cells) isolated from the ovaries of virgin wild-type mice and cultured repeatedly before transplantation into recipient mice [25].
2. Human model: Human ovarian carcinoma cell lines (A2780 or IGROV1) established in vitro from patients [24, 27].

2.3 Patient-Derived Tumors (PDX)

Clinical specimens from ovarian cancer patients were engrafted as tumor fragments subcutaneously (s.c.) or as a cell suspension (i.e., ascites) i.p. as described by Ricci et al. [8]. PDX are maintained as ascites for serial passages in nude mice by transplantation of 10×10^6 tumor cells i.p., or as solid tumors by transplantation of tumor fragments (*see* **Note 3**). Cell suspensions for i.p. or i.b. transplant were obtained from ascites harvested from the peritoneal cavity or from subcutaneously growing tumors or peritoneal tumor masses, enzymatically digested.

2.4 Media and Solutions

1. Culture medium for ID8 cell line: Dulbecco's modified Eagle medium (DMEM), 10% v/v fetal calf serum (FCS), and 1% v/v l-glutamine.
2. Standard cell culture medium appropriate for A2780 and IGROV1 cell lines: Roswell Park Memorial Institute (RPMI) 1640 medium, 10% v/v fetal calf serum (FCS), and 1% v/v l-glutamine.
3. Washing mediums: Phosphate-buffered saline (PBS) and Ca^{2+}/Mg^{2+}-free Hanks' balanced salt solution (HBSS).
4. Trypsin–EDTA solution: 0.25% w/v Trypsin and 0.02% w/v EDTA in Ca^{2+}/Mg^{2+}-free PBS.
5. Trypan blue solution (0.4% w/v).

2.5 Orthotopic Intrabursa Transplant

1. A 25 μL Hamilton syringe with a 26G needle.
2. Surgery table at 37 °C.
3. Sterile surgical instruments: Scalpel, scissors, and forceps.
4. Surgical thread (nylon, 70 cm, RB-1 needle) and metal wound clips (9 mm).
5. Inhalational anesthetic isoflurane (induction of anesthesia: 3–4%; maintenance: 2–3%).
6. Betadine antiseptic solution.

3 Methods

3.1 Preparation of the Tumor Cell Suspension from Culture

1. Cultured tumor cell lines are prepared using standard protocols (*see* **Note 4**) standardized for ID8, A2780, or IGROV1 cell culture, as detailed below; other cell lines might require modifications.
2. Four or five days before the experiment, split the cells (1:10–1:20) and plate them in 75 cm^2 flasks ensuring that they do not grow over semi-confluence. Calculate the time required to obtain approx. $6–8 \times 10^6$ cells in each flask (*see* **Note 5**).
3. Change the culture medium 24 h before harvesting cells for injection in the mice.

4. Control the condition of the cells before detaching, empty the medium, and wash the monolayer once with PBS.
5. Empty PBS from the flask, overlay with trypsin–EDTA solution, and pour off (leave a thin layer).
6. A minute later, tap the flask until the cells come away from the surface.
7. Add 10 mL of complete medium containing FCS (to neutralize the trypsin), pipette up and down in order to obtain a single-cell suspension, and then transfer into a 50 mL polypropylene conical tube (*see* **Note 6**).
8. Pellet the cells by centrifugation ($290 \times g$ for 10 min), wash twice again with HBSS, and pellet each time.
9. Count cells using trypan blue exclusion dye and adjust the cells to a concentration of 2×10^8/mL.

3.2 Preparation of Patient-Derived Tumor Cell Suspensions

1. Kill mice bearing tumors, harvest ascites, as described by Oliva et al. [18], or collect subcutaneously growing tumor or tumor masses from the peritoneal cavity as described by Ricci et al. [8].
2. Centrifuge ascites or cells obtained after enzymatic digestion (*see* **Note 7**) of solid tumor masses ($290 \times g$ for 10 min), wash twice again with HBSS, and pellet each time.
3. Count cells using trypan blue exclusion dye (or any other standard procedure) and adjust the cells to a concentration of 1×10^8/mL (*see* **Note 8**).

3.3 Injection Under the Ovarian Bursa

Cell suspension is obtained from cell lines, or from ascites, or from enzymatic digestion of solid tumor masses, as described above.

1. Anesthetize mice with isoflurane and place on the surgery table warmed at 37 °C. If necessary, shave mice on one side to allow rapid, clean surgery. Work in aseptic/sterile conditions.
2. Disinfect the skin with Betadine.
3. Make a 1–2 cm lateral midline skin incision to access the left ovary (*see* **Note 9**) and exteriorize the ovary and the oviduct.
4. Inject 1×10^6 ovarian cancer cells in 5–10 μL HBSS under the bursa of the ovary of the mice, using a Hamilton syringe with a 26-gauge needle (Fig. 1a).
5. Replace the ovary in the peritoneal cavity and close the incision with surgical thread and the skin with metal wound clips. Disinfect the skin with Betadine.
6. Follow tumor formation in the ovary and check abdominal distention twice a week. To monitor tumor formation over time (once a week) non-invasive bioluminescence or fluorescence optical imaging techniques can be used for cell lines carrying the luciferase or a fluorescent gene (e.g., A2780-luc, IGROV1-luc,

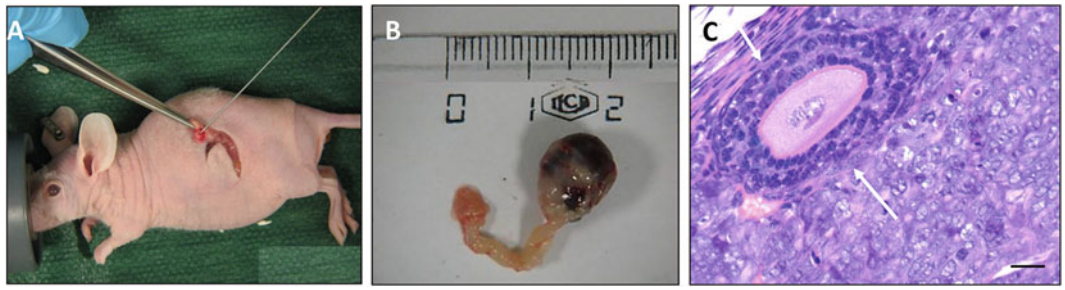

Fig. 1 Orthotopic transplant procedure. (**a**) Picture representing tumor cell injection into the left ovary, as detailed in the text. (**b**) Representative photo of the reproductive tract of a mouse bearing a PDX orthotopically in the ovary and removed at autopsy. (**c**) Representative histological image of ovarian structures (follicles with oocytes, *white arrows*) recognizable in some neoplastic masses, indicating the accuracy of injection. Scale bar = 50 μm

or ID8-luc cell lines [18, 24]) (*see* **Note 10**). Otherwise, for tumors that cannot be labeled with the dyes (e.g., PDX), tumor formation over time can be followed by non-invasive ultrasound (US) or magnetic resonance imaging (MRI) (*see* **Note 11**).

7. Kill mice at the first sign of discomfort and record the time as survival. For ethical reasons, 3–5 mL of ascites (corresponding to 20% of increased body weight) and 1.5–2.0 g of estimated tumor weight (considering 1 $cm^3 = 1$ g) are considered the endpoints of the study.
8. At autopsy, harvest ascites, record the volume, and collect the peritoneal organs to establish tumor burden and dissemination. Images and measure of tumor in the ovary and peritoneal cavity organs can be acquired with a macrodigital imaging system (Fig. 1b). Two independent scientists should do a complete autopsy on each mouse, using a dissemination/invasion score to rate the representative organs of the peritoneal cavity (liver, diaphragm, omentum, pancreas, uterus/ovary, and lymph nodes [18, 26]).
9. Fix tissues in formalin and embed in paraffin (FFPE) or snap-freeze for further histological (Fig. 1c), immunohistochemical, or molecular analyses [27] (*see* **Note 12**).

4 Notes

1. To ensure reproducible results, we recommend standardization of the animal source and characteristics and carefully monitoring husbandry conditions and animal health. For guidelines for laboratory animal care and use we refer the reader to ref. 29.
2. All cell lines growing in vitro (murine and human) can be manipulated to express luciferase or fluorescent proteins such as

green fluorescent protein (GFP) [30], red fluorescent protein (RFP) [31], near-infrared proteins (mCherry [32], Katushka [33]), or infrared fluorescent proteins [34], in order to facilitate the imaging and monitoring of tumor development and progression in the mouse ovary, and metastasis formation in vivo, in a rapid and sensitive manner within days or weeks. We suggest the lentivirus infection based on the Gateway® Technology [35], which provides stable expression of the gene of interest [24].

3. PDX should be used at the earliest passage possible after establishment from patients and should not be maintained in mice for too many passages (approx. 3–5). PDX of different passages should be stocked frozen in liquid nitrogen; a new batch from the stock should be recovered to guarantee the phenotypic stability of PDX.
4. Cell lines should be grown and stocks stored frozen in liquid nitrogen. Stocks should be checked and should be free of mycoplasma. Cell lines should not be maintained in culture for long periods in order to avoid changes in their growth and metastatic behavior. Once every 1–2 months (approx. 10–15) of continuous in vitro culture, a new batch from the stock should be recovered to guarantee the phenotypic stability of the cell line and reproducibility of the results.
5. Culture confluence affects tumor growth and metastatic behavior. It is important that the cell culture is in growth phase. Cells maintained in culture for too long without passage are hard to detach from the plastic (*see* use of trypsin in **Note 6**), and will be difficult to dissociate and produce in a cell suspension, ultimately, losing their viability.
6. The length of trypsinization affects tumor growth and the metastatic potential of cells; therefore make sure that you do not over-trypsinize. Cells need to be evenly dispersed. Use only suspensions containing single cells with >90% viability. Dead cells do not form tumors; but they influence the behavior of the viable cells. The single-cell suspension is influenced by how the cells are prepared. Most small clumps can be eliminated by gentle pipetting. Try to avoid using small-bore pipettes or syringes, as too small a diameter can result in cell death.
7. Enzymatic digestion: Cut tumors into small pieces (1–3 mm) keeping them in chilled medium. Transfer pieces to a clean tube, add digestion medium (collagenase I, 200 U/mL + DNAse, 270 U/mL), and leave on ice for 20 min to allow the enzymes to soak in. Agitate at 37 °C for 30 min to allow enzymes to act on fragments. Allow aggregates to settle for 5 min and slowly decant the single-cell suspension through 100 μm cutoff Falcon strainers. Centrifuge the suspension at 200 $\times g$ for 10 min at 4 °C and wash twice with medium without serum.

8. An accurate count is not always possible because of cell clumps. To avoid errors try to standardize the counting method.
9. Injection into the left ovary is preferable, as the spleen and pancreas can help locate the ovary in order to permit a smaller skin incision.
10. A cell line expressing luciferase (e.g., ID8-luc, A2780-luc, IGROV1-luc) can be used to monitor tumor development and progression in the ovary of mice, and metastasis formation in vivo, in a rapid and sensitive manner within days or weeks, using non-invasive bioluminescence imaging (BLI). "Luc" cells are obtained by transfecting or infecting cells with the luciferase gene (e.g., *luc*2) and are inoculated in mice as described above. Luciferase generates bioluminescence on conversion of its substrate, luciferin, into oxyluciferin. Luciferin is injected i.p. to the mice (150 mg/kg body weight), and the resulting bioluminescence is imaged after 10 minutes with the use of an optical imaging system. Alternatively, cells can be labeled with fluorescent proteins and tumor growth under the bursa of the mouse ovary is monitored by fluorescence imaging (FLI) techniques.
    To quantify tumor burden, light emission from a single mouse is quantified as total photon counts. Photon emission is recorded as pseudo-color images representing the spatial distribution of photons emerging from active luciferase of fluorescent cells in the animal. Overlaying the grayscale (body of reference photograph) and pseudo-color images enables one to locate tumors in the animal (Fig. 2a). For each group and each time point, the mean BLI or FLI signal in the selected ROI is calculated and plotted against days after tumor transplantation in a histogram (Fig. 2b) [18, 24].
    We suggest shaving C57BL/6 black-haired mice and in general mice with fur or using depilatory cream to expose the skin and allow a higher BLI or FLI signal.
11. Tumor development and progression in the ovary of mice, and metastasis formation in vivo, can be followed in days or weeks with US or MRI. These techniques are useful for fresh tumors, such as PDX or GEMs, which cannot be labeled with bioluminescent or fluorescent dyes. For US, tumor growth is imaged using a transducer with the appropriate frequency for the desired resolution; US images are recorded digitally and tumor areas measured by manually tracing the outline of the tumor using the dedicated software. The software then calculates the area within the outline [36, 37], representative of tumor burden. For MRI, gadolinium-based contrast agent should be injected to permit high-resolution serial imaging with minimum scanning duration, allowing quantification of the tumor volume over time. MRI data are comparable to caliper-based measurements taken at autopsy [38].

12. To analyze tumor vasculature and angiogenesis in the orthotopic tumor or study its function (permeability and perfusion), US and photoacoustic images are taken in vivo, using air microbubbles as contrast agents [39, 40]. We suggest shaving C57BL/6 black-haired mice and in general mice with fur or using depilatory cream to improve the application of the aqueous ultrasonic gel on the skin and avoid background signals.

    At the end of the imaging analysis, mice are killed, and tumor in the ovary or disseminating in the peritoneal cavity can be harvested, fixed in formalin, or frozen for immunehistological analysis with selected antibodies against vascular and lymphatic structures, tumor and host cells, or elements of tumor microenvironment [24, 27].

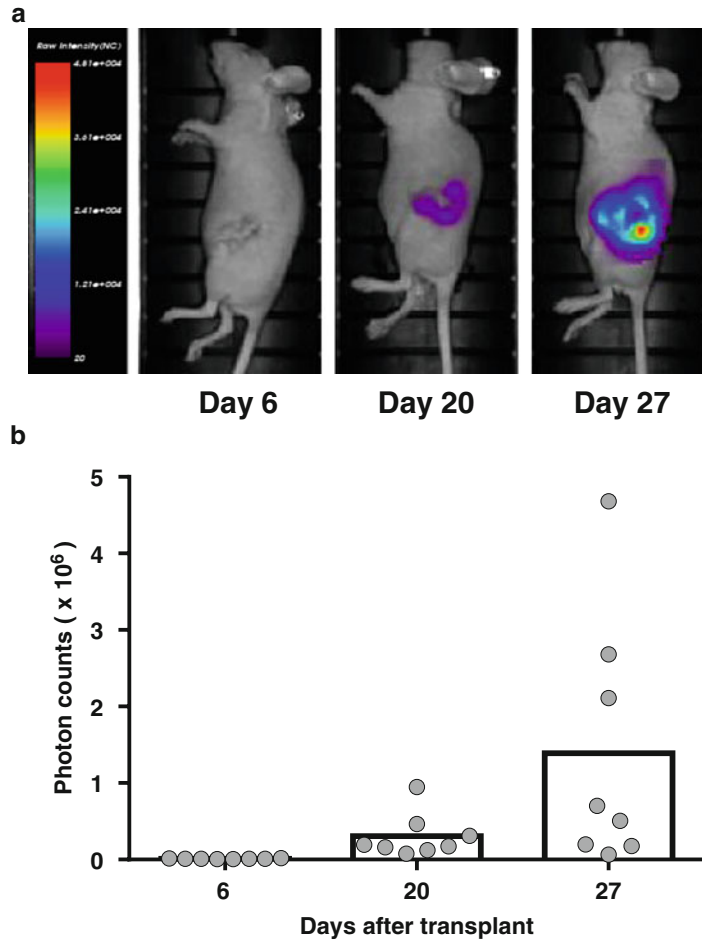

Fig. 2 Orthotopic tumor growth. Nude mice transplanted with IGROV1-luc under the bursa of the ovary were monitored by BLI for tumor formation and progression in the ovary. (**a**) A representative mouse imaged on days 6, 20, and 27 after tumor cells injection. (**b**) Tumor burden in the ovary expressed as photon counts at different time points. *Grey dots* represent single mice, *white columns* are mean photon counts of mice imaged on days 6, 20, and 27 (8 mice)

Acknowledgements

This study was supported by a grant from the Italian Association for Cancer Research (AIRC) no. IG14532 to R.G. A.D. is the recipient of a fellowship from the Umberto Veronesi Foundation, Milan, Italy. We thank J.D. Baggott for editing.

References

1. Siegel RL, Miller KD, Jemal A (2015) Cancer statistics, 2015. CA Cancer J Clin 65(1):5–29
2. Stuart GC, Kitchener H, Bacon M, duBois A, Friedlander M, Ledermann J et al (2011) 2010 Gynecologic Cancer InterGroup (GCIG) consensus statement on clinical trials in ovarian cancer: report from the Fourth Ovarian Cancer Consensus Conference. Int J Gynecol Cancer 21(4):750–755
3. Jayson GC, Kohn EC, Kitchener HC, Ledermann JA (2014) Ovarian cancer. Lancet 384(9951):1376–1388
4. Eskander RN, Tewari KS (2014) Incorporation of anti-angiogenesis therapy in the management of advanced ovarian carcinoma—mechanistics, review of phase III randomized clinical trials, and regulatory implications. Gynecol Oncol 132(2):496–505
5. House CD, Hernandez L, Annunziata CM (2014) Recent technological advances in using mouse models to study ovarian cancer. Front Oncol 4:26. doi:10.3389/fonc.2014.00026
6. Kuhn E, Tisato V, Rimondi E, Secchiero P (2015) Current preclinical models of ovarian cancer. J Carcinog Mutagen 6(2). doi:10.4172/2157-2518.1000220
7. Lengyel E, Burdette JE, Kenny HA, Matei D, Pilrose J, Haluska P et al (2014) Epithelial ovarian cancer experimental models. Oncogene 33(28):3619–3633
8. Ricci F, Bizzaro F, Cesca M, Guffanti F, Ganzinelli M, Decio A et al (2014) Patient-derived ovarian tumor xenografts recapitulate human clinicopathology and genetic alterations. Cancer Res 74(23):6980–6990
9. Weroha SJ, Becker MA, Enderica-Gonzalez S, Harrington SC, Oberg AL, Maurer MJ et al (2014) Tumorgrafts as in vivo surrogates for women with ovarian cancer. Clin Cancer Res 20(5):1288–1297
10. Alkema NG, Tomar T, Duiker EW, Jan Meersma G, Klip H, van der Zee AG et al (2015) Biobanking of patient and patient-derived xenograft ovarian tumour tissue: efficient preservation with low and high fetal calf serum based methods. Sci Rep 5:14495
11. Colombo PE, du Manoir S, Orsett B, Bras-Goncalves R, Lambros MB, MacKay A et al (2015) Ovarian carcinoma patient derived xenografts reproduce their tumor of origin and preserve an oligoclonal structure. Oncotarget 6(29):28327–28340
12. Tentler JJ, Tan AC, Weekes CD, Jimeno A, Leong S, Pitts TM et al (2012) Patient-derived tumour xenografts as models for oncology drug development. Nat Rev Clin Oncol 9(6):338–350
13. Langdon SP (2012) Animal modeling of cancer pathology and studying tumor response to therapy. Curr Drug Targets 13(12):1535–1547
14. Peterson JK, Houghton PJ (2004) Integrating pharmacology and in vivo cancer models in preclinical and clinical drug development. Eur J Cancer 40(6):837–844
15. Daniel VC, Marchionni L, Hierman JS, Rhodes JT, Devereux WL, Rudin CM et al (2009) A primary xenograft model of small-cell lung cancer reveals irreversible changes in gene expression imposed by culture in vitro. Cancer Res 69(8):3364–3373
16. Ricci F, Broggini M, Damia G (2013) Revisiting ovarian cancer preclinical models: implications for a better management of the disease. Cancer Treat Rev 39(6):561–568
17. Hasan N, Ohman AW, Dinulescu DM (2015) The promise and challenge of ovarian cancer models. Transl Cancer Res 4(1):14–28
18. Oliva P, Decio A, Castiglioni V, Bassi A, Pesenti E, Cesca M et al (2012) Cisplatin plus paclitaxel and maintenance of bevacizumab on tumour progression, dissemination, and survival of ovarian carcinoma xenograft models. Br J Cancer 107(2):360–369
19. Kurman RJ, Shih Ie M (2010) The origin and pathogenesis of epithelial ovarian cancer: a proposed unifying theory. Am J Surg Pathol 34(3):433–443
20. Nunez-Cruz S, Connolly DC, Scholler N (2010) An orthotopic model of serous ovarian cancer in immunocompetent mice for in vivo tumor imaging and monitoring of tumor immune responses. J Vis Exp (45). doi:2146 [pii] 10.3791/2146

21. Fu X, Hoffman RM (1993) Human ovarian carcinoma metastatic models constructed in nude mice by orthotopic transplantation of histologically-intact patient specimens. Anticancer Res 13(2):283–286
22. Shaw TJ, Senterman MK, Dawson K, Crane CA, Vanderhyden BC (2004) Characterization of intraperitoneal, orthotopic, and metastatic xenograft models of human ovarian cancer. Mol Ther 10(6):1032–1042
23. Tamada Y, Aoki D, Nozawa S, Irimura T (2004) Model for paraaortic lymph node metastasis produced by orthotopic implantation of ovarian carcinoma cells in athymic nude mice. Eur J Cancer 40(1):158–163
24. Decio A, Taraboletti G, Patton V, Alzani R, Perego P, Fruscio R et al (2014) Vascular endothelial growth factor c promotes ovarian carcinoma progression through paracrine and autocrine mechanisms. Am J Pathol 184(4): 1050–1061
25. Greenaway J, Moorehead R, Shaw P, Petrik J (2008) Epithelial–stromal interaction increases cell proliferation, survival and tumorigenicity in a mouse model of human epithelial ovarian cancer. Gynecol Oncol 108(2):385–394
26. Decio A, Cesca M, Bizzaro F, Porcu L, Bettolini R, Ubezio P et al (2015) Cediranib combined with chemotherapy reduces tumor dissemination and prolongs the survival of mice bearing patient-derived ovarian cancer xenografts with different responsiveness to cisplatin. Clin Exp Metastasis 32(7):647–658
27. Cesca M, Morosi L, Berndt A, Fuso Nerini I, Frapolli R, Richter P et al (2016) Bevacizumab-induced inhibition of angiogenesis promotes a more homogeneous intratumoral distribution of paclitaxel, improving the antitumor response. Mol Cancer Ther. 15(1):125–35
28. Bankert RB, Balu-Iyer SV, Odunsi K, Shultz LD, Kelleher RJ Jr, Barnas JL et al (2011) Humanized mouse model of ovarian cancer recapitulates patient solid tumor progression, ascites formation, and metastasis. PLoS One 6(9):e24420
29. Workman P, Aboagye EO, Balkwill F, Balmain A, Bruder G, Chaplin DJ et al (2010) Guidelines for the welfare and use of animals in cancer research. Br J Cancer 102(11):1555–1577
30. Yang M, Jiang P, An Z, Baranov E, Li L, Hasegawa S et al (1999) Genetically fluorescent melanoma bone and organ metastasis models. Clin Cancer Res 5(11):3549–3559
31. Amoh Y, Bouvet M, Li L, Tsuji K, Moossa AR, Katsuoka K et al (2006) Visualization of nascent tumor angiogenesis in lung and liver metastasis by differential dual-color fluorescence imaging in nestin-linked-GFP mice. Clin Exp Metastasis 23(7–8):315–322
32. Shaner NC, Campbell RE, Steinbach PA, Giepmans BN, Palmer AE, Tsien RY (2004) Improved monomeric red, orange and yellow fluorescent proteins derived from Discosoma sp. red fluorescent protein. Nat Biotechnol 22(12):1567–1572
33. Shcherbo D, Merzlyak EM, Chepurnykh TV, Fradkov AF, Ermakova GV, Solovieva EA et al (2007) Bright far-red fluorescent protein for whole-body imaging. Nat Methods 4(9): 741–746
34. Shu X, Royant A, Lin MZ, Aguilera TA, Lev-Ram V, Steinbach PA et al (2009) Mammalian expression of infrared fluorescent proteins engineered from a bacterial phytochrome. Science 324(5928):804–807
35. Landy A (1989) Dynamic, structural, and regulatory aspects of lambda site-specific recombination. Annu Rev Biochem 58:913–949
36. Snyder CS, Kaushal S, Kono Y, Tran Cao HS, Hoffman RM, Bouvet M (2009) Complementarity of ultrasound and fluorescence imaging in an orthotopic mouse model of pancreatic cancer. BMC Cancer 9:106
37. Sastra SA, Olive KP (2013) Quantification of murine pancreatic tumors by high-resolution ultrasound. Methods Mol Biol 980:249–266
38. Hensley H, Quinn BA, Wolf RL, Litwin SL, Mabuchi S, Williams SJ et al (2007) Magnetic resonance imaging for detection and determination of tumor volume in a genetically engineered mouse model of ovarian cancer. Cancer Biol Ther 6(11):1717–1725
39. Gerling M, Zhao Y, Nania S, Norberg KJ, Verbeke CS, Englert B et al (2014) Real-time assessment of tissue hypoxia in vivo with combined photoacoustics and high-frequency ultrasound. Theranostics 4(6):604–613
40. Paproski RJ, Heinmiller A, Wachowicz K, Zemp RJ (2014) Multi-wavelength photoacoustic imaging of inducible tyrosinase reporter gene expression in xenograft tumors. Sci Rep 4:5329

Chapter 14

The Rip1Tag2 Transgenic Mouse Model

Ruben Bill and Gerhard Christofori

Abstract

The Rip1Tag2 transgenic mouse model of β-cell carcinogenesis has been instrumental in studying various aspects of tumor angiogenesis and in investigating the response to anti-angiogenic therapeutics. Thereby, the in-depth assessment of blood and lymphatic vessel phenotypes and functionality represents key experimental analyses. In this chapter, we describe basic protocols to assess tumor blood vessel morphology (pericyte coverage), functionality (perfusion, leakiness, and hypoxia), lymphatic tumor coverage, and tumor cell proliferation and apoptosis based on immunofluorescence microscopy analysis.

Key words Rip1Tag2, PNET, Insulinoma, Tumor angiogenesis, Anti-angiogenic therapy, Endothelial cells, Immunofluorescence

1 Introduction

Generated in 1985, the Rip1Tag2 transgenic mouse model of pancreatic neuroendocrine tumors (PNETs) has ever since served as a versatile tool to study various aspects of tumor angiogenesis. In this model, the simian virus 40 large T-antigen (*Tag*) oncogene is expressed under the control of the rat insulin gene promoter (*Rip*) leading to multifocal development of insulin-producing β-cell carcinoma (insulinoma) of the islets of Langerhans in the pancreas [1]. Whereas all β-cells present in the approximately 400 islets of Langerhans contain the property to express the *Tag* oncogene at birth, stochastically occurring additional genetic and epigenetic events are required for successful stepwise carcinogenesis. Such an event is for example the acquired capability to express insulin-like growth factor 2 (IGF2). Only about 1–2 % of all islets eventually progress into highly vascularized solid tumors [2]. Finally, Rip1Tag2 mice start to die between weeks 12 and 14 of age due to the tumors' excessive production of insulin resulting in fatal hypoglycemia (*see* **Notes 1** and **2**, [3]).

Primary tumor growth in the Rip1Tag2 mouse model is highly dependent on active tumor angiogenesis. The acquisition of new

Domenico Ribatti (ed.), *Tumor Angiogenesis Assays: Methods and Protocols*, Methods in Molecular Biology, vol. 1464,
DOI 10.1007/978-1-4939-3999-2_14,

blood vessels (i.e., the angiogenic switch) has been shown to be a critical event in order to progress from hyperplastic lesions to adenoma, which is a prerequisite for further development into invasive tumors (carcinoma) [4]. Furthermore, tumor growth is prevented in Rip1Tag2 mice with a β-cell-specific deletion of the major pro-angiogenic molecule VEGF-A [5]. In the following years, the Rip1Tag2 model has revealed important insights into the functions of key angiogenesis mediators by their β-cell-specific deletion or transgenic expression [6–12]. In addition, this PNET mouse model has proven highly instrumental for preclinical validation of eligible biological or pharmacological anti-angiogenic compounds, some of which have been subsequently successfully implemented into clinical practice [13].

Tumor angiogenesis is generally considered to be overshooting, producing abnormal vessels with poor pericyte coverage and a highly fenestrated endothelial layer, thus promoting leakiness and increased interstitial fluid pressure. Intriguingly, despite an abundance of pro-angiogenic factors, regional differences in blood vessel perfusion can result in hypoxic areas with low pH [14]. The delivery of chemotherapeutic agents to tumors is hampered because of hypo-perfused areas and increased interstitial fluid pressure caused by the abnormal vasculature. Vessel-normalizing interventions have been shown to increase chemotherapy availability in tumors [15, 16]. Key to the identification of quantitative and qualitative tumor blood vessel characteristics, i.e., vessel functionality, are methods based on immunofluorescence (IF) analysis.

In this chapter, we provide a simple workflow for routine assessment of the most important parameters of tumor blood vessel characteristics in Rip1Tag2 mice. Analysis of blood vessel microvessel density (MVD; i.e., the number of CD31-positive blood vessels per tumor area) provides quantitative insights into the extent of angiogenesis. This can be further complemented by injecting fluorescently labeled lectin (typically fluorescein/FITC or Texas Red) into the mice prior to euthanization to label the vessel lumen and to assess the percentage of actually patent (i.e., perfused) tumor blood vessels. Similarly, leaky vessels are identified by extravasation of FITC-labeled dextran. Pericytes are perivascular cells localized on the abluminal site of endothelial cells, sharing a common basement membrane and stabilizing the vessel tube. To date, a marker exclusively expressed by pericytes has not been identified [17]. However, the marker neuron-glia antigen 2 (NG2) known to be expressed by pericytes is commonly used to assess pericyte coverage of tumor blood vessels in the Rip1Tag2 model when combined with a staining for CD31 [3]. In the Rip1Tag2 model, staining for α-smooth muscle actin, a marker often used to visualize perivascular cells, only results in a strong staining around large blood vessels, but not around capillaries. To estimate the consequences of an experimentally altered MVD on tumor

oxygenation, the aforementioned characterization of the tumor vasculature can be complemented with the assessment of tumor hypoxia. Intraperitoneally (i.p.) injected pimonidazole hydrochloride (HCl) is chemically reduced in hypoxic areas, and the resulting pimonidazole adducts can be visualized by IF staining.

Lymphatic vessels represent an alternative route for metastatic spread in addition to tumor blood vessels. Indeed, the transgenic expression of VEGF-C or D in β-tumor cells of Rip1Tag2 mice, VEGF family members known to induce lymphangiogenesis, massively increased peritumoral lymphatic coverage and promoted lymph node metastasis [10, 18]. Assessing the peritumoral lymphatic coverage of tumors of Rip1Tag2 mice therefore provides insights into lymphangiogenesis-promoting or -inhibiting mechanisms (*see* **Note 3**).

The ultimate readout of most experimental manipulations in the Rip1Tag2 mouse model is the impact on tumor volumes (*see* **Note 4**). To assess the basis of changes in tumor growth, analysis of tumor cell proliferation by staining for phospho-histone H3 (pH3) and of tumor cell apoptosis by staining for cleaved caspase 3 (cCasp3) can give first insights into the mechanisms underlying a potentially altered tumor burden. In addition, performing a combination staining for CD31 with pH3 or cCasp3 reveals the amount of proliferating and dying endothelial cells, respectively.

The methods presented in this chapter are meant to allow a routine workflow as a basis for further morphological, biochemical, and molecular biology experiments. While the protocols presented here have been specifically described for the use with the Rip1Tag2 transgenic mouse model, they have proven to be functional in a variety of other mouse models of cancer, including xenograft and syngeneic tumor transplantation models and other transgenic mouse models of cancer.

2 Materials

Rip1Tag2 mice

Depending on the source and genetic background, Rip1Tag2 mice start to die approximately at the age of 12–14 weeks. Due to this short survival, the mouse colony has to be constantly bred to prevent loss of the line. In addition, due to the complications caused by the tumor insulin production during pregnancy and nursing, Rip1Tag2 females are not being used for breeding. Rip1Tag2 mice should be strictly kept in a C57BL/6 background, since the genetic background of the mice significantly affects tumorigenesis [19]. Hence, heterozygous transgenic males are bred with wild-type C57BL/6 females. Both heterozygous females and males are used for experiments. Although no apparent gender-dependent phenotypic differences in terms of tumor development have been

observed, it is recommended to stratify experimental groups based on sex. Genotyping of the mice is performed by employing the primers Tag1 5′GGACAAACCACAACTAGAATGCAG and Tag2 5′CAGAGCAGAATTGTGGAGTGG. The resulting PCR product has a size of 449 kb.

2.1 Lectin or Dextran Injection and Mouse Perfusion

1. Fluorescein Lycopersicon Esculentum (Tomato) Lectin (FITC-Lectin; Vector Laboratories/Reactolab), diluted in sterile PBS to 1 mg/ml.
2. Dextran Fluorescein (FITC-Dextran; Life Technologies), anionic, lysine fixable, 70,000 MW, dilute in sterile PBS to 1.25 mg/ml.
3. Pimonidazole Hypoxyprobe (TM-1 Omni Kit Hydroxyprobe Inc.), pimonidazole HCl plus rabbit antisera, dilute in sterile PBS to 6 mg/ml.
4. Ethanol 70 % spray.
5. Surgical scissors.
6. Forceps.
7. Insulin syringe, BD Micro-Fine, 29G.
8. Anesthetic, according to the locally licensed compounds for terminal anesthesia (e.g., Pentobarbital).
9. “Butterfly,” BD Valu-Set, 25G.
10. Syringe, 10 ml.
11. PBS (sterile for diluting lectin, dextran, and pimonidazole; non-sterile for mouse perfusion and tissue processing).
12. PBS/4 % PFA.

2.2 Tissue Fixation and Cryopreservation

1. PBS/4 % PFA.
2. PBS/20 % sucrose.
3. Optimal cutting temperature (OCT) compound (Tissue-Tek).
4. Embedding mold for frozen tissues.
5. Dry ice pellets.
6. Ethanol 100 %.

2.3 Cryosectioning and Immunofluorescence Staining

1. Cryotome.
2. Microscope slides.
3. Cover slips.
4. Liquid blocker, Super Pap Pen (Daido Sangyo Co., Ltd. Tokyo, Japan).
5. PBS (non-sterile).
6. PBS/0.2 % Triton X-100.
7. PBS/5 % or 20 % normal goat serum (ngs).

8. DAPI 1:10,000.
9. Fluorescent Mounting Medium (Dako) (*see* **Note 5**).
10. Primary antibodies, dilutions:

    CD31, rat (BD Pharmingen, 550274), 1:50.

    Cleaved Caspase-3 (cCasp3; Cell Signaling, 9664), 1:50.

    Insulin, guinea pig (Dako, A0564), 1:200.

    LYVE-1, rabbit (RELIATech, 103-PA50S/0412P02-2), 1:200.

    NG2, rabbit (Chemicon, AB5320), 1:100.

    Phospho-Histone H3 (pH3), rabbit (Millipore, 06-570), 1:200.

    Pimonidazole, rabbit (Hypoxyprobe Inc.), antibody included in "Pimonidazole Hypoxyprobe TM-1 Omni Kit", 1:25.

    SV40 Large T antigen, rabbit (Santa Cruz, sc-20800), 1:50.
11. Secondary antibodies, Alexa labeled (Molecular Probes/Life Technologies).

3 Methods

3.1 Injections, Systemic Perfusion, and Excision of Pancreas (See Also Note 6*)*

1. Inject all animals with pimonidazole 60 mg/kg (inject 100 µl per 10 g mouse body weight of a 6 mg/ml solution) intraperitoneally 1–2 h prior to euthanization (*see* **Note 7**).
2. If the anesthetic licensed for terminal anesthesia provides fast narcosis, the intravenous (i.v.) injection of FITC-lectin or FITC-dextran can be performed in non-anesthetized animals, followed by anesthesia (methods adapted from refs. 16, 20, 21).
3. For the injection of FITC-lectin, inject 100 µl of FITC-lectin i.v. into the tail vein (0.1 mg/mouse, perfuse after 10 min).
4. For the injection of FITC-dextran, inject 200 µl of FITC-dextran i.v. into the tail vein (0.25 mg/mouse, perfuse after 5 min).
5. For the perfusion, anesthetize the mouse with an ultra-deep (terminal) and fast-acting anesthesia as licensed by the local veterinary office (*see* **Note 8**).
6. Pin the extremities of the animal on a dissection pad, spray it with ETOH 70%, and incise the skin and the underlying peritoneum with a horizontal cut immediately *caudal* of the costal arch using scissors. Now, the *caudal* surface of the diaphragm should be visible.
7. Grab the *processus xiphoideus* with forceps and induce a pneumothorax by incision of the diaphragm. The resulting collapse of the lungs prevents them from damage potentially caused during the dissection procedure. Introduce the scissors carefully along the interior surface of the ribs in direction of the axilla

and cut the ribs. Repeat this on the other side. Free the resulting flap containing the cut ribs and the *sternum* from remaining *caudal* attachments to the diaphragm, fold it, and pin it over one of the shoulders on the surface. Now, a free look on the collapsed lungs and the heart should be possible.

8. Introduce the needle of the butterfly into the left ventricle of the heart (due to the oxygenated arterial blood it shows a lighter red color than the right ventricle) and cut into the right *atrium* to open the circulation and provide an opening for the perfused solution.
9. For the perfusion of FITC-lectin-injected animals, perfuse the FITC-lectin-injected animal slowly with 10 ml ice-cold PBS/4% PFA for immediate fixation, immediately followed by 10 ml ice-cold PBS (*see* **Note 9**).
10. For the perfusion of FITC-dextran, perfuse the FITC-dextran-injected animals slowly first with 10 ml ice-cold PBS to wash out the intravascular dextran, immediately followed by the perfusion with 10 ml ice-cold PBS/4% PFA for fixation (*see* **Note 10**).
11. In order to dissect the pancreas (and other abdominal organs such as the liver), widen the existing abdominal incision to have free access to the abdominal organs. Move the intestine to the right side of the animal and identify the spleen. Pull the spleen carefully. This helps to identify the pancreas, which is the yellowish tissue containing red, vascularized tumors and is connected via the *ligamentum pancreato-lienale* to the spleen.
12. Dissect the pancreas, rinse it briefly in PBS to get rid of blood, measure the diameter of the macroscopic tumors using a ruler, and fix the tissue as soon as possible in cold PBS/4% PFA. Incubate the tissue in PBS/4% PFA for 2 h while rotating at 4 °C, followed by overnight incubation at 4 °C in PBS/20% sucrose.
13. On the next day, prepare a bath with dry ice pellets covering the floor of a Styrofoam container and add ethanol 100% (*see* **Notes 11** and **12**). Snap-freeze the tissues in optimal cutting temperature (OCT) freezing solution in the ethanol/dry ice bath. Store samples at −80 °C.

3.2 Cryosectioning and IF Staining

1. Put frozen OCT blocks at −20 °C (into cryotome or freezer) >30 min before starting sectioning (*see* **Notes 13–15**).
2. Cut 7–10 μm thick sections (*see* **Note 16**).
3. Let it dry for at least 30 min.
4. Encircle the sections with a liquid blocker and let it dry for some additional minutes.
5. Rehydrate in PBS 3 × 5 min (*see* **Note 17**).

6. Permeabilize in PBS/0.2% Triton X-100 for 20 min.
7. Wash in PBS 3×5 min.
8. Block with blocking buffer (PBS/5% ngs) for 1 h in a humid chamber. For staining with the anti-cCasp3 antibody perform the blocking with PBS/20% ngs.
9. Replace the blocking buffer with the desired antibodies diluted in blocking buffer. Incubate in a humid chamber overnight at 4 °C (*see* **Note 18**).
10. On the next morning, wash the specimen 3×5 min in PBS at room temperature.
11. Incubate for 1 h at room temperature with secondary antibodies directed against the species of the corresponding primary antibodies and labeled with Alexa fluorochromes suitable for the filters of the fluorescence microscope available.
12. Wash in PBS 3×5 min.
13. Incubate with DAPI diluted 1:10,000 in PBS at room temperature for 10 min in a humid chamber.
14. Wash in PBS 3×5 min.
15. Mount slides with cover slips using DAKO mounting medium (*see* **Note 19**). Avoid air bubbles.
16. Let slides dry (in the dark) for some hours at room temperature. Then transfer them to 4 °C and analyze the slides within few days.
17. We recommend acquiring the images using a 20× magnification for the assessment of MVD, pericyte coverage, vessel perfusion, and leakiness. For the analysis of the hypoxic area fraction, a 10× magnification is recommended.
18. For image analysis we routinely employ ImageJ image processing and analysis software.

4 Notes

1. Although the Rip1Tag2 mice used in different laboratories around the globe originate from the same founder line, breeding in isolation over years has led to interesting phenotypic differences even when kept in a pure C57BL/6 background. Notable differences in survival, lymph node, and liver metastasis at baseline and upon anti-angiogenic therapy, and the extent of intra- and peritumoral lymphangiogenesis, can be detected when screening the literature [3, 11, 21–26].
2. Rip1Tag2 mouse survival can be extended by the administration of food pellets consisting of 60% glucose starting from the age of around 9 weeks.

3. Insulinoma in the Rip1Tag2 model only rarely displays intratumoral lymphatic vessels. Instead, they can be found at peritumoral location. Whereas peritumoral lymphatic vessels in Rip1Tag2 single transgenic mice only cover less than 10% of the tumor circumference, almost complete lymphatic coverage can be achieved by intercrossing Rip1Tag2 mice with Rip1-VEGF-C or D transgenic mice [3, 10].
4. Tumor volumes of macroscopic tumors (≥1 mm diameter) are assessed by measuring the diameter of each tumor, calculating the volume assuming a spherical shape (volume = (4/3)*π* (diameter/2)^3), and summing up the resulting volumes per mouse.
5. DAKO mounting medium can be replaced with Mowiol.
6. Blood vessel perfusion and leakiness can in principle be analyzed in the same mouse by co-injecting FITC-dextran and Texas-Red-labeled lectin. However, this reduces the possibilities of future IF co-staining, since the "green" and the "red" channels are occupied in this setting. Additionally, please note that DAPI is always accompanying the IF stainings. Therefore, we usually split the mouse cohorts into three groups. All the animals receive an injection of pimonidazole, one-third of the animals FITC-lectin or FITC-dextran, respectively, and one-third pimonidazole only. Furthermore, tissues from the latter group can be conveniently used for RNA or protein isolation, since the pimonidazole injection alone does only require a (immediate) post-dissection fixation in PBS/4% PFA, but not a systemic PBS/4% PFA perfusion prior to organ dissection, as it is the case for FITC-lectin- and FITC-dextran-injected animals.
7. Pimonidazole HCl displays a half-life of about 0.25 h in mice. To avoid artifacts introduced by hypoxia/anoxia during the euthanasia and dissection procedure, pimonidazole levels in the systemic circulation should therefore be sufficiently low at the time of euthanasia. Therefore, the manufacturer recommends to dissect the mice 1–2 h (the chosen time point should be strictly kept for all the animals in the same experiment) after injection, using a fast euthanasia technique (cervical dislocation rather than CO_2 suffocation) [27].
8. In principle, mice could also be perfused shortly after death by CO_2 suffocation. If mice are co-injected with pimonidazole, however, CO_2 suffocation should be avoided (*see* **Note** 7). In this case, any terminal anesthesia method licensed by the relevant veterinary office can be employed to obtain a humane peri-mortal perfusion.
9. Changing from the syringe containing 10 ml PBS to the 10 ml syringe containing PBS/4% PFA should ideally be performed by a second assisting person. Like this, the needle can remain

in the exact same position in the left ventricle preventing the creation of holes in the myocardium of the left ventricle that could reduce the perfusion quality.

10. If the perfusion with PBS is incomplete, remaining intravascular FITC-dextran can be distinguished from extravascular (i.e., leaking) FITC-dextran by visualizing the blood vessels with a staining for the endothelial cell marker CD31.
11. Styrofoam containers, which are often used to ship laboratory materials, can easily be recycled for the purpose of freezing tissues. Please make sure that you take a container that does not leak.
12. To prevent vanishing of markings made on the embedding molds, use an alcohol-resistant lab marker and fill the ethanol only to a level below the markings.
13. Prevent prolonged handling of OCT blocks at room temperature because the OCT solution should not thaw. If rapid transfer from the –80 °C freezer to the cryotome or –20 °C freezer is not possible, transport the OCT blocks cooled.
14. Short-term storage of OCT blocks at –20 °C for a few days is possible, although not recommended. In addition, avoid leaving the OCT blocks in the cryotome overnight, since some machines display temperature fluctuations.
15. Protect sections from light throughout the whole experiment, especially if FITC-lectin or FITC-dextran is present in the respective tissue.
16. Since cutting sections of larger experiments containing numerous OCT blocks often take some hours, the time the different sections are drying may vary. To account for potential "batch effects," the order of the OCT blocks processed should not be according to the experimental groups, but random instead.
17. All washing and the permeabilization step (if not otherwise indicated) can be performed by putting the sections as a batch in one container gently shaking on a tumbling table at room temperature.
18. Alternatively to overnight incubation with the primary antibodies, the incubation can also be shortened to 1 h at room temperature in a humid chamber (do not forget to protect the specimen from light).
19. Insulinoma can be easily distinguished from the surrounding exocrine pancreas based on the more dense distribution pattern of the DAPI-stained nuclei. Pancreatic lymph nodes display a densely packed nuclei distribution pattern as well, but nuclei are more densely distributed and smaller than observed in insulinoma. If required, tumor cells can be specifically visualized by staining for insulin or SV40 large T antigen.

Importantly, it has been described that a subpopulation of insulinoma in the Rip1Tag2 mouse model loses insulin expression but remains positive for SV40 large T antigen expression [28]. Therefore, SV40 large T antigen appears to be a more sensitive marker to detect tumors (and metastases) in this model. On the other hand, the quality of the IF staining on cryosections for insulin is significantly better than that for SV40 large T antigen.

Acknowledgement

This work was supported by a Swiss National Science Foundation MD-PhD student fellowship to R.B.

References

1. Hanahan D (1985) Heritable formation of pancreatic beta-cell tumours in transgenic mice expressing recombinant insulin/simian virus 40 oncogenes. Nature 315:115–122
2. Christofori G, Naik P, Hanahan D (1994) A second signal supplied by insulin-like growth factor II in oncogene-induced tumorigenesis. Nature 369:414–418
3. Bill R, Fagiani E, Zumsteg A et al (2015) Nintedanib is a highly effective therapeutic for neuroendocrine carcinoma of the pancreas (PNET) in the Rip1Tag2 transgenic mouse model. Clin Cancer Res 21:4856–4867
4. Folkman J, Watson K, Ingber D et al (1989) Induction of angiogenesis during the transition from hyperplasia to neoplasia. Nature 339:58–61
5. Inoue M, Hager JH, Ferrara N et al (2002) VEGF-A has a critical, nonredundant role in angiogenic switching and pancreatic beta cell carcinogenesis. Cancer Cell 1:193–202
6. Albrecht I, Kopfstein L, Strittmatter K et al (2010) Suppressive effects of vascular endothelial growth factor-B on tumor growth in a mouse model of pancreatic neuroendocrine tumorigenesis. PLoS One 5:e14109
7. Bergers G, Brekken R, McMahon G et al (2000) Matrix metalloproteinase-9 triggers the angiogenic switch during carcinogenesis. Nat Cell Biol 2:737–744
8. Fagiani E, Lorentz P, Kopfstein L et al (2011) Angiopoietin-1 and -2 exert antagonistic functions in tumor angiogenesis, yet both induce lymphangiogenesis. Cancer Res 71:5717–5727
9. Gannon G, Mandriota SJ, Cui L et al (2002) Overexpression of vascular endothelial growth factor-A165 enhances tumor angiogenesis but not metastasis during beta-cell carcinogenesis. Cancer Res 62:603–608
10. Mandriota SJ, Jussila L, Jeltsch M et al (2001) Vascular endothelial growth factor-C-mediated lymphangiogenesis promotes tumour metastasis. EMBO J 20:672–682
11. Paez-Ribes M, Allen E, Hudock J et al (2009) Antiangiogenic therapy elicits malignant progression of tumors to increased local invasion and distant metastasis. Cancer Cell 15:220–231
12. Schomber T, Kopfstein L, Djonov V et al (2007) Placental growth factor-1 attenuates vascular endothelial growth factor-A-dependent tumor angiogenesis during beta cell carcinogenesis. Cancer Res 67:10840–10848
13. Tuveson D, Hanahan D (2011) Translational medicine: cancer lessons from mice to humans. Nature 471:316–317
14. Carmeliet P, Jain RK (2011) Principles and mechanisms of vessel normalization for cancer and other angiogenic diseases. Nat Rev Drug Discov 10:417–427
15. Jain RK (2001) Normalizing tumor vasculature with anti-angiogenic therapy: a new paradigm for combination therapy. Nat Med 7:987–989
16. Mazzone M, Dettori D, Leite de Oliveira R et al (2009) Heterozygous deficiency of PHD2 restores tumor oxygenation and inhibits metastasis via endothelial normalization. Cell 136: 839–851
17. Armulik A, Genove G, Betsholtz C (2011) Pericytes: developmental, physiological, and pathological perspectives, problems, and promises. Dev Cell 21:193–215

18. Kopfstein L, Veikkola T, Djonov VG et al (2007) Distinct roles of vascular endothelial growth factor-D in lymphangiogenesis and metastasis. Am J Pathol 170:1348–1361
19. Hager JH, Hodgson JG, Fridlyand J et al (2004) Oncogene expression and genetic background influence the frequency of DNA copy number abnormalities in mouse pancreatic islet cell carcinomas. Cancer Res 64: 2406–2410
20. Kuzmanov A, Hopfer U, Marti P et al (2014) LIM-homeobox gene 2 promotes tumor growth and metastasis by inducing autocrine and paracrine PDGF-B signaling. Mol Oncol 8:401–416
21. Maione F, Capano S, Regano D et al (2012) Semaphorin 3A overcomes cancer hypoxia and metastatic dissemination induced by antiangiogenic treatment in mice. J Clin Invest 122:1832–1848
22. Anderberg C, Cunha SI, Zhai Z et al (2013) Deficiency for endoglin in tumor vasculature weakens the endothelial barrier to metastatic dissemination. J Exp Med 210:563–579
23. Rigamonti N, Kadioglu E, Keklikoglou I et al (2014) Role of angiopoietin-2 in adaptive tumor resistance to VEGF signaling blockade. Cell Rep 8:696–706
24. Sennino B, Ishiguro-Oonuma T, Schriver BJ et al (2013) Inhibition of c-Met reduces lymphatic metastasis in RIP-Tag2 transgenic mice. Cancer Res 73:3692–3703
25. Sennino B, Ishiguro-Oonuma T, Wei Y et al (2012) Suppression of tumor invasion and metastasis by concurrent inhibition of c-Met and VEGF signaling in pancreatic neuroendocrine tumors. Cancer Discov 2:270–287
26. Singh M, Couto SS, Forrest WF et al (2012) Anti-VEGF antibody therapy does not promote metastasis in genetically engineered mouse tumour models. J Pathol 227:417–430
27. Hypoxyprobe, Inc. http://www.hypoxyprobe.com/faq.html. Accessed 27 Aug 2015
28. Hunter KE, Quick ML, Sadanandam A et al (2013) Identification and characterization of poorly differentiated invasive carcinomas in a mouse model of pancreatic neuroendocrine tumorigenesis. PLoS One 8:e64472

Chapter 15

Tumor Blood Vessel Visualization

Clarissa Gillmann and Tobias Bäuerle

Abstract

Noninvasive multimodal imaging of tumor blood vessels allows the qualitative and quantitative assessment of morphological, functional, and molecular features of tumor angiogenesis longitudinally in a living organism. In this chapter we focus on the application of magnetic resonance imaging (MRI), computed tomography (CT), ultrasound (US), and positron emission tomography (PET) in tumor blood vessel visualization on the example of breast cancer bone metastasis in a nude rat model. Thereby, materials and methods are described that are needed to obtain complementary data on tumor vascularization from these imaging techniques.

Key words Magnetic resonance imaging, Computed tomography, Ultrasound, Positron emission tomography, Angiogenesis, Tumor vessels, Angiography, Dynamic-contrast-enhanced imaging

1 Introduction

Angiogenesis is an essential feature of cancer growth and metastasis formation. Experimental imaging techniques from radiology and nuclear medicine allow the investigation of various aspects of tumor blood vessels longitudinally in a living organism. Thus, angiogenesis might be characterized on the morphological, functional, and molecular level using noninvasive in vivo imaging without the need of repetitive histological evaluations.

For tumor blood vessel visualization in small animals, various imaging modalities are employed that differ significantly concerning methodology and acquired information. Here, the focus is on complementary techniques from radiology and nuclear medicine such as computed tomography (CT), magnetic resonance imaging (MRI), ultrasound (US), and positron emission tomography (PET). CT and MRI are utilized to visualize blood vessel morphology and architecture, but also functional data like regional blood volume, perfusion, and vessel permeability can be acquired by dynamic image acquisition after contrast media application (dynamic contrast-enhanced CT or MRI; DCE-CT, DCE-MRI) [1–3]. Particular

Domenico Ribatti (ed.), *Tumor Angiogenesis Assays: Methods and Protocols,* Methods in Molecular Biology, vol. 1464,
DOI 10.1007/978-1-4939-3999-2_15,

strengths of US and PET are on the molecular level regarding vessel function that might be determined in real time by US and PET imaging of molecular epitopes of endothelial cells assessed with molecular probes [4, 5]. Related to the different methodology of these imaging modalities, the available contrast agents and radiotracers differ accordingly. For MRI and CT, gadolinium- and iodine-containing agents may be used, respectively, while ultrasound requires the intravenous application of gas-filled microbubbles. For PET, positron emitters are administered (e.g., ^{18}F or ^{68}Ga), e.g., attached to a specific ligand and the respective epitope for molecular imaging.

Here, we focus on CT, MRI, US, and PET presenting materials and methods for tumor blood vessel imaging in vivo. The following protocols were optimized for visualizing angiogenic processes in experimental breast cancer bone metastases growing in the hind leg of nude rats and may be adapted for other purposes and species (*see* ref. 6 for details on the animal model).

2 Materials

For noninvasive imaging of tumor blood vessels, appropriate imaging modalities and contrast agents or radiotracers are needed along with consumables for animal preparation. Analysis of imaging data is performed with image processing software (*see* **Note 1**).

2.1 Imaging Modalities

Dedicated preclinical scanners are available from various companies, e.g., small animal MRI systems from Bruker (Ettlingen, Germany), hybrid scanners for PET/SPECT/CT like the Inveon system from Siemens (Erlangen, Germany), or the ultrasound devices from FujifilmVisual Sonics (Toronto, Canada). As an alternative, scanners for human use might be used, often at the cost of decreased temporal and spatial resolution. Nevertheless, optimization of clinical scanners with suitable hard- and software may result in appropriate imaging properties for small animal imaging.

For the protocol described here, we used a human MR system (1.5T Symphony, Siemens, Germany) in combination with a home-built radiofrequency excitation and detection coil dedicated for rat imaging. The coil was designed as a cylindrical volume resonator with an inner diameter of 83 mm and a usable length of 120 mm. CT scans were performed on a prototype of a flat panel equipped volumetric computed tomograph (Volume CT, Siemens, Germany). The clinical system Acuson Sequoia 512 with a 15L8 linear transducer was used for US investigations (Siemens-Acuson, Mountain View, USA) and PET studies were performed on an ECAT EXACT HR+ scanner (Siemens, Germany).

2.2 Intravenous Administration

Contrast agents and PET tracers (compare Subheading 2.3) are administered intravenously in the tail vein via a catheter (*see* **Note 2**). For rats we use Introcan Safety W (24 G×3/4″, 0.7×19 mm, B. Braun, Germany) catheters in combination with a 1 ml Soft-Jet syringe (Henke Sass Wolf, Germany). For mice, a needle (Sterican 30 G×1/2″, 0.3×12 mm) inserted in a flexible tube (Smiths Fine Bore Polyethylene Tubing, 0.28 mm inner diameter, 0.61 mm outer diameter, Smiths Medical, USA) might be used. How to insert a catheter into the tail vein as well as how to prepare a catheter for mice are explained in Subheading 4.

2.3 Contrast Agents and PET Tracers

Various contrast agents and PET tracers are available. For our studies, we administered the following concentrations of the given products:

1. MRI: 0.1 mmol/kg Gd-DTPA (Magnevist, Bayer-Schering, Germany).
2. CT: 1 g Iodine per kg (Imeron 400, Bracco, Germany).
3. US: 1.6 ml/kg (SonoVue, Bracco, Italy).
4. PET: 5–10 MBq ^{18}F-deoxyglucose (^{18}F-FDG, from any local vendor).

As alternative to the abovementioned radiotracer for PET (^{18}F-FDG), specific radiopharmaceuticals for specific imaging of molecular structures of angiogenic vessels may be synthesized, e.g., for integrins alpha (v) beta 3 and 5 (for more specific information, *see* ref. 5).

Weigh each animal and calculate the individually needed amount of contrast agent (weight adapted administration). Dilute contrast agent/tracer with sodium chloride (NaCl) (concentration: 9 g 154 mmol/l Na^+ and 154 mmol/l Cl^- in 1000 ml) to obtain the appropriate concentration/activity. The total injection volume (contrast agent/tracer diluted in NaCl) should be approximately 0.5 ml for each animal (rat; approx. 0.1 ml for mice) (*see* **Note 3**).

2.4 Image Postprocessing

Dedicated software tools (e.g., Osirix Imaging Software, ImageJ) can visualize image data saved in Digital Imaging and Communications in Medicine (DICOM) format (*see* **Note 4**). Morphologic parameters of blood vessel formation (e.g., from angiography) can be determined with (semi-)automatic or manual segmentation tools (e.g., Chimaera GmbH, Germany). The quantification of functional parameters such as amplitude A (associated with blood volume) and exchange rate constant k_{ep} (associated with perfusion and vessel permeability) obtained from dynamic contrast-enhanced studies requires specific analysis tools (e.g., Dyna Lab (Mevis Research, Bremen, Germany) or Osirix' DCE plug-in (Osirix Imaging Software) for DCE-MRI and DCE-CT and Qontrast (Bracco, Italy) for DCE-US).

3 Methods

Following animal preparation (Subheading 3.1), multimodal data acquisition (Subheading 3.2–3.5), postprocessing, and analysis (Subheading 3.6) are the most important methods for tumor blood vessel visualization. The respective procedures are described below.

3.1 Animal Preparation

1. Anesthetize the animal with inhalation of oxygen (0.5 l/min) and isoflurane (1.5 vol.%). As an alternative, intraperitoneal injection anesthesia might by administered.
2. Apply moist cream to the animal's eyes to prevent drying during anesthesia due to incomplete closure of the eyelids.
3. For US, animals should be shaved in the respective imaging region, or as alternative, a depilatory cream might be used.
4. Insert a catheter into the tail vein for contrast agent/tracer application and connect a syringe to the catheter that contains the respective contrast agent/tracer.

3.2 Magnetic Resonance Imaging

1. Maintaining the inhalation anesthesia, place the rat in the MR system with the volume of interest (tumor) being close to the most homogeneous part of the coil.
2. Tune the volume coil according to the animal's weight (*see* **Note 5**).
3. Start imaging with a localizer-sequence.
4. Manually adjust frequency, transmitter, and 3D shim (*see* **Note 5**).
5. Use a short, low-resolution morphologic sequence to locate the tumor and to determine the volume of interest (e.g., a T2-weighted turbo spin echo sequence with the following scan parameters: repetition time (TR): 3240 ms, echo time (TE): 81 ms, resolution: 0.6×0.2 mm^2, slice thickness: 1.5 mm, averages: 3, acquisition time (TA): 3:40 min).
6. Apply a T1-weighted pre-contrast sequence to obtain morphology before contrast agent injection (e.g., a 3D Fast low angle shot (FLASH) sequence with TR: 1430 ms, TE: 58 ms, flip angle: 35°, slice thickness: 1.5 mm, TA: 5:30 min).
7. Determine an appropriate region of interest (either a single slice or a volume) and start the sequence for DCE-MRI (e.g., a saturation recovery turbo flash sequence, TR: 373 ms, TE: 1.86 ms, nominal resolution: 1.5×1.5 mm^2, slice thickness: 5 mm, measurements: 512, averages: 1, TA: 6:55 min). After approximately 30 s, begin to inject the contrast agent over a time period of 10 s.
8. Copy the T1-pre-contrast sequence and apply it again to obtain post-contrast images.

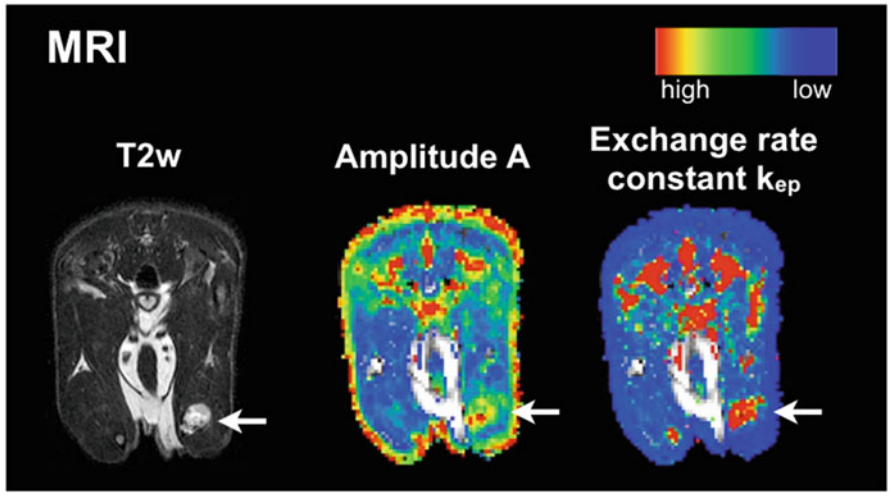

Fig. 1 Axial MR sections. *Left panel*, T2w MRI; *middle panel*, amplitude A (DCE-MRI, associated with blood volume); *right panel*, exchange rate constant k_{ep} (DCE-MRI, associated with perfusion and vessel permeability) according to the pharmacokinetic model of Brix. *Arrows* point at bone metastases. The color map for DCE-MRI data ranges from *red* (high values) to *blue* (low values). *Arrows* point at bone metastasis. Figure reprinted with permission from [14]

9. The total time for the abovementioned procedures to perform a magnetic resonance imaging (MRI) examination is approximately 20–25 min per animal.
10. Using the protocol described above, examples from morphological and functional MR imaging of a breast cancer bone metastasis in a rat's hind leg are shown in Fig. 1.

3.3 Computed Tomography (CT)

1. Place the rat on the scanner under inhalation anesthesia.
2. Use the following scan parameters: tube voltage: 80 kV, tube current: 50 mA, rotation speed: 10 s, frames per second: 120, matrix: 512 × 512, slice thickness 0.2 mm, and scan time: 51 s.
3. Inject the contrast agent during the second rotation of the flat panel system (acquire at least one rotation before administration of the contrast agent to obtain the baseline level of unenhanced images).
4. The total time for the abovementioned procedures to perform a CT examination is approximately 5–10 min per animal.
5. Reconstruct images with a modified Feldkamp Davis Kress (FDK) cone-beam reconstruction algorithm (kernel H80a, Afra, Germany).
6. Using the protocol described above, examples from morphological and functional CT imaging of a breast cancer bone metastasis in a rat's hind leg are shown in Fig. 2.

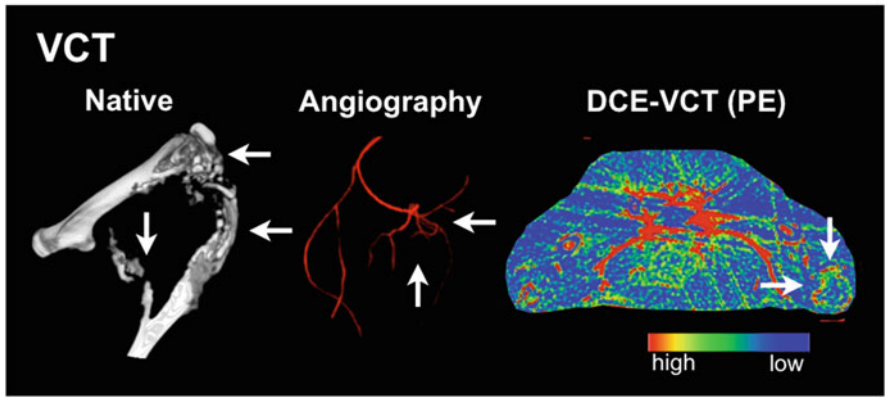

Fig. 2 3D CT reconstructions of the osteolytic bone metastasis (*left panel*) and an angiography (*middle panel*) as well as a DCE-CT section in axial orientation from the parameter peak enhancement (associated with blood volume, *right panel*). The color map for DCE-CT data ranges from *red* (high values) to *blue* (low values). *Arrows* point at bone metastasis. Figure reprinted with permission from [14]

3.4 Ultrasound (US)

1. Maintaining anesthesia, place the rat under the transducer and fix the US transducer on the respective volume of interest using a tripod.
2. Apply US gel between the transducer and the skin of the animal (rub the gel mildly onto the skin to avoid air bubbles).
3. Perform B-mode imaging (transmission frequency: 17 MHz; mechanical index: 0.51) to determine the region of interest within the tumor (e.g., largest diameter) and fix the transducer in this position. Add Doppler signal on B-mode images for information on tissue perfusion.
4. For dynamic contrast-enhanced US (DCE-US) set the US device in cadence-contrast pulse sequencing (CPS) mode (transmission frequency: 7 MHz; mechanical index: 0.18). Inject the microbubbles and record a cine loop of 90 s length.
5. Performing a US examination with the abovementioned procedures takes approximately 10–15 min per animal.
6. Using the protocol described above, examples from morphological and functional US imaging of a breast cancer bone metastasis in a rat's hind leg are shown in Fig. 3.

3.5 Positron Emission Tomography

As the animal's diet usually contains glucose, animals should fast at least for 4 h before positron emission tomography (PET) imaging (*see* **Notes** 6 and 7).

1. Position the animal in the axial plane of the PET scanner to maintain best resolution in the center of the system.
2. Perform a transmission scan (10 min) to account for attenuation correction of dynamic emission data.

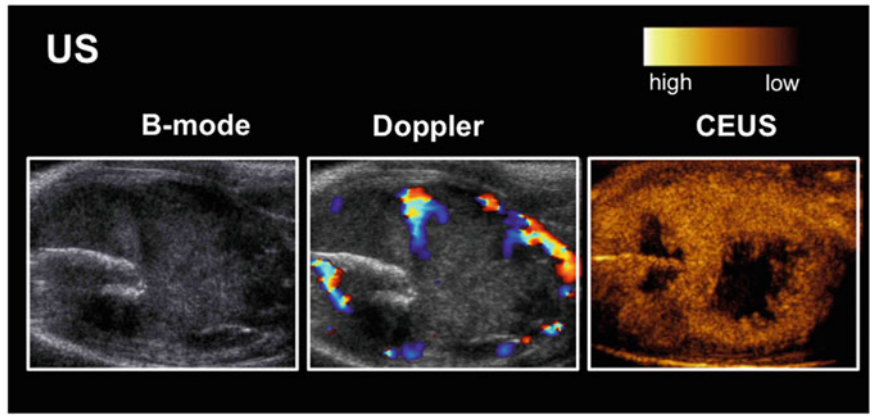

Fig. 3 US images from B-mode (morphology, *left panel*), Doppler (perfusion, *middle panel*), and contrast-enhanced US (CEUS; *right panel*, peak enhancement after injection of microbubbles from real-time imaging of vascularization) of a bone metastasis. Figure reprinted with permission from [14]

3. Inject radioactivity (here: ^{18}F-FDG).
4. Start PET protocol. Dynamic acquisition over 60 min including 28 frames: ten frames of 30 s, five frames of 120 s, eight frames of 300 s, nominal resolution: $2.3 \times 2.3 \times 2.4$ mm^3. For static acquisition, the time of imaging is reduced, accordingly.
5. When using a hybrid scanner (e.g., PET/CT), a subsequent CT scan might be combined with the PET examination without moving the animal that facilitates easy co-registration (*see* **Note 8**).
6. Using the protocol described above, examples from PET imaging of a breast cancer bone metastasis in a rat's hind leg are shown in Fig. 4(*see* **Note 9**).

3.6 Postprocessing and Analysis of Imaging Data

1. Morphological information from MRI, CT, and US can be used to determine location, size, and volume of the soft-tissue tumor (MRI, US) and the skeletal destruction (CT) (*see* **Note 10**).
2. Branching pattern of vessels and the altered macrovessel architecture in tumors (angiography) can be visualized by both CT and MRI data. Reconstruct 2D or 3D images using the information of the arterial phase. For MRI, subtract pre-contrast from post-contrast T1-weighted images (Sequences 6 and 8 in Subheading 3.2) to obtain a subtraction image for determination of strongly vascularized regions.
3. The vascular parameters amplitude A (associated with blood volume) and exchange rate constant k_{ep} (associated with perfusion and vessel permeability) can be obtained by analyzing DCE-MRI data with Dyna Lab software (Mevis Research, Bremen, Germany) based on pharmacokinetic models (e.g.,

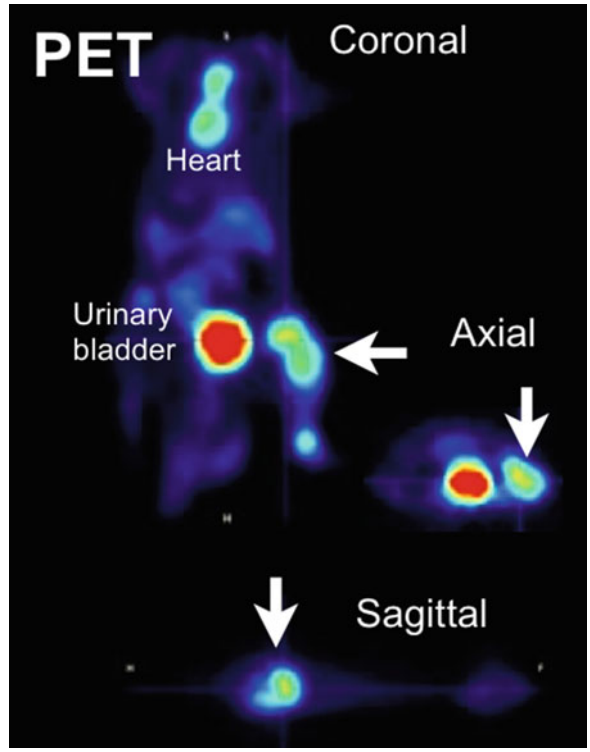

Fig. 4 ^{18}F-FDG PET images in coronal (*left panel*), axial (*right upper panel*), and sagittal orientation (*lower panel*) of a bone metastasis. Besides FDG uptake in the bone metastasis, there is physiological accumulation in the heart and urinary bladder by blood and urine, respectively. *Arrows* point at bone metastasis

the two-compartment model of Brix [7] or Tofts [8]). As alternative quantification method of vascular parameters from DCE data, parameters derived from the signal-intensity-versus-time curve can be associated with vascularization and perfusion (e.g., area under the curve, peak enhancement, time to peak; *see* ref. 2).

4. DCE-US can be quantified by analyzing cine-loops according to the implemented bolus injection model (e.g., with Qontrast post-processing software, Bracco, Italy). Place the region of interest (ROI) over the tumor and determine either descriptive factors (e.g., area under the curve) or (semi-) quantitative parameters from color-coded maps, e.g., regional blood volume, regional blood flow, and filling time.
5. Time-activity curves from volumes of interest (VOIs) can be retrieved by analysis of PET data. Place one VOI over the aorta to obtain the blood concentration of the tracer. Position other VOIs over the tumor and normal tissue. Apply partial volume correction according to the size of the VOIs. The recovery is 0.85 for a diameter of 8 mm and 0.32 for a diameter of 3 mm.

The standard model for FDG is a two-tissue compartment model, providing the following parameters: the transport parameters for ^{18}F-FDG into and out of the cell (k1 and k2), the parameters for phosphorylation and dephosphorylation of the intracellular ^{18}F-FDG (k3 and k4), and the fractional blood volume (VB, also called vessel density) that reflects the amount of blood in the volume of interest [9–11].

4 Notes

1. All procedures and methods used in small animals require the approval of the respective local animal committee.
2. For inserting a catheter into the tail vein: Anesthetize the rat. Moderately warm the tail, i.e., with warm water or an infrared lamp, until veins are clearly visible (please be careful with the heat). Insert the needle into the tail vein. Then fix the catheter on the tail using tape and replace the syringe containing NaCl with a syringe containing contrast agent.
3. In the calculation of the contrast agent injection volume, bear in mind possible dead volumina and boli (syringe, etc.). Do not allow any air bubbles in the catheter. Rinse the catheter and all possible dead volumes with NaCl before injecting contrast agent.
4. Monitoring systems are useful to monitor the animal during imaging (especially breathing and temperature). MR-compatible systems are available, e.g., from SA Instruments, New York, USA.
5. Tuning the MRI volume coil becomes the more important the smaller the coil is as small coils are more sensible to loading than big volume coils are. Furthermore, perform manual adjustments of frequency, transmitter, and 3D shim for each MRI examination (for each animal): Manual adjustments are usually done after the localizer and before start of the imaging protocol. In addition, make sure that the subsequent sequences of the protocol adopt the manual adjustments.
6. For multimodal comparison of the respective data between the techniques, all four imaging modalities can be performed sequentially in the same animal. Co-registration of images from the different modalities is facilitated when the same positioning device is used, at least for MRI, CT, and PET.
7. The noninvasive character of imaging furthermore allows the investigation of therapeutic effects upon anti-angiogenic or standard therapies for vascularized tumors in longitudinal studies. Choose the most suited modality and imaging technique according to the drug's mechanism of action. As an example, for assessing treatment response to vascular endothelial growth factor (VEGF) inhibitors or multityrosine kinase inhibitors (e.g., including VEGF/VEGFR), DCE-MRI, DCE-CT, and

DCE-US are feasible. Thereby, DCE-MRI and DCE-US revealed response to therapy within 2 days after onset of the multityrosine kinase inhibitor sunitinib malate (Bayer Healthcare, Germany) [4].

8. Furthermore, molecular and metabolic aspects of targeted treatments might be acquired with PET by specific radiotracers and kinetic modeling of imaging data. As an example, the small-molecule inhibitor of integrins alpha (v) beta 3 and 5 cilengitide (Merck, Germany) could be monitored calculating the vascular fraction VB from dynamic ^{18}F-FDG PET acquisition [9]. Furthermore, specific radiotracers like ^{68}Ga-DOTA-E[c(RGDfK)] [2] might directly visualize alpha (v) beta 3 and 5 expression in tumors [5].
9. For the validation of noninvasively acquired imaging parameters, the correlation of these surrogate parameters with histologic results is pivotal. Quantitative data from kinetic modeling such as blood volume and vessel permeability depend largely on vessel maturation and diameter that can be determined by immunostainings for smooth muscle actin (SMA) and collagen IV [12].
10. When using different species like mice or rabbits, the given materials and methods have to be adjusted regarding animal preparation (e.g., contrast agent dosage), scanner and hardware proportions (e.g., scanner gantry, MR coils), imaging protocols (e.g., acquisition time, sequence parameters), and postprocessing (e.g., presettings for kinetic modeling). Most experimental scanners for CT, MRI, and PET are suitable for mice and rats, while rabbits are often examined in human systems. Experimental US devices are usually suited for mice, rats, and rabbits.

    Further information and examples of applying these imaging techniques in a nude rat model with bone metastases growing in the hind leg can be found, e.g., in the following references: MRI: [3, 12, 13]; CT: [1, 2]; US: [4]; PET: [5, 9]; Correlation of imaging data with histology: [12].

References

1. Bäuerle T, Hilbig H, Bartling S, Kiessling F, Kersten A, Schmitt-Gräff A et al (2008) Bevacizumab inhibits breast cancer-induced osteolysis, surrounding soft tissue metastasis, and angiogenesis in rats as visualized by VCT and MRI. Neoplasia 10(5):511–520
2. Bäuerle T, Bartling S, Berger M, Schmitt-Gräff A, Hilbig H, Kauczor H-U et al (2010) Imaging anti-angiogenic treatment response with DCE-VCT, DCE-MRI and DWI in an animal model of breast cancer bone metastasis. Eur J Radiol 73(2):280–287
3. Bäuerle T, Merz M, Komljenovic D, Zwick S, Semmler W (2010) Drug-induced vessel remodeling in bone metastases as assessed by dynamic contrast enhanced magnetic resonance imaging and vessel size imaging: a longitudinal in vivo study. Clin Cancer Res 16(12):3215–3225
4. Merz M, Komljenovic D, Semmler W, Bäuerle T (2012) Quantitative contrast-enhanced ultrasound for imaging antiangiogenic treatment response in experimental osteolytic breast cancer bone metastases. Invest Radiol 47(7):422–429

5. Mühlhausen U, Komljenovic D, Bretschi M, Leotta K, Eisenhut M, Semmler W et al (2011) A novel PET tracer for the imaging of αvβ3 and αvβ5 integrins in experimental breast cancer bone metastases. Contrast Media Mol Imaging 6(6):413–420
6. Bäuerle T, Adwan H, Kiessling F, Hilbig H, Armbruster FP, Berger MR (2005) Characterization of a rat model with site-specific bone metastasis induced by MDA-MB-231 breast cancer cells and its application to the effects of an antibody against bone sialoprotein. Int J Cancer 115(2):177–186
7. Brix G, Semmler W, Port R, Schad LR, Layer G, Lorenz WJ (1991) Pharmacokinetic parameters in CNS Gd-DTPA enhanced MR imaging. J Comput Assist Tomogr 15(4):621–628
8. Tofts PS, Brix G, Buckley DL, Evelhoch JL, Henderson E, Knopp MV et al (1999) Estimating kinetic parameters from dynamic contrast-enhanced T(1)-weighted MRI of a diffusable tracer: standardized quantities and symbols. J Magn Reson Imaging 10(3):223–232
9. Bretschi M, Cheng C, Witt H, Dimitrakopoulou-Strauss A, Strauss LG, Semmler W et al (2013) Cilengitide affects tumor compartment, vascularization and microenvironment in experimental bone metastases as shown by longitudinal ^{18}F-FDG PET and gene expression analysis. J Cancer Res Clin Oncol 139(4):573–583
10. Pan L, Mikolajczyk K, Strauss L, Haberkorn U, Dimitrakopoulou-Strauss A (2007) Machine learning based parameter imaging and kinetic modeling of PET data. Soc Nucl Med Annu Meet Abstr 48(Supplement 2):158P
11. Cheng C, Komljenovic D, Pan L, Dimitrakopoulou-Strauss A, Strauss L, Bäuerle T (2011 Apr) Evaluation of treatment response of cilengitide in an experimental model of breast cancer bone metastasis using dynamic PET with 18F-FDG. Hell J Nucl Med 14(1):15–20
12. Merz M, Seyler L, Bretschi M, Semmler W, Bäuerle T (2015) Diffusion-weighted imaging and dynamic contrast-enhanced MRI of experimental breast cancer bone metastases—a correlation study with histology. Eur J Radiol 84(4):623–630
13. Bäuerle T, Komljenovic D, Merz M, Berger MR, Goodman SL, Semmler W (2011) Cilengitide inhibits progression of experimental breast cancer bone metastases as imaged noninvasively using VCT, MRI and DCE-MRI in a longitudinal in vivo study. Int J Cancer 128(10):2453–2462
14. Bäuerle T, Komljenovic D, Berger MR, Semmler W (2012) Multi-modal imaging of angiogenesis in a nude rat model of breast cancer bone metastasis using magnetic resonance imaging, volumetric computed tomography and ultrasound. J Vis Exp 66:e4178

Chapter 16

Uncovering Metabolic Effects of Anti-angiogenic Therapy in Tumors by Induced Metabolic Bioluminescence Imaging

Stefano Indraccolo, Stefan Walenta, and Wolfgang Mueller-Klieser

Abstract

Induced metabolic bioluminescence imaging (imBI) is an imaging technique which enables detection of various metabolites associated with glycolysis in tumor sections. Signals captured by imBI can be used to chart the topographic distribution of lactate, glucose, pyruvate, and ATP and quantify their absolute amount. ImBi can enable us to perform metabolic classification of tumors as well as to detect metabolic changes in the glycolytic pathway associated with certain therapies, such as anti-angiogenic drugs.

Key words Tumor xenografts, Bioluminescence, Glycolysis, Angiogenesis, Imaging

1 Introduction

Angiogenesis plays an essential role in tumor growth and metastasis and tumor angiogenesis pathways have been identified as important therapeutic targets in many types of cancer. Vascular endothelial growth factor (VEGF) is one of the key cytokines driving tumor angiogenesis. By targeting the tumor-associated microvasculature, VEGF signaling inhibitors cause vessel pruning, which is followed by hypoxia and reduced supply of other nutrients [1–4]. Since anti-angiogenic drugs do not have, in general, direct effects of tumor cells, the therapeutic activity of these drugs is almost entirely dependent on its modulation of the supportive functions of the tumor microenvironment. Albeit still hypothetical, it is quite possible that the metabolic status of tumor cells can enable them to either succumb or adapt to the starving effects on anti-angiogenic therapy. Tumor metabolism could eventually represent a factor that influences tumor response to VEGF inhibitors.

Imaging techniques are extremely valuable both to perform metabolic profiling of tumors and to uncover metabolic fluctuations caused by drugs. With regard to anti-angiogenic therapy, some of these techniques have been used to measure the uptake of selected metabolites in tumors, such as PET [5], whereas others,

Domenico Ribatti (ed.), *Tumor Angiogenesis Assays: Methods and Protocols,* Methods in Molecular Biology, vol. 1464,
DOI 10.1007/978-1-4939-3999-2_16,

including hyperpolarized ^{13}C spectroscopy [6] and proton NMR [7], enabled quantitative assessment of certain metabolites in experimental tumors.

We were the first to exploit a technique termed induced metabolic bioluminescence imaging (imBI) to investigate metabolic perturbations associated with anti-VEGF therapy [5, 8]. Notably, although somewhat limited by the small number of metabolites which can be analyzed, imBI provides an accurate representation of the steady-state levels of the metabolites, matching them to the histology of the tumor section.

The imBI technique has been developed in the laboratory at the University of Mainz to detect metabolites in cryo-sections from snap-frozen tissue in situ [9–11] (*see* **Note 1**). The data obtained therefore reflect a "snapshot" of the momentary metabolic status of biological tissues. Self-made kits containing definite exogenous enzymes and cofactors are used as "metabolic sensors" to achieve high specificity and sensitivity. Heat inactivation of endogenous enzyme activities in the tissue sections of interest immediately before imBI measurement avoids interference with exogenous enzymes within the kit. Substrate saturation is prevented by providing all components of the kit in excess. The enzymatic activity induced by the metabolite of interest in the target tissue is biochemically coupled via the $NAD(P)H + H^+$ redox system to luciferases leading to light emission, i.e., to bioluminescence. The intensity of this low-level light emission is proportional to the tissue content of the respective metabolite. The biochemistry for the detection of ATP, glucose, pyruvate, and lactate via imBI is illustrated diagrammatically in Fig. 1. Since a specific enzyme mixture has to be prepared for each metabolite of interest, the imBI technique allows for the detection of only one metabolite per section. On the other hand, section thickness is adjusted in most cases to values in the range of 10–20 μm, and thus different metabolites can be determined in serial sections at a quasi-identical location within a tissue. Furthermore, a specific computerized overlay technique using metabolic and structural imaging allows for the determination of metabolite concentrations within selected histological tissue areas.

The rest of this chapter is devoted to the methodologic description of this valuable imaging technique and its applications in the field of tumor angiogenesis. It is important to remark that both experimental and clinical tumor samples can be analyzed by imBI, as reviewed elsewhere [9] (*see* **Note 2**).

2 Materials

2.1 Cells

The ovarian cancer cell line OC316 was a kind gift of Dr. Silvano Ferrini (IST, Genova, Italy) and can be purchased from the IRCCS AOU San Martino core facility ICLC (http://www.iclc.it).

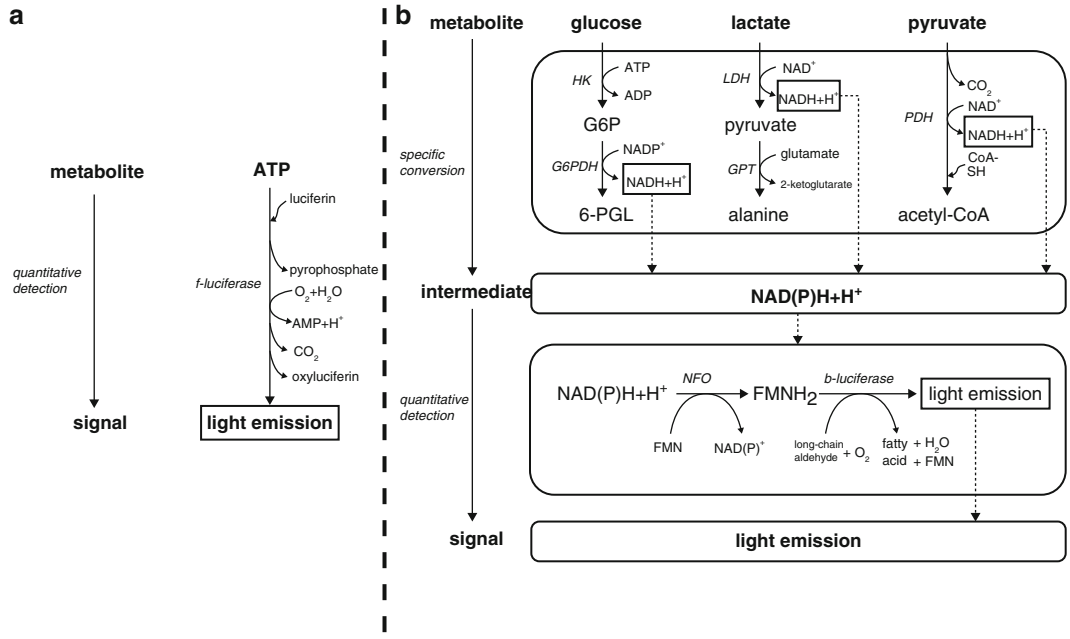

Fig. 1 Schematic of the biochemistry of induced metabolic bioluminescence imaging (imBI): Detection of (**a**) ATP and (**b**) glucose, lactate, pyruvate. (**a**) ATP immediately takes part in the bioluminescence reaction of fireflies (*Photinus pyralis*). (**b**) Glucose, lactate, and pyruvate are enzymatically converted to a common intermediate metabolite, NADH + H^+ or NADPH + H^+. Subsequently, the coenzyme enters the bioluminescence reactions of *Photobacterium fischeri* yielding light emission proportional to the initial metabolite concentration (modified according to [9]). *Abbreviations:* Enzymes: hexokinase (HK), glucose-6-phosphate-dehydrogenase (G6PDH), lactate dehydrogenase (LDH), glucose-pyruvate-transaminase (GPT), pyruvate-dehydrogenase (PDH), NAD(P)H:FMN-oxidoreductase (NFO), bacterial luciferase (b-luciferase), firefly luciferase (f-luciferase). Metabolites: glucose-6-phosphate (G6P), 6-phospho-gluconolactone (6-PGL)

2.2 Mice

Eight-week-old SCID mice were purchased from Charles River (Calco, Italy).

3 Methods

3.1 Generation of Subcutaneous Tumor Xenografts

Procedures involving animals and their care conformed with institutional guidelines that comply with national and international laws and policies (EEC Council Directive 86/609, OJ L 358, 12 December, 1987). For tumor establishment, 8-week-old SCID mice (Charles River) were subcutaneously injected into both flanks with $0.3–0.5 \times 10^6$ tumor cells mixed at 4°C with liquid Matrigel (Becton Dickinson). Tumor volume (mm^3) was calculated as previously reported [8].

Starting from the day of inoculum, the animals were inspected twice weekly and tumors measured by caliper; tumor volume was calculated as $(\text{length} \times \text{width}^2) \times 0.5$. At the end of the experiment,

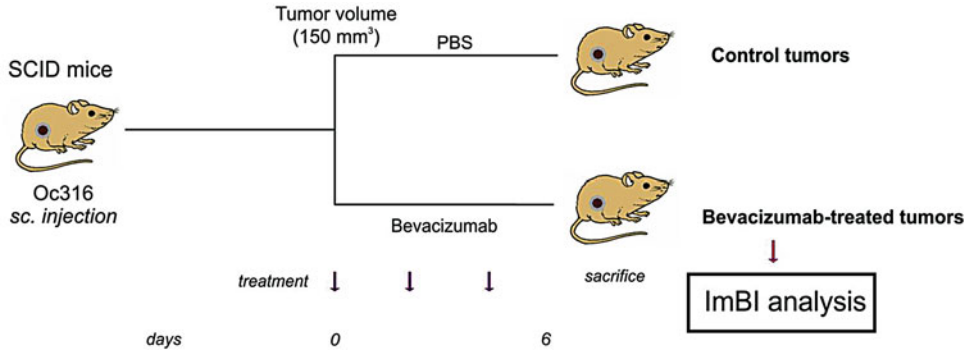

Fig. 2 Schematic of the protocol used to generate subcutaneous tumor xenografts and treatment with the anti-angiogenic drug bevacizumab

the mice were killed by cervical dislocation. The tumors were harvested by dissection, weighted, and snap-frozen in LN2 for imBI analyses (*see* **Note 3**).

3.2 Anti-angiogenic Treatment

In a set of experiments, when the average tumor volume had reached 150 ± 50 mm³, the anti-human VEGF monoclonal antibody (mAb; bevacizumab) was administered intraperitoneally at 100 mg/dose every other day three times, and mice were sacrificed 48 h after the last treatment. Control mice received intraperitoneal injections of PBS (Fig. 2) [8].

3.3 ImBI Analysis

3.3.1 Specific Detection of Tissue Metabolites

1. For processing of the tissue specimens the frozen biopsy is embedded in Tissue Tek® (O.C.T.™ Compound; Sakura Finetek Europe B.V., Alphen aan den Rijn, The Netherlands) on a sample holder of a cryomicrotome (SLEE cryostat, Type MEV; SLEE, Mainz, Germany).
2. Serial sectioning is then performed precisely at a temperature between –20 and –12 °C depending on the tissue composition of the specimen. As indicated in the upper panel of Fig. 3, two parallel channels are driven into each biopsy by a specially designed "micro-fork." Sectioning perpendicular to these channels leads to two holes in each section. These holes make it possible to precisely overlay sequential sections and, thus, to co-localize different parameter values in different adjacent sections.

3.3.2 Localization of Tissue Metabolites

1. The spatial resolution of imBI is generated by a sandwich technique providing a homogeneous contact between enzyme cocktail and tissue section (Fig. 3).
2. An excess volume of enzyme solution is pipetted into a casting mold within a metal slide.
3. A cover glass with a tissue section adhered is laid upside-down onto the enzyme solution within the casting mold. This pro-

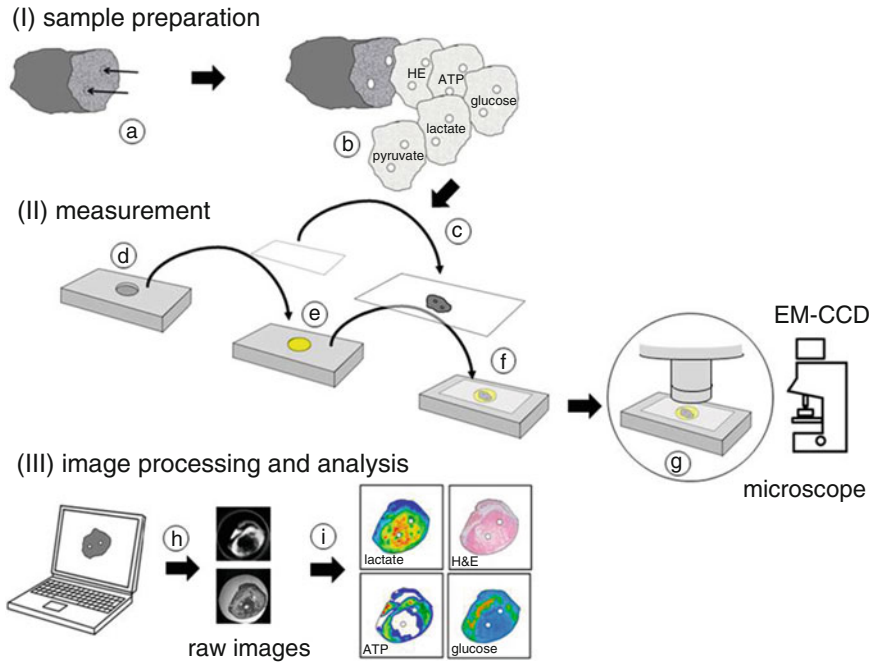

Fig. 3 Schematic of the procedure of induced metabolic bioluminescence imaging (imBI). (*I*) Sample preparation: The frozen tissue sample is precisely punctured by a small fork (**a**). Subsequently, serial cryo-sections are prepared (**b**). Each section is adhered on a cover glass (**c**) and heat-inactivated (not shown). (*II*) A casting mold (**d**) is filled with an appropriate enzyme solution (**e**). Immediately before measurement, a section on a cover glass is immersed into the enzyme solution (**f**). This "sandwich" is inserted into a thermostated chamber mounted on the stage of a microscope (**g**). The light emission is registered by an EM-CCD camera connected to a computer. (*III*) Using an image analysis software (**h**), the raw images are processed, analyzed, calibrated, and finally expressed as color-coded images (**i**). Pinpricks (**a**) within the biopsy provide landmarks for a correct overlay of corresponding images

vides complete contact between tissue and enzyme solution, which has been kept in a liquid state at the measuring temperature. The contact between substrate and enzyme mixture then initiates the bioluminescence reaction.

4. The sandwich is put on the thermostated stage of a microscope (Axiophot, Zeiss, Oberkochen, Germany) within a light-impervious chamber.
5. An ultrasensitive back-illuminated EM-CCD camera (iXonEM+ DU-888; Andor Technology PLC, Belfast, UK) connected to the microscope enables the registration of the low-light bioluminescence intensity with the optics focused on the tissue section plane.
6. The image signal is transferred to a computer for image analysis. By integrating the light emission intensities over a selected time interval, a two-dimensional density profile is obtained representing the two-dimensional metabolite distribution across the tissue section.

3.3.3 Quantification of Tissue Metabolites

1. Using appropriate standards, which are handled in exactly the same way as the tissue of interest, bioluminescence intensities can be transformed into absolute tissue concentrations of the respective metabolite, e.g., in micromoles per gram of tissue (μmol/g) which corresponds approximately to mM in solution.
2. Routine standards are obtained by mixing cryo-embedding medium (Tissue-Tek®) with defined amounts of substrate.
3. The frozen medium is then cryo-sectioned and processed in the same way as the tissue of interest.
4. The calibration allows for the illustration of the two-dimensional substrate distribution in a color-coded manner, as indicated in Fig. 4.

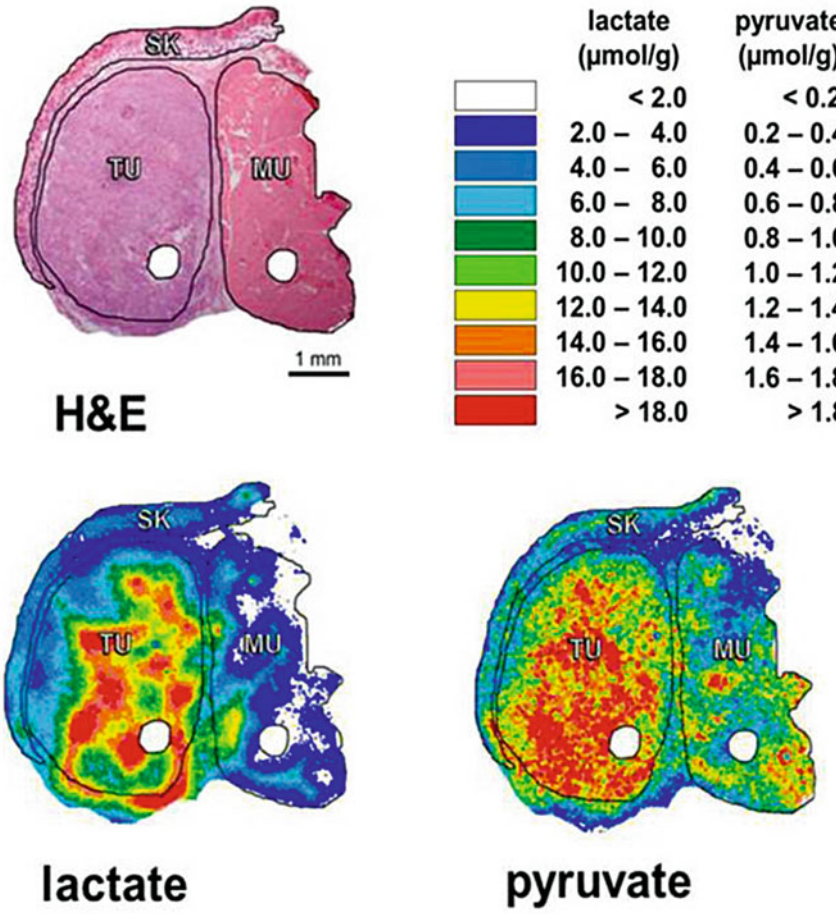

Fig. 4 Induced metabolic bioluminescence imaging (imBI) of lactate and pyruvate in a human head and neck squamous cell carcinoma (HNSCC) xenografted in a nude mouse. Sequential cryo-sections (each showing two punched holes for overlay) were used for hematoxylin and eosin (H&E) staining and imaging of lactate and pyruvate concentrations. For structure-associated evaluation, defined histological areas were delineated: tumor tissue (TU), skeletal muscle (MU), and skin (SK) (modified according to [9])

5. This procedure is applicable to all metabolites specified above.
6. Light intensity is also influenced by the microscopic magnification, since pixel density per unit image area and, hence, light intensity are much lower at a high magnification and vice versa. Other factors with impact on light intensity are the viscosity of the enzyme solution, the measuring temperature, the light integration interval, or the quantum efficiency of the bioluminescence reaction itself. And all these factors are mutually related and not at all independent of each other. In essence, the concert of these factors determines the sensitivity of the technique being on the micromolar level.

3.3.4 Combined Quantification and Localization of Metabolites

1. High sensitivity and high spatial resolution are contradicting demands, but the advantage of imBI is its versatility in adjusting the measuring conditions towards either resolution or sensitivity depending on the requirements of an actual experiment.
2. Spatial resolution is restricted at a low viscosity and high temperature of the enzyme solution and at long light integration interval. Such conditions favor lateral diffusion of metabolites and enzymes resulting in a "smearing out" the gradients in the metabolic profiles.
3. For most measurements in tumor biopsies, experimental settings are chosen in a way that the minimum detectable substrate concentration is around 100 μmol/g with a spatial linear resolution of around 100 μm (*see* **Note 4**).
4. Keeping the former sensitivity of detection, the spatial resolution can be adjusted to 20 μm in imaging metabolic gradients in multicellular spheroids adjusting an appropriate registration temperature and viscosity of the enzyme solution.

3.3.5 Structure-Associated Metabolite Detection and Co-localization

1. Using serial sections, a section can be stained for the histological structure, e.g., with hematoxylin and eosin (H&E), followed by sections stained for the various metabolites.
2. The "two-hole technique" allows for an exact, computer-assisted overlay between the sections. Such an overlay makes it possible to detect the bioluminescence signals in a structure-associated way, i.e., within selected histological areas, such as viable tumor regions, stromal areas, or necrosis. The strategy is exemplified in Fig. 4.
3. Co-localization studies can be extended to virtually all parameters which can be visualized in cryo-sections, e.g., mRNAs detected by in situ hybridization, proteins assessed by immunostaining, or functional parameters, such as blood perfusion imaged by fluorescent stains or hypoxic cells identified by pimonidazole [12].

3.4 Conclusions: Applications of ImBI in the Field of Tumor Angiogenesis

ImBI proved to be an extremely useful technique to investigate modulations in the concentration of metabolites in tumors treated with anti-angiogenic drugs. In tumor xenografts, we observed a dramatic reduction in glucose and ATP levels in the tumor microenvironment following anti-VEGF therapy (Fig. 5) [8]. Such changes, nicely visualized and quantified by imBI, led us to speculate that glucose-addicted tumors could be particularly vulnerable to the effects of VEGF blockade. In line with this prediction, the amount of necrotic area in the highly glycolytic tumors was much larger compared with values found in poorly glycolytic tumors [8], thus connecting a metabolic trait of tumor cells to a histologic pattern of response to VEGF neutralization. Importantly, the hypothesis that highly glycolytic tumors could be highly responsive to antiangiogenic drugs has been recently validated in a clinical trial with the antiangiogenic drug cediranib [13].

4 Notes

1. It is highly recommended that metabolic tissue banks (in liquid nitrogen) should be set up by big clinical centers. We have shown [9] that metabolites can be cryo-preserved for more than 10 years.
2. The speed of cryo-fixation is indeed critical, but it can be done and organized in an appropriate way even in the clinical setting in the operation hall.
3. To prevent loss of ATP, it is critical to remove tumors from the subcutaneous tissue and freeze them in liquid nitrogen within 20 s.
4. In our routine technology, the minimum detectable substrate concentration is around 100 μmol/g of viable tissue. Taking a given thickness of the cryosection used of 10 μm and a section area of 1 cm^2, this corresponds to a minimum detectable absolute amount of substrate (i.e., the substrate content of one cryosection) of around 10 pg. By reducing the section thickness, increasing the enzyme components in the detection cocktails, and optimizing the photon registration technique it is possible to detect minimum substrate concentrations in the nmol/g range.

Funding

This work was supported by grants from AIRC (IG grant 14295), the Deutsche Forschungsgemeinschaft (Mu 576/15-1, 15-2), and the German Federal Ministry of Education and Research ("ISIMEP"; 02NUK016A).

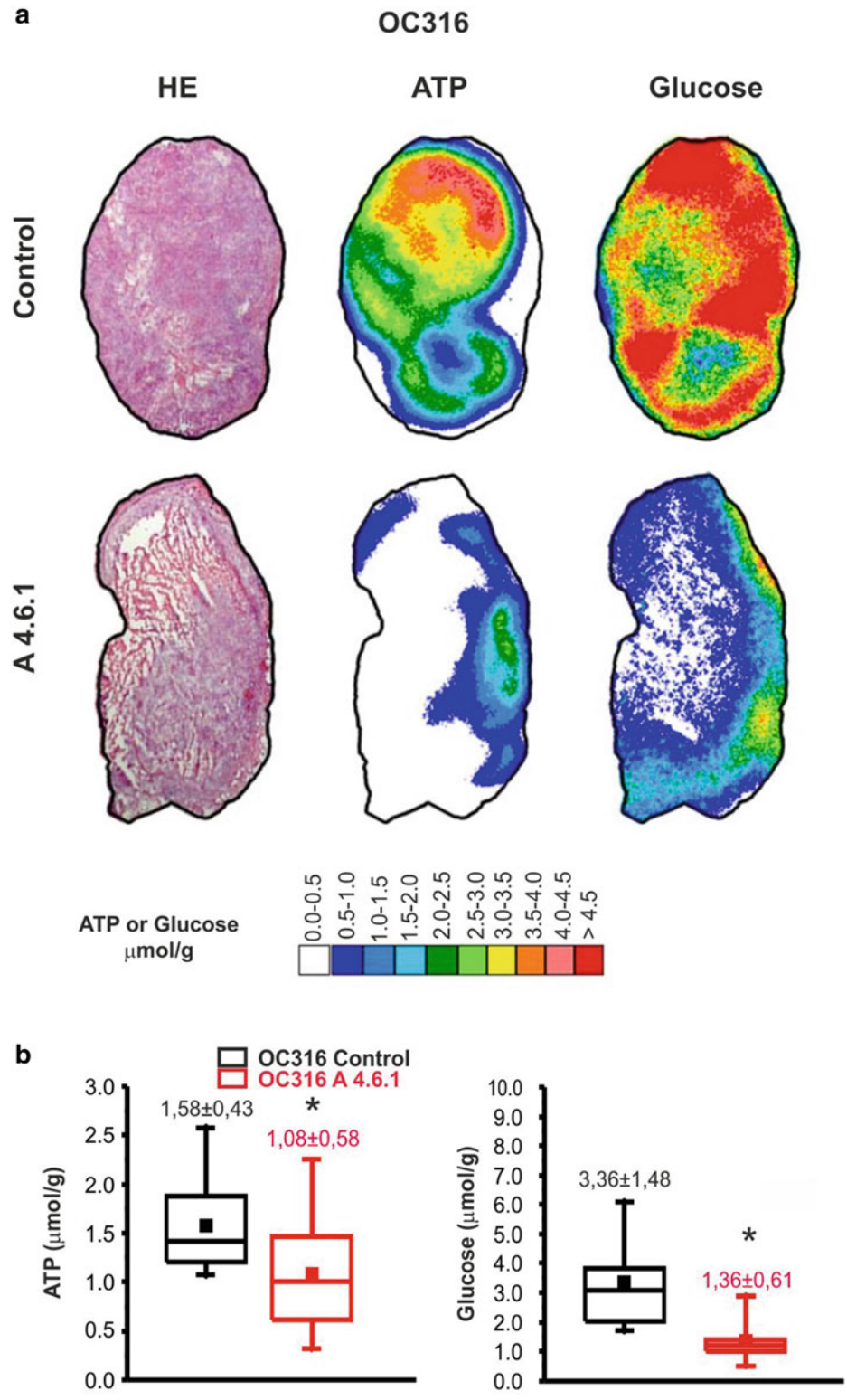

Fig. 5 Metabolic effects of anti-VEGF therapy in tumors measured by bioluminescence imaging. **a**: H&E staining as well as color-coded distributions of ATP and glucose in sequential cryo-sections from representative OC316 tumors treated or not with the anti-VEGF mAb A4.6.1 (100 µg/dose, three doses given every other day). The concentration values were color-coded, with each color corresponding to a defined concentration range in µmol/g. **b**: Metabolite concentrations in OC316 tumors treated or not with A4.6.1. Values were derived exclusively from vital tumor regions. ATP and glucose values were calculated from $n = 12–32$ sections from 4 to 10 different tumors (reproduced from [8])

References

1. Carmeliet P, Jain RK (2011) Principles and mechanisms of vessel normalization for cancer and other angiogenic diseases. Nat Rev Drug Discov 10(6):417–427
2. Grothey A, Galanis E (2009) Targeting angiogenesis: progress with anti-VEGF treatment with large molecules. Nat Rev Clin Oncol 6(9):507–518
3. Heath VL, Bicknell R (2009) Anticancer strategies involving the vasculature. Nat Rev Clin Oncol 6(7):395–404
4. Jayson GC, Hicklin DJ, Ellis LM (2012) Antiangiogenic therapy—evolving view based on clinical trial results. Nat Rev Clin Oncol 9(5):297–303
5. Curtarello M, Zulato E, Nardo G, Valtorta S, Guzzo G, Rossi E, Esposito G, Msaki A, Pasto A, Rasola A et al (2015) VEGF-targeted therapy stably modulates the glycolytic phenotype of tumor cells. Cancer Res 75(1):120–133
6. Bohndiek SE, Kettunen MI, Hu DE, Brindle KM (2012) Hyperpolarized (13)C spectroscopy detects early changes in tumor vasculature and metabolism after VEGF neutralization. Cancer Res 72(4):854–864
7. Keunen O, Johansson M, Oudin A, Sanzey M, Rahim SA, Fack F, Thorsen F, Taxt T, Bartos M, Jirik R et al (2011) Anti-VEGF treatment reduces blood supply and increases tumor cell invasion in glioblastoma. Proc Natl Acad Sci U S A 108(9):3749–3754
8. Nardo G, Favaro E, Curtarello M, Moserle L, Zulato E, Persano L, Rossi E, Esposito G, Crescenzi M, Casanovas O et al (2011) Glycolytic phenotype and AMP kinase modify the pathologic response of tumor xenografts to VEGF neutralization. Cancer Res 71(12):4214–4225
9. Walenta S, Voelxen NF, Sattler UGA, Mueller-Klieser W (2014) Localizing and quantifying metabolites in situ with luminometry: induced metabolic bioluminescence imaging (imBI). In: Hirrlinger J and Waagepetersen HS (eds) Brain energy metabolism. Humana Press (Springer), New York, pp 195–216
10. Walenta S, Mueller-Klieser WF (2004) Lactate: mirror and motor of tumor malignancy. Semin Radiat Oncol 14(3):267–274
11. Walenta S, Schroeder T, Mueller-Klieser W (2004) Lactate in solid malignant tumors: potential basis of a metabolic classification in clinical oncology. Curr Med Chem 11(16):2195–2204
12. Yaromina A, Quennet V, Zips D, Meyer S, Shakirin G, Walenta S, Mueller-Klieser W, Baumann M (2009) Co-localisation of hypoxia and perfusion markers with parameters of glucose metabolism in human squamous cell carcinoma (hSCC) xenografts. Int J Radiat Biol 85(11):972–980
13. Pommier AJ, Farren M, Patel B, Wappett M, Michopoulos F, Smith NR, Kendrew J, Frith J, Huby R, Eberlein C et al (2015) Leptin, BMI, and a metabolic gene expression signature associated with clinical outcome to VEGF inhibition in colorectal cancer. Cell Metab 23(1):77–93

Chapter 17

Quantitation of Tumor Angiogenesis In Vitro: An All-In-One Angiogenesis Assay

Mahtab Bahramsoltani and Ward De Spiegelaere

Abstract

In vitro angiogenesis systems enable the analysis of pro- or anti-angiogenic compounds. Most in vitro models do not reproduce the entire angiogenic cascade, from cell migration and proliferation to tube formation. Here, we describe an all-in-one angiogenesis assay that mimics the entire angiogenic cascade in vitro, rendering this model an ideal tool for the in vitro testing.

Key words In vitro angiogenesis, Quantitation, All-in-one assay, Tumor-induced angiogenesis, Pro-angiogenic factors, Angiogenic cascade

1 Introduction

In vitro models of angiogenesis represent a cost-efficient tool for quantitation as well as investigation of the cellular and molecular mechanisms of tumor-induced angiogenesis [1–4]. They allow identification of direct effects on endothelial cell function and the analysis of isolated processes that contribute to angiogenesis [2]. Most of these models are based on static systems using monocultures of microvascular endothelial cells [5, 6]. According to the phases of sprouting angiogenesis in vivo, most of the in vitro assays are designed to quantify migration, proliferation, or tube formation of endothelial cells [1, 2, 4, 7–10]. Therefore, quantitation of angiogenesis in vitro is carried out most frequently using three different angiogenesis assays to consider all phases of the angiogenic cascade [1–4, 11].

The all-in-one in vitro angiogenesis assay presented here is based on long-term cultivation of microvascular endothelial cells. Observation of endothelial morphology during long-term cultivation reveals a similar cascade of events and morphological changes of endothelial cells to angiogenesis in vivo also angiogenesis. Although these morphological changes are not equal to the

Domenico Ribatti (ed.), *Tumor Angiogenesis Assays: Methods and Protocols*, Methods in Molecular Biology, vol. 1464,
DOI 10.1007/978-1-4939-3999-2_17,

morphology of angiogenesis in vivo, they form a close mimic to the in vivo changes of angiogenesis [12–15]. By long-term cultivation of microvascular endothelial cells and staging the morphological changes during the process of angiogenesis in vitro, quantitation of all phases of the angiogenic cascade can be carried out in one single assay [12].

2 Materials

1. Human microvascular endothelial cells of different origin (Lonza Biosciences, Verviers, Belgium) (*see* **Note 1**).
2. EGM-2 MV BulletKit (Lonza Biosciences, Verviers, Belgium).
3. ReagentPack Subculture Reagents (Lonza Biosciences, Verviers, Belgium).
4. Factors/substances/tumor-conditioned media to be tested.
5. 1.5% Gelatine in 0.01 M PBS, pH 7.4.
6. Culture well plates, 6- and 24-well.
7. Medium for negative controls by supplementing the basal medium only with 2% FBS (*see* **Note 2**).
8. Medium for positive controls by mixing the growth medium as suggested by the distributors (*see* **Note 3**).
9. Medium for the samples by adding the substances or growth factors to be investigated (also tumor-conditioned media can be used) to the basal medium supplemented with 2% FBS.

3 Methods

Carry out all procedures that require the opening of the well plates in a laminar flow hood.

3.1 Thawing and Expansion of Microvascular Endothelial Cells

1. Prepare the endothelial cell growth medium containing all supplements according to the distributor's instructions. Warm up the medium at 37 °C in a water bath.
2. Add 1 ml 1.5% gelatine in each well of 6-well plates and put the well plates for 30 min in an incubator at 37 °C. Remove the remaining gelatine and cover the wells with culture medium in order to prevent the gelatine from drying out. Put the 6-well plates back to the incubator.
3. Thaw the microvascular endothelial cells as suggested by the distributors. Seed the cells in a concentration of $2.1–2.3 \times 10^5$ cells per well into the gelatine-coated 6-well plates.
4. Subculture the cells before reaching confluence until attainment of a sufficient cell yield for the experiments (*see* **Note 4**).

3.2 Seeding and Cultivation of Microvascular Endothelial Cells

1. Prepare four gelatine-coated wells (as described in Subheading 3.1, **step 2**) of 24-well plates for each case: negative controls, positive controls, and each sample (*see* **Notes 5** and **6**).
2. Seed the microvascular endothelial cells in a concentration of $4.1–4.5 \times 10^4$ cells per well.
3. Cultivate the microvascular endothelial cells over a period of 30 days by refreshing the media every 3 or 4 days.

3.3 Documentation, Staging, and Quantitation of Angiogenesis In Vitro

1. After seeding of the cells, randomly choose four visual fields in each well (two visual fields from the border area and two visual fields from the center of the well) using phase-contrast microscopy (*see* **Note 7**). Save the coordinates of the visual fields automatically if possible; otherwise list them manually.
2. Beginning with day 2, when the vast majority of the cells become adherent, take photographs of the defined visual fields every second day using phase-contrast microscopy (*see* **Note 8**).
3. Assign to each photograph one of the defined stages of angiogenesis in vitro (*see* **Note 9**) based on subjective assessment (*see* **Note 10**) as follows:

   Stage 1: Confluent monolayer (*see* **Note 11**). More than 50% of the cells are polygonal shaped (Fig. 1).

   Stage 2: Endothelial sprouting. More than 50% of the cells are elongated shaped (Fig. 1).

   Stage 3: Linear side-by-side arrangement. More than 50% of the cells are linearly arranged (Fig. 2).

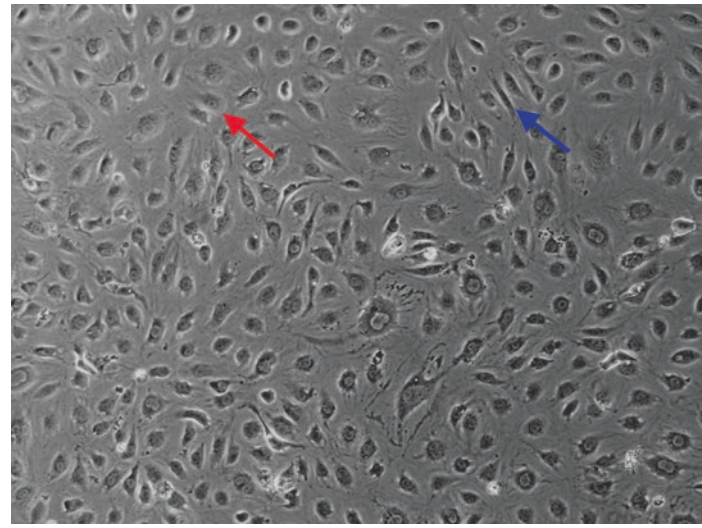

Fig. 1 Human microvascular endothelial cells derived from the skin. Polygonal (*red arrow*) and elongated (*blue arrow*) shaped cells. Phase-contrast microscopy, 100×

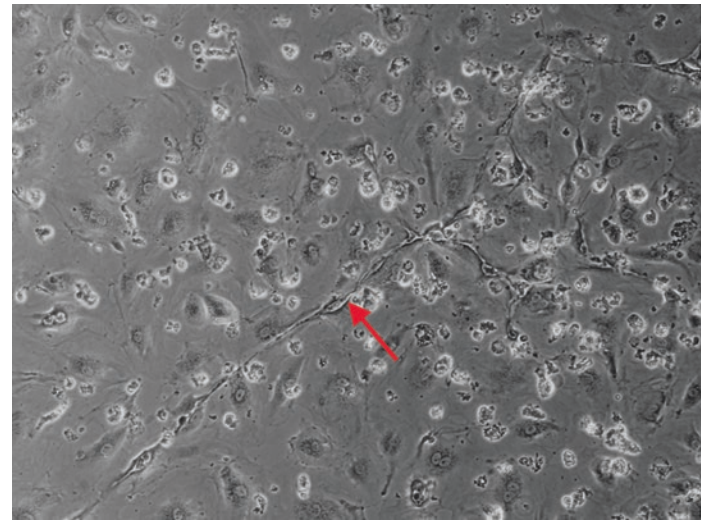

Fig. 2 Human microvascular endothelial cells derived from the skin. Linearly arranged cells (*arrow)*. Phase-contrast microscopy, 100×

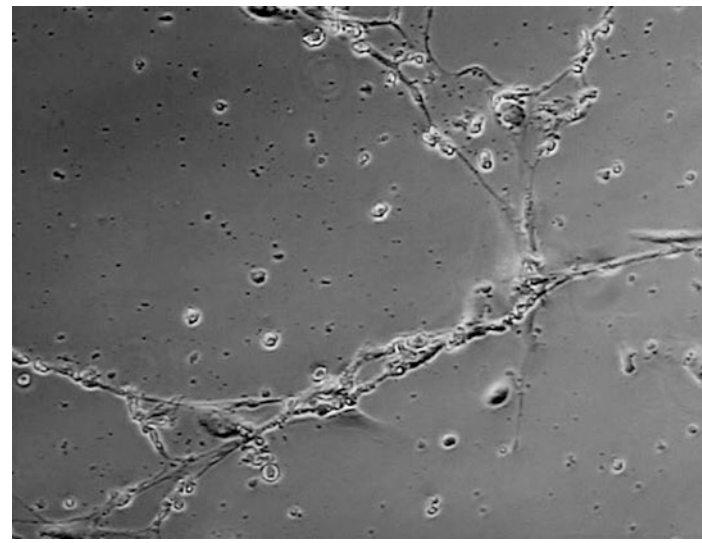

Fig. 3 Human microvascular endothelial cells derived from the heart. Network of linearly arranged cells. Phase-contrast microscopy, 100×

Stage 4: Networking. The linearly arranged cells detach from the monolayer and form an overlying network (Fig. 3). The cell layer on the bottom of the well starts to dissolve and loses confluence (*see* **Note 12**).

Stage 5: Three-dimensional organization, early phase. Appearance of the first capillary-like structures within the network (Fig. 4). Capillary-like structures are defined as linear

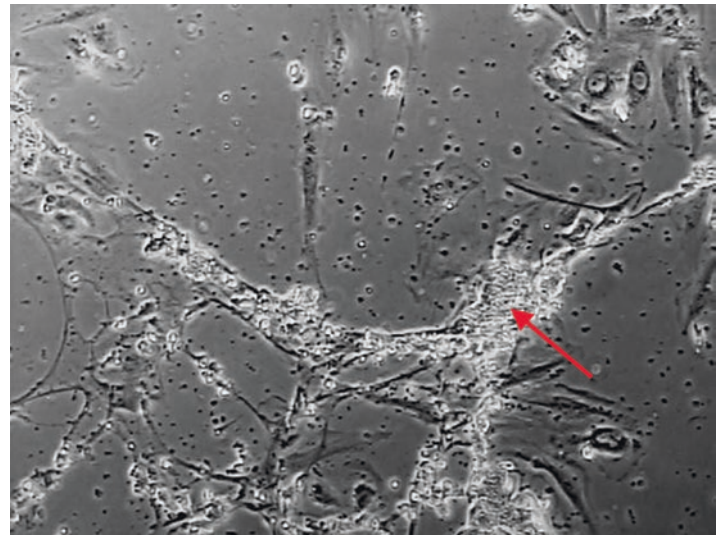

Fig. 4 Human microvascular endothelial cells derived from the heart. Capillary-like structure (*arrow*) within a network of linearly arranged cells. Phase-contrast microscopy, 100×

structures of endothelial cells with a diameter of more than 28 μm (*see* **Note 13**). Dissolution of the cell layer proceeds on the bottom of the well (*see* **Note 14**).

Stage 6: Three-dimensional organization, late phase. Linear structures of endothelial cells represent capillary-like structures predominately.

4. For quantitation of angiogenesis calculate first the sum of the assigned stages for each visual field and second the arithmetic mean of the sums for the 16 visual fields of each case ($\overline{S_j^{\text{case}}}; j = 1,\ldots,16$), i.e., negative controls, positive controls, and each sample.
5. For determination of the proangiogenic effect of the substances to be tested within the samples, calculate the ratio of the arithmetic mean of the visual fields of each sample and the arithmetic mean of the visual fields derived from the cells for positive control incubated in the growth medium ($\overline{S^{\text{sample}}} / \overline{S^{\text{positive control}}}$).

4 Notes

1. This model can also be performed with human umbilical vein endothelial cells (HUVEC).
2. This medium composition serves for the negative controls as it turned out to retain cell survival but did not result in any angiogenic response of the endothelial cells.

3. This medium composition serves for positive controls as it stimulates angiogenic endothelial cells to run through all stages of angiogenesis in vitro within 30–40 days.
4. Preliminary studies showed that the results for each batch of microvascular endothelial cells do not differ using the cells until passage 5.
5. It is recommended not to use the wells on the margins of the well plate as the morphology of the cells in these wells turned out to be very different from the other wells.
6. Internal validation studies revealed that representative quantitation can be carried out in four wells of 24-well plates [16].
7. Internal validation studies revealed that representative quantitation can be carried out in four visual fields per well [16].
8. Even using a motorized stage the visual fields adjusted differ slightly at the different investigation days. However, this fact does not have any influence on the results, as the morphology of the cell layer does not alter abruptly.
9. Applying the growth medium, batches of microvascular endothelial cells are defined as angiogenic, which run through the stages of angiogenesis in vitro reaching at least stage 4. Batches of microvascular endothelial cells reaching not more than stage 3 are defined to be non-angiogenic [14, 15]. As the last mentioned are not useful for angiogenesis assays, it is recommended to test the angiogenic potential of each batch of microvascular endothelial cells by cultivating the cells in the provided growth medium prior to their application in the study.
10. Internal validation studies include staging of angiogenesis in vitro by different investigators [16]. The results showed that staging carried out by equally experienced investigators only lead to slight differences in stage assignment of at most one stage in the early stages 1–3 of angiogenesis in vitro. As the same visual field was assessed repeatedly in the same way by the same investigator, it is recommended to carry out staging by one individual.
11. There are some batches of microvascular endothelial cells which do not form a confluent monolayer. The cells of these batches exhibit predominantly an elongated shape over the whole cultivation time. In these batches dissolution of the monolayer cannot serve for staging.
12. There are some batches of microvascular endothelial cells which exhibit a confluent monolayer on the bottom of the well during the whole cultivation time. Also in these batches dissolution of the monolayer cannot serve for staging.

13. Transmission electron microscopically investigations revealed an internal lumen within linear endothelial structures with a diameter of more than 28 μm [16].
14. In batches of microvascular endothelial cells, which form a confluent monolayer initially followed by the dissolution of the monolayer, the dissolution of the monolayer can be considered for staging if no capillary-like structures are present in the respective visual field.

References

1. Auerbach R, Lewis R, Shinners B et al (2003) Angiogenesis assays: a critical overview. Clin Chem 49:32–40
2. Bahramsoltani M, Plendl J, Janczyk P et al (2009) Quantitation of angiogenesis in vivo, ex vivo and in vitro—an overview. ALTEX 26:95–107
3. Goodwin AM (2007) In vitro assays of angiogenesis for assessment of angiogenic and anti-angiogenic agents. Microvasc Res 74:172–183
4. Staton CA, Stribbling SM, Tazzyman S et al (2004) Current methods for assaying angiogenesis in vitro and in vivo. Int J Exp Pathol 85:233–248
5. Minami T, Aird WC (2005) Endothelial cell gene regulation. Trends Cardiovasc Med 15:174–184
6. Aird WC (2012) Endothelial cell heterogeneity. Cold Spring Harb Perspect Med 2:a006429
7. Hata Y, Miura M, Nakao S et al (2008) Antiangiogenic properties of fasudil, a potent Rho-Kinase inhibitor. Jpn J Ophthalmol 52:16–23
8. Jabbour MN, Elder JB, Smeulson CG et al (2009) Abberant angiogenic characteristics of human brain arteriovenous malformation endothelial cells. Neurosurgery 64:139–146
9. Limaye V, Xia P, Hahn C et al (2009) Chronic increases in sphingosine kinase-I activity induce a pro-inflammatory, pro-angiogenic phenotype in endothelial cells. Cell Mol Biol Lett 14:424–444
10. Shrader CD, Bailey KM, Konat GW et al (2009) Insulin enhances proliferation and viability of human umbilical vein endothelial cells. Arch Dermatol Res 301:159–166
11. AlMalki WH, Shahid I, Mehdi AY et al (2014) Assessment methods for angiogenesis and current approaches for its quantification. Indian J Pharmacol 46:251–256
12. Bahramsoltani M, De Spiegelaere W, Janczyk P et al (2010) Quantitation of angiogenesis in vitro induced by VEGF-A and FGF-2 in two different human endothelial cultures—an all-in-one assay. Clin Hemorheol Microcirc 46:189–202
13. De Spiegelaere W, Cornillie P, Van den Broeck W et al (2011) Angiopoietins differentially influence in vitro angiogenesis by endothelial cells of different origin. Clin Hemorheol Microcirc 48:15–27
14. Bahramsoltani M, Harms T, Drewes B, Plendl J et al (2013) Searching for markers to identify angiogenic endothelial cells: a proteomic approach. Clin Hemorheol Microcirc 55:255–269
15. Bahramsoltani M, Slosarek I, De Spiegelaere W et al (2014) Angiogenesis and collagen type IV expression in different endothelial cell culture systems. Anat Histol Embryol 43:103–115
16. Bahramsoltani M, Plendl J (2004) A new in vitro model to quantify angiogenesis. ALTEX 21:227–244

Index

A

Affinity calculation 83
Aldehyde dehydrogenase (ALDH) 50, 56–57, 61
Angiogenesis ..... v, 1, 2, 4–10, 13, 14, 17, 19–21, 25–32, 63–71, 75, 85, 86, 90–91, 93, 94, 108, 115–118, 120–125, 127, 129–137, 147, 152, 163, 175, 185–191
Angiography 165, 168, 169
Anti-angiogenesis 3, 6–8, 10, 17, 20, 63, 85, 86, 88–90, 92–94

B

Bioluminescence 143, 146, 175–178, 180–182

C

Cancer ..... v, 5, 8–10, 13, 14, 17, 20, 25, 26, 28–32, 49, 50, 52, 60, 97, 115, 129, 130, 140, 153, 163, 164, 167–169, 175
Cancer cells 32, 68, 70, 71, 97, 104, 129, 131, 141, 143, 176
Cancer initiating cells (CICs) 27, 49
Cancer stem cells (CSCs) 49–61
Chick embryo 2, 97–102, 104
Chorioallantoic membrane (CAM) 2, 3, 97–102, 104
Coculture 35–40, 42–44, 46, 47
Collagens 8, 30, 64, 66–69, 120, 132, 172
Computed tomography (CT) 163, 164, 167–168
Confocal 121–123, 125, 126

D

Drug screening 87
Dynamic-contrast enhanced imaging 163, 165

E

Endothelial cells (EC) 3, 6, 8, 9, 14, 16, 18, 19, 29–31, 35–40, 42–44, 46, 47, 64, 70, 86, 92, 107, 117, 118, 124–126, 152, 153, 159, 164, 185–187, 189–191
Exosomes 25–32

F

Fluorescence 46, 55–57, 61, 101, 102, 108, 116, 117, 121, 123–126, 143, 146, 157

G

Gateway cloning system 108
Glycolysis 182

H

Heparin 3, 73–78, 80–84
History of medicine 1, 2, 4–10

I

Imaging 46, 86, 89–90, 93, 97, 102, 107, 116, 117, 121–125, 135, 141, 144–147, 163–169, 171, 172, 175–178, 180–182
Immunofluorescence (IF) 152, 154–155
Insulinoma 151, 158–160
Intercellular interactions 25, 28
Intrabursal transplant 139
Intravital microscopy 115–118, 120–125, 127

M

Magnetic resonance imaging (MRI) 144, 146, 163–167, 169, 171, 172
Matrigel 35, 52, 58, 61, 67, 70, 120, 130–133, 136, 177
Mesentery 85, 86, 88–93
Metastasis 5, 7, 26–32, 49, 97–102, 104, 140, 145, 146, 153, 157, 163, 167–170, 175
Microenvironment 5, 17, 25, 27–30, 32, 97, 130, 140, 147, 175, 182
Microvascular network 85–87, 89–93
Microvessels 5, 7, 20, 21, 69–70, 87
Multiphoton 121

N

Neovascularization 2, 5, 20, 63

O

Optical imaging 107, 143, 146
Orthotopic transplant 140, 142, 144
Ovarian cancer 50, 70, 71, 139–147, 176

P

Pancreatic neuroendocrine tumors (PNETs) 151, 152
Patient-derived xenografts 52, 132, 140

Domenico Ribatti (ed.), *Tumor Angiogenesis Assays: Methods and Protocols*, Methods in Molecular Biology, vol. 1464,
DOI 10.1007/978-1-4939-3999-2, © Springer Science+Business Media New York 2016

Pericytes 9, 10, 14, 18, 20, 30, 35, 36, 41–43, 46, 47, 64, 70, 86, 87, 94, 152, 157
Positron emission tomography (PET) 163–165, 168–172
Preclinical anticancer therapy 129, 130
Pre-metastatic niche 26–29, 32
Pro-angiogenic factors 3, 10, 14, 17, 20, 29, 152
Protein binding 75, 82, 83

Q

Quantitation 185–191

R

Rip1Tag2 ..... 4, 10, 151–160

S

Sensorchip 73, 74, 76–83
Side-population (SP) 50, 54–56
Small intestinal submucosa 45
Surface plasmon resonance 73–78, 80–84

T

Tissue culture 36, 51, 53, 64, 66, 67, 85, 86, 88–90, 92–94, 98, 132
Tol2 system 108, 109, 111
Transgenesis 108–111, 113
Tumorigenicity 27, 49, 52, 58, 61
Tumors ..... v, 1–2, 4–10, 14, 16–18, 20–22, 25–32, 49, 50, 52–60, 85, 97–102, 104, 115–118, 120–127, 130–137, 140–147, 151–153, 156, 158–160, 166, 168–172, 175–178, 180–183
  angiogenesis ..... v, 1, 2, 4–10, 13, 14, 17, 19–21, 25–32, 63–71, 76, 108, 115–118, 120–125, 127, 151, 152, 175, 176, 182, 185–191
  growth 1–4, 6, 8–10, 14, 20, 28, 30, 97, 116, 121–123, 129–137, 141, 145–147, 151–153, 175, 176
  models 14, 130, 153
  vessels 2, 9, 14–18, 20, 125, 126, 147, 152, 153, 163–172
  xenografts 14, 58, 132, 177–178, 182
Tumorspheres 52, 57

U

Ultrasound (US) 144, 163, 164, 168

X

Xenografts 14–16, 22, 58, 121–123, 129–137, 140, 153, 180

Z

Zebrafish embryos 107